A CONTINUOUS LOW-COST GPS-BASED VOLCANO DEFORMATION MONITORING SYSTEM IN INDONESIA

CRAIG ROBERTS

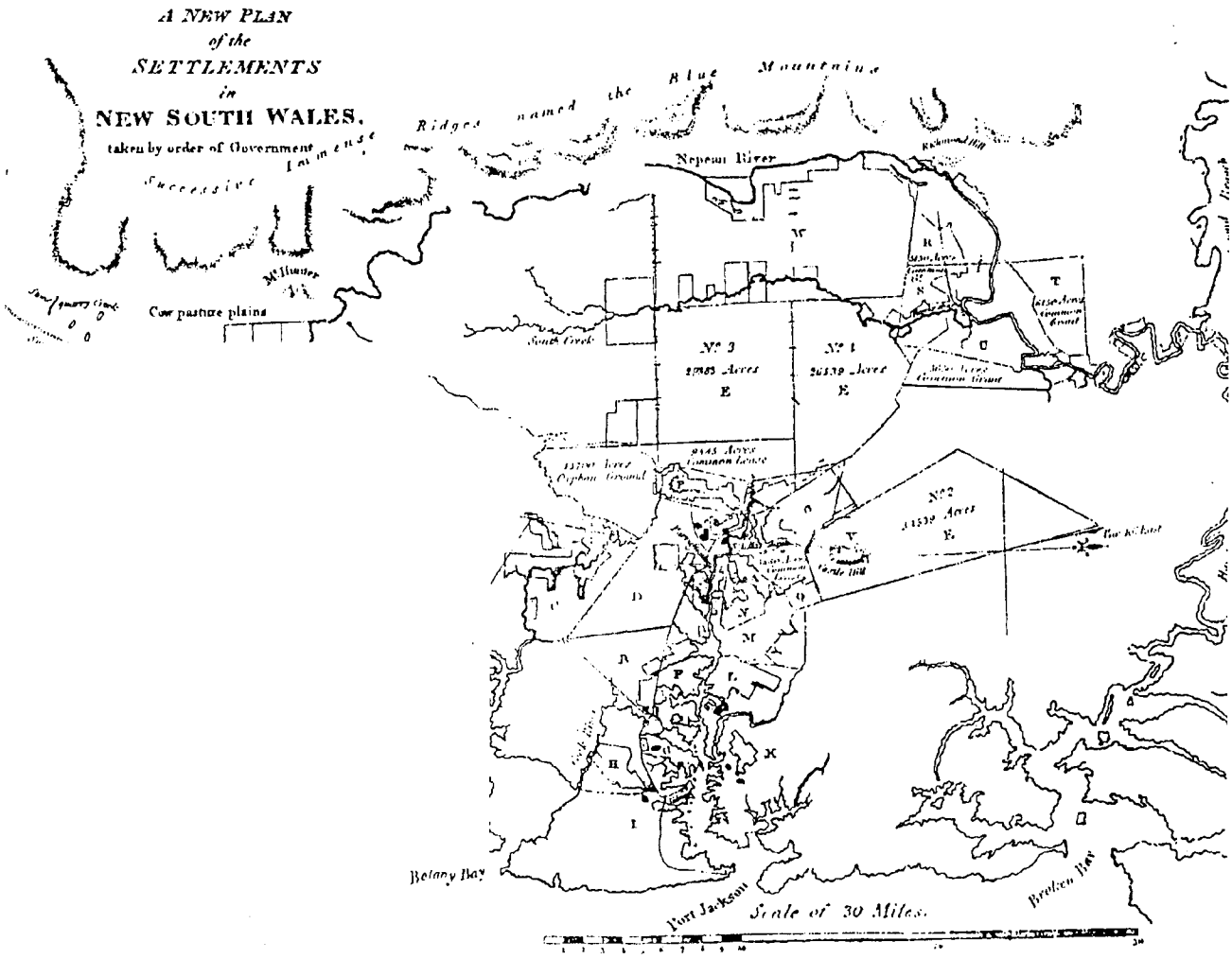

UNISURV S-73, 2002

Reports from

SCHOOL OF SURVEYING
AND SPATIAL INFORMATION SYSTEMS

THE UNIVERSITY OF NEW SOUTH WALES UNSW SYDNEY NSW 2052 AUSTRALIA

UNISURV REPORT S-73, 2002

A CONTINUOUS LOW-COST GPS-BASED VOLCANO DEFORMATION MONITORING SYSTEM IN INDONESIA

CRAIG ROBERTS

Received: October 2002
Accepted: November 2002

SCHOOL OF SURVEYING AND SPATIAL INFORMATION SYSTEMS
(formerly GEOMATIC ENGINEERING)
UNIVERSITY OF NEW SOUTH WALES
UNSW SYDNEY NSW 2052
AUSTRALIA

UNISURV REPORTS

Series Editor: Dr. J. M. Rüeger

National Library of Australia

Card No. and ISBN 0 - 7334 - 1976 - 3

FOREWORD

Research into the development, testing and deployment of a low-cost GPS-based system for the monitoring of deformation associated with volcanic activity has been undertaken at The University of New South Wales (UNSW) since the mid-1990s. Two Australian Research Council (ARC) Large Grants (one commencing in 1996, the other in 1998) have supported this research. Since 1996 Craig Roberts has been associated with this research. The project has had a number of components. Firstly there was the development of the monitor station hardware, consisting of a low-cost L1-only OEM (Original Equipment Manufacturer) GPS receiver board integrated within a robust box with a low-power PC computer. This "box" was connected to an antenna, to a power sub-system (consisting of batteries that are trickle charged with solar panels), and a UHF radio modem for communicating the GPS data to a base station. Secondly software was developed to process the static baselines (base to monitor stations). Finally there was the issue of deploying and operating the system. For this the project was able to benefit from close collaboration with Indonesian colleagues at the Institute of Technology Bandung and the Volcanological Survey of Indonesia. Three monitor stations and one base station were deployed on the Papandayan volcano, approximately 60 km from the city of Bandung in eastern Java. The system was deployed for several weeks at a time on three occasions: July 1999, February 2000, July 2001.

This thesis report describes all aspects of Craig's project. All aspects of the hardware development are described. Unfortunately there were problems with the reliability of the PC computer board, otherwise the system definition was within the parameters specified, i.e. low-cost, and low-power. (A new hardware architecture is presently under development, and it is hoped an improved version will be able to be tested in 2003.) This report also describes the observation model used in the data processing software, and in particular the method of treating the tropospheric delay (as the baselines from base to monitor stations are inclined). Tests were carried out with several datasets, apart from those collected in Indonesia (which were found to be contaminated by excessive ionospheric delay) to confirm the improvements in the data processing strategy used. This was a very demanding project, and in hindsight many factors conspired to prevent reliable, high-quality results from being obtained. The physical environment was indeed challenging, although Craig did a great job of managing the deployment in Indonesia.

However, in addition to the need to deploy in equatorial, jungle conditions, the late 1990s – early 2000s was also a period of very high ionospheric activity (due to the 11 year solar cycle). This meant that the L1-only results were very erratic. An improved configuration consisting of several dual-frequency receivers supporting the L1-only network has been designed and is the subject of study by another graduate student.

The support of colleagues in Indonesia, as well as several members of the Satellite Navigation and Positioning (SNAP) group at UNSW, is gratefully acknowledged. In particular, the considerable assistance of Dr. Hassanuddin Abidin, of the Department of Geodetic Science, Institute of Technology Bandung, Indonesia, must be mentioned. During his research, Craig Roberts was supported from the following sources: a Trimble scholarship (2 years), the ARC and the SNAP group at UNSW.

Professor Chris Rizos
November 2002

ABSTRACT

Ground deformation due to volcanic magma intrusion is recognised as an important precursor of eruptive activity at a volcano. The Global Positioning System (GPS) is ideally suited for this application. The methodology requires the measurement of changes in GPS baseline easting, northing and height components over time. With the advent of inexpensive OEM GPS receiver boards, the primary motivation of this thesis is to develop a low-cost GPS-based volcano monitoring system. This thesis reviews the characteristics of existing GPS continuously operating reference station networks. The major design considerations for GPS-based volcano monitoring systems are described, together with the dominant error sources, culminating in the definition of the design specifications for the UNSW system. A low-cost, GPS-based system was developed, tested and deployed on the Gunung Papandayan volcano, West Java, Indonesia. The hardware and software components utilised in the UNSW system are described, as well as the special challenges in deploying and operating such a system in an inhospitable environment. Differential tropospheric signal delay between GPS receivers with a large change in height is identified as a significant error source. Standard atmospheric models, radiosonde data, temperature lapse rate, refractive index, troposphere modelling and mapping functions are investigated. Two 21-day data sets from the mid-latitude SAGE-NZ network and the equatorial Papandayan network are analysed with a view to reducing the variability (specifically in the height component) of the time series. Issues such as modelling versus parameter estimation, and varying the observation session length, are investigated in order to determine the optimal procedure. The estimation of an additional residual relative zenith tropospheric delay parameter is found to be the most suitable means of dealing with the effects of differential tropospheric delay. Multipath in the time series is mitigated using digital signal processing techniques. The Allan Variance is introduced as a novel way of characterising a time series of baseline results, and provides a temporal measure of the upper limit of the accuracy. The variability of the Papandayan time series is significantly higher than the SAGE-NZ time series due to the higher ionospheric activity at the equator. Dual-frequency data measured at the Papandayan network and processed using an ionosphere-free linear combination demonstrated a considerably lower variability, confirming the fact that the ionospheric signal delay is the major limiting factor to accuracy. It is therefore concluded that single-frequency data is not suitable for volcano monitoring applications in equatorial regions during a solar maximum.

ACKNOWLEDGEMENTS

It has been a wonderful experience and a privilege to work with so many talented people from all walks of life during the course of this project. I have very many people to thank due to its broad nature.

Firstly, I must thank and acknowledge the Trimble Navigation Company for financial support for this project.

I want to thank my many colleagues from the SNAP group; the late Bernie Hirsch, Ken Wong, Lienhart Troyer, Horng-Yue Chen, Chalermchon Satirapod, Volker Janssen, Liwen Dai, Clement Ogaja, Michael Moore, Dr. Tsuiji Toshiaki, Linlin Ge, Dr. Jingling Wang and Jun Zhang. Special thanks also to Xiujiao Han and Dalia Hammady who worked specifically to produce the software that ran the system. Also many thanks to the support staff at the School of Surveying and Spatial Information Systems in particular Phillip Lam, Brian Donnelly, Chris Ryan, Leon Daras, Maria Ponce and Helve Frangoulis.

Thanks also to the many folks outside of the University who offered advice and expertise during the design and construction of the hardware. Thanks go to Ron Wilson and Paul Simpson for their endless patience whilst testing the radios. Thanks to Mick Viber for expert advice on the behaviour of the JED PCs in the GPS/PC modules. Thanks to Andersen Products Pty Ltd for fibreglass pole design, PIP Industrial Services for assistance with the monuments and Samuelson Cases (Australia) Pty Ltd for the design of solar panel cases for transportation to Indonesia. Thanks also to Greg James, David Small and Tim Hailes for some useful conversations regarding the hardware design. Special thanks to Berntsen International Inc. who donated the four 3D survey marks used on Papandayan.

Thanks to Dr. Gerry Mader and his team at the NGS for producing APCV computations for the GPS antennas. Thanks also to Dr. Rob Largent from the Centre for Photovoltaics whose infectious enthusiasm for all things solar led to a great power system design at the slave stations.

Extra special thanks go out to Graeme Hooper who designed and built the GPS/PC modules and was always ready to answer my many (often stupid) questions during testing of the system.

Thanks for the support of my many postgraduate friends from varying disciplines at UNSW. Their advice and comradery during the tough times was a constant source of motivation.

My gratitude goes out to my friends and colleagues at the ITB; Dr. Hasanuddin Abidin, Prof. Joenil Kahar, Irwan Meilano, Mipi Kusuma, Dudy Darmawan, Dina Sarsito, Gamal, and the ever cheerful driver Ohan for explaining to me the endless cultural intricacies of life in Indonesia. As well, for remaining so open and helpful with every task I attempted. Thanks also to the many students who volunteered their help in the field. To the punks Heri and Ally, to Asep, Susilo, Denny, Irawan and Denny a big Hatur Nuhun.

I would also like to express my appreciation to the Heads of the Vulcanological Survey Institute, Mr. Sukhyar and Mr. Wirakusumah whose advice during the early stages of my project was invaluable. To the VSI observers at the base station, Momon, Achmad and Kresno many thanks. A special thankyou to Ony Suganda whose infinite patience and experience was crucial during the first three visits to Bandung.

I want to recognise the efforts of the many local farmers who dropped everything to come in the field and work with me, often at short notice. To Ibu Ipah, who kept me warm and fed in her Warung (near the crater of Papandayan) after long days working on the volcano, I thank you.

An extra special thankyou to Sarif; a local farmer and perhaps the most valuable helper during the fieldwork of the project. Without his initiative, skill, responsibility and reliability, this project would certainly have suffered. I very much enjoyed our trips up and down the mountain and the ensuing lessons in Sundanese language en-route.

My PhD has given me a terrific opportunity to engage in detailed academic conversations with many of the leaders in their respective fields. Thanks go out to

A/Prof. Jean Rüeger, Dr. Ken Hudnut, Prof. Fritz Brunner, Dr. Stefan Schaer, Dr. Markus Rothacher, Dr. Chuck Meertens, John Braun, Dr. Lou Estey, Dr. Chris Rocken, Dr. Michael Jackson, Dave Mencin, Dr. Henry Fooks, Dr. Virgilio Mendes, Dr. Pierre Fridez for replying to my e-mail questions. Particular thanks to Dr. John Beavan for allowing me to use data from the SAGE-NZ network for my studies and Dr. Yehuda Bock for making data available from the SCIGN network.

My co-supervisor Dr. Shaowei Han offered great guidance during my studies and was always ready to help in any way.

To the unstoppable A/Prof. Peter Morgan; I've enjoyed so much our coffee sessions with pen, paper and frantic hand waving. Many thanks for all of your time invested into the project.

To my supervisor Prof Chris Rizos, who, from our first telephone conversation between Potsdam and Oberpfaffenhofen, empowered me with a sense of certainty and assurance that I could tackle this project. I've enjoyed his pragmatic approach to researching, writing, presenting, and I believe I've learnt more from his approach to problems than he realises. Thankyou so much for all your support and giving me a chance.

Thanks to my big brother Greg for convincing me to have a go at a PhD. It was your conviction that decided it for me.

Thankyou to my mum who started me down this path by selflessly encouraging me to go abroad to UNAVCO and the GFZ soon after the sudden death of her husband and my father. Her boundless love and support is immeasurable.

To my dear (late) father, who, through lack of his own opportunity and education, worked selflessly and tirelessly to ensure the education and opportunity of his sons.

And most importantly of all, to Jessica and our new baby Nelson for giving me a reason to strive on and finish.

TABLE OF CONTENTS

LIST OF ABBREVIATIONS

AC	Alternating Current
APCV	Antenna Phase Centre Variation
AR	Ambiguity Resolution
ARC	Australian Research Council
C/A	Coarse Acquisition or Civilian Access code
CINA	Commission Internationale de Navigation Aerienne
cm	Centimetre
CMC	Canadian Marconi Company
CORS	Continuously Operating Reference Stations
Cusum	Cumulative Summation approach
DC	Direct Current
DefNet	Deformation Network (Popocatépetl Volcano)
DFT	Discrete Fourier Transform
DoD	Department of Defence
EDM	Electronic Distance Measurement
FIR	Finite Impulse Response
FTP	File Transfer Protocol
GByte	Gigabyte
GEONET	GPS Earth Observation Network
GFZ	GeoForschungsZentrum
GOCA	GPS-based Online Control and Alarm system
GPS	Global Positioning System
GSI	Geographical Survey Institute (Japan)
Hz	Hertz
IAVCEI	International Association of Vulcanology and the Chemistry of the Earths' Interior
IDNDR	United Nations International Decade for Natural Disaster Reduction
IERS	International Earth Rotation Service
IGS	International GPS Service
ISDN	Integrated Services Digital Network
ITB	Institute of Technology Bandung
ITRF94	International Terrestrial Reference Frame

IUGG	International Union of Geodesy and Geophysics
JPL	Jet Propulsion Laboratory
L1	First frequency sent out by GPS satellites (1.5GHz)
L2	Second frequency sent out by GPS satellites (1.2 GHz)
LC	Ionosphere-free linear combination
mm	Millimetre
NGS	National Geodetic Survey (NOAA)
OEM	Original Equipment Manufacturer
PAGAS	Permanent Automatic GPS Array System
PC	Personal Computer
PSD	Power Spectral Density
RHS	Right Hand Side
RTK	Real-Time Kinematic
Rx	GPS Receiver
SAGE	Southern Alpine Geodetic Network (New Zealand)
SCIGN	Southern California Integrated Geodetic Network
SNAP	Satellite Navigation and Positioning Group
STFT	Short Time Fourier Transform
SV	Satellite Vehicle
SWEPOS	Swedish GPS Reference Station Network
TDMA	Time Division Multiple Access
TEC	Total Electron Content
UHF/VHF	Ultra High Frequency/ Very High Frequency
UNAVCO	University Navstar Consortium
UNSW	University of New South Wales
USGS	United States Geological Survey
UV	Ultra-Violet
VLBI	Very Long Base Interferometry
VSI	Vulcanological Survey of Indonesia
WGS84	World Geodetic System 1984

Chapter 1
INTRODUCTION

1.1 Volcano Hazards

Historical records suggest that in the past 10 000 years, over 1300 separate volcanoes have erupted somewhere on the Earth (Simkin & Siebert, 1999). Volcanoes have been categorised as active, dormant or extinct. This classification has been shown to be misleading, as extinct volcanoes may become active. The relatively short historical records of volcanic activity do not consider long dormant repose periods for volcanoes, which may subsequently reawaken. Instead, the 10 000-year record is used to identify *historically active* or *Holocene volcanoes* as those exhibiting some activity during this period.

The definition of a volcano tends to describe the magmatic source rather than its surface manifestation. Hence over 1000 magma systems (on land only) have been identified as likely to erupt in the future (Ibid, 1999). The ever increasing world population, and therefore the increased competition for land, means that more people than ever live dangerously close to historically active volcanoes, particularly in developing countries.

Volcanoes are unevenly distributed on the surface of the Earth, with over 80% situated north of latitude 10°S and two-thirds located around the so-called Pacific *ring of fire* (Blong, 1984). The location of historically active volcanoes is closely related to plate tectonic boundaries. Most volcanoes are located at convergent plate boundaries (subduction zones) or divergent plate boundaries (oceanic spreading ridges). Other well-known volcanoes, such as the Hawaiian Island chain, occur due to the location of a hotspot (see Fig 1.1).

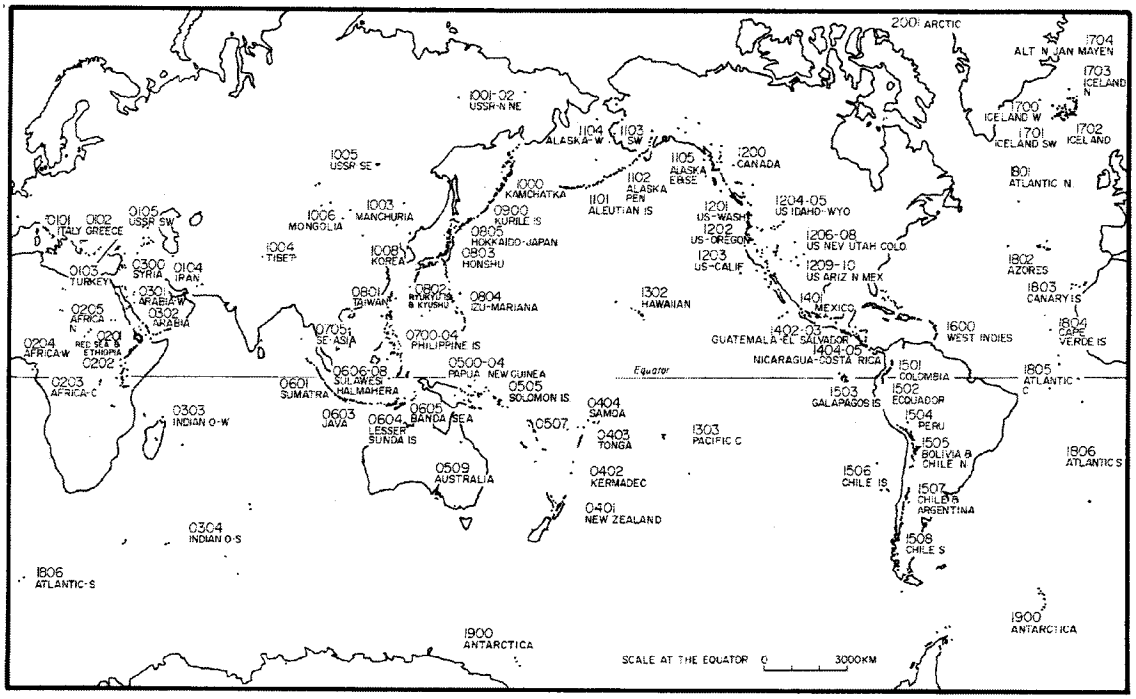

Figure 1.1 – *Location of historical volcanoes. The numbers refer to the regional numbering scheme adopted by Simkin & Siebert, (1994).*

The behaviour of these three distinct types of volcanoes complicate classification of volcanoes in terms of hazard. Hawaiian volcanoes erupt frequently and produce large, continuous lava flows, however these eruptions are not explosive and are relatively predictable. While they present a hazard, it is easily avoided and can actually be studied. Divergent plate margins usually occur under the ocean. These volcanoes are generally not explosive, being contained by the pressure of the overlying water. Although the volume of erupted material may be large, the resulting hazard is negligible, as humans do not live in close proximity. A notable exception is Iceland, which owes its existence to the volcanoes produced along the Atlantic plate margin. Over 1000 years of recorded data suggest that Icelandic volcanoes undergo periodic fissure eruptions which can be catastrophic, not due to their explosiveness, but rather because of secondary effects. An example of this is the 1783-4 eruption of Laki, which killed one-fifth of Iceland's population due to the subsequent famine (Simkin & Siebert, 1994).

The most explosive eruptions occur at volcanoes formed along convergent plate margins. The majority of surface volcanoes, such as those along the spine of Sumatra and Java in Indonesia, and most of the volcanoes around the Pacific ring-of-fire, map

these convergent plate margins. As oceanic crust subducts into the mantle, it is dehydrated and material ascends through the overlying continental crust to form subduction zone volcanoes (see Fig 1.2).

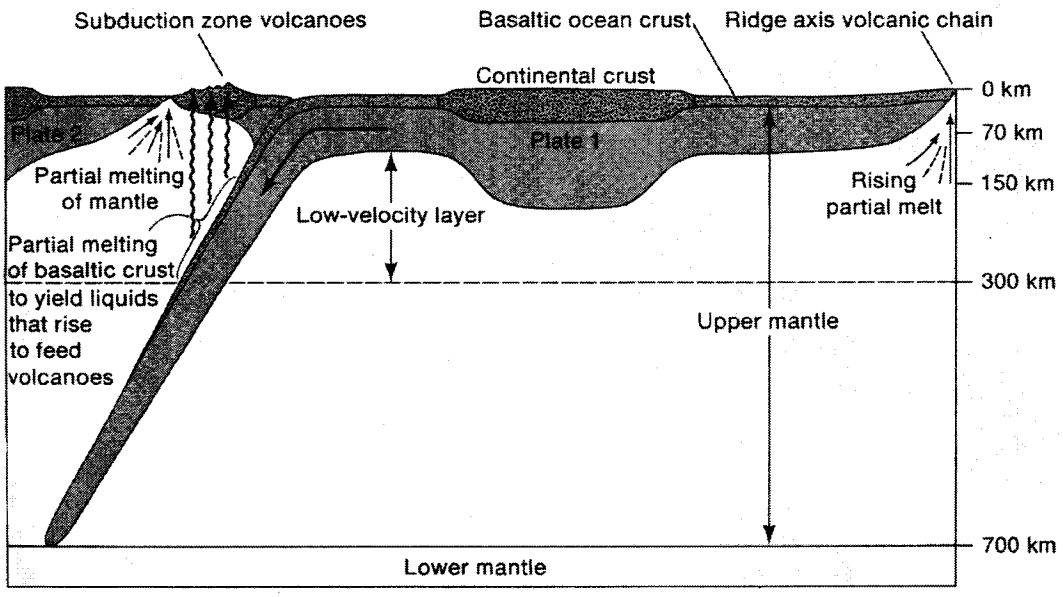

Figure 1.2 – *Diagram of the formation of subduction zone volcanoes (Decker & Decker, 1997).*

Subduction zone volcanoes do not erupt as frequently or for as long as those along divergent plate margins, however they are considered more hazardous as they are located in close proximity to human populations.

The hazard presented by a volcano can be measured either by the size of an eruption or by its effect on the human population. It is commonly believed that the largest and most explosive eruption affords the greatest hazard, but this may not be true. The Krakatau eruption of 1883 was a violently explosive eruption in terms of intensity and destructive potential, however the Mauna Loa eruptions in 1859 and 1950 were as large in terms of the volume of erupted material and total energy released. If the number of people killed is the measure of hazardousness, then Krakatau was a more hazardous volcano.

Newhall & Self (1982) have tried to address the issue of the size of an eruption by introducing the volcanic explosivity index (VEI). The VEI is a logarithmic scale ranging

from 0-8 and considers the total volume of erupted material, duration of the main eruptive phase, height of the eruption cloud and several other descriptive characteristics (Blong, 1984). For the example given above, the magnitude of the Mauna Loa eruptions of 1859 and 1950 were only around VEI 1, in contrast to that of Krakatau which was VEI 6. Interestingly there is only one recorded magnitude VEI 7 eruption; Tambora in 1815. There are no recorded VEI 8 eruptions. Historical records suggest that Yellowstone erupted around 2 million years ago with an intensity of VEI 8. Simkin & Siebert (1999) gives a graphical representation of the VEI scale.

It is instructive to describe a volcano in terms of its behaviour, however its impact is a much clearer measure of its hazard. The number of people killed as a direct result of an eruption, the number of people who die due to secondary effects of the eruption, and the economic damage caused will determine the magnitude of a volcano hazard (see Fig 1.4).

1.1.1 Hazards

In order to understand the hazard caused by a volcano, the major volcanic effects need to be considered. Tephra falls, pyroclastic flows, lahars, earthquakes and ground deformation, tsunamis, atmospheric phenomena and lava flows are briefly described (Fig 1.3).

Tephra falls

Tephra refers to all airborne products (pyroclastic material) produced during a volcanic eruption, except for the gases. It therefore includes volcanic ash, ballistic projectiles (sometimes called volcanic bombs) and pyroclastic flows. Tephra is generally produced at subduction zone volcanoes. Volcanic bombs may be as large as several metres across and be projected kilometres away from their source. An eruption plume contains tephra particles or volcanic ash and as the cloud rises the larger and heavier particles fall to the ground. A large eruption cloud can cause daytime darkness and deposit huge volumes of ash up to several metres in thickness. The Galunggung eruption of 1982 produced huge tephra falls and displaced thousands of people from the cities of Tasikmalaya, Garut and surrounding villages.

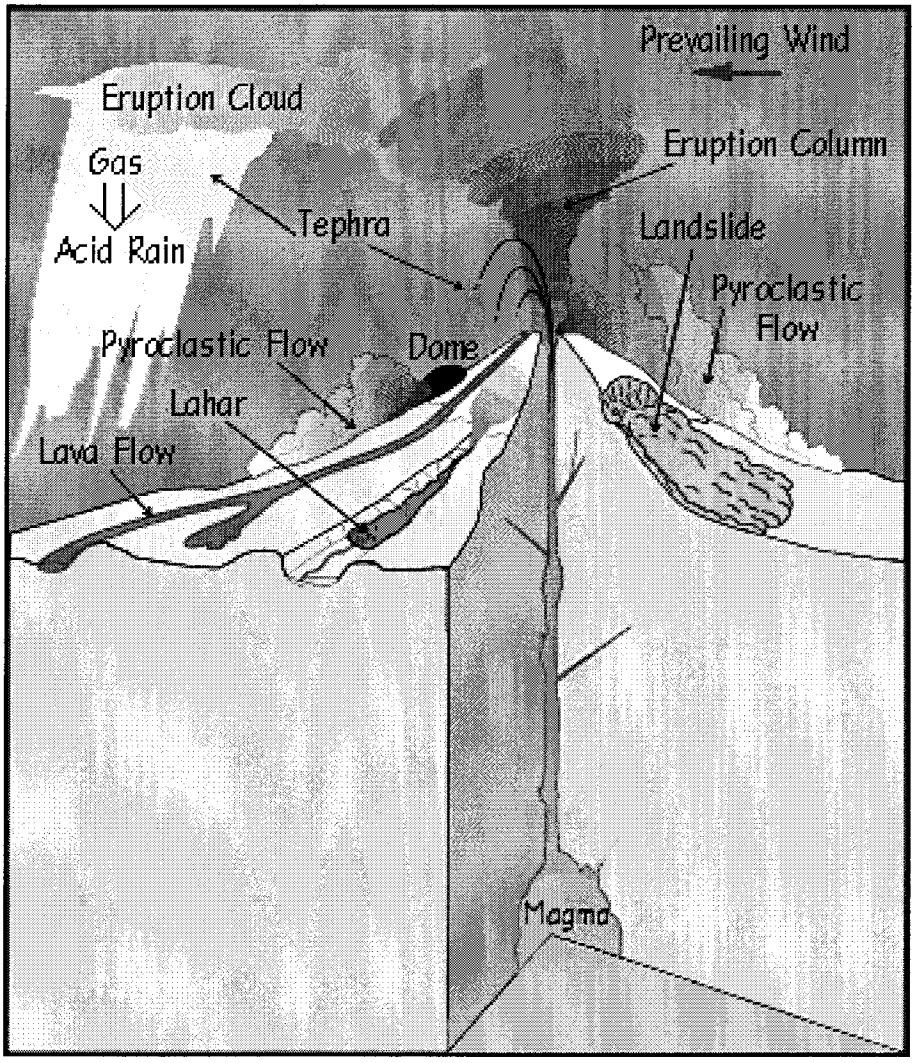

Figure 1.3 – *Schematic diagram of volcano hazards (USGS, 2001a).*

Pyroclastic flow

Pyroclastic flow was mentioned above as tephra but it can be classed as a separate hazard. Hot gases reaching temperatures of 1000°C mixed with a mass of hot, dry rock fragments are ejected from the volcano at speeds of 200km/h or more and flow down the flanks. Pyroclastic flows cover areas as wide as 600 km^2 as was the case for the Mt St. Helens (1980) eruption (Hoblitt et al, 1981). The velocity, temperature and magnitude of the flows determine their potential hazard.

Lahars

Lahar is an Indonesian name for a volcanic mudflow. Lahars are difficult to define as they may arise from a number of sources. Some occur at the end of a pyroclastic flow as it cools and liquefies. Lahars may also form after heavy rain which can transform dry

volcanic ash into a liquid mud which moves downhill. Snow and ice on the summit of large volcanoes can also be a source of meltwater that create lahars.

Earthquakes and ground deformation

Earthquakes can be defined as either tectonic or volcanic. Tectonic earthquakes are generally much larger in magnitude and are easily distinguished using seismic measurements. Volcanic earthquakes reflect magma movements inside a volcano. The movement of magma can be tracked over time, and provides a good indication of when and where a volcano may erupt. When magma approaches the Earth's surface, the ground deforms, providing further indication of some pending activity. Volcanic earthquakes and associated ground deformation cause damage local to the volcano.

Tsunami

The Japanese word *tsunami* refers to a great sea wave produced by a submarine earthquake or volcanic eruption. The most famous example of such a phenomenon occurred after the violent 1883 eruption of Krakatau Island in the Sunda Strait, Indonesia. Wave heights of up to 40m were reported and 36 000 people were reported killed as a result (Decker & Decker, 1997).

Atmospheric phenomena

The sound of an explosive eruption can be heard great distances from the source of the explosion. It was reported that the Krakatau eruption could be heard 4700 km away on Rodriguez Island. This is remarkable indeed but does not present a great hazard. The pressure wave created by such an explosion can cause damage to buildings up to several hundred kilometres away (Blong, 1984). The gaseous discharge of fine particles associated with volcanic eruptions can create violent lightning storms around the volcano with strikes recorded up to 9km away from the volcano (Shepherd et al, 1979). Also the volume of ash ejected into the atmosphere can change the global climate. The eruption of the Indonesian volcano Tambora in 1815 adversely affected 1816 crop yields in the continental USA (Sigurdsson, 1999).

Lava flows

Lava is magma or molten rock that has reached the surface. The two most common forms of lava are the *pahoehoe* and *aa* lavas. Pahoehoe lava is quite thin and flows relatively quickly in sheets. Overlying sheets may form skins of lava or it may develop lava tubes which transport the molten lava further from the source. Aa lava flows are more viscous and move more slowly. They are often thicker and carry rough fragments on their exterior. They follow watercourses and can be up to 30m thick. Pahoehoe lavas sometimes form into aa lavas. A less common form of lava is called block lava which is similar to aa lavas except that the surface contains large polyhedral blocks.

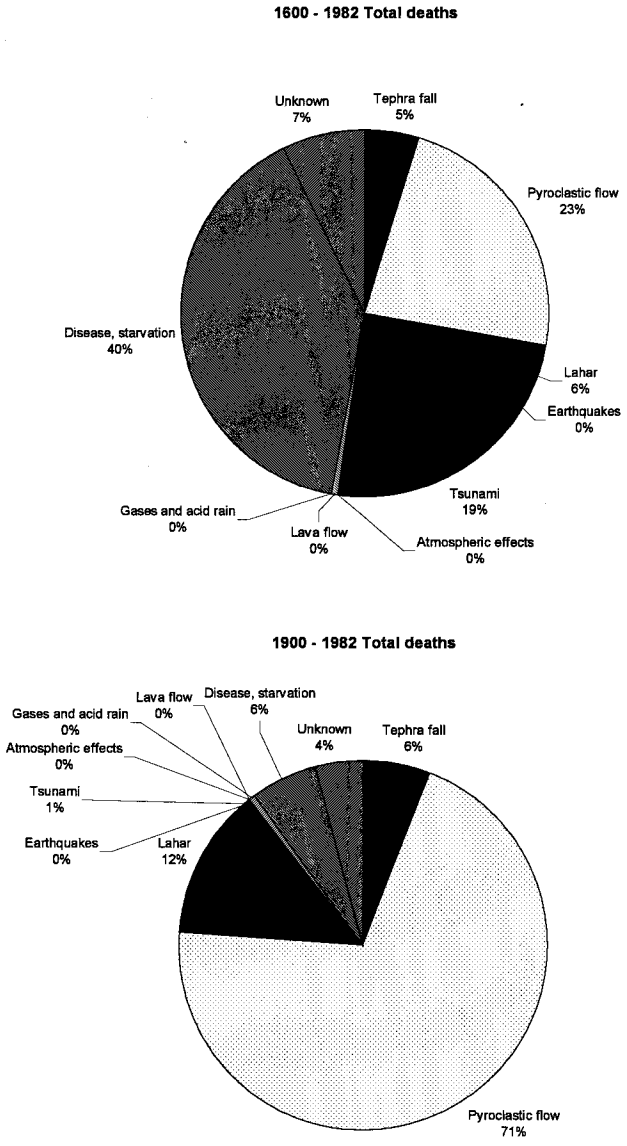

Figure 1.4 – *Deaths by volcanic hazards (adapted from Blong, 1984).*

Blong (1984) presents a table of historical records of the number of deaths due to volcanic hazards for the periods 1600 – 1982 and 1900 – 1982. Figure 1.4 presents this data as pie charts.

For the period from 1600 – 1982, the majority of casualties arose from disease and starvation, tsunamis, pyroclastic flows, lahars and tephra falls. For the period 1900 – 1982, a subset of the first data set, the major cause of death is clearly from pyroclastic flows, lahars and tephra falls. It should be noted that the unusually high number of deaths as a result of the Krakatau eruption of 1883 from tsunamis has biased the data set. Also the Tambora and Laki eruptions in 1815 and 1783 respectively killed many by starvation.

Pyroclastic flows, lahars and tephra falls are regarded as significant hazards. With improved communications and a more globalised society, the effects of disease and starvation can be better addressed than was previously possible. Improved building standards reduce the effects of earthquakes. Lava flows can be redirected away from population centres to a limited extent by constructing earth banks to steer their flow. Most other volcanic hazards can only be avoided. Accurate and timely prediction and forecasting strategies provide more time to evacuate those at risk.

Damage to communications infrastructure upon which emergency services may rely is a significant secondary effect. The loss of agricultural land, crop damage and the resultant lack of food causes longer term problems, and can also be classed as a volcanic hazard.

1.1.2 Risk

Volcano hazards can be considered in terms of risk management, and follow what Blong (1999) calls the risk management chain:

Identification → Analysis → Reduction → Transfer

The focus of this thesis is on identification of a volcanic hazard. For any volcanic environment this requires recognition of the type of volcanic hazards to which it is

exposed, and implementing techniques to detect a potential threat. The vulnerability of populations and infrastructure that could be affected by volcanic activity are also part of the risk identification.

Risk analysis utilises historical records and scientific data to better understand volcanic behaviour in order to assess potential consequences. This information can be used to implement risk reduction strategies such as development of evacuation procedures, introducing improved building standards and generating hazard zone maps. Earth barriers can be constructed to redirect lava flows, revegetation of recent tephra falls reduce the effects of lahars, and drainage of crater lakes (which could present a hazard) decrease risk. Risk transfer involves apportioning part of the risk reduction to organisations, communities, governments or the like in the form of disaster relief or insurance. Whilst this does not remove the risk, it can help save life and lessen suffering during a crisis, and help to quickly reinstate essential services and infrastructure shortly afterwards.

Blong (1999) defines the fundamental equation of risk reduction as:

Hazards x Vulnerability = Risk

The hazard part of this equation deals with tephra falls, pyroclastic flows, lahars, earthquakes and ground deformation, tsunamis, atmospheric phenomena, lava flows etc, as described above. The vulnerability measures the degree to which humans, buildings, agriculture and other economic activity is exposed to volcanic hazards. This is clearly not a precise equation as there is much subjectivity involved, but it does give some quantifiable indication of the effect of volcanoes.

Merging all aspects of the risk management chain together can help to provide effective early warning and evacuation systems, reduce the effects of known hazards, minimise loss, both human and economic, and help a community re-establish itself as quickly as possible after a crisis.

1.2 Introduction to GPS

The United States Department of Defense (DoD), Global Positioning System (GPS) is a satellite-based radio ranging navigation system (Parkinson & Spilker, 1996). It consists of three segments. The space segment nominally comprises 21 satellites (+ 3 spares) in 6 orbital planes with an inclination of 55° to the equator, and an orbit period of half a sidereal day. The control segment consists of five ground stations which provide satellite tracking, orbit computations and telemetry and daily control of the space segment. The user segment refers to the many positioning and navigation applications available to both military and civilian users.

The GPS satellites broadcast two L-band ranging signals at a frequency of 1575.42MHz (L1) and 1227.6MHz (L2). In order to distinguish satellites, two pseudo-random noise (PRN) codes are modulated onto the L-band carrier frequencies. These are the 1-millisecond long C/A-code (coarse acquisition) and a week-long segment of the P-code (precise). The L-band carriers are also modulated with a navigation message which includes ephemeris information describing the satellite position and predicted satellite clock correction terms, as well as other information. The L2 carrier does not include the C/A code modulation.

Code measurements are used to compute the time of transmission of a GPS signal from the satellite to a user equipped with a GPS receiver. The time of transmission multiplied by the speed of light gives the range between the satellite and receiver for a particular time. Actually this is called a pseudo-range because the time systems of the satellite and receiver are not equivalent due to the non-synchronisation of the clocks. Four simultaneous pseudo-range measurements (ie observing to four satellites), provides a three dimensional position. This is GPS navigation.

GPS surveying uses two or more GPS receivers and simultaneously observes the same constellation of satellites. Differencing the measurements between satellites and receivers (double differencing), effectively eliminates the clock errors and improves the relative positioning between the antennas. Good explanations of the principle of GPS surveying can be found in Hofmann-Wellenhof et al (1994), Leick (1995), Rizos

(1997a) and Wells et al, (1987). The GPS system is thoroughly described in Parkinson & Spilker (1996).

The L1 and L2 carrier signals have a wavelength of 19 and 24 mm respectively. Measuring the integer number of wavelengths (the ambiguity) between the satellite and the receiver provides millimetre level range measurements. Note this is not possible with GPS navigation and can only be achieved using GPS surveying techniques. Collecting many epochs of data and employing double-differencing techniques can resolve these integer ambiguities, thereby providing sub-centimetre relative positioning. Han & Rizos (1996b) provide a review of ambiguity resolution (AR) techniques.

GPS surveying is subject to a number of systematic biases. The GPS satellite positions that are broadcast in the navigation message are only known to the metre level and therefore can bias baseline solutions. The ionosphere and troposphere layers delay the GPS signals as they propagate through to the Earth's surface. Multipath occurs when reflected signals are received at the GPS antenna. These error sources and strategies to model and mitigate them are described in more detail in chapter 3.

The advantages offered by GPS surveying include:

- no requirement for intervisibility of stations,
- operates in all-weather,
- operates 24 hours/day,
- provides three-dimensional coordinates,
- provides sub-centimetre level relative accuracy,
- the baseline length can extend to 1000's of kilometres,
- stations can operate automatically,
- stations can be located remotely, and
- the technique is relatively inexpensive.

1.3 Motivation for Research

Volcanoes present a real hazard to many communities around the world, particularly in developing countries. Many organisations monitor the activity of volcanoes and seek to predict their behaviour. Seismology currently is widely accepted as the most convenient and effective means of monitoring volcanic activity. The monitoring of ground deformation precursory to some volcanic activity could *bootstrap* the seismology and help better predict a potentially violent eruption (Dvorak & Dzurisin, 1997).

In the past half decade or so there has been increasing interest in the use of permanent, continuously operated GPS stations, and a small number of continuous networks have been deployed in the USA, Japan, Canada and several other developed countries. An important justification for permanent GPS arrays is that natural hazards research will be furthered because of the *continuous* measurement of a deformation phenomenon, rather than a *periodic* measurement. However, only in Japan has it been possible to establish a country-wide continuous GPS network to support seismic research, and ultimately contribute to hazard mitigation. Even with such a dense network of dual-frequency GPS receivers as established by Japan's Geographical Survey Institute, the station separation is of the order of 15km or more. There are, however, applications of GPS deformation systems which require receiver densities of the order of just a few kilometres. Furthermore, the high cost of such GPS systems means that most countries cannot possibly afford to establish such systems. Applications of permanent GPS arrays include monitoring of volcano flanks, micro-faults, ground subsidence due to underground mining or fluid extraction, slope stability, and even engineering structures such as dams, etc.

Therefore the cost of a continuously operating GPS array system must be reduced significantly (ideally by at least a factor of five to ten) if the technology is to contribute to hazard mitigation. The introduction of Original Equipment Manufacture (OEM) GPS receiver boards onto the market presented an opportunity to investigate a low-cost approach to volcano monitoring. This thesis describes the development and testing of a low-cost volcano deformation monitoring system GPS.

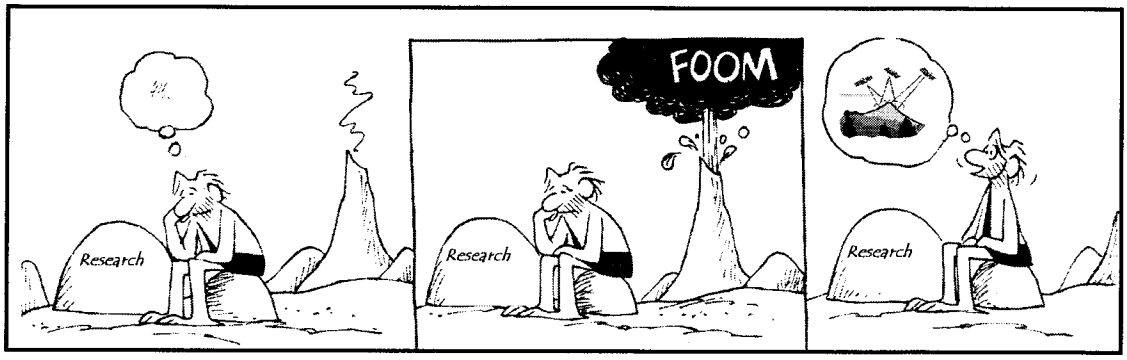

(adapted from the comic strip BC by Johnny Hart)

The United Nations International Decade for Natural Disaster Reduction (IDNDR) was declared from 1990 - 2000, and provided a further impetus for this thesis. The report, "Reducing volcanic disasters in the 1990s", by the International Association of Vulcanology and the Chemistry of the Earths' Interior (IAVCEI) Task Group recommends that "more effective volcano surveillance and other initiatives designed to mitigate the effects of erupting volcanoes over the remainder of this century and into the next, be implemented."

The International Union of Geodesy and Geophysics (IUGG) General Assembly in Vienna in 1991 selected 9 volcanoes as *decade volcanoes* to focus the limited research funding of various cooperating international institutions onto a few significant volcanoes. Although Gunung Papandayan, the subject volcano in this thesis, is not included in this list of decade volcanoes, the Australian Research Council (ARC) grant awarded for this research was successful largely due to the heightened activity initiated by the IDNDR project.

The Satellite Navigation and Positioning group (SNAP) at the University of New South Wales (UNSW) focuses on precise GPS applications. This, in conjunction with UNSW's 25-year cooperation with the Department of Geodetic Engineering at the Institute of Technology Bandung (ITB), were prime motivations to deploy a low-cost, GPS-based volcano monitoring system on an Indonesian volcano. Additionally, the ITB also has a strong collaboration with the Vulcanological Survey of Indonesia (VSI), who are the government department overseeing all volcano monitoring in Indonesia. This

project has reinforced a strong partnership with the ITB and initiated an on-going partnership with the VSI.

A large proportion of the world's historically active volcanoes are located in Indonesia. 67% of deaths recorded from 1600 – 1982 caused by volcanic eruptions have occurred in Indonesia (Blong, 1984). In Indonesia, over 200 million people live on a land mass approximately the size of Queensland, and it is estimated that 10% of Indonesians live dangerously close to active volcanoes. In total 129 historically active volcanoes are identified, and of those 60 are regularly monitored by the VSI (Abidin & Tjetjep, 1996).

Aside from Gunung Merapi in central Java, very little GPS-based volcano monitoring had been tested in Indonesia at the commencement of this project. Indonesia is a developing country seeking a low-cost GPS solution. The advantages of GPS-based monitoring coupled with the opportunity to develop an automatic, continuous monitoring system were important reasons to carry out this research. Indeed the IDNDR suggest that ground deformation monitoring be ideally measured using GPS (McGuire et al, 1995).

Off-the-shelf GPS systems have tempted non-geodesists to commence monitoring campaigns on volcanoes and interpret erroneous GPS derived signals as indicating some geophysical phenomena. Mis-modelled systematic biases or user inexperience may render GPS-derived movements incorrect and geophysical interpretations meaningless. It is important that experienced GPS users provide reliable measures of ground deformation which are interpreted by those who understand geophysics and volcanic behaviour.

1.4 Methodology

One of the surest precursors to eruptions is geodetic measurement of horizontal and vertical deformations of the volcano (Ibid et al, 1995). Ground deformation is a phenomenon ideally suited for study using GPS. GPS can measure the *change* in length (as well as height difference and orientation) of baselines connecting receivers in a carefully monumented ground network. This is done by repeatedly measuring the same

baseline vector to an accuracy commensurate to (and preferably much higher than) the expected baseline component changes. A stable base station located away from the zone of deformation is the point to which all movements are referred.

A network of permanent GPS receivers must be deployed in an inhospitable environment, in which they must operate reliably, on a continuous basis. The GPS observations must then be telemetered by radio to a central computing facility where data processing occurs in near-real-time, to generate precise baseline results. The analysis of the time series of baseline results then takes place in order to detect any change in the baseline components between successive solutions attributable to ground deformation that may signal an imminent eruption. Furthermore, the nature of volcano flank deformation poses its own problems, not the least of which is that a volcano may be dormant for many years, then suddenly undergo a rapid vertical deformation, followed by violent eruptive activity, then a deflation.

The distance between VSI observatories on Indonesian volcanoes and the active volcanic edifice is rarely more than 15 kms. This allows single-frequency GPS receivers to be used under the assumption that ionospheric and (to a lesser extent) tropospheric biases will be negligible. The major focus of this research is to develop a low-cost methodology. Therefore inexpensive single-frequency GPS OEM boards are custom-integrated with low-cost personal computer boards. The short baselines require low-power VHF radios for a telemetry link. The remote slave stations are powered by 12 V lead acid batteries, recharged continuously by solar panels. The low power requirements of all components reduces the size of the solar panels and batteries, and therefore the cost.

In later versions of this methodology, the single-frequency network will be surrounded by an external fiducial network comprising high quality, dual-frequency GPS receivers. The fiducial network will provide corrections to the internal network to improve baseline accuracy. The effects of large differential heights on tropospheric estimation and ionospheric bias, particularly during a solar maximum, need to be especially considered.

It is not anticipated that ground deformation monitoring alone will provide a sure indicator of pending eruptive activity, rather it will augment existing systems and provide some additional information. For example, seismicity can pinpoint where magma movements occur under the ground. A carefully located GPS monitoring system can confirm these pressure sources based on detectable ground deformation using the Mogi model (Mogi, 1958), and indicate more precisely when and where the magma may intersect the ground surface.

1.5 Outline of Thesis

This thesis consists of seven chapters and three appendices.

Chapter 1 gives a concise explanation of volcanoes and volcano hazards followed by a brief introduction to GPS. The factors motivating this research are summarised and a conceptual outline of the proposed methodology is presented. The contributions to research are then listed.

Chapter 2 provides a brief historical account of volcano monitoring using geodetic techniques. Existing GPS-based continuously operating reference systems (CORS) are classified by type and previous work is reviewed. Considerations specific to GPS volcano monitoring networks, such as network configuration, forecasting and detection are then discussed, and specifications for the UNSW designed system are defined.

The major design considerations for a generic continuous GPS deformation monitoring system appropriate for volcanic applications are discussed in chapter 3. The main hardware components are described as well as issues affecting the performance of the monitoring stations. Reference is made to existing systems to provide context. The dominant error sources for GPS surveying are introduced and strategies for mitigating and eliminating these effects are described.

Chapter 4 focuses on the small scale, low-cost continuous GPS network installed on Gunung Papandayan. The equipment chosen, the error mitigation strategies adopted and the budget for the UNSW design are described with regard to the factors outlined in

chapter 3. The collaboration and management through to the installation of the system over several visits to Indonesia highlights the experience gained. (It is intended that this chapter along with appendix B could serve as a quasi-manual for subsequent researchers.)

Chapter 5 concentrates on differential troposphere as a significant error source. This chapter details standard atmospheres, radiosondes, temperature lapse rate, refractive index, troposphere modelling and mapping functions. A local temperature lapse rate is computed for Java based on local radiosonde data. Local meteorological values are compared with standard troposphere models. Residual tropospheric parameter estimation techniques are introduced.

Parameter estimation is compared with troposphere modelling in chapter 6. In the absence of a "clean" time series of data, 21-days of data from the mid-latitude SAGE-NZ network is used to demonstrate the proposed methodology introduced in chapter 5. Initially a 24-hour segment of data is tested with various processing strategies before the entire 21-day series is processed. Data from the Papandayan 2001 campaign is processed and compared with the SAGE-NZ results. The time series data are analysed using digital signal processing techniques and Allan variance plots are introduced to describe the performance of the monitoring system over time.

Chapter 7 summarises findings and presents some concluding remarks. Recommendations for further research are given.

Appendix A is included for completeness of section 3.2.2 on multipath. Appendix B provides a user guide for the operation of the GPS deformation monitoring system installed on Gunung Papandayan, a troubleshooting guide and setup diagrams. Appendix C investigates the effect of changing the temperature lapse rate on the Saastamoinen model.

1.6 Contributions to Research

The contributions to research described in this thesis can be split into two major categories; 1) The design and implementation of a low-cost, GPS-based volcano monitoring system in Indonesia; and 2) an investigation of the processing strategies appropriate for this network.

GPS monitoring stations were designed, built and tested in a volcanic environment for one-tenth the cost of comparable dual-frequency systems. The hardware components were designed specifically to withstand the harsh conditions on an equatorial volcano. A GPS network was established on Gunung Papandayan for future research and to augment the monitoring capabilities of the VSI at Gunung Papandayan.

Investigations into the effects of differential troposphere on the determination of the height component revealed that standard troposphere modelling was an inappropriate method of correcting for tropospheric bias. Local meteorological data used in the standard models decreased the accuracy. The local temperature lapse rate for Java was computed and shown to differ negligibly from the global value. Estimating a relative residual zenith troposphere correction to the a-priori Saastamoinen model decreased the repeatability in the height component. The time series was also more centred on a mean value and (unlike modelling) was unaffected by local weather changes.

In the absence of ground planes, multipath was accounted for by using digital signal processing techniques. Power spectral density plots identified a definite multipath signal for the time series computed using the parameter estimation technique. The erratic nature of time series results using modelling masked the multipath signal. This further proved the inappropriateness of modelling. Fast Fourier Transform filtering eliminated the multipath signal. The Allan variance representations of the time series results provided a novel approach to characterising an upper accuracy boundary of a deformation monitoring system over time.

Despite the short baseline length, ionospheric effects rendered the single-frequency data from the Papandayan 2001 network too inaccurate for volcano deformation monitoring

applications. Global ionospheric models contribute very little to improving the repeatability of baseline resolution in equatorial regions during a solar maximum. Dual-frequency data is required for a centimetre-level accuracy GPS network located in an equatorial region during a solar maximum. Despite the short baseline length, the gains made by employing the ionosphere-free linear combination outweigh the losses due to the increased noise level incurred when using this approach in equatorial regions.

Chapter 2
GPS AND VOLCANO MONITORING

2.1 Introduction

Prior to a dramatic volcanic event such as an eruption, the volcano flanks will deform in some way, reflecting magmatic movements below the earth's crust. This surface deformation may range in magnitude from centimetres to metres, and may occur minutes, days or weeks before the actual eruptive event. Dvorak & Dzurisin (1997) state that, "The pattern and rate of surface displacement reveal the depth and rate of pressure increase within shallow magma reserves", and "GPS offers the possibility of revealing changes in surface strain both local to a volcano and over a broad region that includes the volcano." Murray et al (1999) further state, "For many volcanoes, ground deformation is among the most useful indicators of the general state of the volcano and any impending eruption." Deformation may constitute expansion as a subterranean magma chamber swells or deflation after magma is released from the chamber (see Fig 2.1). These observations therefore provide the primary motivation for the research reported in this thesis.

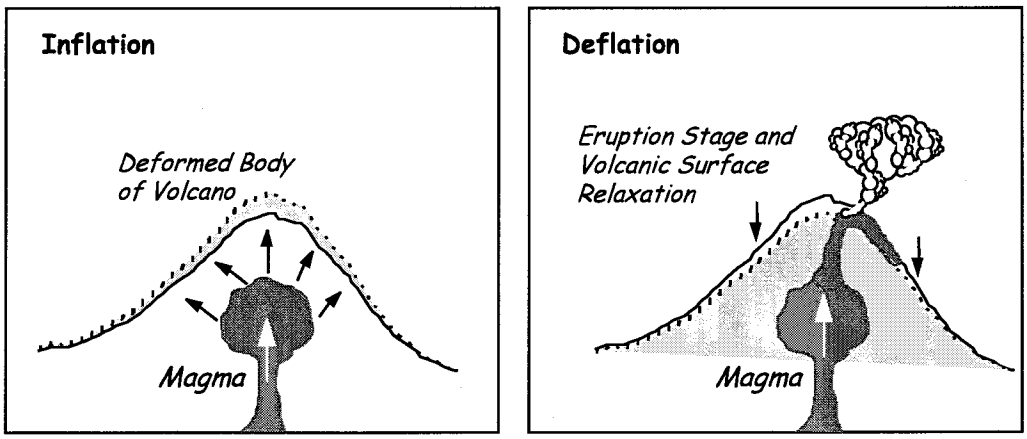

Figure 2.1 - *Ground deformation from magmatic activity (Abidin, 1998b).*

In this chapter a brief history of volcano monitoring is presented, with particular emphasis on ground deformation monitoring techniques. Several geodetic techniques will be briefly discussed before introducing the GPS satellite surveying technique. An attempt is made to categorise the different permanent continuous GPS networks that

currently exist in order to highlight their distinguishing features. Suitable applications for these various forms of GPS monitoring networks will then be discussed.

2.2 Volcano Monitoring using Ground Deformation Techniques

Observations of volcanic behaviour date back to ancient times. In Greek mythology it was believed that volcanic eruptions were battles between Olympian gods and the Titans - great giants imprisoned in the earth. Indeed Mt. Etna in Italy was believed to be a huge dungeon hurled down from the heavens by Zeus himself to entrap the rebellious Typhon, the largest monster that ever lived. Volcanic eruptions of Mt. Etna were believed to be stirrings of Typhon from his subterranean prison (Sigurdsson, 1999).

The magnitude and ferocity of volcanoes was always associated with spiritual or supernatural beliefs. The Aztecs, for example, named Mt. Popocatépetl (near Mexico City) after one of their gods. Some ancient cultures even believed that human sacrifices had to be made in order to appease the gods, and to preserve the calm of nearby volcanoes. Mt. Coseguina was one such volcano, where Nicaraguans believed that it would only remain dormant if a child was thrown into the crater every 25 years. The Javanese up until recently sacrificed humans on the Mt. Bromo volcano, and even now still throw chickens into the crater once a year.

Ancient philosophers hypothesised on the causes of volcanic eruptions. The earliest known hypothesis concerning volcanoes dates from the 5th century BC when the ancient Greek philosopher Anaxagoras suggested that when great winds from within the earth channelled to a narrow outlet, that this would result in an eruption. He hypothesised that the friction caused by the compressed air in the winds would melt the surrounding rock, forming magma (Ibid, 1999).

Perhaps the first scientific expedition to study the behaviour of a volcano took place in 79 AD by Pliny the Elder, who set out on a small boat from his home to Mt. Vesuvius, to observe the erupting mountain. He died in the attempt but his nephew, Pliny the Younger, witnessed the eruption from 30 km away and wrote the first account of a volcanic eruption (Ibid, 1999).

Sigurdsson (1999) presents a useful chronological history of volcanology. With regard to ground deformation measurements, perhaps the most indicative document was the first quantitative study presented by William Hamilton. A series of eight sketches illustrating the expanding edifice of Mt. Vesuvius during the eruption period from July – October, 1767, shows clear evidence of the relationship between ground deformation and an impending eruption (See Fig 2.2).

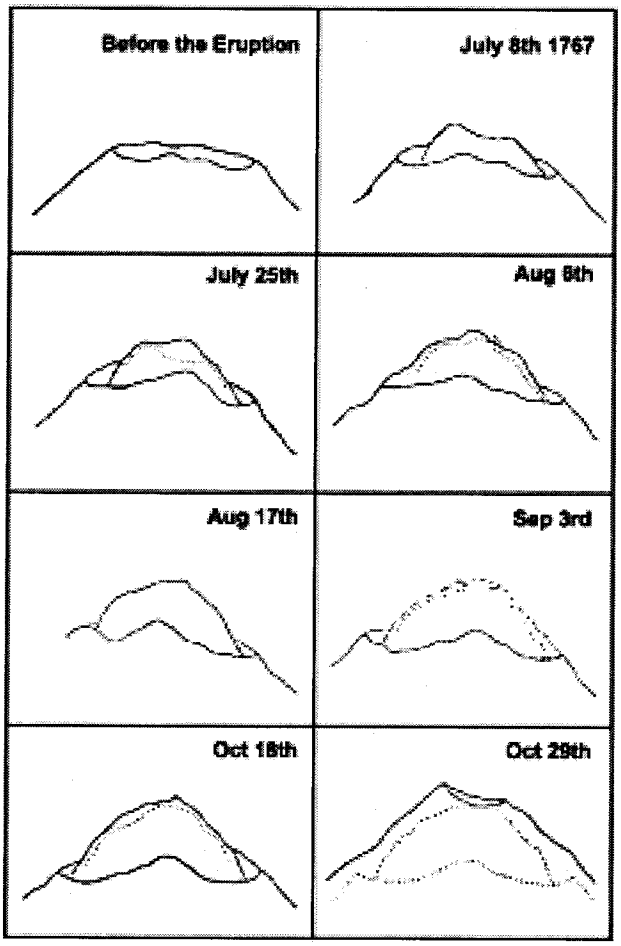

Figure 2.2 - *Outline of the expansion of Mt. Vesuvius during the 1767 eruption as drawn by William Hamilton (Sigurdsson, 1999).*

In 1847, the first volcano observatory *Observatorio Vesuviano* was opened on the flanks of Mt. Vesuvius to monitor its behaviour. Protecting the dense population surrounding the volcano was the primary motivation. However, this new scientific initiative also helped shed light on the volcano's behaviour. Other volcano monitoring observatories were established in the early 1900s in Japan and Hawaii.

Omori (1914) first documented ground deformation associated with a volcanic event. His investigations indicated vertical ground displacements on the Mt. Usu volcano in Japan of up to two metres, when conducting precise levelling surveys before and after the eruption of 1910. A 100-metre upheaval of the ground surface was also recorded close to the crater at the time of eruption. A similar comparison between two precise levelling surveys measured in 1895 and 1914 revealed a significant deflation of the ground at the Sakura-jima volcano of up to two metres (but usually at the several decimetre level) (Ibid, 1914).

At around the same time, Wilson (1935), from the University of Hawaii, was also investigating the ground deformation associated with the shield volcano Mt. Kilauea in the Hawaii islands. He employed various techniques including continuous tilt measurements, precise levelling and triangulation, as well as periodic measurements of the crater depth and seismometric observations. Wilson recorded remarkable deformations of the ground surface during the 1924 eruption of Mt. Kilauea. Precise levelling surveys were carried out in 1912, 1921 and 1927, and were connected to a tide gauge for absolute level control. The continuously operating tilt-meters recorded a sudden movement in the ground surface at the time of the 1924 eruption, and the crater was found to have subsided by around 300m!

Kiyoo Mogi, in his 1958 seminal paper, "Relations between the eruptions of various volcanoes and the deformations of the ground surfaces around them" (Mogi, 1958), attempted to describe the mechanism of a volcanic eruption. He used the observations of Wilson (1935) and Omori (1914), as well as ground deformation observations from the 1929 Komagatake eruption and the 1940 Miyake-sima eruption, to develop a mathematical representation of a volcanic eruption. Mogi hypothesised that the ground deformation is caused by a spherical source (magma chamber) located under a volcano edifice which exerts hydrostatic pressure upwards to the ground surface. He proposed that the earth's crust behaves elastically at the time of eruption. However, for the long period deformation after the eruption, the crust behaves as a visco-elastic medium.
Using elastic theory, Mogi (1958) produced a model that was able to derive the position and depth of a magma source based on ground deformation measurements and their locations. This model, while relatively simple, has proven remarkably resilient over the years and is still used to define the position of magma sources. More recently, the Mogi

model considers three-dimensional volcano topography and more complicated shaped magma chamber sources.

In the 1960s through to the 1980s ground deformation was measured by traditional surveying techniques. Spirit levelling determined movements in the vertical to millimetre accuracy, while theodolites were used to measure triangulation networks resolving movements to centimetres. With the advent of electronic distance measuring (EDM) techniques relatively long distances could be quickly and accurately measured to sub-centimetre accuracy between permanent survey marks, and repeat surveys could indicate movements of the monuments on the volcano over time. Usually a fixed permanent mark was established away from the zone of deformation and considered a benchmark to which all subsequent measurements could be referred.

Ground deformation measurements have also been successfully applied on much smaller scales. For example, between 1980 – 82 on Mt. St. Helens, repeated steel tape measurements across cracks near the centre of an expanding magma dome provided valuable information on the magnitude and rate of swelling of the dome. These measurements, combined with other techniques, led to the successful prediction of 13 eruptions during this period (Swanson et al, 1983). This technique, while cheap and fast, is however not without its risks. Ewert & Swanson (1992) present a comprehensive review of the ground deformation techniques used by staff at the Cascades Volcano Observatory from 1980 - 90.

Suganda (1993) reports a 2m change of horizontal distance between points spanning the crater of Mt Merapi in Indonesia. In this report, four campaigns of EDM measurements were conducted between 1988 – 1992, revealing a significant ground displacement.

The emergence of GPS in the late 1980s as a geodetic tool contributed further to ground deformation studies. GPS could deliver measurements over long distances in three dimensions without the need for intervisibility of benchmarks, 24 hours/day, in all weather and, considering its capability for sub-centimetre accuracy, was relatively cheap.

2.3 Ground Deformation Monitoring using GPS

Ground deformation due to volcanic magma intrusion, crustal motion due to tectonic activity, ground subsidence, etc., are phenomenon ideally suited for study using GPS. Since the late 1980s, high precision GPS applications have included the study of geodynamic phenomena. GPS was a revolutionary tool for the geoscientist who, for the first time, could detect plate tectonic movements over a relatively short period of time, ie months or years. The *change* in length, height difference and orientation of baselines connecting GPS receivers in a carefully monumented ground network can be monitored. This is done by repeatedly measuring the same baseline components to an accuracy commensurate to, but preferably much higher than, the expected baseline component changes. Such GPS techniques are based on the *campaign* principle: the periodic (often annual) re-survey of a network of control points. A changing baseline length between campaigns indicates the magnitude and direction of a plate tectonic movement.

What is the optimal time period between GPS re-surveys? The following comments may be made:

(1) If the rate of change of the baseline components is *constant* with time, the surveys can be repeated at convenient intervals (typically on an annual basis) for a sufficient number of times to ensure a reliable estimate of the (average) rate.

(2) If the deformation varies with time, there will be a sampling problem, as the instantaneous rate (derived from two consecutive GPS surveys) may bear little relation to the average rate, and the frequency characteristics of the deformation may remain unobserved.

(3) If the deformation under study is such that *failure* will occur when the rate climbs above some unsustainable value - as in the case of a precursory uplift due to magma intrusion inside a volcano before it erupts catastrophically, or the deformation of a dam wall before it fails - then GPS may be used as a monitoring tool, rather than simply to measure deformation.

The latter two comments are particularly relevant to localised deformations which may be better studied using *permanent continuous GPS networks*.

Over the last decade or so, there has been a growing interest in the deployment of continuous GPS monitoring networks. The factors responsible for this trend include the declaration of Full Operational Capability of the GPS system in 1995, the establishment of the International GPS Service (IGS) in 1994, and the steady decrease in price, size and power requirements of geodetic GPS receivers. Important additional factors have been the high cost of annual GPS campaigns (manpower, travel, logistics, etc.), as well as the fact that geo-scientific research can be furthered because of the continuous measurement of a deformation phenomenon, rather than its periodic measurement.

The disadvantages inherent in a campaign-style GPS survey approach can be summarised as:

- Periodic surveys only provide a snapshot of the phenomenon, and are unlikely to catch an event such as an earthquake as it happens,
- stability of the monuments became more of an issue as researchers began to realise that the geodynamic signal was often contaminated by systematic biases such as centring errors of a tripod, movement of marks due to changing local environmental conditions, or theft/vandalism of the marks themselves,
- antenna mixing introduced biases (particularly in the vertical component),
- the cost of planning and executing a GPS campaign soon became the largest expense, not the cost of the instruments themselves,
- establishing in-country collaborators, and obtaining permission to work in these countries, was often time-consuming and convoluted,
- equipment had to be shipped in and out of the country, and cleared in and out of customs,
- in-country observers, often inexperienced, had to be trained as GPS surveyors in intensive courses prior to a survey, and hence there was no guarantee that all stations would be observed correctly,
- in-country archiving of the data also risked data loss in harsh environments, and

- processing of all of the data was often not completed satisfactorily until months after the data capture survey had been completed.

Many of these factors served to degrade the final quality of the results obtained from a campaign-style GPS survey, and have served as a primary motivation for adopting a continuous monitoring approach in this project.

Despite these disadvantages, local GPS campaigns are still used to monitor dome growth in conjunction with EDM distance measurements on, for example, Mt Etna, Italy. In addition, the Institute of Technology Bandung (ITB) conducts quarterly campaigns on Gunung Guntur and Gunung Papandayan in West Java, Indonesia (Abidin et al, 1998a).

One of the first continuous GPS networks was established in March 1988 on the Izu Peninsula in central Japan to support earthquake prediction research. Daily observations of this network led to the first GPS measurements of surface deformation as they happened. Shimada et al (1990) reported that, "We have, for the first time, used GPS fixed-point measurements to follow the evolution with time of the crustal movements; such measurements provide a continuous uninterrupted record of deformation."

Another continuous GPS network was established in southern California in the late 1980s for the purpose of crustal deformation monitoring and earthquake research (Bock et al, 1997). Subsequent networks include the Geographical Survey Institute (GSI) network in Japan, which now covers the entire country and consists of almost 1000 sites with an average spacing of about 20km (Sagiya et al, 1997; Kato et al, 1998). The Swedish GPS reference station network (SWEPOS) (Jaldehag et al, 1996) consists of 21 stations the data from which is intended to measure post-glacial rebound in the Fennoscandia region, as well as supporting GPS surveys across Sweden. These networks comprise high quality, dual-frequency GPS receivers, sophisticated communications hardware and software, and cover large areal extents. The GSI and SWEPOS networks are nationwide networks.

Such networks, however, are not suitable to measure the ground deformation surrounding a volcano. Continuously operating reference station (CORS) GPS networks

can therefore be further categorised into large scale and small scale networks. Small scale networks can be subdivided into static networks, real-time kinematic networks and low-cost networks. The differences between the various types of continuous GPS networks will be briefly discussed below, with reference to existing networks, in order to frame the approach adopted in this project.

2.3.1 Large scale CORS GPS networks

A CORS GPS network overcomes many of the disadvantages of the campaign-style survey approach listed earlier. Establishing in-country collaborators and obtaining permission to work becomes a *once only* process. Clearing scientific research equipment through customs, a process if not approached correctly can significantly delay a project, is also only required once. The possibilities of human error are markedly reduced, though not entirely eliminated, by setting up permanent sites. The time delay between observation and processing is also significantly reduced.

For large scale networks, many of the stations are nowadays identified with the IGS (Fig 2.3). Although their data may not be used to assist the precise GPS satellite orbit computation task (a core set of 20-30 well distributed stations is generally enough (Rizos & Galas, 1996)), they are realisations of the terrestrial reference frame to which local GPS surveys can be connected.

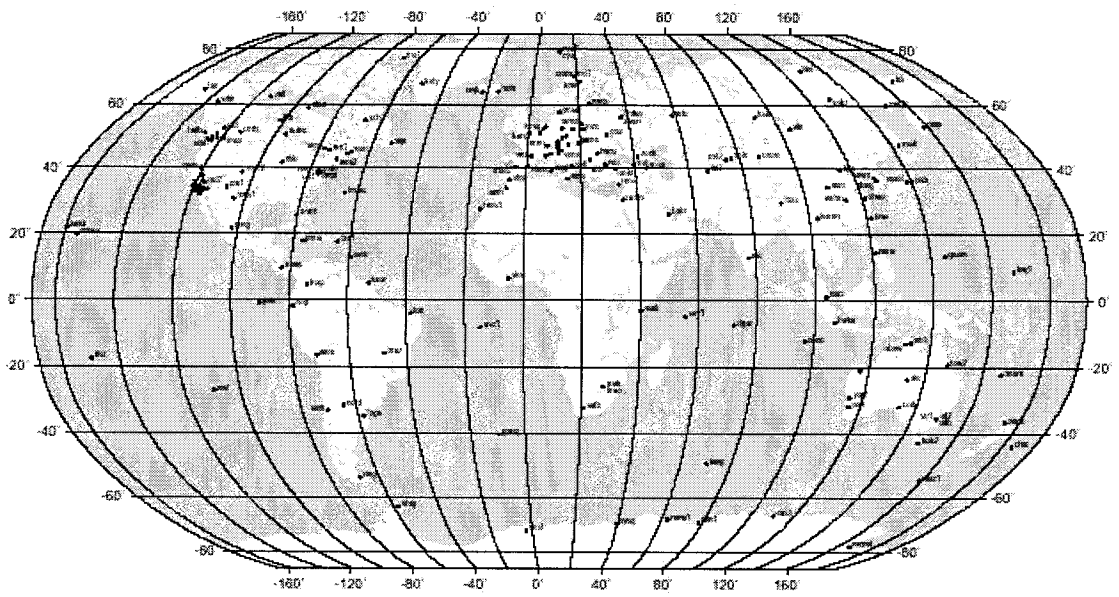

Figure 2.3 - *IGS network map (IGS, 2001).*

Increasingly these permanent GPS stations are being established in the form of sub-nets that can be used for deformation monitoring. For the first time, patterns of deformation occurring over very short time scales, from a matter of a few minutes or hours, to several weeks, can be detected and studied. The 1994 Landers earthquake for instance was measured by the Southern Californian Integrated Geodetic Network (SCIGN) and the 1994 Hokkaido-Toho-Oki earthquake was measured by the Japanese GSI network (Tsuji et al, 1995). These are examples of a continuous measurement strategy that has advantages over a 'periodic' approach for natural hazard mitigation research.

Clearly, network design and receiver station density is crucial if a reliable interpretation of the deformation pattern is to be made. Such design is constrained somewhat by the requirement, for example, for the network stations to be connected to mains power and a phone-line for download of the data on a regular basis. In the case of the SCIGN, GSI and SWEPOS networks mentioned earlier, 24-hour sessions are downloaded and coordinates computed at central computing facilities. The difference between the current and the previous baseline results would indicate any deformation. There is therefore no information in these networks about any sub-diurnal baseline effects that may be apparent over the course of the day.

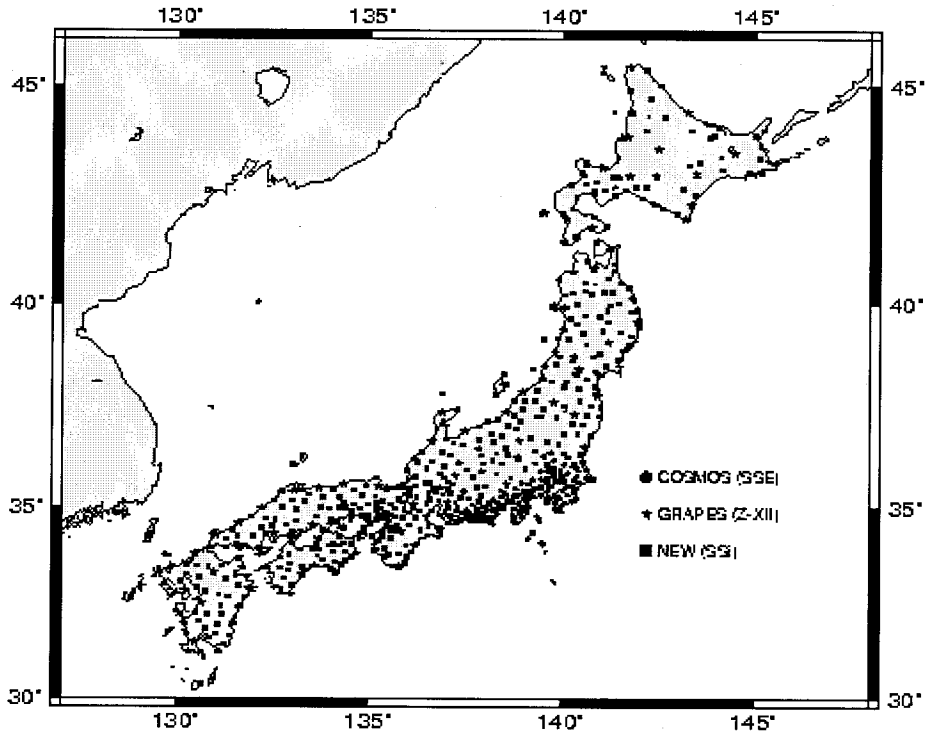

Figure 2.4 – *Network configuration of the GSI's GEONET (Rocken et al, 1999).*

GEONET

Perhaps the best example of a large scale network is the GPS Earth Observation Network (GEONET) of the Geographical Survey Institute (Fig 2.4). The charter of the GEONET is to provide geodetic control for Japan, as well as continuous monitoring of crustal deformation ultimately for earthquake and volcanic eruption prediction (GSI, 2001). Several GEONET stations also contribute data to the IGS global network. Continuous GPS data observed throughout Japan is transmitted to a central processing facility located in Tsukuba. Processed baselines are monitored to detect extraordinary crustal movements which could indicate some pending earthquake threat. Post-processed deformation analysis over longer time periods is also conducted to contribute further to crustal deformation research. Recently, during July-August 2000, the GEONET measured up to 80 cm of horizontal movement and over 1m of subsidence at the Miyake and Kozu Islands in eastern Japan.

GEONET provides the framework for all national spatial data used for land development and management, disaster prevention, volcanic land condition maps and active fault maps in Japan. Contributions to research on monitoring changes in the global environment using space technologies such as environmental sensing,

ionospheric mapping and precipitable water predictions are also made. The GEONET is like a large scale, open-air laboratory, and is used to facilitate technical exchange with foreign researchers, and even to help improve the mapping and survey techniques of developing countries.

Drawbacks of large scale continuous deformation arrays are:

- Network design must be sufficiently dense, whilst still covering a relatively large area, resulting in an expensive system.
- Requirement for mains power and a phone-line constrains network design.
- Due to its high quality baseline results, monumentation must be extremely stable to reliably distinguish between geodynamic signals and local biases.
- Some receiver maintenance is required.
- Sophisticated communications hardware and software are required.
- Sub-diurnal scale deformations are averaged out in the 24-hour baseline result.

Despite these drawbacks, the benefits of a continuous array can not be underestimated. There is hardly any lag time between surveys and coordinate results. No in-field archiving is required as data is automatically downloaded. Logistical problems such as customs clearance for out-of-country networks, and transport of equipment on-site for installation, must only be done once. An entire network can be monitored from a central computing facility. Furthermore, antenna mixing problems and centring errors can be eliminated.

2.3.2 Small scale CORS GPS networks

The GSI, SCIGN and SWEPOS networks are examples of large scale, CORS GPS networks for near-real-time crustal motion monitoring. However, smaller scale GPS arrays, such as those on the Augustine volcano (Alaska), the Popocatépetl volcano (Mexico), the Kilauea volcano (Hawaii), and the Rabaul volcano (Papua New Guinea), reflect a growing interest in local continuous GPS volcano monitoring systems. GPS is also increasingly used to monitor engineering structures such as dams, bridges, buildings, offshore drill platforms, etc.

Developing an automatic GPS receiver array system for such small scale monitoring applications is an engineering and software challenge. A network of permanent GPS receivers needs to be deployed, often in an inhospitable environment in which they must operate reliably on a continuous basis. The GPS observations must be telemetered to a central computing facility where data processing occurs with minimum delay. Analysis of the time series of baseline results then takes place in order to detect any baseline component change between successive solutions that may be a precursor to failure or eruption. What are the bases of small scale monitoring systems? Often the solution has been simply to purchase commercial *off-the-shelf* real-time-kinematic (RTK) GPS systems. This is the high cost option, yet there are several hundred active volcanoes in the world, many located in the less developed countries, and the cost of GPS monitoring systems must be significantly reduced if the technology is to contribute to volcano hazard mitigation. An alternative approach is to develop a system based on single-frequency GPS receivers, integrated with communications and in-field computer sub-systems.

2.3.2.1 Small scale CORS GPS networks – Static networks

Many smaller scale arrays are being developed to monitor deformations on a local scale. One of the first such networks was set up by the United States Geological Survey (USGS) (USGS, 2000) on the Augustine volcano, Alaska (Fig 2.5). Three Ashtech dual-frequency, carrier phase tracking GPS receivers were used. Radio modems send data from the two remote stations located on the flanks and summit of the volcano to a base station. The data is then sent on to another facility 80km away for baseline processing (Dzurisin, 1996). Other examples of such systems include the DefNet array on the Popocatépetl volcano in central Mexico installed in 1996 (UNAM, 2000). The DefNet system uses Turbo-rogue dual-frequency GPS receivers and rigorous data processing (using JPL's GIPSY) software following the approach of Heflin et al (1992) and Blewitt et al (1992). A similar system monitors the Mt. Kilauea volcano in Hawaii (Owen, 2000).

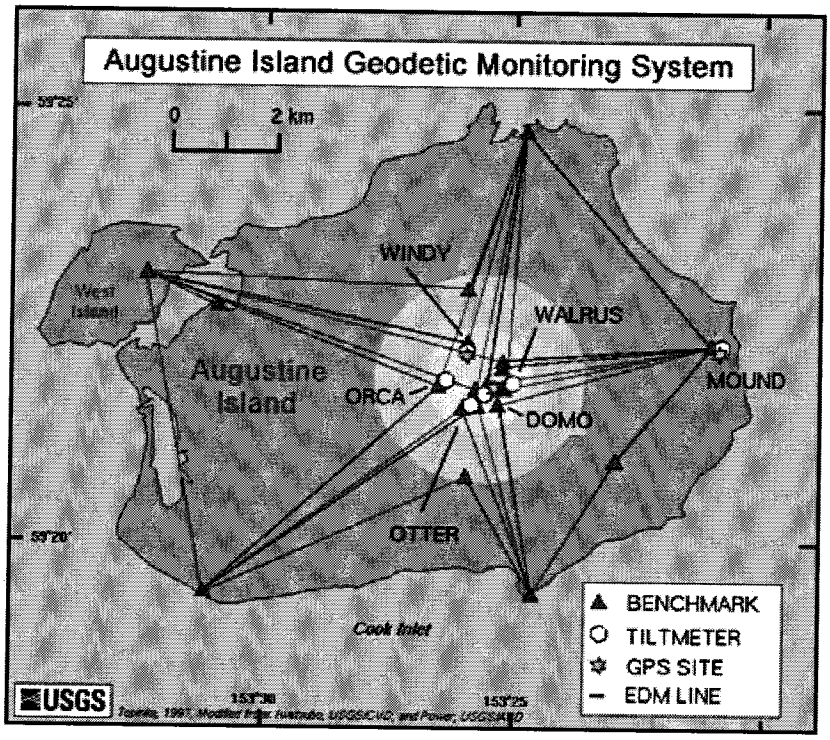

Figure 2.5 - *Augustine small-scale static network (USGS, 2000).*

Unlike the large scale CORS networks, often the station locations for these smaller scale arrays are extremely remote. Power for the stations must be supplied on-site using batteries and solar panels, and all data must be transmitted by some form of wireless link. The logistical challenge for setting up the system therefore is greater. The length of the observation session per baseline is usually a compromise between how often a baseline result is required and how long the information stored on-site at a remote station will take to transmit via the radio link. At the Augustine network it is possible to dial up the GPS stations and command a low power controller to turn GPS receivers on or off. Due to the high power requirement, during the first year of operation only, one 2-hour session per week was recorded (Dzurisin, 1996).

A feature of all of these systems is that they use high quality, expensive, dual-frequency GPS receivers. This high expense severely restricts the number of GPS stations which can be deployed in a local network. The advantages and disadvantages of this type of small scale monitoring system are listed below.

Advantages:

- Can locate GPS stations almost anywhere.
- Smaller scale network implies a higher density of GPS stations, and therefore better resolution of the deformation pattern.
- Continuous measurements are possible.
- No in-field archiving required.
- *One-off* logistical problems.
- Ability to monitor the entire network from a central facility.
- No centring errors or antenna mixing problems.

Disadvantages:

- Expensive, dual-frequency GPS receivers.
- Hardware maintenance is required.
- Sophisticated communications hardware and software are required.
- Number of GPS stations in network limited by communication link considerations.
- Usually a higher power requirement, therefore more batteries and larger solar panels are needed to power the system.
- Initial logistics are arduous.
- Threat of vandalism to system.

2.3.2.2 Small scale CORS GPS networks – RTK mode

In the mid-1990s the technique of Real-Time Kinematic (RTK) GPS surveying was introduced. This technique combines two high quality, dual-frequency GPS receivers with a radio link. Carrier phase measurements are simultaneously observed at a rover and a base station, and data is transmitted to the rover. These double-differenced data are processed at the rover receiver where a position to centimetre accuracy is obtained in real-time. Continually updated, centimetre-level, positions are an excellent option for some deformation monitoring applications.

The commercial deformation monitoring systems are off-the-shelf RTK products developed by several GPS manufacturers. Although intended to perform routine tasks such as engineering surveys, they are increasingly being used for engineering deformation applications. One system was modified to specifically address the requirements for volcano monitoring, and has been deployed for several years at the Rabaul volcano, in Papua New Guinea (Lowry, 1997). It works essentially as a reverse RTK system by computing the position solutions at the rover and then transmitting these results back to the base facility; in effect doubling the volume of transmissions. This in turn limits either the number of GPS stations in the network (as only one station at a time can transmit its data to the base), or the sampling rate between epochs. The following comments can be made with regard to such systems:

- The hardware, software, field computer and telemetry components are relatively expensive.
- Due to limitations of the telemetry sub-system (generally UHF/VHF radios), and the standard double-differenced observation model that is used in such systems, the receiver array scale is generally less than about ten kilometres.
- There is no software that monitors the (changing) baseline solutions to ensure that the variability being observed is really due to a deformation signal, and not simply GPS system noise mapped into the baseline components (see Fig 2.6).
- Many deformational phenomena cannot be characterised as *kinematic* (except under extreme conditions just before a failure or eruption), but may be considered to be *static* over a period of one hour or longer.

RTK systems are therefore not always appropriate options for dense GPS deformation monitoring networks where receiver movement is expected to be comparatively slow.

The Furuno landslide monitoring system is another example of an RTK system where the base facility receives the computed positions of its roving stations (Kondo & Cannon, 1995). This system uses 8 channel GPS receivers capable of outputting raw C/A code and carrier phase at a 0.5Hz data rate. The receivers communicate via a wire connection, limiting the baseline length to a maximum of 1200m between any two receivers (in most cases only 800m). Up to 10 relay stations can be used in the network.

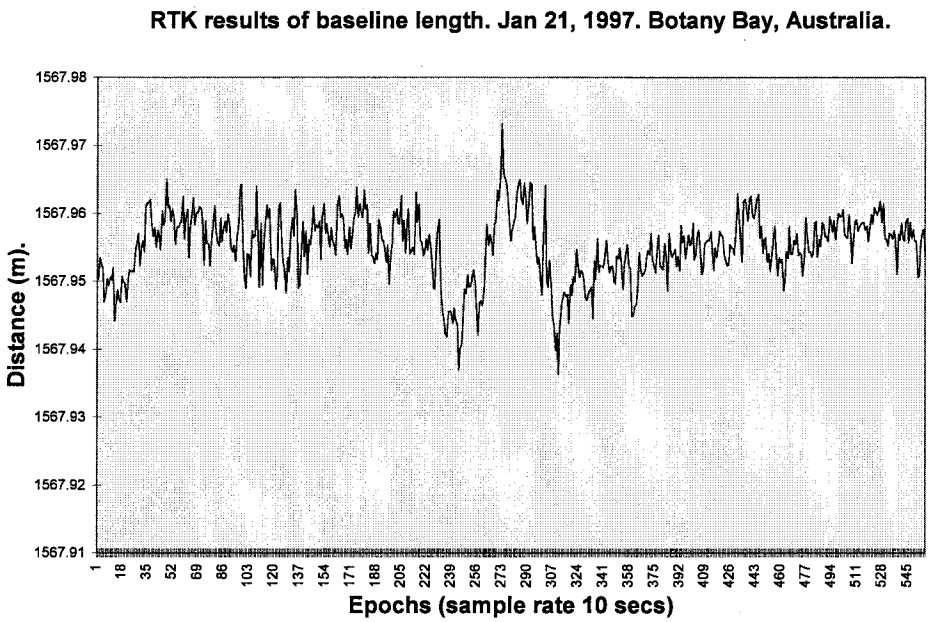

Figure 2.6 - *Typical epoch-by-epoch variability of RTK solutions.*

The system continuously determines real-time positions of several receiver locations to an accuracy of 2cm and indicates if any displacements have occurred over time (Ibid, 1995). Such a system, however, is severely limited by the wire connection between GPS sensors and would be entirely unsuitable for the volcano monitoring application.

The GPS-based On-line Control and Alarm (GOCA) system is a software infrastructure that is designed to receive GPS baseline solutions from any combination of single or dual-frequency GPS systems. Kälber et al (2000) states that GOCA can be set up as an early warning system to monitor landslides, earthquakes and volcanic activity. Data from the base receiver is transmitted to the rover receivers where the baselines are computed. Radio modems then transfer the estimated baseline vectors to the GOCA centre, where network adjustment software analyses the resulting baselines, and indicates any motions between observation epochs. Deformation network points may be occupied permanently or intermittently, permitting a higher degree of flexibility.

Recently, Magellan has developed an off-the-shelf, real-time monitoring software package called Condor (Condor, 2000) which uses a slightly different approach. The static nature of the monitoring stations is exploited. After a period of initialisation, a Kalman filter, augmented by triple-differenced and double-differenced data solutions, provides epoch-by-epoch filtered solutions. This software can process data from single

or dual-frequency receivers, or a combination of the two. The manufacturers claim mm-level accuracy for this system. It would seem that continuous GPS deformation monitoring systems could not possibly improve on this design, but it comes at a high cost. In addition, a high-end desktop PC is recommended for running the software. The problems of power supply and protection against the elements still need to be addressed, and are very much dependent on the application. The Condor system has been installed by the USGS at the Long Valley Caldera in 1999, and more recently at the Hawaiian Volcano Observatory and the Rabaul Volcano in PNG.

Advantages of RTK-based continuous monitoring systems:

- Real-time coordinates of the rover stations available at the base facility.
- Smaller scale network implies higher density of stations, and therefore better description of deformation pattern.
- Can locate GPS stations almost anywhere.
- No in-field data archiving required.
- One-off logistical challenges.
- Ability to monitor the entire network from a central facility.
- No centring errors or antenna mixing problems.

Disadvantages:

- Cost of GPS stations can be prohibitive.
- Real-time positions give no indication of longer period effects.
- The variability in epoch-by-epoch solutions, resulting from RTK-based systems, is not likely to be entirely due to a deformational signal, but may just be system noise, (see Fig 2.6).
- The mm-level accuracy refers to repeatability between epochs and may not necessarily be the accuracy of the solution.
- Higher demand on communications link.
- Vulnerable to vandalism.

2.3.2.3 Small scale CORS GPS networks – Low-cost option

The above monitoring systems require expensive GPS receivers. In recent years low-cost original equipment manufacturer (OEM), single-frequency GPS receivers have been released on the market at a fraction of the cost of standard dual-frequency receivers. These receivers can be integrated into custom-built systems that output code and/or phase measurements for baseline determination.

A lower system cost means that a larger number of stations can be deployed on any one project. The station hardware is suitable for remote locations, ie will have their own power in the form of batteries and solar panels. Radio modems transmit raw data to the base facility, and a computer controls data management and the communications software. The lack of peripheral components to the GPS receiver and computer (ie screens, hard disks) significantly reduces the power usage of the system. As a result, the size of the battery bank and the solar panels can be reduced, which translates to further cost savings.

A single-frequency carrier phase tracking GPS receiver is appropriate for small scale CORS networks if the baseline lengths are no longer than about 10 kilometres. This *rule-of-thumb* implies that the differential ionospheric delay between the two receivers is essentially zero (because single-frequency systems cannot eliminate the ionospheric delay), and therefore does not impact on the baseline result. An advantage is lower noise on the signal and perhaps better detection criteria (see section 3.2.4.1). Orbit bias over such short distances can also be ignored (see section 3.2.5).

An example of such a system is the GPS volcano monitoring system developed by the University Navstar Consortium (UNAVCO). A commercial single-frequency GPS carrier phase tracking receiver is integrated with a Time Division Multiple Access (TDMA) radio data modem network. "The compact size, low power consumption and lower cost of the L1 GPS receivers make them feasible to be deployed in dense arrays to monitor sub-centimetre small scale crustal deformation; a situation ideal for active volcano deformation monitoring" (Meertens, 1998).

The UNAVCO system was deployed on Popocatépetl volcano near Mexico City in April 1999 to augment the DefNet network already in operation. Five remote stations were installed with one at 5100m elevation, and just 300m below the summit from a continuously erupting crater. The harsh conditions are considered a challenging test site for the GPS system (Fig 2.7). It is planned to construct several of these L1-only GPS networks along the Trans-Mexican Volcano Belt.

Figure 2.7 - *Remote L1 GPS station on Popocatépetl volcano (UNAM, 2001a).*

Chapter 4 of this thesis describes in detail the UNSW-designed volcano monitoring system. This system also uses an OEM GPS receiver, integrated with a PC board, low-cost VHF radios and a low-cost GPS antenna. Short session static baselines are post-processed using in-house GPS baseline software. Considering the equatorial location of the network, and with the sunspot activity reaching a maximum in 2001, achieving centimetre level accuracy even over 10km baselines is a significant challenge.

Han & Rizos (1996a) have proposed a correction algorithm which maps the ionospheric conditions around a volcanic environment using sparse external 'fiducial' network of dual-frequency GPS receivers. This network operates simultaneously with the internal L1-only GPS network, and generates corrections that ensure high-quality baseline results from a L1-only system. Rizos et al (2000) describe improvements in the L1

baseline results when implementing corrections derived from such an external fiducial network.

In-house baseline processing software is extremely advantageous for such a low-cost system, where software and algorithm enhancements can help compensate for lower quality hardware, and still ensure high accuracy.

Advantages:

- Low-cost systems are more appropriate for developing countries.
- Potentially more receivers in a local array provide better monitoring of deformation.
- Can locate stations almost anywhere.
- No in-field data archiving required.
- One-off logistical problems.
- Ability to monitor the entire network from a central facility.
- Ability to connect low-cost system into an existing continuous fiducial GPS network.
- Custom-built software implies access to source code for algorithm improvement.

Disadvantages:

- Session solutions perhaps every hour, ie it is not an RTK system.
- Low-cost GPS system implies less stable monuments.
- Autonomous communications hardware and software are required.
- On-site power required for remote stations.
- Limited to small-scale surveys due to radio communications considerations and ionospheric effects.
- L1 noise is lower than L2 noise (and therefore LC noise) ie single frequency networks are higher accuracy over short distances.
- Sparse outer fiducial GPS network required to maintain high accuracy.
- Vulnerable to vandalism.

2.3.3 Summary of Continuous GPS Deformation Monitoring Systems

It is well established that GPS is a suitably mature technology for the continuous monitoring of deforming bodies. The various types of GPS monitoring systems have been briefly described, and will be referred to in subsequent chapters. The appropriate type of monitoring system to be used is primarily defined by the application.

Table 2.1 - *The distinguishing features of different continuous GPS networks.*

FEATURE	LARGE SCALE	SMALL SCALE STATIC	SMALL SCALE RTK	SMALL SCALE LOW-COST
Component expense	High	High	Relatively high	Low
Accuracy	mm-level	mm-level	cm-level	mm-cm level
Quality of the monumentation	Highly stable Expensive	Good stability Expensive	Stable Inexpensive	Stable Inexpensive
Power type	AC Power	AC or remote	Batteries/Solar panels	Batteries/Solar panels
Power demand	High	High	High	Low
Data transmission	Phone lines	Phone lines/ Radio	Radio	Radio
Session length	24-hour	1 - 24-hour	epoch to epoch	1 – 3 hour
Threat of vandalism	Low	Low (location dependant)	Potentially high	Potentially high
On-site data archiving	Daily-central facility	Daily to Base station PC	Base station PC with display	Base station hard disk
GPS receiver quality	High Dual freq	High Dual freq	High Dual freq	OEM Board Single freq
GPS antenna quality	High Dual freq	High Dual freq	High Dual freq	Lower Single freq

A larger scale system requires high quality, high cost components and relies on communications infrastructure in order to support crustal motion studies. (The GPS data from such a network may also be used for troposphere and ionosphere sensing studies, and/or supports a GPS service for local users.) A smaller scale system can relax the accuracy requirements and therefore reduce the quality and cost of its components. A regional network may be small enough to maintain high accuracy using L1-only GPS

receivers. A correlation therefore exists between size, quality and cost of a continuous GPS network (Table 2.1).

2.4 Factors to Consider in Designing GPS Volcano Monitoring Systems

Section 2.3 dealt generally with any continuous GPS monitoring system. Volcano monitoring requires certain extra considerations to be taken into account. The following section briefly discusses these issues at a conceptual level. Chapter 3 details specific design considerations for the volcano monitoring application.

2.4.1 GPS Configuration

A volcanic environment is generally of small scale, ie no larger than perhaps 10 –15km across. A small scale approach is therefore suitable for a GPS volcano monitoring system. One or more stable base stations must be located away from the zone of deformation. Remote observing stations are required to be located on the volcano edifice.

Selection of GPS receivers and antennas

The selection of GPS receiver for a volcano monitoring network is the most significant factor. The choice between dual-frequency and single-frequency receivers is determined by the budget of the project, as well as the desired accuracy of the system. Dual-frequency data can be used to account for ionospheric effects, provides more data for reliable ambiguity resolution, and generally guarantees high quality data. Laboratory test results at UNSW and UNAVCO show that the L1 carrier tracking loops inside single-frequency GPS receivers are as good as those in dual-frequency receivers. This was further tested during the Papandayan 2001 survey (see section 6.5).

Together with the choice of GPS receiver, the selection of GPS antenna is also significant. A low-cost network will seek to use the most inexpensive antenna without compromising the accuracy requirement of the desired signal (Roberts et al, 1998). For highest accuracy results, a choke-ring style dual-frequency antenna should be used at all stations (see section 3.1.4). If a network is comprised of different GPS antenna types,

the effects of antenna phase centre variation (APCV) must be taken into account (see section 3.2.1).

Selection of optimal station location

These remote stations will often be exposed to harsh environmental conditions (see section 3.1.6). Sensitive hardware components, such as the GPS receiver, on-board PC and radio sub-systems need to be protected from corrosive gases, temperature extremes, wind, rain and possibly even flying volcanic debris on extremely active volcanoes (Fig 2.7). Remote stations can be subject to vandalism, and should be protected as far as is possible. This can be done by emplacing a fence around the site (unfortunately also increasing the multipath effects), or locating the site where it is difficult to access.

Station location must also consider the stability of the marks, the magnitude of the deformation expected, avoidance of extremely corrosive locations, and selection of suitable geodetic sites for GPS surveying (see section 3.1.3). It is important to locate stations away from known local tectonic effects often associated with volcanic terrain.

Measuring strategy

How much GPS data will be sufficient to determine the deforming behaviour of the volcano? How long should a GPS session log data? What data rate should be recorded? How many sessions/day? Measuring 24-hour sessions will average out any diurnal effects on the one hand, but measuring 24 1-hour sessions may not be enough data to resolve 24 sufficiently accurate GPS baselines on the other hand. Longer baselines will require longer observation sessions. To conserve power at the remote stations, the system could measure six 2-hour sessions/day with a 2-hour down-time between sessions. A 30 second data sample rate compared to a 1 Hz data rate will reduce the volume of data archived, and therefore the power required by the on-site radios when transmitting the data to the base facility. A transmitting radio uses the most power of any system component (see section 4.2.3). Perhaps an RTK approach could be triggered prior to some anticipated activity based on ground deformation or seismic measurements. The configuration of the system will be determined by many factors, and is likely to be unique to each environment and application.

Data transmission and communications

Data transmission is best accomplished using UHF/VHF radios (see section 3.1.2). Radio data systems are a reliable technology and provide error checking of transmitted data. Many different radio systems are available to cater for varying network configurations. In some environments, a cellular telephone network is available. However, call charges are expensive over long periods and such an infrastructure is not always reliable.

All system components require reliable power to operate continuously. For a base station, generally located in a safe building, AC power can provide a reliable power source. However, in some developing countries the power may be intermittent or unstable. Section 4.3.1 describes the power system design at the base station of the low-cost system established at Gunung Papandayan to illustrate this point. The remote observing stations need to provide power using 12 V DC batteries, continuously recharged by an array of solar panels. Considerations such as the latitudinal location of the network, power requirement, size of battery bank, recharge rate, amount of sunlight etc., influences the design of the remote power systems. Section 4.2.4 provides a detailed description of the power budget for the UNSW low-cost system.

Elimination of errors and biases

Generally, the height difference between a stable GPS base station and a remote station located on the flanks or summit of a volcano will be significant. Applying conventional troposphere models during processing will give erroneous results. Correcting for the differential troposphere between these stations, particularly in equatorial regions where there exists more water vapour, complicates the GPS baseline processing step. Chapter 5 focuses on this issue.

Given that continuous volcano monitoring systems generally cover a small areal extent, the effect of the ionosphere can be dealt with either by using dual-frequency GPS receivers to calibrate the effect, or by ignoring it for short baselines. However, with the maximum in solar activity in 2000/2001, and particularly for volcanoes located in equatorial or polar regions, it is unwise to ignore the effect of the ionosphere at this time. For an L1-only system therefore an outer fiducial network of dual-frequency GPS receivers could map the ionospheric conditions and provide corrections for single-

frequency receivers (see section 3.4.4)(Wanninger, 1995; Rocken et al, 2000). The fact that large scale continuous GPS arrays already exist, and are becoming more prevalent all over the world, offers the opportunity to utilise these networks as the backbone for smaller scale, low-cost type networks (Rizos, 1997c). RTK networks use dual-frequency data.

The effects of multipath cannot be avoided in the case of volcano monitoring networks. Stations should be located to avoid multipath effects as much as possible, however stations located on the flanks of the volcano will have a masked skyview, which can cause multipath. Because the GPS network remains fixed, the multipath signal at the receiving antenna will repeat on a daily basis (minus ~4 minutes). This repeatability can be exploited using digital signal processing techniques in order to account for multipath (see sections 3.2.2 & 4.6.2). A more expensive solution would be to equip all stations with high-cost multipath-resistant antennas. However, it is very difficult to eliminate all multipath effects using a hardware approach only.

Broadcast ephemerides are considered accurate enough for short baseline applications (see section 3.2.5). However, a well-equipped base station connected to the Internet can easily download the latest IGS orbit products, so that they can be utilised during baseline processing. Similarly, the starting coordinates adopted for the base station(s) can be computed rigorously, to the highest accuracy, or less rigorously and adopted as the fixed coordinate to which subsequent deformation results can be compared (see section 3.2.6).

Selection of software

The choice of GPS baseline processing software offers many options. An off-the-shelf commercial software may offer a simple user interface and some instructive graphical representations, however more sophisticated changes to the software maybe restrictive. For example, tropospheric estimation capabilities, the inclusion of improved algorithms or the ability to process in a choice of operating system environments is limited. Scientific software such as Bernese or Gamit offer many options to the skilled user, however may be too cumbersome for a regional network. Custom-written software can combine the advantages of both styles of software, but must be written and tested by

that research group. Chapter 6 describes the processing software and options used for the UNSW-designed low-cost volcano monitoring system.

2.4.2 Forecasting Eruptive Activity

Volcano monitoring has the stated goal of improving our understanding of how volcanoes function, and why and when they erupt (McGuire et al, 1995). Reliable forecasting of pending eruptive activity is crucial for hazard mitigation. Swanson et al (1985) distinguishes between a *forecast* and a *prediction*. A *forecast* considers estimates of historical records, maybe decades prior, which give a general indication of the behaviour of the volcano. It is a relatively imprecise statement of the time, place and nature of expected activity. A *prediction,* however, is generally more accurate and short term. It is a relatively precise statement of the time, place and ideally the nature and size of impending activity (McGuire et al, 1995). Predictions may be announced months or days prior to an event, and may recommend an evacuation of local residents.

Abidin (1998, personal communication) suggests that to really understand the behaviour of a volcano, the researcher must "marry" the volcano. This humorous assertion is valid as all volcanoes are unique and therefore display different characteristics. Only after gathering historical records over decades can a researcher understand better what Tilling (McGuire et al, 1995) terms the *baseline data* of a particular volcano. Baseline data constitutes empirically derived time series of recurring events. This data can be used to determine if recent activity is characteristic behaviour or indeed a potential threat. As more data is gathered, the reliability of patterns of behaviour will improve.

Similarly, it is crucial to understand the accuracy of the measurement technology used to monitor a volcano and be familiar with its overall performance. Systematic biases of the instruments must not be interpreted as some geophysical signal. This issue is particularly relevant to continuous GPS monitoring systems which are susceptible to the influence of different error sources. Section 3.2 deals with this issue in more detail.

The dilemma facing vulcanologists is to decide if a prediction based on their measurements warrants the evacuation of a large number of people. To over-react, and to unnecessarily evacuate the population, leads to a loss of confidence and heightened

aggravation by the local authorities and the community. However, to not act could lead to a major loss of life and property, as well as damage to the professional reputation of vulcanologists. McGuire et al (1995) gives an example of "crying wolf" during the 1976-7 eruption of Soufrière, where 72,000 residents were evacuated for four months due to a mis-interpretation of data (Fiske, 1984). Conversely, the threat of the Nevado del Ruiz disaster of November 13, 1985 was well understood by vulcanologists and appropriate authorities were warned in advance. However, a combination of poor communications, indecisiveness and lack of appreciation of the seriousness of the threat by the relevant authorities led to the deaths of about 22,000 people (Voight, 1990).

The problems set out in points 2 and 3 of section 2.3 are relevant to volcano monitoring. The sampling problem for a non-linear deformation may not be detected between routinely measured sessions, particularly when session lengths are up to 24 hours. A volcano may remain dormant and inactive for many years and suddenly undergo significant deformation. The challenge of a GPS monitoring system is to detect any sudden movement as early as possible. The method of detection could be in the form of a software innovation. Comparing the newest baseline result with the previous baseline may indicate nothing, yet comparing with a baseline from the week prior may indicate some trend (see Fig 2.8).

2.4.3 Time Series Analysis

How the baselines determined by a continuous GPS monitoring system are utilised is a consideration unique to volcano monitoring. It is expected that the largest signal during some deformation episode will occur in the vertical component at the observing stations located on the volcano (Mogi, 1958). However, for GPS surveying, the vertical component is the least accurate to measure. Careful error mitigation of all effects influencing the accuracy of the baselines reduces systematic biases in the resulting data. Time series analysis can filter the results, improving the repeatability further. The accuracy limitations of a monitoring system must be well known in order that the system can be used for prediction/forecasting. The challenge of a monitoring system is to be able to distinguish between what constitutes ground movement, and what is simply measurement noise.

2.4.3.1 Filtering

Filtering is used to eliminate data that has non-desirable characteristics such as outlier data or unwanted frequency content. Filtering removes or down weights outliers and hence improves the quality of the resultant time series.

Outliers

Perhaps the simplest form of filtering is the process of removing blunders or outliers. In GPS measurements, outliers generally occur as a result of incorrectly resolved ambiguities. Ambiguities may be incorrectly resolved due to poor receiver-satellite geometry, short observation sessions, incorrectly modelled ionosphere or troposphere, large numbers of cycle slips, excess multipath, an incomplete navigation message or due to an unhealthy satellite.

The detection of outliers may not be straightforward. If good data is assumed to be an outlier and is rejected, then the outlier detection method is at fault and a type I error has been committed. Conversely, a type II error occurs when data, assumed valid, is in fact an outlier. The statistical t-test can be applied for outlier detection (Baarda, 1968). The w-test for outlier detection and the concept of the marginally detectable error are explained in Cross (1983, 1999).

Fourier Analysis

A data series may contain a repeatable systematic signal which is not visible in the time domain. Time series data can be transformed into the frequency domain using a Discrete Fourier Transform (DFT) (Proakis & Manolakis, 1996). Fourier analysis is a mathematical technique for transforming our view of the signal from time-based to frequency-based. A signal is broken down into constituent sinusoids of different frequencies. The more efficient Fast Fourier Transform (FFT) algorithm is used for computing the DFT of a data sequence. Frequency peaks (in the frequency domain) will indicate a repeatable effect buried in the data, such as multipath, low frequency troposphere effects, a diurnal ionospheric signal etc. A Finite Impulse Response (FIR) filter can be designed to remove these signals in the time domain. Armed with this frequency information, FIR filters can also be used in the frequency domain in which

case a reverse FFT process returns the resulting data series to the time domain. Han & Rizos (1997) describe a filter designed to mitigate multipath effects.

Adaptive Filtering

An extension of the FFT technique is the adaptive finite-duration impulse response filter, based on a least-mean-square algorithm. Ge et al (2000) used this filter to mitigate multipath effects by first deriving a multipath model, and then removing the multipath effect from the time series data. Ibid (2000) claims a reduction in the standard deviations of residual time series of 25% for pseudoranges, and approximately one half for carrier phase measurements.

Short-time FFT (STFT)

Fourier analysis, discussed above, can detect frequencies within a data series but there is no indication of when this frequency occurred. If data is *stationary* (ie does not change over time) then Fourier analysis is sufficient. However, effects such as drifts, trends and abrupt changes will be missed. Fourier analysis applied to small sections of data STFT sought to address this shortcoming by *windowing* a signal. By detecting a particular frequency peak for a window of data, time information could be gleaned as to changes in the stationarity of a signal. This is a fairly discretised approach however, and is restricted by the size of the window chosen.

Wavelets

The natural evolution of the STFT approach is towards wavelets. Here the windowing technique uses variable sized windows. Long time intervals will detect long wavelength effects, and shorter windows will indicate high frequency information. The advantage of wavelets over a FFT and STFT is that frequency peaks are identified and their associated time information is preserved. The vibration of a building in an ever-increasing wind (ie changing frequency over time) could then be monitored using wavelets. Fu & Rizos (1997) introduce a wavelet-based technique for GPS processing, and Satirapod et al (2001) demonstrate improved GPS analysis using wavelets. The wavelet approach however is more complicated in the analysis and the concept of a time-frequency region is replaced by a time-scale. In other words, a particular range of frequencies may occur at one time. The relationship between frequency and scale

considers a central frequency, a nominated scale and a sampling period giving a pseudo-frequency related to that scale (The Mathworks, 2000).

Power Spectral Density Analysis

Like the FFT approach, estimation of the power spectra permits the detection of frequency signals hidden in a noisy time series. Power spectral density plots evolve from short sections of the FFT technique with the overlap sections joined by a Hanning (or some other) window (The Mathworks, 1998). This approach is similar to the STFT approach, though the presentation of the results is different. Chapter 6 uses this technique to identify a diurnal multipath signal in time series height data.

2.4.3.2 Detection

A time series of data may exhibit a long term trend, a sudden jump or a shorter term motion which may be considered unusual based on the measurement history. When is a measurement considered constant, and when does it indicate a geophysical signal? Some popular tests that can be used to detect such movements are described below. The implications of such a discovery are important for volcano monitoring (see section 2.4.2), as the system must be certain that a detected movement is indeed significant before alerting local authorities of a potential hazard. Some outliers will always be detected. The consistency of the movement will also be a prime indicator. Ogaja (2001) describes integrity tests that can be applied to GPS measurements, that deal with false alarms and anomalous behaviour.

t (Student) Distribution Test

The Student *t*-test is a classic statistical tool that compares a sample mean with a population mean (Harvey, 1994; Wolf & Ghilani, 1997). Such a test could be used for volcano monitoring by comparing the mean value derived from a sample GPS measurement with a known mean (or adopted mean) value, based on the assumption that the points are not moving. The *t*-test determines whether a mean value is statistically similar to, or significantly different from the known mean, at a predefined confidence interval (usually 95% or 99%). A value considered significantly different from a mean value indicates either a potential movement of the volcano edifice, or perhaps a poorly processed baseline; an outlier. The *t*-test is similar to the normal

distribution but is preferred in surveying as it deals comfortably with fewer than 30 samples. The F-test, another statistical tool (Ibid, 1994; 1997), can provide a similar indicator based on variances. This detection method is less frequently used.

Control Charts

Quality Control Charts used for industrial applications to test for defective products can also be applied to deformation monitoring. A chart of GPS baseline results for all components vs. time indicates the variation between baselines (see Fig 6.11). Certain limits can be set (see Fig 6.13, which shows a limit of two standard deviations of the mean) which define the maximum allowable tolerance before the observation will be identified as either an outlier or a potential movement. Scheaffer & McClave (1990) and Juran & Blanton-Godfrey (1999), suggest the following upper and lower bound control limits:

$$\mu \pm 3\left(\frac{\sigma}{\sqrt{n}}\right) \qquad \text{- (2.1)}$$

where;

μ – mean

σ – standard deviation

n – number of samples

(Note: 3 is the constant adopted for most control charting)

Thus, the interval has a 99.73% chance of including the new baseline computation, providing the system is "in control". This corresponds to the confidence level of the system. Note that for a continuous system, it is prudent to wait for at least 20 samples before setting control limits.

It would be remiss to assume a geophysical movement on the basis of one observation alone. Perhaps a series of results, indicating a definite trend, must first be derived before assuming a deformation. However, this too is dangerous, as demonstrated for day 9 in Fig 6.13. Several points in the height component time series fall well above the adopted mean value and appear to follow a similar trend. The easting and northing components

show no such trend, and the results suddenly return to within the control chart limits late on day 9. This could be a result of an unhealthy SV corrupting baseline results or perhaps an incomplete navigation message. It indicates the level of sensitivity to which a detection system must be capable. Similarly, s-charts monitor the standard deviation of a time series of data.

Cusum tests

Control charts indicate sharp changes in time series data, but also increase the risk of false alarms. The cumulative summation (Cusum) approach was developed in the 1950s as a quality control indicator. Accumulating the difference between a sample and an established mean over time shows trends in the time series, and can detect sharp changes as well as slight changes in trends. Accordingly, the *slope* of a Cusum chart requires interpretation rather than the departure from a mean value. Changes in slope will indicate steps in the control chart and can show how a process changes over time. The accumulation of deviations from a mean value make them suitable for prompt detection of off-standard conditions. It can also locate the onset of changes and measure their magnitudes. It is an arithmetically simple test to implement. More complex adaptations of Cusum charts deal with decision rules, consideration of an appropriate mean value as well as detection and measurement of trends or drifts. Bissell (1984) provides an excellent reference for Cusum charts. Mertikas & Rizos (1997) recommend Cusum tests as a statistical tool for ground deformation monitoring.

Allan Variance

A time series of GPS baseline components is correlated between successive samples. This is particularly so for short session lengths (ie 1-hour), where a similar constellation of satellites may be used for successive sessions. This correlation will therefore influence a detection algorithm. Additionally, in order to detect a longer-term movement or trend, comparison between a baseline determination and the previous measurement will often be far too imprecise. Perhaps comparison between a baseline solution and its corresponding baseline a day, a week or even a month, previous may indicate a significant movement over time. Figure 2.8 illustrates the vertical component of a baseline result taken from the DefNet network on the Popocatépetl volcano in Mexico. It shows daily results and a trend line over approximately a month of data. Such a trend is not apparent over one day only.

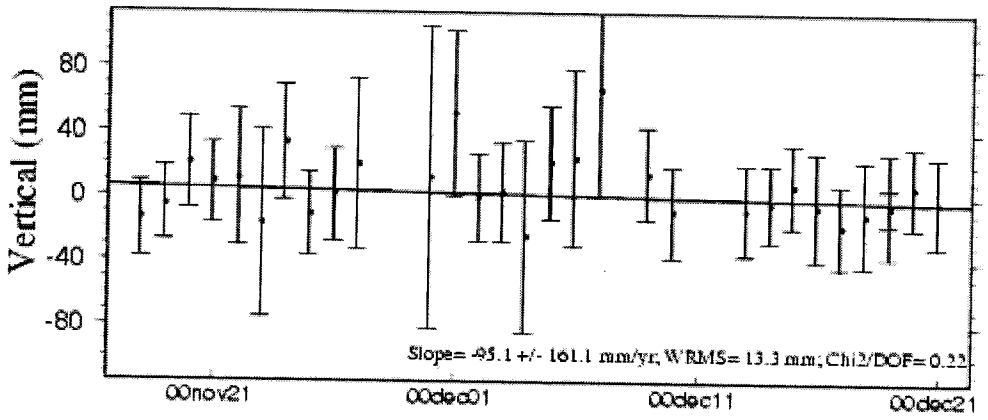

Figure 2.8 – *POPN – POSW dual-frequency baseline from the DefNet network on Popocatépetl Volcano, Mexico (UNAM, 2000).*

Allan variance (or pair-variance) can provide an accuracy limit above which a sample could be considered a movement and analysed more carefully. The Allan variance for a specific time interval τ is given by (Hellwig, 1977):

$$\sigma = \sqrt{\frac{addition\_of\_squares\_of\_differences\_between\_successive\_readings}{2 \times total\_number\_of\_differences\_used}} \quad \text{-(2.2)}$$

The Allan variance is defined as (Allan et al, 1974):

$$\sigma_y^2(\tau) = \frac{1}{2}\left\langle (\Delta y)^2 \right\rangle \quad \text{- (2.3)}$$

where $\langle\ \rangle$ denote an infinite time average.

The Allan variance is approximated using a series of samples because an infinite time average is not practical. Therefore:

$$\bar{y}_k = \frac{\phi(t_k - \tau) - \phi(t_k)}{2\tau} \quad \text{- (2.4)}$$

For N samples, the Allan variance is:

$$\sigma^2_{Allan}(\tau) = \frac{1}{2(N-1)} \sum_{k=1}^{N-1} \left(\bar{y}_{k+1} - \bar{y}_k\right)^2 \qquad \text{- (2.5)}$$

The use of the Allan variance was introduced in the early 1970s to look at the frequency stability of atomic oscillators. Note that clock stability is usually expressed in terms of the deviation, $\sigma_{Allan}(\tau)$. Chapter 6 introduces Allan variance as a novel way to look at the quality of a deformation monitoring system and to provide an upper accuracy limit for different time samples.

2.5 Specifications for the UNSW Design

Permanent CORS GPS networks have been categorised in this chapter by type. The UNSW–designed system located on Gunung Papandayan, Indonesia, is therefore a small scale, low-cost, continuous GPS network. The general specifications are listed below:

- Small scale, low-cost system,
- remote stations powered by batteries and solar panels,
- remote stations designed for harsh environments,
- L1 OEM GPS boards controlled by PC or micro-controller,
- radio modems modular in design to allow for different range transmissions in different environments,
- in-house developed baseline processing software,
- centimetre accuracy from post-processed static baselines,
- designed for volcano monitoring in equatorial regions,
- suitable for operation in developing countries, and
- allow for inclusion of an external fiducial network to augment the internal network.

These specifications will define the hardware components chosen to build the system. Chapter 3 describes in more detail the various components available for any type of system. Chapter 3 also describes the significant error sources of GPS surveying and some error mitigation strategies. These, in conjunction with the general specifications given above, define the hardware selected and software strategies adopted for the UNSW system. The technical details of all components are provided in chapter 4.

Chapter 3
DESIGN CONSIDERATIONS FOR VOLCANO MONITORING

This chapter details the basic components for all types of volcano monitoring systems. The choices of hardware available and its appropriateness to a particular type of volcano monitoring system with regard to accuracy and cost is presented. The major error sources are then described and strategies to mitigate them are introduced. It is envisaged that this chapter shall highlight the array of options available for a GPS-based monitoring system. This provides a framework for the specific design considerations adopted for the UNSW system described in chapter 4.

Apart from the technical issues, there are challenges of another sort. No project can ever be carried out in isolation in a foreign country. Permission must be granted to allow work to be undertaken, and therefore some form of collaboration with in-country colleagues is vital. It is advisable that like-minded institutions should work in partnership; for instance universities working with universities, or government institutions working with government institutions.

A successful scientific proposal attracting research funds is required in the first instance. In-country institutions, usually expert in the research field, are approached to partner a project. A meeting and subsequent Memorandum of Understanding (MOU) between all parties identifies the various aims, expectations and objectives. An MOU is not unlike a contract between the collaborators (though not with the same legal basis). It therefore must be a visionary document from the outset; general, flexible and anticipatory in nature.

These initial stages of research collaboration can be slow, nerve racking and sensitive. It is important that all parties feel they are making an equal contribution and are gaining something (eg scientific kudos, academic exchange, exposure to new technologies, etc) from the partnership.

Despite the desire for an equal contribution from all, usually one partner is required to lead the project, the principal investigator (PI), and it is his/her management skills which must drive the project to a successful conclusion. Communication between all parties is crucial to building trust. This may take the form of e-mail communication, fax or telephone, but must invariably include face-to-face visits in order to cement relationships.

International collaboration will be further complicated by the different cultural rules and expectations of the participating members. A certain degree of cultural education and sensitivity goes a long way toward improving relations and understanding. Of course, there are no set rules, and all projects have their unique challenges. Reference is therefore made to section 4.1 of this thesis, which details the collaboration and management issues that were addressed in order to have the UNSW low-cost volcano monitoring system installed on Gunung Papandayan.

3.1 Monitoring Station Equipment Issues

The important component parts of a GPS volcano monitoring system are listed below. Their suitability for particular applications is described with reference to existing monitoring systems. There is little point combining a top-of-the-range dual-frequency GPS receiver with a low-cost antenna and an unstable monument. The application criteria defines the equipment selected for the task, such as the size of the network, magnitude of deformational signal to be detected, budget, and location. The equipment chosen for a specific type of monitoring system impacts directly on the error terms in equation 3.1 (see section 3.2).

3.1.1 GPS Receivers

The GPS receiver is of course at the heart of the monitoring. The choice of GPS receiver largely defines the type of monitoring system to be used. For any deformation monitoring system however, the GPS receiver must have carrier phase measuring capability in order to permit the determination of high accuracy (cm-level) baselines.

- *Large scale continuous GPS networks* such as the SCIGN (California) and the GSI network (Japan) use top-of-the-line, dual-frequency GPS receivers. Power requirements and robustness in harsh environments are not such important concerns as these receivers are often housed inside buildings or structures with AC power. Very important is that the data collected by these stations must be of the highest quality, as they may contribute to the IGS network.

- *Small scale continuous GPS static networks* such as at Popocatépetl (Mexico) or the GeoForschungsZentrum (GFZ) system (Indonesia) also use top-of-the-line, dual-frequency GPS receivers. However, the design specifications suffer due to the high power demands of this style of GPS receiver, a particularly important issue when such stations have to be located in remote areas. Such designs often begin as first generation prototype systems, constructed from off-the-shelf components (see Figure 3.1).

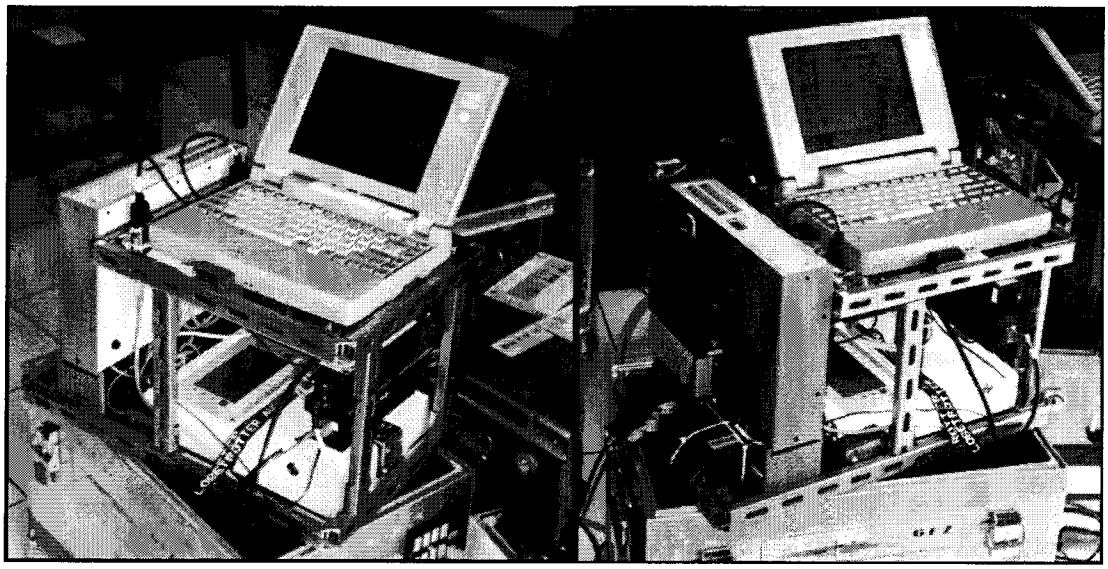

Figure 3.1 - *Small scale static GPS monitoring system on Gunung Guntur, Indonesia comprising Turbo-rogue GPS Rx, laptop computer, DSP modem and radio transceiver.*

- *Small scale continuous GPS RTK networks* such as the PMoS system setup on the Rabaul volcano (Lowry, 1997), or the Condor system (Condor, 2000), also use off-the-shelf packaged systems which cannot be easily customised to suit the particular conditions. These systems may use single or dual-frequency GPS receivers (which obviously impacts on the final cost of the system). The areal extent of the network

will generally be dictated by the range of the communications interface when sending the RTK correction messages, and the efficiency of the ambiguity resolution algorithm.

- *Small scale continuous GPS low-cost networks* typically imply the use of L1 measurements only. Examples include the UNSW system described in chapter 4, or the UNAVCO system deployed at Long Valley Caldera, California (USGS, 2001b). These L1-only receivers draw less power, which is a great advantage for remote locations. In addition, the lower cost of single-frequency GPS receivers makes them feasible for deployment in dense arrays to monitor movements across small areas; a situation ideal for active volcano deformation monitoring. OEM boards can be custom-mounted into ruggedised containers to suit extreme conditions. The scale of the network is restricted mostly by the impact of the unmodelled ionosphere on single-frequency data processing, particularly in equatorial regions and during high sunspot activity (see section 3.2.4). Specially developed software can also be implemented within such systems, but a high degree of expertise is needed to ensure that the completed system is reliable.

In summary, the particular GPS receiver chosen will be dictated by price, power usage, data quality, size, ruggedness and type of application for which it is intended. Accordingly, the instrument noise E_x of the GPS receiver chosen will be determined by the quality of the electronics.

3.1.2 Radio Communications, Data Logging and Archiving

A fundamental difference between a campaign-style GPS survey and a continuous GPS monitoring system is that, in the latter case, all data is automatically transferred to a base facility where it can be processed. The scale and budget of a particular type of monitoring system will determine the method and strategy of GPS data transferred from remote stations.

Differing approaches to radio communications & data logging

For a large scale system such as the SCIGN network, 24-hour data files are typically downloaded once per day via a telephone dial-up (some stations use the cellular phone

network) to a central computing facility. Data files received are automatically uncompressed, translated into the RINEX format (Gurtner & Mader, 1990), subjected to quality control analysis and transferred to archival media which are accessible via FTP and the Internet (Bock et al, 1997). This is also the case for the GSI network in Japan, where data is accessed from the sites via ISDN and public telephone lines on a daily basis. Previously, when the GSI network consisted of 610 stations, approximately one GByte/day of data had to be archived (Rocken et al, 1997). Nowadays the network is almost twice as dense. Clearly, the volume of data quickly becomes unwieldy and one must devote appropriate resources to data archiving.

The GeoForschungsZentrum PAGAS (Permanent Automatic GPS Array System) system is a small scale, high-cost volcano monitoring system with remote stations (see Figure 3.1). Data communications infrastructure must therefore be designed into the system to operate autonomously. One hour sessions are logged at all stations and an on-site laptop computer handles file management. 4 Watt UHF radios with directional Yagi antennas are used to routinely transfer data every hour to the base facility. Session files unsuccessfully sent from the remote stations remain on the remote laptop computers and can be re-sent later, preventing data from being lost due to communications problems. RINEX files are archived to a hard disk and sent to the GFZ for post-processing (Galas, 1997, personal communication).

Lowry (1997) describes a different approach to data communications used for the PMoS system. The RTK system, in this case using UHF half duplex radios, provides position results at the rover station. However, for a monitoring system the baseline results are required at the base facility. Consequently radio communications are effectively doubled as position results and some statistical data must be re-transmitted back to the base facility. Accordingly, power consumption is increased as the radio communications equipment typically draws the most power of all components. The raw GPS data can be logged at the base station to allow post-processing of the observations. The communications are sufficiently sophisticated to allow changes of the remote station parameters to be made from the base facility. The radio communications link must be line-of-sight.

The low-cost L1-only system designed by UNAVCO (see Figure 3.2) for small scale monitoring sends remote station data to the base facility using radio-modems configured according to a Time Division Multiple Access (TDMA) format. These are intelligent radios, which rather than sending logged data files, send GPS data epochs continuously according to predefined time slots. The base station receives binary data at a 10 second rate from all stations simultaneously and sorts the data into their respective addresses (Meertens, 1998). These data are then sent via a serial port connection to a processing computer. This negates the need for file management software at the remote stations but also requires a higher level of radio sophistication. The TDMA format therefore allows for operation as a small scale static monitoring system or a single-frequency, reverse RTK system. The remote stations can additionally act as repeater stations if data communications are interrupted for some reason and must be re-routed via a different path. This system requires that the radios operate constantly, thereby increasing the power usage. A base facility can handle up to 75 remote stations in one network, implying that the project budget is the major limiting factor when designing such a network.

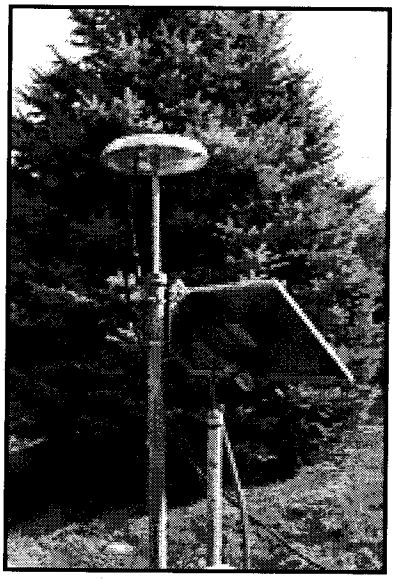

Figure 3.2 - *The compact UNAVCO GPS monitoring system (UNAVCO, 2001).*

The UNSW (see chapter 4), uses VHF radios with a separate transmit and receive frequency. The system is simple, low-cost and reliable and was designed to be modular (the radio system is separate from the GPS receiver) so that more/less powerful radios can be utilised for different applications and environments. The radios can be used for

static or reverse RTK systems, depending on the nature of the software implemented within the system. At Gunung Papandayan, one-hour binary files are sent every hour to the base facility where they are converted to RINEX files, and archived to a hard disk. Approximately 12 Mb of data per day, comprising 192 files, are archived at the base facility from this 4-station network. Being an L1-only system, the volume of data is significantly less than most other systems. A phone line connection to Bandung would be required to connect the system to the Internet for remote access.

For all of the above radio systems the possibility of interference of the radio signal is always present. It is advisable to conduct a radio propagation study of the subject region before deciding on the frequency and power of the radio communications equipment to be employed. Television/telephone repeater stations or microwave transmitters can cause interference for both the radio and GPS signals, and should always be avoided. The appropriate radio licence maybe required, depending on the transmitter power and the location of the network.

Archiving

The observed data from the remote GPS stations located on the deforming body and from the associated base station(s) should be archived for possible post-processing (even if only to verify a suspect solution). Continuous monitoring systems assemble the data from all stations at a central base facility. This base facility may sort the data into appropriate files, and perhaps automatically process the baselines. However, these results are only available at the base facility. How can this data be made available to various users?

The SCIGN network is connected to the Internet and publishes RINEX data and baseline results which can be accessed from anywhere in the world. The DefNet small scale static network on Popocatépetl transfers data from its remote base facility via a point-to-point radio link 60 km to Mexico City, where it is then connected to the Internet. UNAVCO systems have been recently installed at the Long Valley caldera, Hawaii, and the Popocatépetl volcano. Data is also transferred via radio links to Internet connections and archived in Boulder, Colorado.

The volume of data being archived is growing rapidly and one needs to ask how much data is necessary and for how long should it be kept? Volcano forecasting with the aid of GPS is a relatively new science and the behaviour of each volcano is unique. Historical data, such as a long time series, may provide valuable clues to the behaviour of a volcano. Conversely, nothing may happen for hundreds of years, leaving the vulcanologist with masses of useless data! To quote Johnson & Wyatt (1994), "It takes a long time to measure a signal which takes a long time to develop." Such is the nature of volcano science.

Another data archiving issue is the readability of the stored data. A vulcanologist may have little experience with GPS but just needs ground deformation results (and their accuracy) for volcano studies. The archived data should be easy to understand. A good example of this is the niche software from Condor, which processes GPS data and displays the results graphically (Condor, 2000). Archived data can be viewed in different screens, including an RTK mode and a time series history mode showing movement over a specified period of time. However, only RTK data is archived. It is not possible to process a session of data for a longer period, as raw GPS data is not recorded. There is therefore total reliance on the quality of the RTK solutions. The volume of archived baseline results is significantly smaller than in the case for the raw observation data.

3.1.3 Monumentation

Continuous monitoring systems avoid the problem of centring errors and height-of-antenna measurement blunders that can plague campaign-style GPS surveys. Establishing monuments once, at carefully selected sites, eliminates these blunders. These sites must be sufficiently stable to detect the desired deformation signal. It makes little sense to seek to measure a geophysical signal with a network of unstable ground marks. Similarly, it is equally important to locate monuments such that the desired signal will be detected, and not some local tectonic effect such as a microfault. Factors to consider when establishing monumentation include:

- skyview,
- station location sensitive to the deformation signal,

- stability of the ground,
- line-of-sight for radio comms link (depends on type of data transmission used),
- station location with regard to environmental factors (sulphur gas, wind, etc.) and vandalism,
- tectonic activity in the vicinity,
- radio disturbance,
- accuracy requirement of the monitoring system,
- ease of accessibility,
- flatness of site for ease of remote installation, and
- on-site facilities (ie AC power, shelter, phone line access, etc.).

The different types of monitoring networks typically utilise different designs for station monuments. A small scale, low-cost network with remote stations would require a stable point to a level of a centimetre or less. On the other hand a large scale network, perhaps connected to the IGS global network, requires a considerably more stable monument. These specifications of course impact on the cost of a system. Investigations have been conducted into the stability of monuments.

No monument can be considered perfectly stable. Because it is only possible to detect a geophysical signal using GPS techniques from the surface of the earth, then station locations will be affected by surface weathering; even in the case of monuments located in surface outcrops of bedrock. Investigations conducted by Wyatt (1982) revealed that for massive concrete and granite monuments housed in underground, temperature-controlled vaults, random movements of the order of ± 1mm $yr^{-1/2}$ were still occurring (Johnson & Wyatt, 1994).

Langbein et al (1995) characterises monument movement according to three error sources: a time-independent error related to the measurement noise, a seasonal component reflecting ground fluctuations due to varying ground moisture and temperature conditions, and a long-period time-dependent motion of the monument also due to ground conditions but Brownian in nature. The studies suggest that monuments embedded in bedrock outcrops may demonstrate a higher stability, however the upper surface of the bedrock will still be weathered and fractured causing mm level

movement. Deeply anchored monuments have been designed to reduce this top layer instability (Wyatt et al, 1989).

Bock et al (1997) describes deeply anchored monuments emplaced for the Southern California Integrated GPS Network. These monuments consist of sections of steel pipe driven into the ground until refusal (often as deep as 12m) comprising a vertical shaft and four oblique sections for bracing. The top section is further decoupled from the upper ground surface to reduce local disturbances. Langbein et al (1995) make a detailed comparison of the stability of deeply anchored monuments vs. monuments installed to depths of 2m (similar to those used on Gunung Papandayan, see section 4.3.1) using a two-colour EDM and 1.5 years of observations. It is indeed demonstrated that deeply anchored monuments provide greater stability.

In the case of the SWEPOS network in Sweden, originally designed to measure post-glacial rebound, 3m tall pillars mounted on bedrock are used. Due to the extremely cold conditions the pillars are insulated and surrounded by heating coils. Six pins surrounding the pillars act as recovery marks, and annual surveys are conducted with theodolite and prism to confirm the stability of the pillars. "In 30 months of operation, no significant motion of the pillars was detected" (Bifrost, 1996).

Figure 3.3 - *Continuous GPS SWEPOS station Joenkoeping. An example of a very stable, expensive monument (SWEPOS, 2001).*

A lower cost, but still a comparatively high accuracy monument design uses the Bevis pin (Hudnut, 1996). The Bevis pin is a 6" x 1" pin glued into a pre-drilled hole in bedrock. The accuracy of the mark is contingent on the quality of the surface bedrock to which it is affixed. A good understanding of the geology is therefore necessary. However, these marks were designed for campaign-style surveys only. Hence, while the mark itself demonstrates excellent stability it is not suitable for continuous systems because the only way to set up over these marks is by using a tripod and tribrach.

The GFZ also designed a similar pin, but included a screw thread on the top to allow an antenna to be directly attached. Careful installation of these marks negates the need for a tribrach, as the mark is emplaced in the level plane. These marks were originally designed for campaign-style surveys to eliminate height and centring errors, but they do suffer from multipath problems and it is often difficult to find a truly clear skyview. These marks are mounted at pillars on the GFZ Guntur network.

Berntsen International Inc. (Berntsen, 2001) manufactures a 3D-control monument that is low-cost and relatively stable. Aluminium sections are driven into the ground surface until refusal, and a plastic sleeve surrounding the upper section, filled with grease, de-couples the aluminium rod from the less stable upper layer. The measured movement of the mark will then be the movement of the lower sections, which are firmly and deeply mounted (see section 4.3.1).

The error term δX_{monu} has been included in equation 3.1 (see section 3.2) to accommodate errors due to monument movement which could range from sub-millimetre for deeply anchored monuments to sub-centimetre for low-cost networks.

3.1.4 GPS Antennas

As GPS technology has matured, many different types of GPS antenna designs have been used over the years. Antenna designs range from very low-cost, single-frequency vehicle tracking antennas, to high-end, geodetic standard, dual-frequency, choke-ring antennas. The considerations for antenna design include (Parkinson & Spilker, 1996):

- The gain pattern with respect to the azimuth and elevation of the incoming signals.

- Multipath rejection.
- Phase stability and repeatability.
- Size & profile.
- Interference rejection.
- Environmental conditions.

Some of these considerations can be dealt with together. For example, designing a gain pattern that excludes low elevation satellites can also reduce interference and multipath, which are typically greater at low elevations. GPS signals are righthand circularly polarised (RHCP), however multipath effected signals will be lefthand circularly polarised or linearly polarised. Designing the antenna gain pattern to optimise only the reception of RHCP signals will further reduce multipath (see section 3.2.2).

Although many different types of antenna designs exist, most common GPS antennas nowadays comprise a microstrip patch to receive the GPS signal. Microstrip antennas are simple to construct, rugged and small. They can be designed to receive single or dual-frequency signals (although dual-frequency patch antennas use a wider bandwidth, which increases noise). It is also possible to use two patch antennas, one tuned to L1 and the other to L2, and mount them in the same antenna. They do, however, have a relatively low gain pattern, which therefore requires the implementation of a low noise preamplifier (Wells et al, 1987).

Much research has been conducted on the effects of using an antenna groundplane to reduce multipath. A plate placed underneath the antenna base can improve the performance of a GPS antenna, particularly in high multipath environments. The purpose of the groundplane is to stop reflected signals from corrupting direct signals measured at the electrical phase centre (see Fig. 3.4 or Fig. 2.6). Various styles of groundplanes have been used by GPS manufacturers. Testing with a large groundplane made of microwave absorbing foam has also been conducted at UNAVCO, although with limited success (Solheim et al, 1996).

Perhaps the most effective, and indeed the most expensive, groundplane design is the choke-ring. Concentric rings of brass mounted on a circular base surround a microstrip

patch located flush with the plane of the rings. This style of antenna has proven to be very stable in terms of multipath protection and phase centre stability. It is now used as the reference antenna for all antenna phase centre calibrations, and is the standard antenna used by the IGS in their global network. Such an antenna would only be suitable for use in a large scale deformation monitoring network or a high quality (and high cost) small scale network.

An additional problem with the choke-ring antenna has been experienced in the SWEPOS network (Hedling & Jonsson, 1996). Heavy snowfall is caught in the rings of the antenna groundplane, which affects the measured signal and changes the position of the electrical phase centre. Small conical fibre-glass radomes were mounted over the antenna pillars to protect the antennas from accumulated snowfall, however these radomes also led to changes in the location of the electrical phase centre. Various radome designs have been tested at UNAVCO in order to establish the best radome design, and corresponding APCV model (Braun et al, 1997).

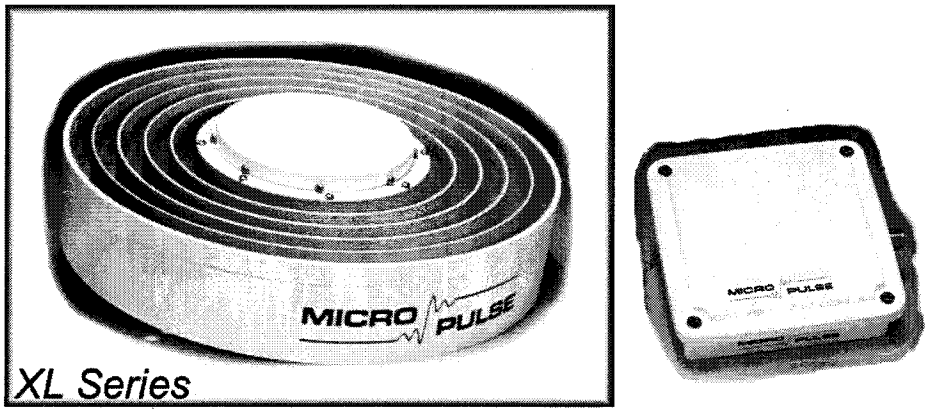

Figure 3.4 - *Choke ring antenna vs. low-cost antenna. (Approx. cost $5000 vs. $500)*

For a low-cost network, the reliability of the GPS antenna used will have a major impact on the resultant accuracy of the system. A compromise between cost and quality needs to be made. Section 4.6.1 lists some of the considerations that need to be taken into account when selecting a suitable antenna. Equation 3.1 (section 3.2) includes the error term δX_{APCV} which refers predominantly to the antenna phase centre variation of a GPS antenna (see section 3.2.1). The stability of an antenna is related to the quality of the hardware and therefore reference is made to this term here.

Low-cost antennas can also be enhanced by the addition of a groundplane to reduce noise due to multipath error in the observations. Meertens (1998) demonstrates a significant improvement in data quality by equipping a MicroPulse 13700 L1 lightweight survey antenna with a "Frisbee" groundplane (see Fig. 3.2). This is a low-cost hardware enhancement. The error term δX_{multi} accounts for errors due to multiapth in equation 3.1 (see section 3.2). Another approach adopted for the UNSW system is to accept that multipath will be present in the data, and to deal with it during post-processing. Sections 4.6.2 and 6.3.1 describe this digital signal processing approach.

3.1.5 Power Supply

It is preferable to power continuous GPS stations using AC power where possible. Often this becomes a major limiting factor in network design, particularly for large scale monitoring systems where the power requirements are larger and hence the need for AC power is more acute. By definition, the AC power supply must be continuous to satisfy the specifications of a continuous GPS monitoring system. This can not be always guaranteed, especially in less developed countries. A backup power supply such as an uninterruptable power supply (UPS) can protect against power surges or spikes, and will automatically and seamlessly switch on in the event of a power blackout. A UPS supplies power from attached batteries, which are continuously charged during normal operation. The batteries must have sufficient capacity to cover blackouts characteristic of the locality.

Another simple solution would be to power the system direct from a battery, which is in turn charged by a battery charger connected to the AC power. Although this approach also guards against surges and spikes, charging and discharging a battery simultaneously is not good for the longevity of a lead-acid battery.

The power system at a remote station is essentially the same as the system described above except that the battery charger can be replaced by solar panels. A solar power regulator must also be included in this configuration. Often voltages of up to 19V DC are generated by the solar panels, and this must be stepped down to a less damaging level for battery recharging (see section 4.2.4.5).

An important consideration for a remote station is the power requirements of the system. If the individual components, such as the GPS receiver, radio, computer require less power, then the size of the battery bank and the solar panels can be reduced, therefore lowering the cost. Generally speaking, there is a direct relationship between the power requirement and quality of the GPS components, ie dual-frequency receivers are more expensive and require more power to run, while single-frequency receivers use less power.

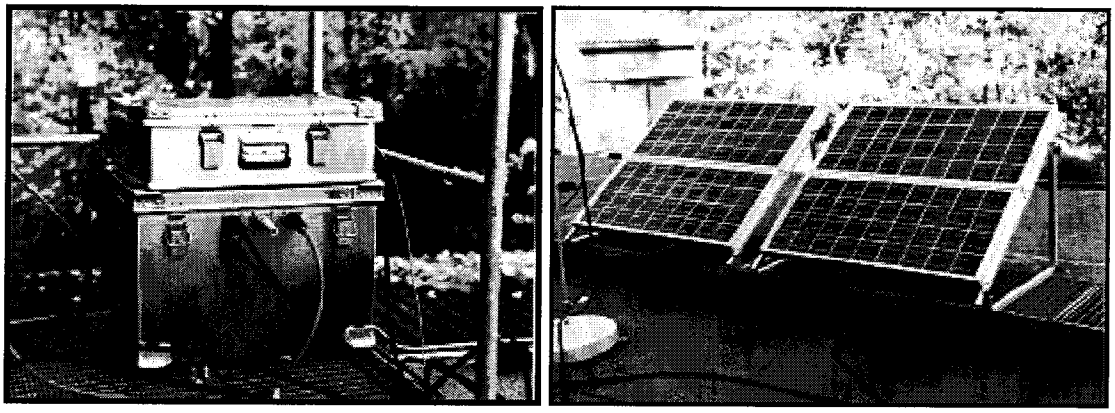

Figure 3.5 - *Battery bank and solar panels for recharging on Popocatépetl, Mexico (UNAM, 2001b).*

3.1.6 Environmental Considerations

Depending on what type of monitoring system is to be deployed, the environmental conditions may vary considerably. Furthermore the environmental considerations may vary from point to point within a network. A volcano will always be a harsh environment in which to operate. A monitoring system must be appropriately designed to deal with such extreme conditions. Often a larger scale network will house the monitoring stations more securely, protecting the system from concerns such as:

- Operating instruments in extreme heat (from the weather above and the surface below the volcano).
- Operating instruments in extreme cold.
- Sulphur gas corrosion.
- Solar conditions for solar panel recharging.
- Lightning protection.

- Wind, rain, monsoon conditions.
- Vandalism and damage by animals.

All electronic instruments have a recommended temperature range in which they operate. On the slopes of an equatorial volcano, the temperature in the sun may be as high as 60°C. Usually instruments are mounted inside some sort of protective box, and inside the box the temperature could be even higher. Added to this is the heat which may be radiating from the ground of an active volcano, and the heat produced by the instruments themselves, and it's clear that keeping the instruments cool during their operation is a significant challenge. Conversely, volcanoes on the Kamchatka Peninsula, or stations on the Swedish SWEPOS network, experience a host of cold temperature problems. Radomes may have to be mounted over antennas to guard against snow build up. Instruments have to remain warm enough to still operate, and batteries perform less efficiently in colder climates.

Around many volcanoes (Gunung Papandayan for instance) sulphur gas is constantly spewed out of fumaroles and gas vents. Sulphur gas is extremely corrosive and will aggressively attack metal objects. When working in such environments it is advisable to design components from materials such as aluminium or fibreglass which resist these acidic gases, or locate stations away from high concentrations of sulphur gas.

Autonomously operating remote GPS stations rely on power from batteries recharged by solar panels. When designing the power system it is important to consider how much sunlight will be incident on the region annually, and to then determine how large the solar panels should be. Rain, dust and cloud cover will also influence the power output (see section 4.2.4). A volcano, by virtue of its shape and size, will attract lightning. Therefore, the GPS antenna cable and radio antenna cable needs to include some form of lightning protection to avoid any damage to the electronic componentry.

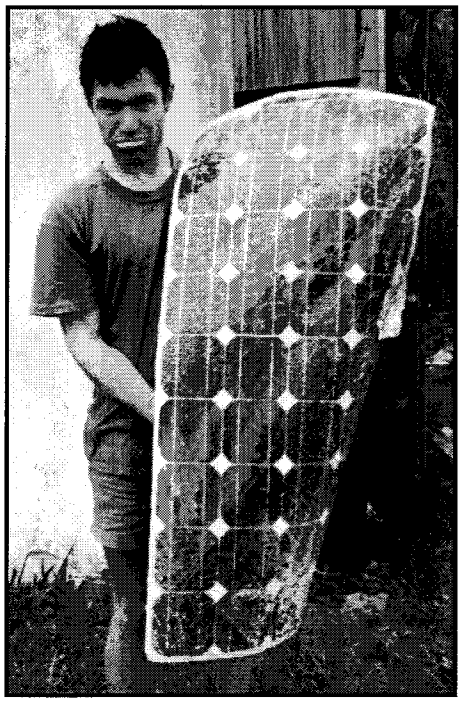

Figure 3.6 - *Strong winds can destroy solar panels. The author at Papandayan.*

Other environmental factors, such as the presence of strong winds in the locality (which may damage solar panels - see Fig 3.6), heavy rains causing erosion around a remote station location, or even the monsoons need to be taken into account. Some monitoring systems are located in tourist destinations and the threat of vandalism is therefore increased. Native animals could also damage the system by gnawing through cables. Protection against all of these factors needs to be considered in order to ensure the longevity of such a monitoring system.

3.2 Error Mitigation

Error mitigation strategies for GPS surveying have been developed and improved over the last 15 years or so. Depending on the type and number of observations taken, and the accuracy required for the system, different approaches can be used to ensure high accuracy resultant baselines. Section 3.1 has described the basic hardware choices available for all monitoring systems. The hardware chosen is closely related to the error budget. The following section briefly describes the major error sources affecting GPS, regardless of scale of network, location or accuracy requirement.

Error Budget for a GPS Monitoring Network

A general formula to describe the positioning error of a GPS monitoring network is equation 3.1:

$$X_P = X_{to} + \dot{X}\,\Delta t + \delta X_{APCV} + \delta X_{multi} + \delta X_{trop} + \delta X_{ion} + \delta X_{orb} + \delta X_{monu} + \delta X_{amb} + E_x$$

Where the position X_p of point p is influenced by:

$\dot{X}$	geodynamic velocity vector,
Δt	time between present and date of computation of starting coordinates,
X_{to}	initial position at epoch t_o (see 3.2.6),
δX_{APCV}	antenna phase centre variation (see 3.1.4, 3.2.1 & 4.6.1),
δX_{multi}	multipath (see 3.1.4 & 3.2.2),
δX_{trop}	tropospheric delay (see 3.2.3 & chapter 5),
δX_{ion}	ionospheric delay (see 3.2.4),
δX_{orb}	satellite orbit bias (see 3.2.5),
δX_{monu}	stability of monuments (see 3.1.3),
δX_{amb}	incorrect fixing of integer ambiguities (see chapter 6),
E_x	instrument noise (see 3.1.1 & chapter 6).

Table 3.1 lists the approximate magnitudes of the error sources and the impact of these on the position solution. Note that the errors δX_{multi} and δX_{amb} could be zero.

The error sources for all GPS-based volcano monitoring systems are discussed in more detail, in the following sections of this thesis. Section 4.6 describes the specific error mitigation strategies adopted for the UNSW volcano monitoring system.

Table 3.1 - *Magnitude of errors on GPS monitoring systems.*

Error Source	Expected magnitude
Geodynamic velocity vector	Up to a few cms/year.
Δt	Up to a few years.
X_{to}	Absolute accuracy better than 10 cms.
δX_{APCV}	When mixing antennas: Horizontal sub-cm, Vertical up to 10 cm.
δX_{multi}	Carrier phase up to 5 – 6 cm.
δX_{trop}	Unmodelled 2m in zenith: Modelled cm level between stations. Differential troposphere up to 20 cm vertical.
δX_{ion}	Unmodelled 20m in zenith: Modelled dm level between stations increasing with baseline length.
δX_{orb}	Short baselines, broadcast ephemerides, sub-cm level. Longer baselines, precise orbits, sub-cm level.
δX_{monu}	Sub-cm for low cost marks, mm level for high quality monuments.
δX_{amb}	Up to dm level.
E_x	mm level.

3.2.1 Antenna Phase Centre Variation

Antenna phase centre variation (APCV) has been identified as a systematic bias which must be addressed for high precision GPS geodesy. For most GPS antennas the physical centre and the so-called electrical phase centre do not coincide. The electrical phase centre can be thought of as the point to which the incoming GPS signals are measured for one particular epoch, for the current constellation of satellites. However, this point is usually not coincident with the physical centre of the antenna, ie the point plumbed over the mark (by whatever means) for a GPS survey.

The electrical phase centre of the antenna will also move with changing azimuth and elevation of the GPS satellite signal. Furthermore, the APCV patterns between the incoming L1 and L2 signals differs (Meertens et al, 1996). Therefore the electrical phase centre offset and variation for any linear combination of the L1 and L2 phase measurements will also be different.

There are two components of APCV, and both can be determined empirically. The first is a mean offset consisting of north, east and up components of the electrical phase centre with respect to the physical phase centre. This could also be thought of as a three dimensional vector. The north and east components can be determined through antenna rotation tests. Ground truth data between antenna stations is required in order to determine the up component. Another method is simply to swap antennas between sessions. This offset can also be determined using an anechoic chamber, but this requires considerably more effort.

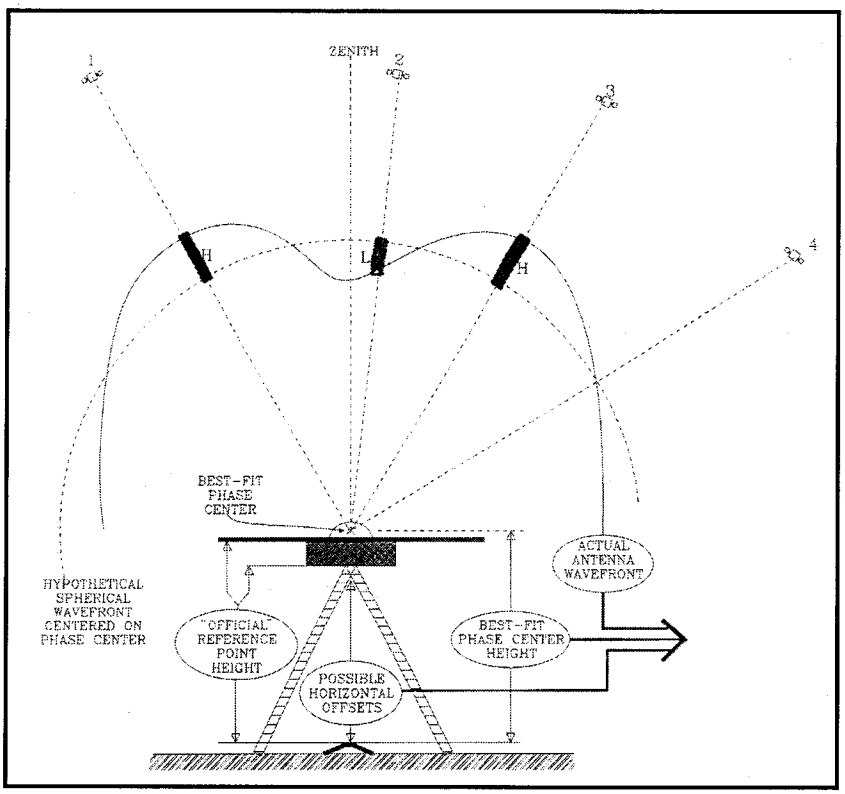

Figure 3.7 - *Antenna Phase Centre Variation components (Clark & Schupler, 1996).*

The second component of APCV changes depending on the elevation angle of the satellite (see Fig 3.7). This correction is variable and is more easily determined in an anechoic chamber because the single point source antenna in the chamber simulates just one satellite. Estimating this variable APCV with GPS field data is always complicated by the fact that more than one satellite is observed for any epoch. Therefore, the APCV will be caused by a mixture of zenith angles from the different satellites observed at the same time. Table 3.2 shows a standard APCV table for the Trimble TR GEOD L1/L2

GP Mod. 22020 type antenna. The offset and zenith dependent components can be more clearly understood by referring to such tables.

For a baseline or network, the problem of APCV between antennas needs to be addressed. Schupler et al (1994) states that when considering microstrip patch antennas (the most popular type of antenna), "...variations among antennas of the same make and model are not significant for geodetic measurements". However, "antennas of a different design, ie not microstrip patch antennas (make and model still the same) may not be as repeatable from unit to unit." From this it can be inferred that microstrip patch antennas of the same make and model display essentially the same APCV patterns. However, the position of the electrical phase centres of antennas of a different make and/or model vary for the same constellation of satellites. Clearly, when mixing antenna types, it may result in a biased baseline solution.

Errors of up to 10 cm in the vertical have been encountered and attributed to this phenomenon (Rocken, 1992). Subsequent studies by Schupler et al (1994) and Rocken et al (1995) have endeavoured to confirm and model this variation.

Antenna testing has been carried out by various institutions since the early 1990s in an attempt to model this variation. The IGS has adopted a standard APCV for certain geodetic quality antennas. A north, east and up component describes the phase centre offset, and a table of zenith angle vs. up component is used to model the variation for both the L1 and L2 signals. It is assumed in this approach that the north and east components do not move appreciably with changing zenith angle, and also that the azimuth of the satellite has a negligible effect on the location of the phase centre. The IGS does not endorse APCV models for single-frequency antennas. The US National Geodetic Survey (NGS) also compute antenna phase centre variation tables.

Table 3.2 - *Example of a phase centre variation table used for correcting GPS data during processing illustrating the N, E & up component and the zenith dependent variation (NGS, 2001). Note values in square brackets refer to zenith distance. All dimensions in millimetres.*

TRIMBLE		TR GEOD L1/L2 GP				Mod. 22020		(13) 96/06/30	
[N]		[E]		[up]					
1.5		-1.2		75.1					
[0]	[5]	[10]	[15]	[20]	[25]	[30]	[35]	[40]	[45]
[50]	[55]	[60]	[65]	[70]	[75]	[80]	[85]	[90]	
0.0	1.8	4.6	8.1	11.7	14.5	16.1	16.9	16.9	16.2
14.9	13.4	11.9	10.4	9.0	7.9	8.2	0.0	0.0	
-1.1		1.7		69.2					
0.0	0.3	0.9	1.8	3.0	4.1	4.9	5.4	5.6	5.6
5.3	4.5	3.6	2.8	2.1	1.2	0.1	0.0	0.0	

The differing methodologies used to determine the APCV model are described below.

3.2.1.1 Anechoic chamber tests

Testing in an anechoic chamber allows one to test a GPS antenna in a controlled environment. However, considerably more effort is required to collect chamber measurements as compared to GPS field data collection (Rothacher et al, 1995). A single fixed point source transmitter simulates a GPS satellite signal for both the L1 and L2 carrier frequencies. The GPS antenna is mounted on a rotating positioner which can be manipulated to simulate changing azimuth and elevation angles.

The position of the mean phase centre is first determined by minimising the APCV for a few different azimuths over a full range of zenith angles. The GPS antenna is shifted - with respect to the physical centre - to this new mean phase centre position. The variable APCV can now be determined by measuring the phase centre variation for a range of zenith angles and azimuths (usually every 5 degrees). Schupler et al (1994) describes the exact procedure followed.

An advantage of chamber tests is that the entire range of antenna-signal angles, in both azimuth and elevation, can be tested without the restriction of satellite visibility. Ibid (1994) also introduces the concept of azimuthal symmetry. Comparing the phase patterns of a Dorne-Margolin choke-ring antenna with that of an Ashtech antenna with attached groundplane, it was shown that the Dorne-Margolin antenna phase pattern is the same regardless of azimuth; ie it displays azimuthal symmetry. This was not the case for the Ashtech antenna. In addition, Braun (1998, personal communication) confirms that the phase centre variation from these chamber tests results in a change to the vertical component vs. zenith angle only. Because of multipath, it is probably reasonable to use only an elevation dependent correction (ie to average over all azimuths). The APCV model published by the NGS reflect these assumptions (see Table 3.2).

3.2.1.2 Antenna phase centre variation using GPS data

The APCV model can be determined from antenna rotation tests using GPS data, thereby eliminating the need for anechoic chamber tests. However, only the differences between antenna APCVs can be derived from GPS. Rothacher et al (1996b) describes a GPS campaign designed to determine the APCV model from GPS data. A variety of antennas were used to log GPS data for four 24-hour sessions. For the first session, all antennas were aligned north. In the second session, all antennas were aligned south, except the two reference antennas. All antennas (except the two fixed antennas) were then swapped between pillars and aligned north, while for the final session, all non-fixed antennas were orientated south.

The processing was a two-stage task: 1) the mean antenna phase centre offset is estimated, and 2) using this new position, the elevation and azimuth dependent APCV is estimated. The Bernese GPS software was used for the processing. Rothacher et al (1996a) describes in detail the processing steps that were followed. An elevation cut-off angle of 20° was used to mitigate multipath, under the assumption that most multipath is caused by low elevation satellites. The antenna phase centre offsets were estimated together with the site coordinates. Because the antennas were rotated between sessions, any phase centre offset will be effectively doubled between sessions. All site coordinates therefore were constrained in all components to within 3 mm to the ground

truth values. All the horizontal offsets were then freely estimated except for the two reference stations which were not rotated between sessions. All vertical offsets were constrained to 5cm.

Determining an azimuth and elevation dependent APCV model is not so straightforward. Rothacher et al (1995) has estimated the coefficients of a spherical harmonic expansion of the APCV model. For most applications however, the assumption of azimuthal symmetry for antennas is valid, requiring that only the elevation dependent term be estimated. In order to determine such an elevation dependent APCV model, the station height component must be fixed to its ground truth value. This procedure only yields the differences between antenna phase variations, and all variations are estimated with respect to a different antenna which is rotated with the pool, ie a non-fixed antenna.

3.2.1.3 NGS approach

In contrast to the approach of double-differencing of field observations used in the above technique, the antenna calibration procedure followed by the NGS uses single-differencing and high quality oscillators to determine the relative phase centre position and phase variations of a series of test antennas, with respect to a reference antenna (Mader & MacKay, 1996).

The reference antenna used for these calibration measurements is a Dorne-Margolin choke-ring antenna type T as used in the chamber tests. This is the antenna used with Turbo-rogue receivers, and is in use throughout the global network of the International GPS Service.

A Dorne-Margolin choke-ring antenna, identical to the reference antenna, is placed on the test pillar in order to determine the location of this antenna's L1 and L2 phase centres on this pillar. These positions are then used as the a-priori positions for the L1 and L2 phase centres of the test antennas. The displacements that are found from the test antenna solutions then give the test antenna phase centre locations relative to the reference antenna.

3.2.2 Multipath

Multipath is a significant disturbance of the GPS signal. At the receiving antenna, the GPS signals are susceptible to reflections from materials surrounding the antenna, resulting in a received signal constituting both direct and indirect components (Fig 3.8). This effect is known as multipath, ie multiple paths of the desired signal are received at the antenna. Of course during the signal processing phase, only one signal, corrupted by the superposition of the direct and indirect signals, will be measured. The challenge is then to determine if indeed this signal has been affected by multipath, and if so, by how much.

Pseudo-range measurements are more affected by multipath than carrier phase observations. Differences in the range of 10 - 20 m between epochs could be expected, and as much as 100 m near buildings for pseudo ranges (Hofmann-Wellenhof et al, 1994). On the other hand, the carrier phase multipath does not exceed ¼ of the wavelength, ie 5-6cm (Rizos, 1997a).

Because the troposphere, clock errors and relativistic effects influence pseudo-range and carrier phase observations by the same amount, multipath can be estimated by using a combination of L1 and L2 code and carrier phase measurements. This is not strictly correct because ionospheric refraction and multipath are frequency dependant, meaning that L1 and L2 signals will be affected by different amounts. Forming the ionosphere-free pseudo-range and carrier phase double-difference combinations will eliminate this ionospheric bias (see section 3.2.4), leaving only multipath (and some instrument noise) as residuals.

The changing geometry of the satellite constellation with respect to the antenna will in turn change the angle of incidence and reflection of the indirect signal. This change will manifest itself in the solution residuals as a sinusoidal. The multipath effect is therefore a function of satellite elevation angle, distance of the antenna from the reflecting surface (either horizontal or vertical) and an attenuation factor. A derivation of this geometric relationship is given in Appendix A. Much research has been conducted in an effort to map these regular sinusoidal multipath signatures, and to then eliminate them from the double-differenced residuals. The period of these patterns generally varies from a few

minutes to up to 30 minutes depending on satellite elevation and distance from the reflecting surface. Signals from low elevation satellites are more susceptible to multipath from the ground surface than from high elevation satellites.

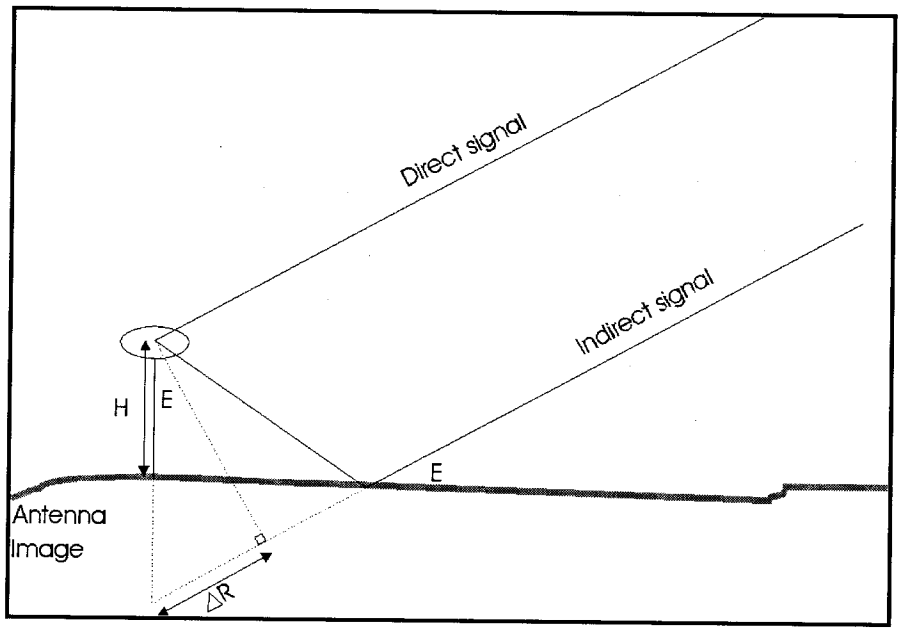

Fig 3.8 - *The effect of multipath showing reflection from a horizontal surface.*

Multipath is a difficult effect to predict and/or to correct for. It can be present at one receiver station of a baseline and not the other. Furthermore it cannot be eliminated by 'data differencing'. Multipath error mitigation is therefore an important consideration for GPS surveying. Perhaps the best method for reducing multipath is careful site selection eg, choosing a site distant from buildings and other reflecting surfaces. Steel objects scattered on the ground around the antenna, water surfaces and even rocks (particularly when they are wet) are potential reflectors. Ironically, ground planes designed to reduce multipath can, at some angles, also produce multipath of their own.

GPS signals are right hand circularly polarised (RHCP). Upon reflection, this polarisation reverses to a left hand circularly polarised signal. Antennas tuned to be more sensitive to receiving RHCP signals will therefore only receive the direct signal, effectively reducing the total multipath. This, of course, is not the whole story. Signals that reflect twice will be received (as they would have changed back to a RHCP wave after the second reflection). In addition, such antennas cannot actually filter out all left hand circularly polarised signals. Other methods of multipath mitigation include digital

filtering (narrow correlator and Strobe correlator technology), wideband antennas and radio frequency absorbent antenna groundplanes, as well as choke-ring antennas. Taking observations at a site for more than 15 minutes can also average out multipath effects (Rizos, 1997a). All of these approaches have only limited success and no single method is capable of *eliminating* all multipath disturbances. Section 4.6.2 details another approach to multipath mitigation using digital signal processing techniques, as used for the UNSW volcano monitoring system.

3.2.3 Troposphere

Atmospheric refraction induces an effective delay on GPS radio signals as they pass through the troposphere. The troposphere can be defined as the neutral (or non-ionised) part of the atmosphere extending to a height of approximately 40km (Fig 3.9). Strictly speaking, the neutral part of the atmosphere extends to the top of the stratosphere (80km in height), however the dominant effect of tropospheric path delay on radio signals occurs in the lower part only (typically below 15km).

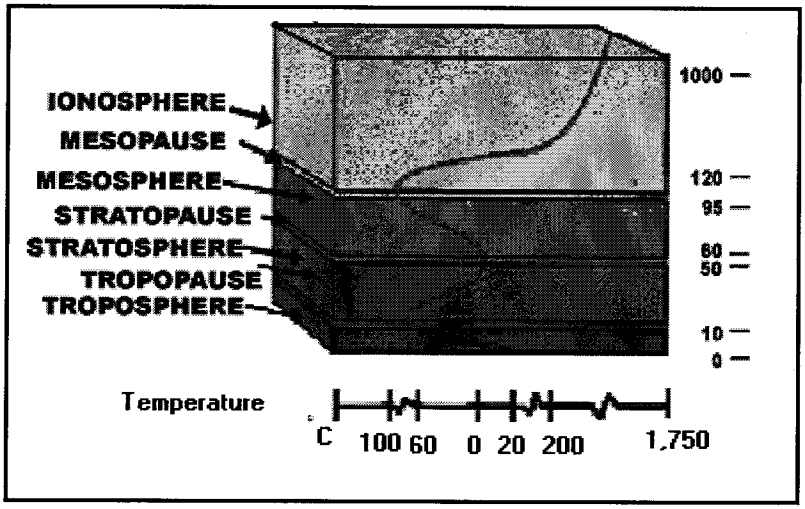

Figure 3.9 - *Atmospheric layers from the ground surface showing the troposphere with relation to the ionosphere and the change in temperature with height (km) (NASA, 2001).*

The neutral atmosphere is a non-dispersive medium with respect to radio waves up to frequencies of 15GHz, and thus the propagation is not dependent on frequency (Hofmann-Wellenhof et al, 1994). This means that the dual-frequency strategy

employed to eliminate ionospheric bias cannot be utilised to correct for tropospheric delay (see section 3.2.4). The L1 and L2 carrier phase and carrier modulation signals are delayed equally (Brunner & Welch, 1993).

The tropospheric delay can be conveniently split up into two components: the wet component and the dry component. The dry component contributes about 90% to the total tropospheric delay. A strong relationship between pressure, temperature and refractivity for the dry component exists, and this component of the tropospheric delay can be estimated to a precision of about 1% (Rizos, 1997a). The wet component contributes the remaining 10% of delay, but is more difficult to estimate due to the dependence on the water vapour pressure (difficult to measure). Ibid (1997) suggests errors of 10-20% are common when estimating the wet component.

The tropospheric path delay at sea level, in the zenith direction, is about 2.3m, and for the same point near the horizon is typically between 20 - 30m. Obviously, the path delay at the horizon is longer as the signal must pass through more atmosphere, and is therefore delayed more. In addition the troposphere will cause the ray path to curve. This curvature is zero at the zenith and less than 1cm at 15° elevation. This correction is incorporated into the formulae for modelling the delay and therefore will not be considered further (Brunner & Welch, 1993) (see section 5.2.4). Tropospheric propagation effects are therefore not a problem for GPS navigation and low-accuracy positioning. However, for geodetic positioning these propagation effects can be a severe limitation.

The effect of not considering the tropospheric delay during baseline processing will mostly be in the estimated vertical component. Various strategies can be used to account for the tropospheric delay. Tropospheric models based on established physical characteristics of the atmosphere can be employed to correct for the delay. Popular models include the Hopfield, Modified Hopfield or Saastamoinen models, but many other models for specific applications have been developed. All commercial GPS baseline processing software use one of these models. For short to medium length baselines (ie up to 15 km) the data between two sites can be differenced (ie ignoring the effect of the troposphere), thereby reducing or eliminating the tropospheric delay, under

the assumption that the GPS signal passes through an almost identical atmospheric column.

This assumption usually valid for points in the mid-latitudes, and when approximately at the same receiver elevation. For the volcano monitoring application however, where a large difference in height between receivers exist, some of the assumptions underlying these models may no longer be valid. This issue is investigated further in chapter 5 with reference to the UNSW volcano monitoring project.

For high precision surveys, an additional parameter can be introduced into the least squares reduction of the observations to estimate the residual tropospheric delay (after modelling). This approach is usually reserved for longer baseline lengths, however Abidin et al (1998) suggests that parameter estimation must be used to deal with the effects of differential troposphere in volcano monitoring applications. Such an approach must be used with caution however, as introducing too many parameters into an adjustment will smear the residual error source across all the estimated parameters in an erratic fashion. The full effect of a tropospheric delay may be dispersed into other similar parameters, particularly the vertical component.

A water vapour radiometer (WVR) can be used to directly measure the water vapour along the ray path of the satellites being tracked. WVRs are cumbersome and expensive. This is a little used, albeit very accurate, solution to the problem of tropospheric delay mitigation. Solheim (1993) comprehensively describes the use of WVRs for tropospheric estimation.

3.2.4 Ionosphere

The ionosphere is the band of atmosphere extending above the troposphere from about 50 km up to around 1000 km above the earth's surface (see Fig 3.9 – note the mesosphere is included as part of the ionosphere). Ultraviolet (UV) radiation from the sun ionises gas molecules in this layer, which release electrons. These free electrons in the ionosphere influence the speed, direction and polarisation of microwave signals as they propagate. The largest effect is on the speed of the signal, and hence the ionosphere primarily affects the measured range (Rizos, 1997a). At the zenith, the magnitude of the

ionospheric delay on range may be as much as 50 metres, and is approximately 3 times greater at the horizon than in the zenith direction.

At GPS radio signal frequencies, the ionosphere is considered a dispersive medium; that is, the refractive index is a function of the signal frequency (Parkinson & Spilker et al, 1996). Therefore for dual-frequency GPS measurements the L1 and L2 signals will propagate at different velocities through the same column of atmosphere. Seeber (1993) expresses the first order approximate refractive index of phase as:

$$n_p = 1 - \frac{40.3 n_e}{f^2} \qquad \text{- (3.2)}$$

where:

n_p - refraction coefficient of ionosphere for phase

n_e - electron density through the column of ionosphere

f - frequency of the propagating signal

The refraction coefficient for pseudo-range n_g:

$$n_g = 1 + \frac{40.3 n_e}{f^2} \qquad \text{- (3.3)}$$

Note that these relations are identical except for a change in sign. This difference can be conceptually explained as the measured pseudo-ranges being 'too long' therefore requiring a negative correction, and the carrier phase measurements being 'too short' compared to the geometric distance between the satellite and receiver. These biases are otherwise referred to as "phase advance" and "group velocity delay". (The range is called group velocity because it refers to ranging codes with different frequencies to the carrier.) The relationship between velocity and refractive index is given as:

$$v = \frac{c}{n} \qquad \text{- (3.4)}$$

where c is the velocity of electromagnetic radiation in a vacuum (m/s). Therefore if the refractive index is larger than one, the resultant velocity will decrease as is the case for ranging (and the opposite is true for phase).

In contrast to the troposphere discussed earlier, the variability of the ionosphere is much higher both spatially and temporally, and is therefore more difficult to model or account for. Note from the equations above that the electron density n_e along the signal path must be known. This is expressed as the number of free electrons per square metre (el/m^2) referred to as the Total Electron Content (TEC). One TEC unit is equal to 1 x 10^{16} el/m^2, and values of TEC range from 10^{16} to 10^{19} el/m^2 along the radio signal path. More specifically, TEC can also be expressed as slant TEC (STEC) along the signal path and vertical TEC (VTEC), the vertical component only of the TEC. The daily variability of the ionosphere from its monthly mean value can be up to ±20 – 25%. Generally, the diurnal ionospheric delay is five times larger during daylight hours, with a maximum two hours after solar noon and a minimum just before sunrise. Spatially, the ionospheric delay is highest along a belt approximately ±30° either side of the magnetic equator and in polar regions. The mid-latitudes experience the least effects from ionospheric disturbances (see Fig 3.10).

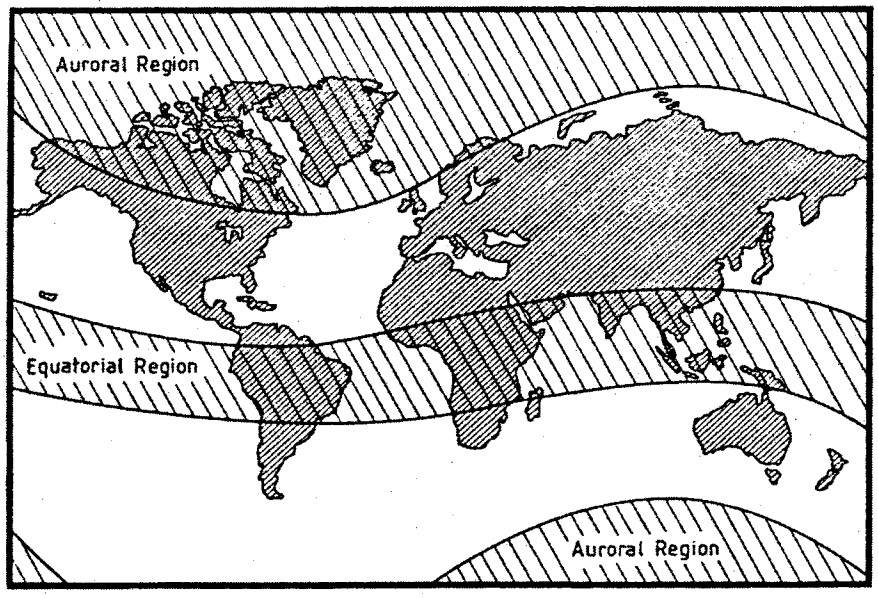

Figure 3.10 - *Regions of the world with high ionospheric activity (Seeber, 1993).*

An 11-year solar cycle (due to sunspot activity) also directly influences the behaviour of the ionosphere (Fig 3.11). The current solar maximum is 2000 - 2001. Periods of solar

maximum increases the occurrence of rapidly varying ionospheric disturbances, which will affect the quality of GPS surveys.

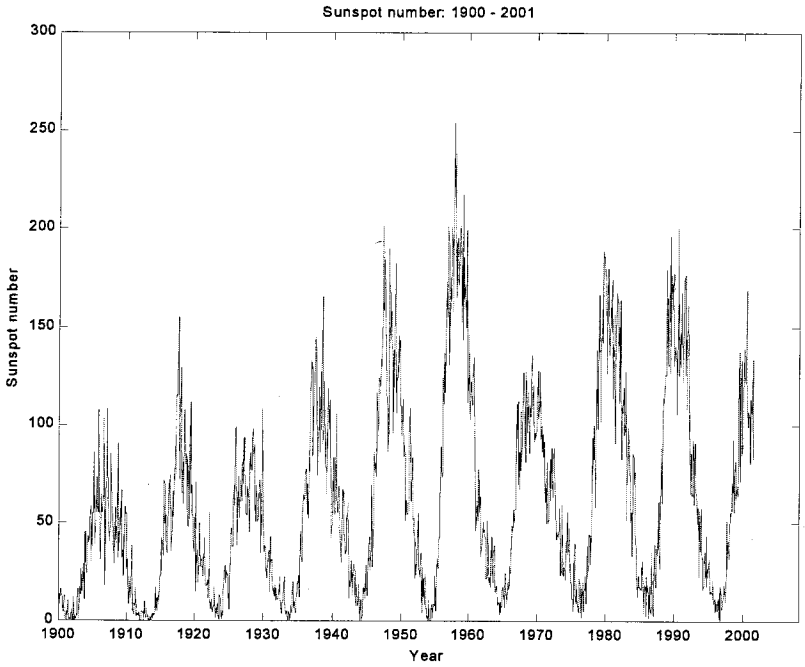

Figure 3.11 - *History of solar cycles.*

Short-term changes in the TEC values along the signal path can lead to ionospheric phase scintillation effects. If the ionosphere produces a phase change faster than the receiver bandwidth can allow, a GPS receiver can lose lock on the signal, resulting in a cycle slip. During periods of high ionospheric activity, eg during a solar maximum, ionospheric cycle slips are frequent. Cycle slips can also be a function of the tracking loop stability. It has also been noted that equatorial scintillations occur most frequently in the period approximately one hour after local sunset until approximately midnight (Klobuchar, 1991).

3.2.4.1 Ionospheric effects for GPS users

For single-frequency GPS point positioning there is little that can be done to account for the ionospheric range errors to centimetre precision (as large as 30m in the zenith direction and scaled up to three times this value for low elevation satellites). The Klobuchar ionospheric correction model (Klobuchar, 1987) is broadcast on the GPS

satellite message and is generally assumed that it can account for around 50% of the ionospheric delay at mid-latitudes. It is also possible to apply a correction derived from the International Reference Ionosphere (Bilitza, 1990). TEC is difficult to model because of its time dependent influences. It is important to note that it is not the absolute magnitude of the TEC that is important, but the rate of change within a portion of the ionosphere. If the portion has more than 10km in extent then rays at either end of a baseline transmit through the same ionosphere. Different methods can be used with GPS phase-based positioning techniques to account for ionospheric effects.

For short baseline GPS surveying (typically up to 10 km) using single-frequency receivers, the GPS signals propagate through effectively the same portion of the ionosphere. Ionospheric effects will therefore be very similar at either end of the baseline, and will mostly cancel during between-receiver differencing. Campbell et al (1984) show that the effect of the residual ionosphere is approximately 1 – 2 ppm of the baseline length, which equates to about 1 – 2cm over 10km. This however, is only valid for short baselines in mid-latitudes, and assuming a quiet ionosphere. Rizos (1997a) claims that for L1 surveying the scale error can range from 0.4ppm to over 3ppm, corresponding to periods of low and high solar activity respectively.

In order to deal with the impact of ionosphere on single-frequency baseline accuracies, a dual-frequency error modelling approach can be adopted. An outer fiducial network of dual-frequency receivers surrounding a single-frequency receiver network attempts to map the ionospheric delay. An epoch-by-epoch and satellite-by-satellite correction model can be applied to the single-frequency receivers (Wanninger, 1995) thereby improving their accuracy and facilitating longer baselines with little loss in accuracy. Han & Rizos (1996a) describe a correction algorithm which has been adopted for the UNSW volcano monitoring system, (described in more detail in section 4.6.4).

For high precision baselines it is best to use dual-frequency GPS receivers to effectively eliminate ionospheric refraction. The dispersive nature of the ionosphere can be exploited with the L1 and L2 observables (the different frequencies will be affected by different amounts). Hofmann-Wellenhof et al (1994) presents a formula for the ionosphere-free linear combination (also sometimes referred to as the LC frequency).

The pseudo-range R measured on the L1 and L2 frequencies can be modelled as:

$$R_{L1} = r + c\Delta t + \Delta_{ion}(f_{L1}) \qquad \text{- (3.5)}$$

$$R_{L2} = r + c\Delta t + \Delta_{ion}(f_{L2}) \qquad \text{- (3.6)}$$

where:

r - geometric range,

c - speed of electromagnetic radiation in a vacuum,

Δt - combined satellite and receiver clock offsets with respect to GPS time,

Δ_{ion} - ionospheric group delay, and

f_{L1}, f_{L2} - L1, L2 frequency respectively.

Combining these two range equations in order to cancel the ionospheric effect results in the ionospheric-free combination for pseudo-ranges (Ibid, 1994):

$$R_{L1,L2} = R_{L1} - \frac{f_{L2}^2}{f_{L1}^2} R_{L2} \qquad \text{- (3.7)}$$

Similarly, the ionospheric-free linear phase combination can be expressed as:

$$\Phi_{L1,L2} = \Phi_{L1} + \frac{f_{L2}}{f_{L1}} \Phi_{L2} \qquad \text{- (3.8)}$$

This linear combination can be used to eliminate the first order effects of the ionosphere during data processing. However this method does suffer some disadvantages:

1. The noise on the LC observable is greater by a factor of 3.2 than that for just the L1 or L2 measurements, which complicates ambiguity resolution.
2. The ambiguity associated with the LC observable is not an integer quantity.
3. Both L1 and L2 simultaneous observations are required to form this combination, ie suffers during loss of lock on L2.

4. For very long and/or high accuracy baselines some assumptions have been made that neglect second order terms, which may influence baseline resolution at the cm level (Seeber, 1993).

Phase scintillations can affect GPS phase-based positioning techniques by causing cycle slips, complete loss of lock, an increase in phase measurement noise and an overall degradation in navigation accuracy regardless of the type of GPS receiver used (Knight & Finn, 1996). Kelley et al (1996) suggests that these phase scintillations can vary in size from a few metres to several kilometres. These effects resemble "blobs" in the ionosphere, the ramifications of which could result in for example, an ionospheric cycle slip at one end of a baseline and not the other, even for very short baselines!

3.2.5 Satellite Orbit Bias

GPS positioning can be thought of as resection-by-distance whereby the satellites represent control points with known coordinates and the receiving antenna is the coordinate to be determined. The coordinates and time of the GPS satellites in space are transmitted to users in the WGS84 Earth Centred, Earth Fixed (ECEF) Cartesian coordinate system. However, these coordinates are not the true values. The difference between the true coordinates of the satellites and the transmitted values is referred to as the satellite orbit bias.

Satellite orbit bias is caused by external, difficult-to-model effects which perturb the orbit of the GPS satellites (Fig 3.12). Orbits are perturbed by such effects as the non-sphericity of the Earth and the gravitational attraction of the sun and the moon. The gravitational effect of the other planets on the GPS satellite orbits is negligible. Non-gravitational effects such as solar radiation pressure, relativistic effects, solar winds and magnetic field forces also result in small perturbing accelerations on the satellite orbit. These orbit biases are typically described by the three components; along track, radial, and cross track error. For GPS satellites, the along-track error is the largest.

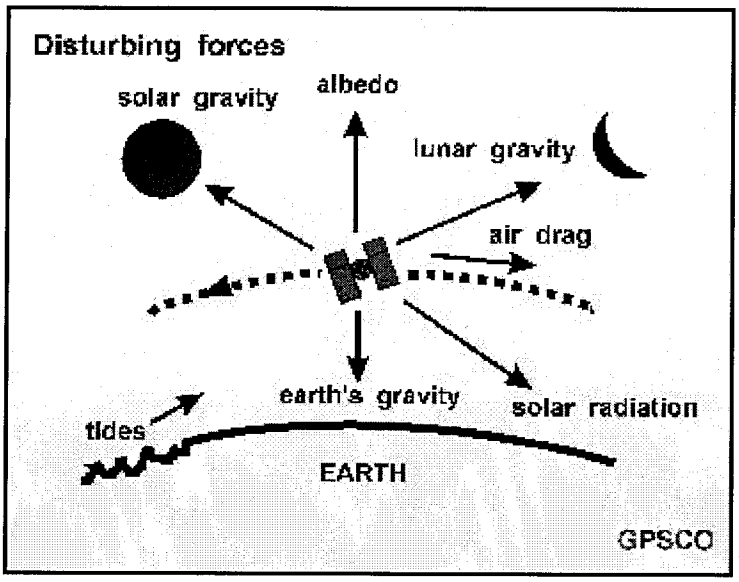

Figure 3.12 - *Satellite orbit bias (Rizos, 2001).*

The GPS Control Segment tracks the constellation of satellites from five tracking stations distributed across the equatorial belt. Observations from these stations are sent to the Master Control Station, where the broadcast ephemerides are computed (Seeber, 1993).

The broadcast ephemerides are uploaded to the GPS satellites via an S-band link. Due to the global distribution of the uplink stations, this upload could occur up to three times a day. Remondi & Hofmann-Wellenhof (1989), state that these ephemerides are accurate to approximately 5m (based on three uploads per day, and 10m if one daily upload is used). The accuracy of the broadcast ephemerides is being improved, and is now conceded as being at the few metre level.

The broadcast ephemerides, which are predictions of the satellite motion, are transmitted to users via the navigation message. The orbital message contains time parameters, and Keplerian and perturbation parameters for each satellite, and is valid for 2-hour arcs. As the 'age' of predictions increases, the orbit accuracy degrades.

For relative positioning, Rizos (1997a), gives a rule-of thumb for the effect of satellite orbit bias on baseline accuracy:

$$Baseline\_error[m] = \frac{d[km]}{20000} OrbitError[m] \quad \text{- (3.9)}$$

where d = baseline length (in km) and 20,000 approximates the satellite altitude (in km).

Assuming a baseline length of 10km and an orbit error of the order of 20m, a baseline error of 1cm (or 1 part per million in relative accuracy) would result. The implication here is that for longer baselines (such as for a large scale monitoring system) broadcast ephemerides may no longer be suitable.

Post-processed ephemerides will provide higher accuracy orbit information. The International GPS Service (IGS) coordinates the operation of a continuous global network of dual-frequency GPS receivers. Table 3.3 lists the various orbit products generated by the IGS.

Table 3.3 - *Orbit products offered by the IGS July 2001(IGS, 2001).*

GPS Satellite Ephemerides	Latency	Updates	Sample Interval	Accuracy
Broadcast	real-time	--	daily	~260cm
Predicted (ultra-rapid)	real-time	twice daily	15 min	~25cm
Rapid	17 hours	daily	15 min	5cm
Final	~13 days	weekly	15 min	<5cm

(Note: IGS accuracy limit based on comparisons with independent laser ranging results. The precision of Rapid and Final orbits is better.)

High quality orbits such as these are required for high precision baseline determination over long distances, typically more than 50km. However, in order to use such orbit products there must be some facility for the baseline processing computer to download this data from the Internet. This may not be suitable for a remote or low-cost network.

On May 1, 2000, the US Department of Defence (DoD) turned off Selective Availability (SA) on all Block II satellites. However, this change has no effect on baseline determination for GPS monitoring networks.

3.2.6 Starting Coordinates

GPS stations designed to detect any geophysical movement in a deformation monitoring system must be referred to some fixed point, or points, that are assumed to be unaffected by the ground displacement. The most notable example is the IGS global network of GPS monitoring stations used to track the GPS satellites for ionospheric monitoring, determination of earth rotation parameters, recovery of precipitable water vapour, as well as continuous monitoring of the tectonic motion of the earth (IGS, 2001). The approximately 130 GPS stations (see Fig 2.3) provide a global infrastructure of absolute, zero-order GPS coordinates to which smaller networks can be connected. Indeed, points in the SCIGN and GSI networks contribute to the IGS network.

However, all points on the earth are moving relative to each other, so it can be stated that the fixed stations in this network are actually the satellites, although they too are moving. An iterative process is used to estimate simultaneously the errors in the satellite orbits and the tracking station coordinates. The absolute coordinate accuracy of IGS core stations is believed to be at the millimetre level and the accuracy of the post-processed precise orbits are around 5cm after 13 days (see Tables 3.3 & 3.4).

Table 3.4 – *Geocentric coordinate accuracies for IGS network July 2001 (IGS, 2001).*

Geocentric Coordinates of IGS Tracking Stations (>130 sites)	Latency	Updates	Sample Interval	Accuracy
Final horizontal positions	12 days	weekly	weekly	3mm
Final vertical positions	12 days	weekly	weekly	6mm
Final horizontal velocities	12 days	weekly	weekly	2mm/yr
Final vertical velocities	12 days	weekly	weekly	3mm/yr

A regional GPS network could specify absolute starting coordinates for a reference station by a number of scenarios (in order of accuracy):

1. rigorously connect one or more or all of its monitoring stations to the IGS network in a global solution using long data sessions and considering all geodetic effects,
2. rigorously connect one or more or all of its monitoring stations to a local section of the IGS network (ie 10 or less stations only) in a regional solution also using long data sessions and considering all geodetic effects,
3. connect to the nearest IGS station and transfer the absolute coordinate to the reference station of the local network, or
4. compute a single point positioning solution of the base station of the local network independent of the IGS network.

The first three methods provide cm-level absolute coordinates, while the last method should provide an absolute coordinate to about 5-10 m accuracy.

The important distinction between absolute and relative coordinates needs to be emphasised again at this point. An absolute starting coordinate for a reference station in a monitoring network at metre level accuracy can still resolve millimetre-level relative coordinates between stations in the network. Rizos (1997a) mentions a rule-of-thumb that, "...20m station coordinate uncertainty is acceptable for 1ppm relative accuracies". Beutler et al (1988) state that a 1" error in the absolute position of a starting coordinate (approximately 30m on the ground) introduces a rotation into the network of about 0".1.

An adopted absolute coordinate for a reference station in a local network can be thought of as a four-dimensional quantity; ie position (X,Y,Z) and a time epoch. Global crustal velocity vectors can be applied to all stations in the network to account for any long period crustal effects (especially important if the network straddles a plate boundary). A pertinent consideration when deciding on a reference station absolute coordinate for a monitoring network therefore is its longevity and contribution to the global infrastructure.

Section 4.6.6 details the procedure for defining the base station absolute starting coordinates on the Gunung Papandayan network. Section 6.2 also compares the quality

of baseline results when using slightly different starting coordinates for observing stations.

Chapter 3 has detailed the design considerations for a generic GPS volcano monitoring system. Building on this, chapter 4 will describe the UNSW designed low-cost GPS volcano monitoring system installed on Gunung Papandayan, Indonesia.

Chapter 4
UNSW SYSTEM DESIGN & INSTALLATION

The UNSW designed GPS-based monitoring system is a small scale, low-cost *type* of volcano monitoring system (section 2.3.2.3). This chapter describes the components, operation and installation of this GPS system on Gunung Papandayan, Papandayan. The components were selected on the basis of their suitability, reliability and cost. These factors cannot be considered in isolation, for each impacts on the other. For instance, reducing the usage of the radios by adopting a static baseline approach (which is appropriate for the intended monitoring application), reduces the power demand, and therefore the size of the battery bank and solar array, thereby reducing the cost. Similarly, choosing OEM GPS receiver boards or low-cost PC boards that are adequate for the task at hand contributes further to this objective. Conversely, sufficiently accurate components, such as the GPS antenna, must be purchased to guarantee data quality. A compromise between quality and cost must therefore be struck.

It is intended that this chapter, in combination with Appendix B (Trouble shooting guide), be considered as a user manual for the system. The remote slave station design and installation will be described first, followed by the base station design, concluding with the operation of all components as a system.

4.1 Collaboration & Management

The School of Surveying and Spatial Information Systems (formerly the School of Geomatic Engineering), The University of New South Wales (UNSW), drafted an agreement with the Department of Geodetic Engineering, Institute of Technology Bandung, Indonesia (ITB), and the Vulcanological Survey of Indonesia (VSI), in May 1998 to facilitate smooth international cooperation. This agreement builds on a 25-year history of collaboration between UNSW and the ITB. Colleagues from the ITB have been concurrently carrying out the project "Monitoring the Volcano Deformation using Repeated GPS Surveys", funded by the Indonesian Department of Education and National Research Council of Indonesia. This project is concerned with encouraging the

use, in Indonesia, of the GPS technology for volcano deformation monitoring. First tests have been made on Mt. Guntur in collaboration with the VSI. The ITB's repeated GPS survey approach complements this project, in that the experience gained from previous work will be of great benefit. In addition, periodic checking of the general trend of the results of the proposed permanent GPS array system would be possible using the independent GPS surveys undertaken by the ITB. Scientists at the VSI are of the firm belief that ground deformation information provides valuable precursory data about the behaviour of a volcano. The VSI's experience of ground deformation monitoring using the campaign style approach will greatly benefit the automation of such techniques, and in turn provides a valuable new tool for volcano hazard mitigation.

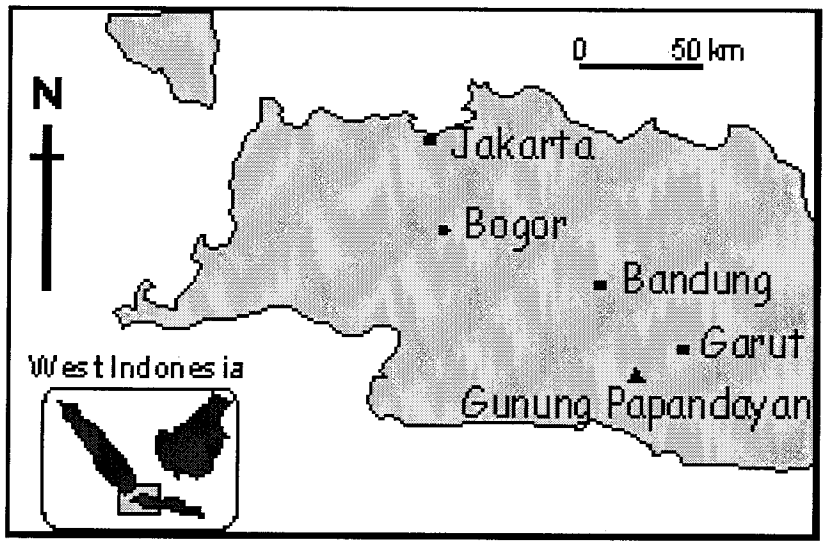

Figure 4.1 - *Map of West Java showing location of Gunung Papandayan.*

In August 1998 the author travelled to Indonesia to meet with ITB and VSI colleagues, and to investigate a suitable volcano on which to deploy the first system. Gunung Gede, located in the popular Gunung Gede/Pangrango National Park was suggested due to its proximity to Jakarta and many vulnerable surrounding villages. An initial site visit, however, revealed that access to the nearest suitable receiver station locations to be at least 5 hours walk away! Gunung Papandayan was then selected as a suitable volcano to make first tests of the proposed volcano deformation monitoring system. This volcano was chosen principally because of its close proximity to the city of Bandung, and the easy accessibility of the receiver stations to be emplaced on the volcano (Fig 4.1). It was anticipated that problems would inevitably arise with the operation of an untried system such as this, and hence field visits to a receiver station should not be too arduous.

Gunung Papandayan is a complex strato-volcano with four large summit craters (Fig 4.2). A collapse of the summit occurred in August 1772, followed by a brief explosive eruption which lasted around 5 minutes only. During this eruption a debris avalanche swept 11km over lowland areas to the east, destroying 40 villages and killing almost 3000 people (Kimberly et al, 1998).

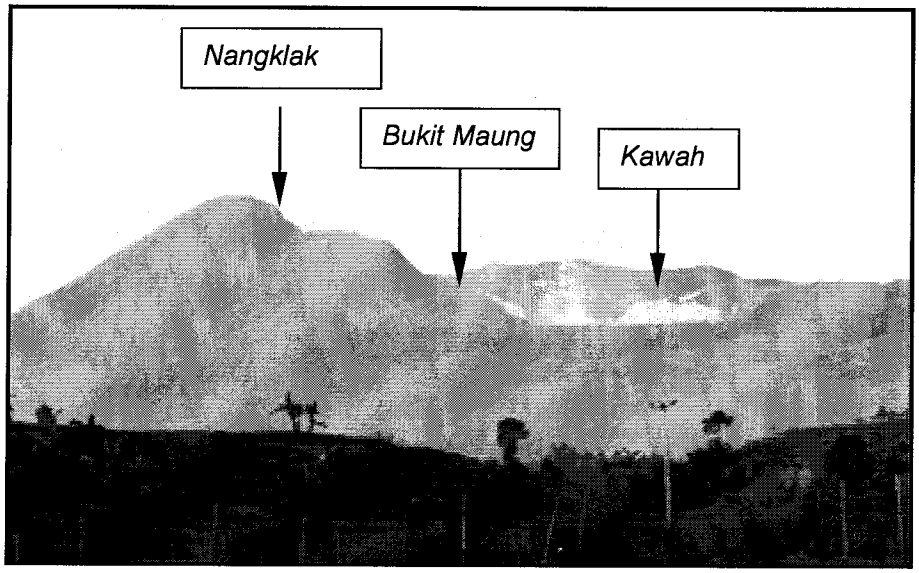

Figure 4.2 - *Photograph of the slave station locations on Gunung Papandayan (photo courtesy of Abidin).*

UNSW staff would visit Indonesia on frequent short-term visits to ensure that problems could be solved, in order to ensure a fair trial of the capabilities of the system. Nevertheless, the key to the ongoing operation (and maintenance) of this system is the involvement of in-country (ITB and VSI) collaborators, and hence these colleagues have been actively involved in the design of the project from the early stages. With such a strategy all parties would be well placed to address technical and non-technical problems as they arise. Furthermore, the local knowledge of the ITB and VSI experts is vital in such a project, for concerns may range from local weather patterns, human and animal vandalism, harsh volcanic environments, to cultural and financial issues. A certain degree of language fluency, and cultural sensitivity, when working in Indonesia is also of great benefit for the smooth running of the project.

Maintenance of the GPS receiver array comes at some cost. More particularly with the difficult financial situation that presently exists in Indonesia, there are few financial

resources to cover the many contingencies that invariably arise. UNSW has therefore setup a bank account in Indonesia to be used by VSI and ITB staff as the need arises. This also instils a sense of mutual responsibility towards, and joint "ownership" of, the system by all the partners. Station visits could be carried out on a regular basis by either VSI staff resident at the observatory/base station at Papandayan, or by motivated final year geodesy students from the ITB. Students will also be encouraged to use the data for their own research purposes. All these measures are intended to strengthen the collaboration between the respective institutions, and in so doing help guarantee a robust and sustainable monitoring system in Indonesia.

4.2 Slave Station

Slave stations are located on the zone of deformation, in this case on the volcano itself (Fig 4.3). They are best located such that any movement of the volcano can be unambiguously detected, and for that reason advice from experts at the VSI was sought when deciding upon station locations on Gunung Papandayan. In fact the three GPS continuous slave stations were located in close proximity to an existing VSI EDM network providing a rough, albeit robust, check of the measurement systems over time. Indeed it is these points that are now used for the ITB/VSI Papandayan campaign surveys, of which eight measurement campaigns have been completed (Abidin, 2001, personal communication).

A low-cost, low-power, single-frequency GPS receiver passively logs GPS data to an 8086 computer. Both of these components are OEM (original equipment manufacture) boards only and are housed inside an aluminium box (Fig 4.4). There is no screen, no keyboard and no hard disk. Memory storage on the computer is restricted to the RAM only. Rudimentary software on-board these GPS/PC modules controls the file creation and radio transmission of the completed sessions to the base station.

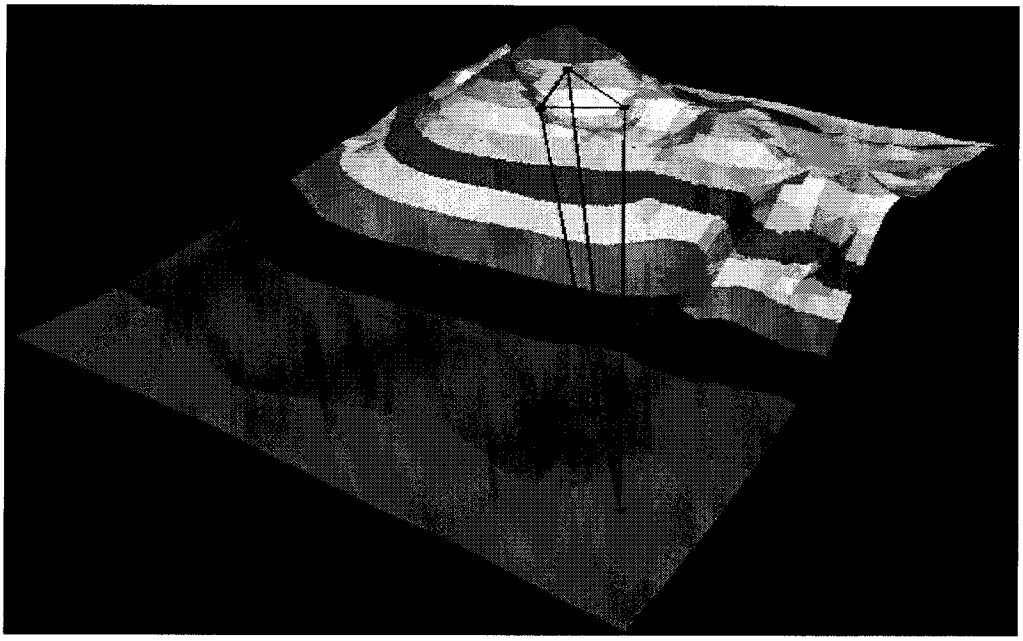

Figure 4.3 - *Diagram of the GPS network emplaced on Gunung Papandayan. The base station is shown at the bottom of the diagram and the slave stations are shown from left to right as Bukit Maung, Nangklak and Kawah.*

A low-power radio is polled routinely every hour by the base station radio, which downloads the previous session of slave station GPS data in binary form. All components in this system require 12V DC power. Power is provided using a 12V wet lead acid battery recharged by a solar panel array (see section 4.2.4).

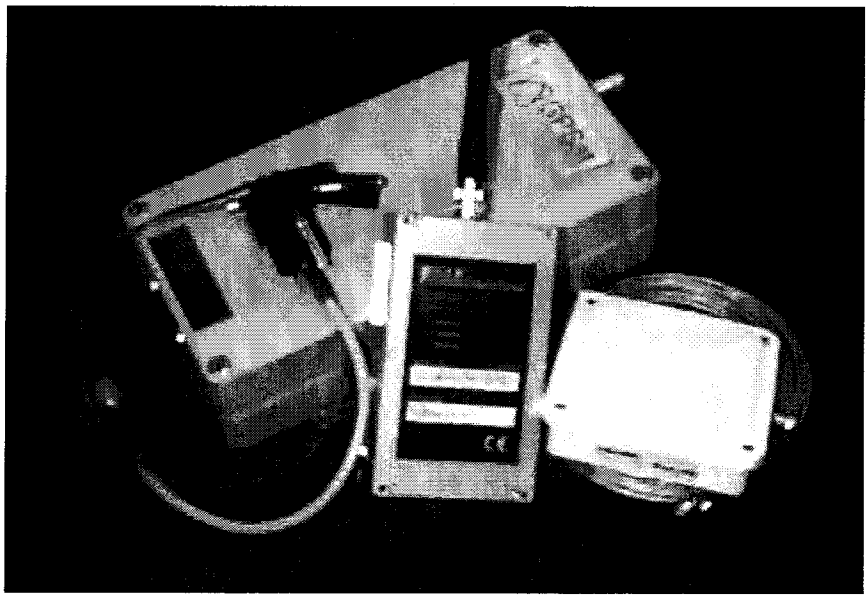

Figure 4.4 - *GPS/PC module, radio and antenna used for the low-cost monitoring system.*

Appendix B-3 shows a schematic diagram of the fundamental components of the slave station operation. Appendix B-4 illustrates in more detail how all components are be installed.

4.2.1 Monumentation

The monumentation for the volcano monitoring system described here was a compromise between cost and stability. It is of paramount importance to ensure that the points being repeatedly measured do not themselves move. A monument emplaced in loose gravel will record a movement of the GPS antenna but this provides no evidence as to the behaviour of the volcano massif. This local 'noise' needs to be minimised.

Bock et al (1997) describe deeply anchored monuments emplaced for the SCIGN network (see also section 3.1.3). It is indeed demonstrated that deeply-anchored monuments provide more stability, but at what cost? Taking into account the effects of rainfall, secular and seasonal variations, Langbein et al (1995) claim a standard deviation of movement of deeply-anchored monuments of a few millimetres. However the cost and logistical complexity of installing such a monument, particularly in a remote volcanic environment, is unwarranted for a low-cost system. Given that the intended error budget of the UNSW system is only at the centimetre level, monuments emplaced to a depth of 2m were considered suitable.

Berntsen 3D survey monuments (Berntsen, 2001) were emplaced on Gunung Papandayan at three locations and a fourth at the base station, considered to be out of the zone of deformation. The location of the volcano sites was chosen according to a number of criteria:

- All sites had a clear line-of-sight to the observatory; a requirement for radio communications.
- As far as possible, sites were located away from the corrosive sulphur gases constantly billowing out of the crater of the volcano.
- Advice from the VSI was sought and it was considered advantageous to locate the continuous GPS sites near the existing EDM network. This EDM network is routinely measured using GPS in a campaign-style approach by collaborators from

the ITB, as part of their project "Monitoring the Volcano Deformation using Repeated GPS Surveys".

- The ground at all sites was deemed to be stable.
- An existing continuous seismic station is located in the vicinity of Kawah, one of the slave stations. Seismic data can be cross-referenced against the GPS data in the future.
- Except for Kawah, sites were located away from the main tourist traffic, to reduce the risk of vandalism to the equipment.
- All sites have a clear skyview.

The sites chosen are described below:

1. Bukit Maung (Tiger Hill) is located on the eastern edge of the Papandayan massif. It is relatively distant from the active crater, and therefore is the least affected by corrosive gases. Despite its proximity to the carpark, access to this site is arduous protecting it from vandalism (Fig 4.5).
2. Nangklak is the highest and most distant site from the carpark, and therefore least likely to be vandalised. It is located above the steep hydrothermally altered headwall of the 1772 eruption (Kimberly et al, 1998). Instruments located here are quite exposed to corrosive gases (Fig 4.5).
3. Kawah (Crater) is located above the active "Kawah Emas" on the debris caused by the collapse of the 1772 eruption (Ibid, 1998). Proximity to the carpark and ease of access make this a highly trafficked site by tourists. Consequently, a fence has been erected around the instruments. This site is the most exposed to corrosive gases from nearby fumarolic vents (Fig 4.8).

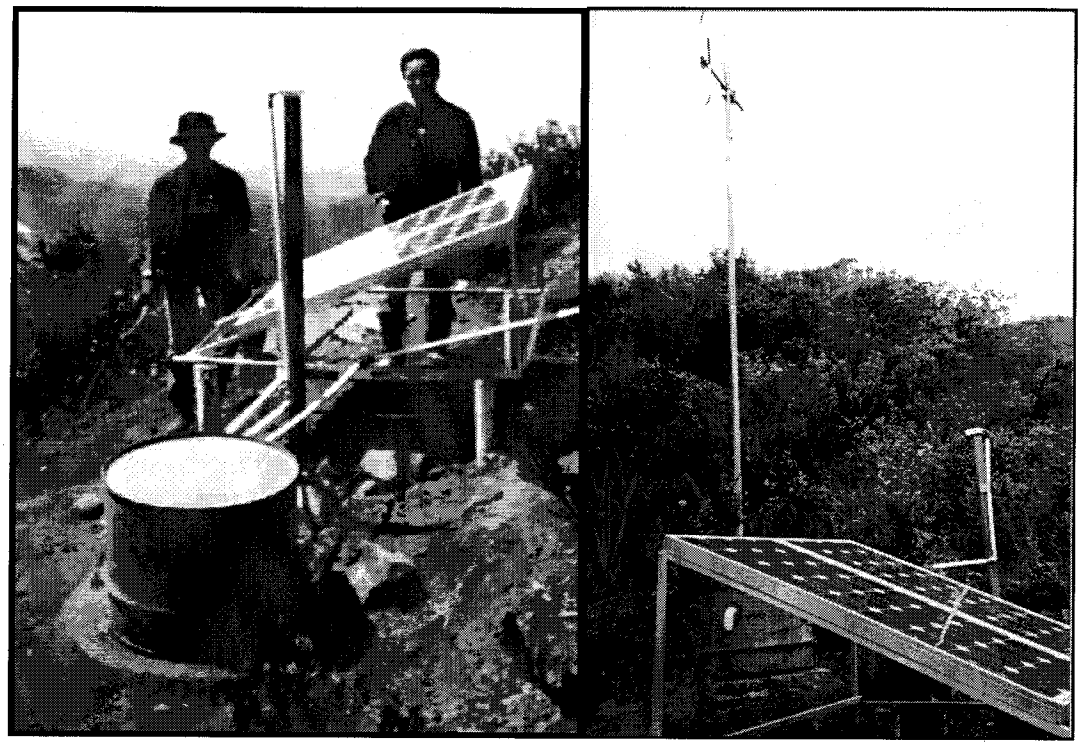

Figure 4.5 – *Slave stations Nangklak (left) and Bukit Maung (right).*

All three sites are located close to the fixed campaign-style GPS network measured routinely by staff and students from the ITB. All sites were located with regard to the local geology, to avoid tectonic faults which might corrupt the deformation analysis with signals other than due to volcanic effects (VSI 1998, personal communication).

The Berntsen 3D monuments consist of 600mm and 900mm screw-in sections of 16mm steel rod driven into the ground until refusal. All sites are between 2 and 3 metres in depth. The top one metre is further stabilised with a 400 x 400 x 1000mm block of reinforced concrete placed in situ around the mark. These monuments were emplaced in August 1998 and left to settle into position before installing the GPS antennas (Fig 4.6 & Appendix B-6).

Figure 4.6 - *Monuments emplaced on Gunung Papandayan, A) Concrete and reinforcing rod extends to a depth of 1-metre, B) the fibreglass rod is braced with a steel mount, C) final concreting around the base of the monument.*

MicroPulse 13700 L1 lightweight survey GPS antennas were tested at UNSW and chosen as a suitable low-cost antenna for this application (see section 4.6.1). The antennas were mounted 1.5m above the ground surface on fibreglass poles. Fibreglass was chosen due to its resistance to corrosion from sulphur gas. The poles are constructed from 50 x 50 x 3mm fibreglass tubing plugged at both ends. The resin plugs provide more stability to the tubing, but more importantly allow for a 3/8" thread and a 5/16" thread to be machined into each end of the pole. The GPS antenna is screwed and glued onto the pole. A locking screw was machined into the pole to further protect the antenna from theft (see Appendix B-5).

The fibreglass pole connects to the Berntsen mark using a 5/16" screw thread, however given the threat of vandalism, this was considered a flimsy design and a steel-mounting bracket was included for further stability (Fig 4.6). The fibreglass pole simply screws onto the fixed Berntsen mark, being careful to orientate the GPS antenna to north on the last turn. Silicon was sandwiched between the mounting bracket and the fibreglass pole for some flexibility and the mounting bracket was then covered by concrete (Appendix B-6).

A TNC elbow connection at the antenna protects the GPS antenna cable from breakage and PVC tubing surrounding the cable protects against animals (Appendix B-5).

4.2.2 GPS/PC Module

The GPS/PC module consists of a GPS receiver board connected to a low-cost PC board for temporary data storage and file management. Initial testing was carried out with two single-frequency GPS receivers: the Rockwell Jupiter board running a Zodiac chipset, and the Canadian Marconi Company (CMC) Allstar. During the course of testing it was established that the oscillator of the Rockwell receiver was noisier than that of the CMC, and the subsequent quality of the pseudo-range and carrier phase measurements was therefore inferior to the CMC.

Independently of the tests conducted at UNSW, scientists at UNAVCO were conducting their own testing for a similar L1 monitoring system. They confirmed, using zero-baseline tests, that due to clock synchronisation problems, the quality of the carrier phase measurements from the Rockwell receiver was unsatisfactory. UNAVCO claim that the CMC receiver is capable of making mm-level carrier phase measurements (Meertens, 1997).

The CMC receiver board is installed within a small aluminium box, and connected to a JED PC104 microcomputer board mounted in the same box (see Fig. 4.7). The GPS/PC modules were custom built by GPSat Systems Pty Ltd, Melbourne.

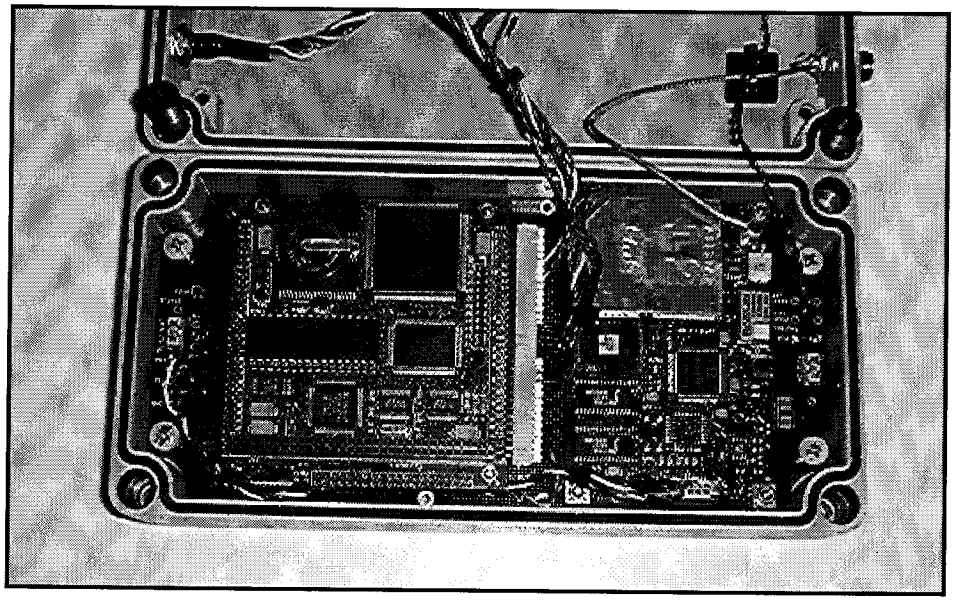

Figure 4.7 - *A custom-built GPS/PC module used on Gunung Papandayan. The JED PC104 can be seen to the left and the CMC Allstar 12 is mounted on the right.*

The JED computers have no screen, no keyboard and no hard disk. They are only required to run file management and communications software. 8086 PC boards with 492Kb of RAM and 240Kb of Flash-PROM are used. Flash-PROM is a data storage device that looks like a chip but acts like a hard disk, in that it can be written to or read from. The base station GPS/PC module however must collect data from all slave stations (and its own receiver), and run the baseline processing software. Therefore a 133 MHz Pentium computer board with 7Mb of Flash-PROM is utilised. The GPS/PC modules run on a 12V DC power supply. The slave stations use approximately 2.5 Watts, while the base station module with the Pentium PC board uses 6 Watts of power.

The slave station GPS/PC modules can be controlled using a terminal program to up-load software and start surveys. At the base station a keyboard and monitor connected to the GPS/PC module operates at all times.

4.2.3 Radio Modems

Radio modems are used to transfer GPS data collected at the slave stations to the base station located 8km away at the VSI observatory. The UNSW system has been designed to address static application requiring the radios to send binary data files on a hourly basis, thereby reducing power usage and simplifying file management. The mobile phone network in Indonesia is also well established. It is reliable (particularly high on the slopes of a remote volcano) and relatively inexpensive. Investigations were made into transferring data using the mobile phone network, however, it was considered that for a continuous system the cumulative cost would become prohibitive. Autonomous stations using radio modems are not reliant on potential faults or outages of the mobile telephony infrastructure.

Almost all of the 60 active volcanoes monitored by the VSI in Indonesia have an observatory based up to 15km away from the zone of deformation, with a clear line-of-sight to the summit. 5 Watt VHF radios from GLB Radio Data Systems are used to transfer the GPS data. Two frequencies (152.375 and 152.475 MHz) are used to transmit and receive data, whereby the 'transmit' frequency for the base station corresponds to the 'receive' frequency for all the slaves, and vice versa. The data is sent in packet mode and the GLB radios provide internal error checking to guard against

corrupted data being received at the base. All the slave stations are equipped with a directional Yagi antenna mounted on a 5-metre mast. The Yagi antennas have line-of-sight view to the base station and are pointed at it. The base station uses an Omni dipole antenna with an all-over gain pattern to enable communications with all the slave stations. The radio antenna cables are encased in PVC tubing to protect against animal damage or human vandalism.

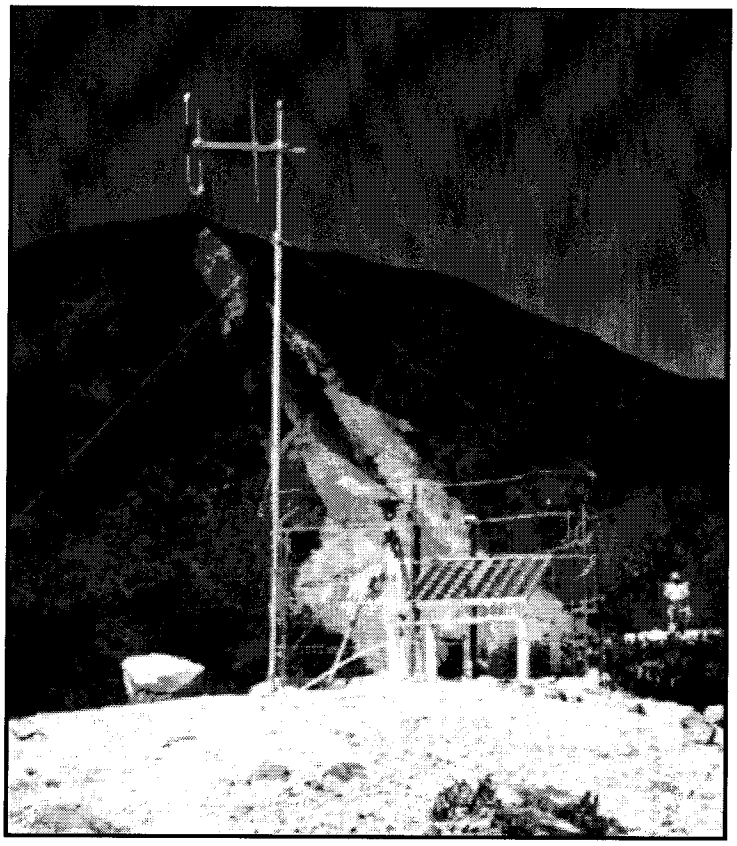

Figure 4.8 – *Slave station at Kawah. (Note the tripod is used for an EDM survey running concurrently).*

4.2.4 Power Budget for Solar Panels

The permanent GPS slave systems located on the remote flanks of Gunung Papandayan are powered by wet lead acid batteries recharged by solar panels. The climatic conditions are not always suited for solar recharging and therefore when estimating the size of the photovoltaic panels and the battery bank many factors need to be considered. It is also prudent to take a conservative approach when estimating the power

requirements, to allow for unforeseen factors while still delivering an uninterrupted power supply to the slave stations.

4.2.4.1 Equivalent Sun Hours (ESH)

Equivalent sun hours (ESH) are a measure of the available daily sun for a particular location. One hour of maximum sunshine received by a solar module equals one equivalent sun hour. Such maximum sunshine occurs between 9am and 3pm daily so ESH would only ever reach a maximum value of six. This factor is used when calculating the size of the solar panel array required for a particular application. ESH also depends on the latitude of the location and the time of year (although year round values are often estimated). The climatic conditions such as average cloud cover and to a lesser extent the temperature must also be considered, either as part of this ESH value or later on in the calculations.

Although Gunung Papandayan is located close to the equator, the summit also reaches 2,622m, attracting frequent cloud cover. For this reason, an ESH value of 3.5 has been adopted for this location.

4.2.4.2 Size of Solar Arrays

The load required by the system must first be calculated by considering all the power requirements of the component parts of the system, and for how long each day they will be operating. It is assumed that the system voltage will be 12V DC. There will always be a loss in the system due to components heating up or resistance along cables. In addition, solar panels are rated by the manufacturer in terms of power output. However, at operating temperatures, the efficiency drops off by about 0.5% / 1°C temperature increase. (Ironically solar panels in Antarctica are more efficient than those located on the equator.) The load per day of the system can be corrected for these losses by multiplying by an appropriate factor (in this case 0.667 (Rob Largent, 1999, personal communication)) to give a corrected load.

The corrected load is used to compute the size of the solar panel array. A similar factor, which accounts for battery inefficiencies when recharging, is adopted to calculate the

size of the battery bank. It is important that the solar panel array is not only large enough to maintain the charge in the battery bank, but also to recharge when the battery charge is low. If, for example, cloudy conditions preclude recharging of the batteries for 3 days, then the solar array needs to be large enough to recharge in a specified time span, ie two days. This is the recharge rate coefficient. (1.5 = 2 day recharge, 1.25 = 4 day recharge). Similarly the battery bank must also be large enough to continue to supply power to the system during periods when no recharging is possible (autonomous mode).

4.2.4.3 Solar Power Equations

The following equations, adapted from the UNAVCO website (1999), can be used to determine solar array size and battery backup requirements based on a 12V nominal system voltage.

Power consumption (W) for each piece of equipment:

Power (W) = voltage (V) × current (A) - (4.1)

Daily amp-hour load (Ah) for each piece of equipment:

$$Amp-hour\_load(Ah) = \frac{Power(W)}{Voltage(V)} \times Hours\_of\_operation\_per\_day(h) \quad \text{- (4.2)}$$

Add up amp-hour load for whole system.

Efficiency and loss-corrected load (Ah) for whole system:

Corrected load (Ah) = amp-hour load (Ah) / 0.75 – (4.3a)

or

Corrected load (Ah) = amp-hour load (Ah) / 0.667 – (4.3b)

Note: the 0.75 factor assumes that high quality solar panels are being used, ie an 8% loss in efficiency at operating temperatures.

The 0.667 factor assumes that lower quality, less expensive solar panels are being used, ie a 20 % loss in efficiency at operating temperatures.
(Approx. 0.5 % / 1°C temperature)

Worst case equivalent sun hours (ESH) (h):

Determine from charts or meteorological data. (see 4.2.4.1 Equivalent Sun Hours)

Solar array power requirement (W) (including recharging):

$$Solar\_power(W) = \frac{Corrected\_load(Ah)}{ESH(h)} \times recharge\_rate\_coeff \times Voltage(V) \text{ -(4.4)}$$

Size of battery bank (Ah):

$$Size(Ah) = \#days\_auton \times Amp-hour\_load(Ah) \times Batt\_rechg\_ineff\_fact \quad \text{- (4.5)}$$

4.3.4.4 Example at Gunung Papandayan

Consider a continuous slave station site with a GPS/PC module consisting of a Canadian Marconi GPS receiver board connected to a PC-104 computer, GLB radio and MicroPulse GPS antenna. The site is located on Gunung Papandayan, West Java, Indonesia, at approximately: $\varphi = 7\,°\,21'$ S, $\lambda = 107°\,35'$ E and elevation 2622 metres.

Power consumption (W) for each piece of equipment:

The GPS receiver tracks satellites 24 hours/day and logs the data to the Flash-PROM of the PC-104. Every hour the master station radio polls the slaves, which then download their data. It could take up to 8 minutes / slave station to download data. Three slave stations will operate.

At a slave station the GPS receiver and antenna will operate continuously. The radio will operate:

8 minutes × 24 times/day = 192 minutes/day or 3.2 hours/day.

The following tables summarise the expected power consumption.

Equipment	Power	Hours/day
CMC GPS/PC modules	2.5W	24
GLB Radios (transmit)	14.4W	3.2
GLB Radios (standby)	3.36W	20.8
MicroPulse antenna	1.2W	24

Daily amp-hour load (Ah) for each piece of equipment:

Equipment	Calculation		Ah
CMC GPS/PC modules	2.5W/12V	× 24h	5.0
GLB Radios (transmit)	14.4W/12V	× 3.2h	3.84
GLB Radios (standby)	3.36W/12V	× 20.8h	5.82
MicroPulse antenna	1.2W/12V	× 24h	2.4
Total			17.06

Efficiency and loss-corrected load (Ah) for whole system:

17.06Ah / 0.75 = 22.747Ah – for high efficiency solar cells

17.06Ah / 0.667 = 25.577Ah – for low efficiency solar cells

Worst case equivalent sun hours (ESH) for Gunung Papandayan, Indonesia:

3.5 hours

Solar array power requirement (W) (including recharging):

High Efficiency Solar cells:

2 day recharge: (22.747 Ah / 3.5 h) × 1.5 = 9.75 A
Power: 9.75 A × 12 V = 117 Watts

5 day recharge: (22.747 Ah / 3.5 h) × 1.2 = 7.80 A
Power: 7.80 A × 12 V = 94 Watts

Low Efficiency Solar cells:

2 day recharge: (25.577 Ah / 3.5 h) ×1.5 = 10.96 A
Power: 10.96 A × 12 V = 132 Watts

5 day recharge: (25.577 Ah / 3.5 h) × 1.2 = 8.77 A
Power: 8.77 A × 12 V = 106 Watts

Based on the above calculations, low efficiency BP Solar BP275 solars panels were chosen to provide power for the system installed on Gunung Papandayan. Two identical panels connected in parallel provide a peak of 150W of power at up to a current of 9.5Amps. (Note: 65 Watt solar panels were not available so it was decided to "over engineer" the power system.)

Size of battery bank (Ah):

The autonomy or reserve time of the battery bank refers to the period the battery bank can continuously supply power to the GPS/PC module and radio without receiving any recharge from the solar panel array, ie in cloudy conditions. In order to compute the size the battery bank required for a nominated period of five days in autonomous mode, then simply use:

17Ah load × 5 days = 85Ah battery will be suitable.

However, inefficiencies in the battery during recharging must be considered. An empirically derived and somewhat conservative figure of 1.25 is adopted and multiplied by the daily amp hour load. This factor infers that there is a 25% loss in efficiency when recharging the battery. The size of the battery bank for 5 days autonomy is therefore:

$17 \times 1.25 \times 5 = 106\text{Ah}$

The discharge rate of the battery refers to how much charge is designed to be taken from the battery bank during these sun-free times. A conservative estimate of 50% for the maximum discharge therefore means that the capacity of the battery bank is designed to be discharged down to 50% of its capacity. Clearly a conservative figure and an educated guess, for one can never know for how long the sun will not shine. This factor also impacts on the cost and size of the system.

For example, choosing five days of autonomy with a 50% maximum discharge and a recharge inefficiency of 25%:

$(5 \text{ days} \times 17.06\text{Ah} \times 1.25) @ 50\% = \underline{213\text{Ah battery bank}}$

The system designed for Gunung Papandayan uses a battery bank of only 120Ah. This size was chosen for reasons of cost and convenience of transport. The discharge rate of 50% was considered too high for a lead acid battery bank and 5 days of autonomy was considered a conservative estimate of sun-free days.

Working backwards therefore, using the above formula, the discharge rate for a specific battery bank capacity can be computed.

$120\text{Ah} = 5 \times 17.06 \times 1.25 \times \text{Maximum discharge}$

$\text{Maximum discharge} = 12\%$

That is, after 5 days without solar recharging, the battery bank will be reduced to a capacity of 12%. This figure is not critically low for a lead acid battery bank.

Recalculating for just 3 days of autonomy would result in a maximum discharge to 47%.

A single 120Ah battery was considered large enough to autonomously supply power to the slave stations for 5 days without discharging to dangerously low levels, and inexpensive enough to satisfy the low-cost requirement of this project.

4.2.4.5 Solar Regulators

The solar regulator ensures that the power output from the solar panel array is 12V DC. Although a solar panel may be rated for 12V DC, actually it may deliver 17 – 21V DC. The regulator restricts the output voltage to 12V DC. Additionally, if more than one panel is required in an array, as is the case for the slave stations on Gunung Papandayan, then identical panels should be used. If two non-identical panels are connected in parallel (as this system will require) their voltages could be incompatible prior to regulation, causing damage to the regulator.

Solar regulators are also rated in terms of their maximum current capacity. When using more than one solar panel, connected in parallel, the current provided by each separate panel should be added to give the total current of the solar panel array. (Note: when connected in series, the voltage is added.) This total current should be less than the maximum allowable current specified for the solar regulator.

As an aside it should be mentioned that the sum of the current in amps delivered by the solar panel array should be less than the maximum recharging current allowed for the battery. In the case of a 75W solar panel the output current is 4.7A. For two panels the sum is less than 10A, which is well under 15A, the maximum allowable recharge current for a 50Ah battery.

Solar regulators may only be suitable for recharging wet, lead acid battery arrays, or sealed, lead acid battery arrays, or both. The solar regulators chosen for Gunung Papandayan are suitable for both wet and sealed, lead acid batteries. Although sealed, lead acid batteries are considered more efficient, wet, lead acid batteries are used at the

slave stations on Gunung Papandayan due to their lower cost and easy availability in Indonesia.

4.2.4.6 Mounting Solar Panels

For maximum efficiency, the solar panels should be mounted on a frame tilted at 15° + the latitude of the location. Therefore aluminium frames were built to tilt the solar panel array at 22° and facing north. This tilt also means that rainwater will run off the face of the panel and in-so-doing clean off any dust that may have accumulated on the panel. The panels must also be mounted slightly above ground level to keep dirt from rain splash off the face. This was done using PVC struts mounted in the ground with the solar panel frame mounted on top of the struts using an insitu holding-down-bolt embedded in concrete. Of course the panels should be located away from any shade (Fig 4.9).

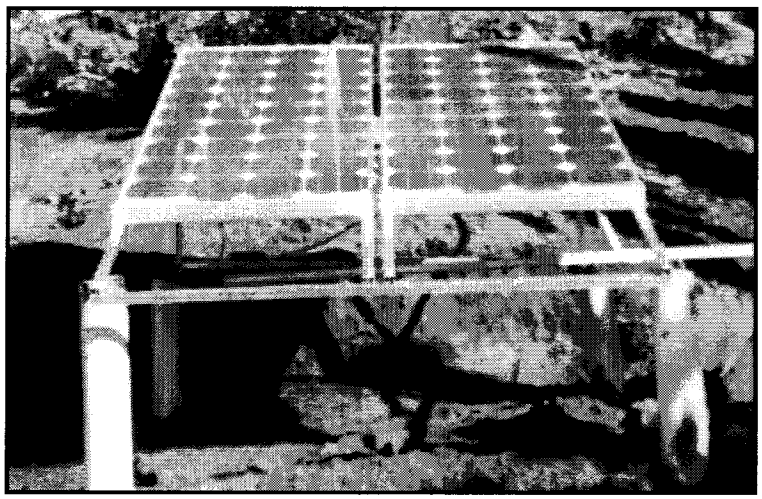

Figure 4.9 - *Solar panels at Nangklak.*

By far the largest threat to the system comes from vandalism, for the solar panels are the most vulnerable component, being large, visible and fragile. Additionally the crater of Gunung Papandayan is a tourist attraction exposing the slave stations to possibly more vandalism. The continuous station located in the crater (Kawah) has a fence erected around it to protect the components from theft or damage. The remaining two slave stations on the flanks of the crater are considered remote enough not to warrant a fence

around them. However, no station will be totally vandal-proof, and this fact indeed is further justification for regular maintenance and inspection of the slave installations.

4.3 Base Station

The base station is essentially of the same design as the slave stations, with the only difference being the quality of the PC in the GPS/PC modules, the complexity of the software and the power system (section 4.3.1). Considerations such as vandalism, protection against corrosive gases and solar power are not a concern at the base station. The monument is of the same design as those on the volcano, as are the GPS antenna and the radio modems. An Omni dipole antenna is used at the base station in preference to a Yagi directional antenna due to its all-over gain pattern.

The communications software at the base station is more 'intelligent' than that of the slave stations. The base station radio polls all slave stations sequentially every hour. It first checks for a radio connection, then downloads the previous session of GPS data, as a binary file, from the slave station. This binary file is then converted to a RINEX file at the base and stored on a hard disk.

At present, baselines are not automatically processed. Data must be manually downloaded from the hard disk at the base station and post-processed. This is a sub-optimal solution, but sufficient to demonstrate a "proof-of-concept" system.

4.3.1 Power Supply at the Base Station

The luxury of AC power at the base station is complicated by the relatively remote location of the observatory and the unreliable nature of AC power in rural Indonesia. Any power system therefore needs to guard against spikes, power surges and blackouts, which can occur for up to 6 hours and as often as every fortnight.

The important components of the volcano monitoring system which require constant power are the GPS/PC module (and therefore the GPS antenna), the radio and the hard disk.

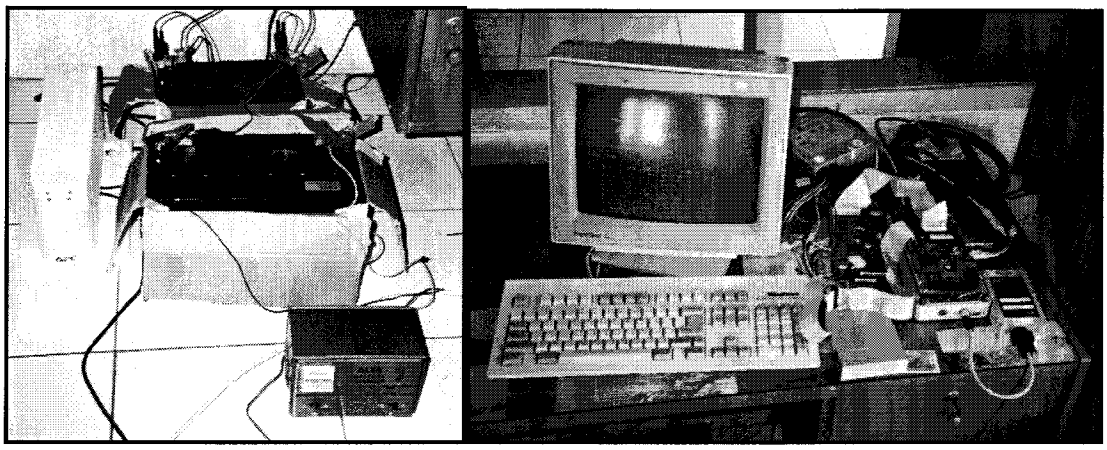

Figure 4.10 - *Power system at the base station (see also Appendix B-2).*

Power is supplied to the base station system using an AC power outlet at the wall. However, the power is quite unreliable and may result in a loss of data. For this reason an uninterruptable power supply (UPS) is connected between the AC power and the base station system. The UPS regulates the power to guard against spikes and also automatically switches to its own on-board battery supply in the event of a blackout. Unfortunately, the on-board battery is only suitable for supplying reserve power for about 20 minutes before it will be exhausted. At the observatory it is not unusual to experience 4 – 6 hour power blackouts. The small 7 Ah battery included in the UPS has been replaced by a larger battery bank backup. A 70 Ah and a 45 Ah 12V wet, lead acid battery have been included in the power system. Although the UPS includes a battery charger, which constantly charges the backup battery, it is only designed for a 7 Ah battery. A more powerful battery charger is used for the larger battery bank.

From appendix B-2 it can be seen that the monitor and a computer power supply are connected directly to the UPS. The computer power supply is used to power the hard disk. The GPS/PC module and radio receive power exclusively from the 12V battery. The battery is continuously charged by a battery charger connected to the wall AC power. The battery charger automatically trickle charges when the battery approaches a full charge. In case of a power blackout, the 12V battery should be able to continue to power the whole system for up to 2 days.

The UPS also indirectly powers the hard disk. Powering the hard disk, however, is more complicated. A hard disk requires both 12V & 5V DC, therefore an external PC power

supply is used to power the hard disk. In the event of a power failure the UPS will quickly switch to the battery to continually power the system.

The GPS/PC module is connected to a monitor and keyboard, as well as the GPS antenna and a data link to the radio. The radio is connected to an Omni dipole antenna mounted on the roof of the observatory. The monitor is not considered crucial to the system and should be switched off during continuous operation to save power, particularly during blackouts when the system is only running off backup batteries. It can be switched on at any time for periodic checking.

4.4 Installation

The installation of the volcano monitoring system required many logistical factors to be taken into account. The benefit of in-country collaborators is most obvious during this stage of the project. Their linguistic and cultural familiarity as well as technical knowledge is crucial to the success of the project, and is also extremely enjoyable and rewarding.

The degree of collaboration between the VSI, ITB and UNSW has been refreshing. All groups have different skills and responsibilities, which augers well for cooperation. Members from the VSI and ITB have been trained to use the system so that any in-country changes can be easily carried out.

4.4.1 August 1999 Installation

180 kilograms of equipment, constituting most of the component parts of the volcano monitoring system, were air-transported from Australia to west Java in August 1998. Customs clearance can be problematic in Indonesia. Despite the added cost, it is advisable to ship equipment as excess baggage on the same flight as the investigators and to greet colleagues at the airport prior to customs declaration. ITB partners have considerable experience with expediting incoming scientific equipment through customs. Delays of weeks due to customs bureaucracy are not unusual in Indonesia.

Ancillary equipment such as batteries, radio masts, concrete, PVC pipe, drums, etc, were purchased in Bandung in preparation for the field deployment of the four station monitoring system. Hire cars were arranged and co-investigators from the VSI and ITB accompanied the author to Gunung Papandayan.

It took a full four days to install the three slave stations on the volcano and the base station at the VSI observatory. At each slave station site a concrete pad was built, large enough to house the GPS/PC module, radio, solar regulator and a battery inside a cut-off 44-gallon drum. The solar panels were mounted on four PVC pipe struts. The GPS antenna was elevated 1.5m above the ground surface on a fibreglass pole and 5m high masts were erected for radio communications. At Kawah, the most trafficked station, a fence was erected around the installation to guard against vandalism (see Fig. 4.8).

Figure 4.11 – *Close-up picture of steel drum with PVC pipes at Nangklak.*

All cables, such as the radio antenna cable, the GPS antenna cable and the solar panel power cables, were housed in PVC tubing to guard against damage from animals. It was anticipated that the sulphur gas environment could degrade the electronic components inside the GPS/PC modules and radios. Caustic soda was placed inside the drums to react first with sulphur gas present inside the drum and to not deteriorate the electronic componentry (rather like a sacrificial anode on the underside of a boat). Concerns for the GPS/PC module inside the drum overheating, particularly in the dry season, were addressed by adding large airholes with PVC tubing covered by a plastic mesh to allow airflow but prevent animals from entering the drum.

The power system at the base station was also a challenge. Although the system is running on AC power, frequent blackouts of up to six hours duration, and spikes and surges in the power, mean that extra measures need to be taken to ensure that continuous DC power is supplied to all components (section 4.3.1). The base station antenna was located as far from the observatory building as possible to reduce the effects of multipath and also to improve the skyview. The length of the antenna cable, however, restricted this distance. It was decided that, due to the power of the low-noise amplifier inside the MicroPulse antenna and the quality of the antenna cable, a 30m cable was sufficient.

4.4.2 Feb./Mar. 2000 Deployment

The August 1998 installation only achieved limited success. All stations were installed but continuous GPS operation was not successful. At most only two days of continuous data from two slave stations and the base were logged. Additionally the quality of the data was poor (see section 4.4.3).

Despite these setbacks, much experience was gained concerning aspects of the operation of the system. The corrosion due to sulphur gas, while extreme, was not as severe as had been anticipated. It was expected that the steel drums would have to be replaced after 7 months exposure to a high sulphurous environment, particularly at Kawah (the most affected site). However this was not the case. As this system is only a 'proof-of-concept' system, the steel drums are considered sufficient to protect the GPS/PC modules and radios. For a longer term system it would be advisable to build fibreglass covers for this equipment. The fibreglass poles used to elevate the GPS antennas were unaffected by the sulphurous environment, nor were the electrical tape and PVC tubing used in the installation. The solar panels, made from glass and aluminium, were also in good condition after 7 months of exposure. The solar panel frames are made from aluminium, but are held together using steel bolts. The bolts have been severely attacked by sulphur gas and will need to be replaced in the future.

At Kawah one of the two solar panels was destroyed by a strong wind which tore the entire solar panel frame from its concrete mounts on the PVC struts (see Figure 3.6). Miraculously one panel remained undamaged and has been re-installed to supply power

to the Kawah station. The power system had been over-engineered for the slave stations, so given that there are not too many sun-free days, the operation of just one solar panel should be sufficient to supply continuous power. The power system at the other slave stations appears to be reliable. The power system at the base station is indeed continuous, despite the unreliable nature of AC power in rural Indonesia. A power blackout was witnessed by the author without a break in the survey at the base station.

The caustic soda inside the drum seemed to be spent indicating that it had reacted with the sulphur gas inside the box. Perhaps the caustic soda should be replaced every 3 months.

It was found that the 30m GPS antenna cable at the base station was unknowingly cut by farmers despite being housed in PVC tubing. This cable was repaired on-site, tested and reconnected. It was also discovered that the antenna cable and GPS antenna at the Nangklak station was faulty, and these parts were replaced. Many other minor problems, such as blown fuses and some baud rate incompatibilities, were experienced during the March 2000 deployment.

One of the deficiencies of the system is the need to take a laptop computer and laplink cable in the field to start the survey. Not only is this inconvenient and potentially damaging for the computer (particularly in the rainy season) but also it is not possible to check in the field if the survey has started correctly or not. All that can be checked is if the GPS receiver is communicating with the PC inside the GPS/PC module. One has to travel to the base station and check if data is being received, on the hour, from the remote slave stations. This configuration requires frequent station visits in the event that problems arise, a most inconvenient situation. Of course for a reliable, mature system, this initial setup will be a one-off procedure.

The focus now is on demonstrating the longevity of the system in a harsh volcanic environment, and acquiring consistent and high quality data.

4.4.3 Software and Hardware problems

Problems of the Aug 1998 survey

Some data was collected during the August 1998 deployment. The hardware proved to be quite unreliable at this early stage, but it was encouraging to obtain some initial baseline results. However, after processing the data it became clear that the quality of the data was generally poor. Using the UNSW baseline processing software repeatabilities of 6 cm could be achieved for baselines of only 7 km in length. The data also exhibited many small 'jumps' which were too small to be cycle slips. The GAMIT software could not repair these jumps (Peter Morgan 1999, personal communication), and upon further investigation it was discovered that the CMC decoding software had a bug. The decoding software was rewritten to produce identical results to UNAVCO's teqc software, decoding CMC binary data into RINEX data. In addition, a problem was found with the sample rate used for CMC phase measurements. Because a phase measurement is derived from integrating the Doppler measurement, integrating over 15 seconds produces an unrepresentative estimate of the movement of the satellite and therefore corrupts the resultant phase measurement. A new approach was adopted whereby one second samples were integrated and accumulated for 15 seconds thereby producing more accurate phase measurement, which was logged at the GPS station. This was successfully tested at UNSW with a new version of the baseline processing software, before returning to Indonesia in Feb/Mar. 2000.

Problems of the Feb/Mar. 2000 survey

The new decoding software with updated sample rate strategy was uploaded to the slave stations on Gunung Papandayan. Again the hardware operated very unreliably, with frequent stops to the survey. This was finally identified as a memory problem. The PC boards have a small data storage capacity (240 Kb) called "disk-on-chip". This Flash-PROM essentially operates as a hard disk by reading and writing to sectors on the chip. It is only possible to write to a particular sector a finite number of times. Continual use causes some sectors to become 'bad', and can no longer be written to. The size of the Flash-PROM therefore progressively decreases. Because the system only has 240 Kb free, with around half of that being used by software, it is easy to fill up the Flash-PROM. In this case the GPS/PC module will just stop, and hence the survey will stop. A new software upgrade overcame this problem by deleting old files of logged GPS data

(usually around 30 Kb in size), but for some GPS/PC modules only 160 Kb space on the Flash-PROM remained. New chips were obtained and re-installed on the GPS/PC modules, but the survey still stopped after around 50 sessions. Appendix B-1 describes some of these errors.

This problem was later identified as a problem with the RAM at the slave stations, which did not clear itself after each session, gradually filling its buffer and causing the survey to stop prematurely. This effect was reproduced during testing at UNSW and new software was written to address this problem. A 3-week long continuous test of the whole network on campus at UNSW confirmed that the system would run continuously. This new software was used for the July 2001 deployment.

4.4.4 July 2001 Deployment

Two years after first installing the GPS monitoring system on Gunung Papandayan, the original hardware, with new software, was redeployed in July 2001. The solar panels were left at Bukit Maung and Nangklak for the entire 2-year period. The remaining undamaged panel at Kawah was brought back to the observatory at the base station after the Feb/Mar 2000 campaign to guard against vandalism. The aluminium frames remained unaffected by the corrosive sulphur gas, however the zinc-plated bolts holding the frame together were badly corroded (although still strong enough to hold the solar panels).

The fibreglass antenna poles were also unaffected by the sulphur gas, as was the PVC piping encasing all cables. However, the temporary steel drums however were almost entirely rusted away and needed to be replaced. It was decided to replace the steel drums with sulphur gas resistant plastic drums (Fig 4.12). It is anticipated that these drums will be unaffected by corrosive volcanic gases.

Figure 4.12 – *The new plastic drums installed during the July 2001 deployment.*

Two of the slave station batteries were old and needed to be replaced. In addition, the backup batteries at the base station had to be replaced to ensure continuous power.

The slave station at Kawah was badly vandalised and a new fence was erected. The radio antenna cable had also been severed and needed to be repaired. A new solar panel frame was built in Australia and reinstalled at Kawah. Again, only one solar panel was available for the station at Kawah.

4.5 Budget

A design specification, and indeed a major motivation of this project, was to build a low-cost system. All components of the system have therefore been selected with this aim in mind. Rizos et al (1997b) proposed a total cost for one receiver station of around $US3000. The total cost of all components is detailed below and it indicates that for both a slave station and the base station the final design was slightly more expensive than the target budget.

4.5.1 Volcano Slave Station

GPS/PC Module	
Canadian Marconi Company Allstar OEM	$ 650.00
JED Computers PC104 PC	$ 550.00
Packaging of box (GPSat systems labour)	$1000.00
MicroPulse L1 Survey GPS antenna	$ 550.00
GPS antenna cables	$ 50.00
GLB Radio	$1027.00
Yagi antenna	$ 273.00
Radio accessories	
Antenna cable	$ 120.00
Power & interface cables	$ 35.00
Mast	$ 30.00
Mounting brackets	$ 45.00
Solar Panels - BP275F 12V 75W 36 cells x 2	$1071.00
Solar Regulator – BP GCR 1200 M 12A 12/24V (metering)	$ 128.10
Battery – 12V lead acid (wet)	$ 90.00
Monument	
Fibreglass poles	$ 32.00
Mounting brackets	$ 113.00
Miscellaneous	$ 30.00
Labour & materials (concrete/reo)	$ 50.00
Total ($AUD)	**$5844.10**
Total ($US @ 0.65)	**$3798.67**

One of the most expensive items for the slave stations was the cost of the solar panels. The power system was designed to operate for 5 consecutive days without sunshine and be recharged by the solar panel configuration in 3 sunny days thereafter. It could be argued that the power system is 'over designed', therefore escalating the cost of a slave station.

4.5.2 Volcano Base Station

GPS/PC Module	
Canadian Marconi Company Allstar OEM	$ 650.00
JED Computers 150 MHz Pentium	$1050.00
Packaging of box (GPSat systems labour)	$1000.00
MicroPulse L1 Survey GPS antenna	$ 550.00
GPS antenna cable (30m)	$ 50.00
GLB Radio	$1027.00
SMD2 Side mounted Dipole antenna	$ 205.00
Radio accessories	
Antenna cable	$ 120.00
Power & interface cables	$ 35.00
Mounting brackets	$ 45.00
Uninterrupted Power Supply (UPS)	$ 212.50
Backup battery (45 Ah)	$ 37.00
Backup battery (70 Ah)	$ 75.00
Hard Disk	$ 200.00
Monument	
Fibreglass poles	$ 32.00
Mounting brackets	$ 113.00
Miscellaneous	$ 30.00
Labour & materials (concrete/reo)	$ 50.00
Total ($AUD)	**$5481.50**
Total ($US @ 0.65)	**$3562.98**

At the base station the extra cost of the higher performance Pentium processor and the UPS offsets the savings of not requiring expensive solar panels to supply power. The total costs of the base station and slave station configurations are therefore similar.

It is worth pointing out that the total cost of the entire four station configuration is less than $US15,000. This compares favourably to the cost of just one "top-of-the-line" GPS receiver, which can cost of the order of $US20,000 or more!

4.6 Error Mitigation for UNSW-designed System

Whilst section 3.2 deals with error mitigation strategies for all types of volcano monitoring systems as categorised in (section 2.3), the specific error mitigation strategies adopted for the UNSW volcano monitoring system are detailed below.

4.6.1 Antenna Phase Centre Variation

Section 3.4.1 deals in some detail with the issue of APCV, and the various approaches that are used to account for it. At UNSW, attempts were made to model the phase centre variation of a series of low-cost antennas using the APCV estimation from GPS data approach (see section 3.4.1.2). Unfortunately APCV estimation was unsuccessful but the experiment did highlight the need for a certain level of quality when choosing a low-cost antenna for deformation monitoring applications (Roberts et al, 1998).

Tests were conducted using both a very low-cost vehicle tracking antenna and the MicroPulse 13700 L1 lightweight survey antenna, which was subsequently chosen for the UNSW system. It was found that in computing the position of the antennas with respect to a high-quality, geodetic standard antenna, the more expensive survey-grade antenna was considerably more accurate than its vehicle tracking counterpart.

A microstrip patch antenna consists of an in-built groundplane, a feed that supplies RF power, a microstrip surface and a dielectric substrate which separates the two. Major factors that influence the quality of the antenna are (Fooks 1998, personal communication):

1. The lower the dielectric constant, ie closer to 1 (1 for a vacuum, but in reality this constant will be closer to 2) and the thicker the dielectric substrate, the higher the efficiency of the antenna.

2. The size of the patch is often about half the wavelength of the signal. Hence the larger the microstrip patch is, the more efficient the antenna will be. If the size of the microstrip patch is less than half the wavelength, then a higher dielectric constant substrate material should be used, but at the expense of the efficiency of the antenna. This is the case for a vehicle-tracking antenna.

3. Shape, size and thickness of the dielectric substrate change the bandwidth of the antenna, ie the thicker the material the larger the bandwidth and the higher the cost.

4. The microstrip patch is often attached to the substrate using some kind of photolithographic technique. This process is considered to be quite accurate.

5. The change in the permittivity across the dielectric substrate material will determine the quality of the antenna, particularly when the dielectric constant is close to 1. This is batch dependent, during manufacturing.

6. Position of the antenna cable feed should not be in the plane of the groundplane. This could cause an electrical disturbance which could influence the position of the electrical phase centre. The more expensive antennas have the antenna feed extending out of the base of the antenna housing.

7. Microstrip patch antennas are sensitive to changes in ambient temperature.

8. Circularly polarised antennas provide a better chance to pick up the same signal regardless of orientation (Peng, S.Y., 1996).

The results of the UNSW antenna testing are summarised in Table 4.1.

Table 4.1 - *Comparison of low-cost antennas from rotation tests at UNSW.*

	Std. Deviation Easting (m)	Std. Deviation Northing (m)	Std. Deviation Up (m)
MicroPulse 16200 Vehicle Tracking	0.0058	0.0021	0.0025
MicroPulse 13700 L1 Lightweight Survey	0.0007	0.0009	0.0028

Note: Previous rotation tests using the MicroPulse 16200 Vehicle Tracking antenna only have resolved standard deviations in the up component of 0.0067 & 0.0054m indicating a larger scatter than that of the 13700 antenna. This result is to be expected.

It can be seen from Table 4.1 that the scatter in the E & N components for the lightweight survey antenna is considerably lower than for the vehicle-tracking antenna. Based on these tests it was decided to purchase a more reliable survey-grade GPS antenna. The cost comparison of the vehicle tracking and survey antennas was approximately $AUD200 vs. $AUD500.

Because the APCV tests were unsuccessful at UNSW, the MicroPulse antennas were sent to the USA to be calibrated by the National Geodetic Survey (NGS) (section 3.2.1.3). Two antennas were sent in order to check the variability of antennas of the same make and model. The result of the APCV calibration test are presented in Table 4.2 (also see Table 3.2).

Table 4.2 - *Antenna Phase Centre Variation table for the MicroPulse L1 Lightweight Survey Antenna.*

MCP1370

[N]	[E]	[up]							
-2.1	-0.7	60.1							
[0]	[5]	[10]	[15]	[20]	[25]	[30]	[35]	[40]	[45]
[50]	[55]	[60]	[65]	[70]	[75]	[80]	[85]	[90]	
0.0	1.0	2.0	3.1	4.2	5.2	6.2	7.0	7.6	8.0
8.0	7.5	6.4	4.7	2.1	-1.5	-6.1	0.0	0.0	

It may seem curious that so much effort has been invested in these APCV studies, given that there is presently no antenna mixing in this low-cost system. However, for subsequent systems, a fiducial network of high-quality, dual-frequency GPS receivers equipped with choke-ring antennas will surround the low-cost system described here (Janssen et al, 2001).

4.6.2 Multipath

Multipath is the effect where direct and reflected indirect signals superimpose at the antenna to corrupt the measured signal (section 3.4.2). The multipath effect is unique to the station location as it depends on the material composition and geometry of the surroundings. The UNSW approach to multipath mitigation accepts that multipath will be present in the measurements and tries to remove these effects during post-processing. The MicroPulse antenna is equipped with a groundplane housed inside the plastic casing. This antenna is not equipped with an additional groundplane to reduce multipath effects. However some precautions were taken.

The antennas are mounted 1.5m above the ground surface to minimise multipath reflections (Johnson et al, 1995). Meertens et al (1996) state that, "GPS antennas should not be placed near the ground because the scattering from the ground causes low frequency multipath that can be mis-modelled as tropospheric delay resulting in vertical errors as large as several cm." Also, "...measurements using GPS antennas mounted on tripods at 1.5m height are generally more accurate because they are subject to high frequency multipath (high frequency multipath is not easily confused with tropospheric delay)."

Although pseudo-ranges are more highly affected by multipath than carrier phase, precise baseline determination uses carrier phase measurements. Rizos (1997a) states that carrier phase multipath does not exceed a quarter of the carrier wavelength, ie 5-6cm.

The static nature of points in the deformation monitoring array, and the fact that carrier phase multipath is for the most part periodic, can be exploited using digital signal processing techniques. Because the GPS antennas are stationary, the carrier phase

multipath will repeat itself every day at the same time minus approximately 236 seconds (the time difference between a solar day and two periods of the GPS satellites). The multipath signal from the previous day's observations can be identified using a Discrete Fourier Transform (DFT) and subtracted from the present day's data using an appropriately designed Finite Impulse Response (FIR) filter.

Han & Rizos (1997) describe how such an approach was successfully implemented for GPS data measured on the roof of the GAS building at the University of New South Wales. Double-differenced residuals from a 6m baseline indicated a periodic carrier phase multipath signal between successive days (Fig 4.13).

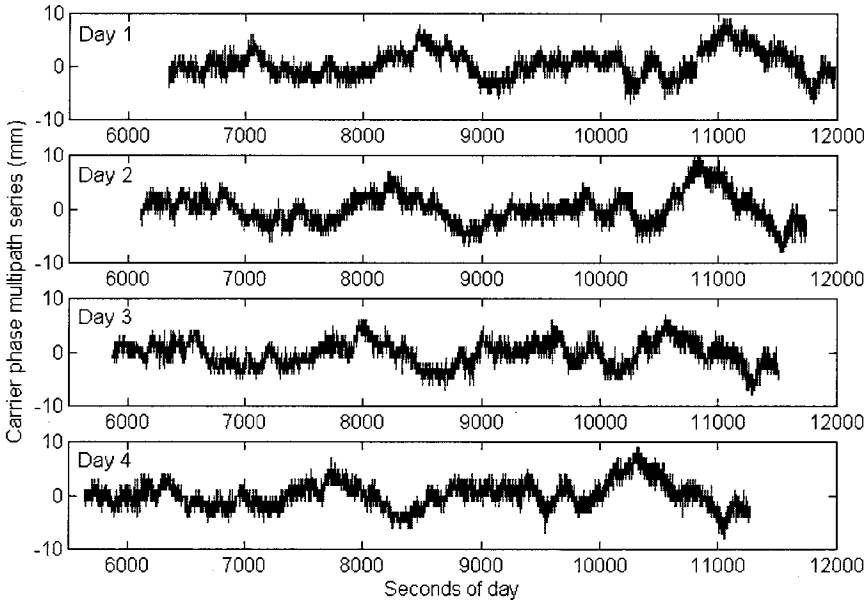

Figure 4.13 - *Multipath series of carrier phase double-differenced observations for four successive days April/May 1997 (Han & Rizos, 1997).*

A few assumptions need to be noted regarding this point:

1. Because the baseline was only 6m in length, tropospheric delay, orbit bias and ionospheric delay are assumed to be absent. The residuals therefore show only double-differenced multipath and some observation noise.

2. Ionospheric, tropospheric and orbit biases are best mitigated by reducing the length of the baseline. This is only partially feasible for volcano monitoring, ie baselines are comparatively short, but may be up to 10km in length.
3. Double-differenced residuals imply a satellite pair. The highest elevation satellite is chosen as the base satellite, and its signals are assumed to be multipath-free. The signal from the second satellite is assumed to be responsible for all multipath.
4. The base station is located in a multipath-free environment.

Han & Rizos (1997) use an auto-correlation function to confirm the randomness of the data and the cross-correlation function gives the time offset between successive days. This value should be about 236 seconds, as mentioned earlier, though the resulting value in this case was 226 seconds due to the satellite orbit period being perturbed by a variety of forces.

The time series data in figure 4.13 can be transformed into the frequency domain using a Discrete Fourier Transform. The frequency domain indicates which periods of temporal data dominate. It is known that multipath has a characteristic period of between a few minutes up to approximately 30 minutes, hence examining the frequency domain can confirm if multipath is present in the data or not.

From Fig. 4.14 it can be seen that the maximum frequency bands exist between 1/2400 Hz and 1/120 Hz. This corresponds to wavelengths between 40 & 2 minutes. Frequencies lower than 1/2400 (or longer wavelength effects) are attributed to other biases, such as tropospheric delay. Frequencies below 1/180 are considered to be observation noise.

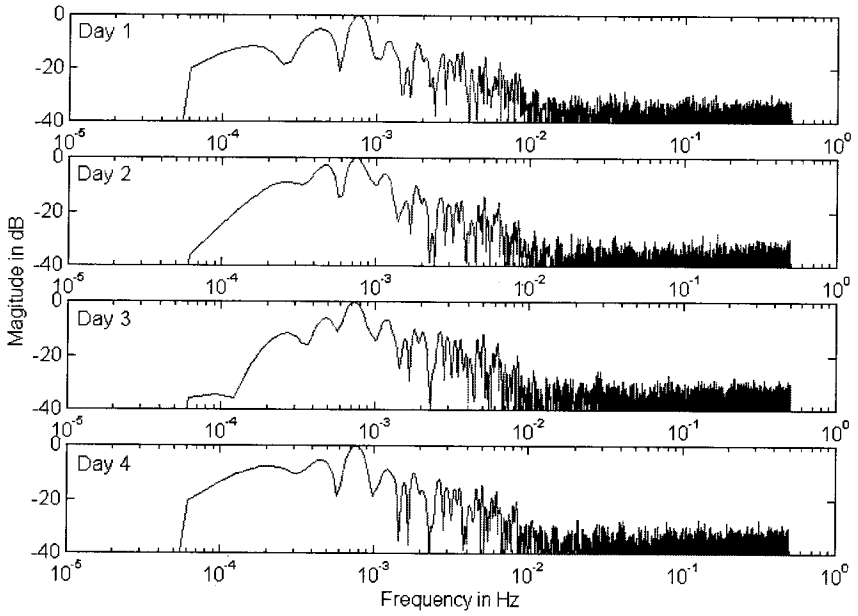

Figure 4.14 - *Frequency-domain representations of multipath on carrier phase data.*

Two digital signal processing approaches can be used on the data. A bandpass filter can be designed to filter out all extraneous noise, and allow only the multipath signal to pass. This characteristic signature can then be used to subtract the multipath effect from the double-differenced residuals, leaving clean, multipath-free (or significantly reduced) double-differenced observations. Due to the design of the filter, there will be a delay for real-time applications of a few tens of minutes between the time of observation and the time of multipath correction.

Secondly, a stopband filter can be designed to mitigate multipath frequencies directly. Stopband filtering also experiences the same delay effects and is therefore unsuitable for real-time positioning.

A second approach assumes that the GPS antennas are permanent and the antenna environment does not change. The characteristic multipath signature for the previous day minus the cross-correlated time shift (close to 236 secs) can be used as a form of template to subtract out the multipath error, in real-time, for the current day.

For the UNSW volcano monitoring system the template approach would not be necessary, as there is no requirement for real-time multipath-corrected data. A stopband

filter applied to the double-differenced residuals between the slave and base receivers would mitigate multipath during the processing stage, because the raw data for that particular session is operated upon. The template approach assumes that the multipath signal for the previous day is identical to that of the present day (minus the sidereal day offset). This is not strictly correct even though the antennas do not move. A wet rock could produce multipath, but a rock in the vicinity of the antenna may not be wet every day.

Such an approach to multipath mitigation is particularly attractive in a volcanic environment where multipath from the up slope of the flank of the volcano is difficult to avoid. At the Kawah station, the threat of vandalism is greater due to the location of the point and the number of tourists who visit this area. A barbed wire fence was constructed around the point to guard against vandalism; but the fence is also expected to significantly increase the multipath. In addition, the solar panels mounted at all slave stations are close enough to the GPS antenna to possibly act as a reflector. Digital signal processing of the carrier phase measurements during the post-processing of the data could be implemented into an automatic baseline processing routine to mitigate multipath without the need for additional expensive hardware enhancements.

Chapter 6 uses a simplified digital signal processing approach on a post-processed baseline time series of data from the SAGE NZ network and identifies a multipath signature in the height component. This multipath effect is removed and the corrected baseline time series is demonstrated to exhibit a lower repeatability, and higher precision.

4.6.3 Troposphere

It is recognised that one of the largest biases impacting on the vertical component arises from mis-modelled tropospheric delay on the GPS measurements (Beutler et al, 1990). This is particularly relevant at Gunung Papandayan which, because of its location in a tropical region, is expected to experience a high moisture content in the lower atmosphere. The characteristics of the wet component of the troposphere are the least precise to measure or model. Also, being a volcano monitoring network, the change in the height between the base station and the slave stations (differential troposphere) is up

to 1400m. This is a significant elevation difference, which is not well accounted for by existing tropospheric models (Brunner & Tregoning, 1994b), particularly in the tropics.

Mendes (1999) suggests that the best existing models of tropospheric delay due to the wet and dry components is the Saastamoinen model. The zenith delay is best transformed to any elevation angle using the Neill mapping function (Neill, 1996). Again, differential troposphere and the moist tropical conditions are not considered. Chapter 5 discusses in more detail the issue of troposphere modelling specific to this application.

4.6.4 Ionosphere

The UNSW-designed volcano monitoring system is comparatively small-scale, and uses single-frequency GPS receivers. The dual-frequency approach described in section 3.2.4.1 cannot be used to eliminate the effects of the ionosphere. Initially the system ignores the ionosphere, based on the assumption that the baseline lengths are less than 10 km, and that the ionospheric effects will therefore largely cancel during between-receiver differencing. However, Gunung Papandayan is located close to the equator and at the time of writing this thesis, a solar maximum was being experienced. Ionospheric effects must therefore be somehow addressed.

A fiducial network of dual-frequency GPS receivers surrounds the single-frequency network on Gunung Papandayan, as proposed by Wanninger (1995) (Fig 4.15). Han & Rizos (1996a) describe a correction algorithm for single-frequency observations based on a mapping of the ionospheric conditions derived from data from the outer fiducial network.

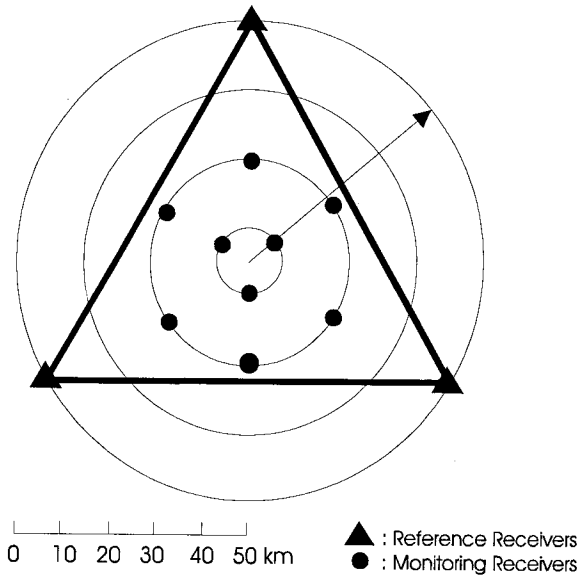

Figure 4.15 - *Configuration of fiducial network.*

The external network should be located away from the zone of deformation but within the local tectonic region. The precise coordinates of the external control stations can be derived with respect to the IGS network (section 4.6.6). These stations operate continuously generating data in order to determine a regional ionospheric model. Although the ionosphere is almost 1000km thick, a single layer model is assumed, typically at a height of 350km, where it is assumed the total ionospheric delay is compressed onto this surface. The slant ionospheric delay measured at external control stations is considered to be in the zenith direction, due to the small areal extent of the fiducial network (side lengths up to 80km). The variation in the ionospheric delay across the network is also assumed to be linear. (This assumption may not be valid during periods of heightened solar activity.)

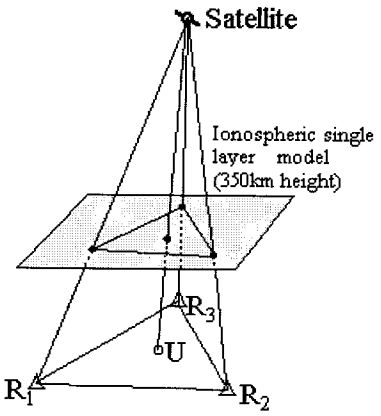

Figure 4.16 - *Differential model of the ionospheric delay (Han & Rizos, 1996a).*

The ionospheric delay for the L1 signal can be determined relative to the reference station, and the reference satellite, every epoch, by (Han & Rizos, 1996a):

$$I_i^j(k) = \frac{f_2^2}{f_1^2 - f_2^2} \cdot \left(\left(\Delta\nabla\Phi_{L1}^{j,i}(k) - \lambda_1 . \Delta\nabla N_{L1}^{j,i} \right) - \left(\Delta\nabla\Phi_{L2}^{j,i}(k) - \lambda_2 . \Delta\nabla N_{L2}^{j,i} \right) \right) \quad \text{-(4.6)}$$

Where:

$$\Delta\nabla\Phi_{L1}^{i,j}(k), \Delta\nabla\Phi_{L2}^{i,j}(k) \quad \text{- (4.7)}$$

are double-differenced observations of the L1 and L2 carrier phase (in units of metres) relative to the reference station and the reference satellite. Note that for a rising satellite, no ionospheric corrections can be applied until ambiguities for that satellite have been resolved.

To illustrate the linear interpolation method across the mapped ionospheric surface consider the following expression (refer to Fig 4.16):

$$I_i^j(k) = x_i . a_N^j(k) + y_i . a_E^j(k) \quad \text{- (4.8)}$$

where the 'a' terms represent the north and east slope components respectively for satellite j, relative to the reference satellite and the reference station for epoch k. The slope parameters are unique to each satellite/receiver pair and change as the satellites move. The 'x' and 'y' parameters refer to the relative location of the reference station for the model. Chen et al (1999) gives examples of this approach for four different data sets.

This correction approach linearly interpolates the Total Electron Content (TEC) value across a surface and approximates the ionospheric delay at any point within the region. However it cannot account for the effects of phase scintillations, which can be very localised.

An outer fiducial network comprising expensive, dual-frequency receivers would seem counter-intuitive when the major thrust of the UNSW design is for a low-cost system. The UNSW system however is a 'proof-of-concept' design, and it is anticipated that with the ever-increasing number of continuous dual-frequency GPS networks being established, these could provide a convenient backbone for densification using a low-cost inner GPS network. Additionally, in environments such as West Java where many active volcanoes are located close to one another, one well designed outer fiducial network could provide corrections for several low-cost networks simultaneously. For example, one fiducial network could service low-cost networks on Mt. Papandayan, Guntur and Galunggung.

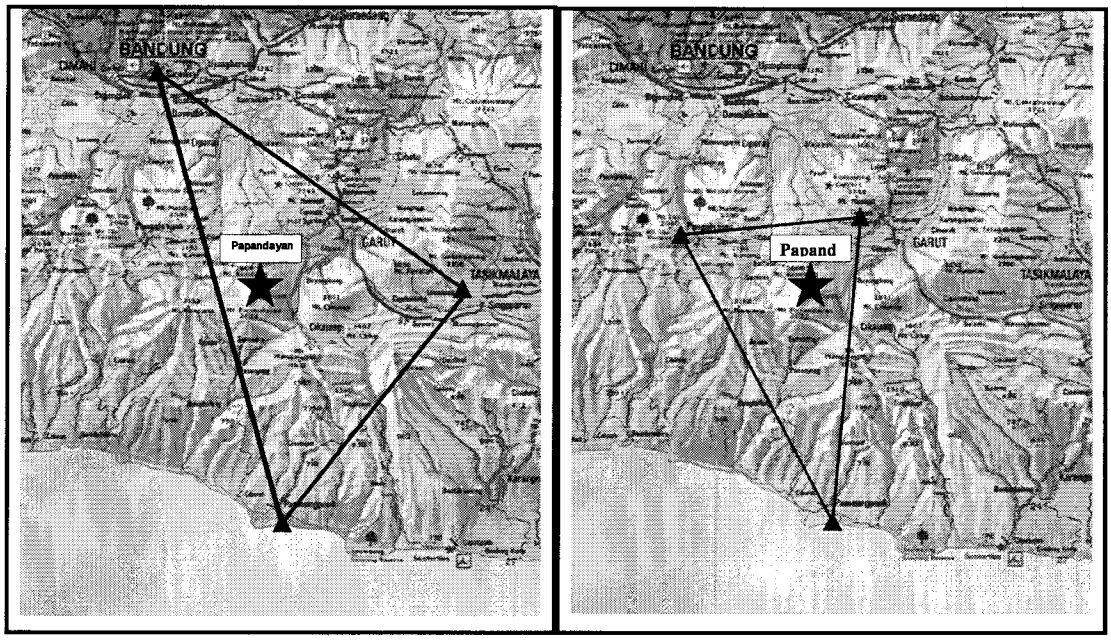

Figure 4.17 – *Diagram of fiducial network for the Feb/Mar 2000 survey on the left and the smaller fiducial network for the July 2001 survey on the right.*

The Feb/Mar 2000 measurement campaign selected three sites as fiducial sites; Bandung, Galunggung and Pameungpeuk (see Fig 4.17). Unfortunately due to the extreme ionospheric noise brought on by the present solar maximum, the baselines lengths were considered too great to provide meaningful correction terms (Janssen et al, 2001). A smaller fiducial network was established for the July 2001 campaign (Fig 4.17) comprising Pameungpeuk, and two new stations at Pengalengan and the Gunung Guntur volcano observatory.

4.6.5 Satellite Orbit Bias

The effect of satellite orbit error on baseline determination was given in equation 3.9, section 3.2.5, and is quantified as a well known rule-of-thumb (Rizos, 1997a). For a 7km baseline using a pessimistic estimate of a 20m orbit bias, a baseline error of 7mm would result. Given the static nature of the deformation network, and the relatively short distances between receiver stations located on the deforming body, the broadcast ephemerides are considered to be of sufficient accuracy for insitu processing. Using post-processed, rapid or even precise predicted IGS orbit products would not contribute significantly to improving the accuracy of this GPS-based, deformation monitoring system. Additionally, the problem of incorporating the IGS orbit products in real-time into the data processing cycle at the Papandayan observatory would require an increase in communications infrastructure, and therefore a significant additional cost.

4.6.6 Starting Coordinates

With reference to section 3.2.6, method (3) is used to derive starting coordinates for the base station at the Gunung Papandayan inner network, in a two-step process. First, the fiducial network established in the Feb/Mar 2000 measurement campaign was connected to the BAKO IGS station whose absolute coordinate accuracy is stated as 1cm (IGS, 2000). Secondly, the derived coordinates for the fiducial stations are then held fixed and the base station coordinates of the inner single-frequency network are computed. The distance between the BAKO site and the Papandayan base station was considered too far to ensure the highest quality result.

The fiducial sites collected data using Leica CRS1000 dual-frequency GPS receivers (with choke ring antennas). 72-hour data files (ie three 24-hour sessions) were used to connect all three fiducial sites independently to the BAKO IGS station. The Bernese software (Rothacher & Mervart, 1996) and precise IGS ephemerides were used to compute the three coordinate values using conventional long static baseline processing procedures. Three coordinate sets were obtained for each fiducial site and the mean was then computed.

The fiducial coordinates were held fixed and three baselines (24-hour data) were processed to obtain the coordinates of the Papandayan base station. The resulting three coordinate sets showed differences of up to 1m possibly due to the high ionospheric activity at the time (baselines up to 60 km long and single-frequency), multipath at the low-cost base station antenna and troposphere effects. A mean value for the base station was generated using the Bernese software, which could be claimed to have an accuracy at the metre level or better. Table 4.3 lists the starting coordinates used hereafter for the single-frequency inner network on Gunung Papandayan (see Section 6.4).

Table 4.3 - *List of WGS84 starting coordinates for the single-frequency inner network on Gunung Papandayan.*

Station	X	Y	Z
Base	-1933614.0131	6025645.7317	-802279.9143
Bukit Maung	-1928406.6847	6027755.3781	-806707.8448
Nangklak	-1927104.2280	6028391.0919	-807450.2857
Kawah	-1927737.2506	6028054.2288	-806646.1924

Chapter 5
TROPOSPHERIC DELAY FOR VOLCANO MONITORING

5.1 Introduction

Regional, small scale GPS networks must demonstrate a reliable repeatability to a specified level of accuracy in order that any measures outside defined threshold limits can be unambiguously identified as deformation. Tropospheric delay of the GPS signals has been identified as a significant bias by virtue of the large change in height between the base station receiver and the slave receivers situated on the volcano. Section 3.2.3 discussed the effect of the troposphere and some standard techniques to account for this bias.

Gurtner et al (1989) state that tropospheric modelling is only true for a 'flat earth'. A large height difference between two the baseline endpoints (as is the case for volcano monitoring) can introduce a bias of the order of 2 – 5 mm per 100m height difference. Thus the assumption that tropospheric effects for short baselines can be ignored is no longer valid in this case. This is due mainly to daily variations of temperature and humidity, causing the tropospheric effects derived from standard models such as the Saastamoinen, Hopfield, Black etc. (section 3.2.3) to be in error, particularly with regard to the heights of points (Ruehrnoessl et al, 1998). Further encouragement for investigation into this bias on Mt. Papandayan is given by Mendes (1999) who states, "...equatorial and tropical regions are clearly the most problematic, likely due to high and variable water vapour content in the atmosphere."

Data from the Southern Alpine Geodetic Network (SAGE) in New Zealand confirms this assertion. Two stations separated by 9.2 km and 1350m in elevation have been installed west of the great divide on the South Island. The data were kindly provided by John Beavan and his research team. (Note that data from the single-frequency network on Gunung Papandayan was not considered suitable for investigations into differential troposphere at this stage. The extreme data noise, believed to be as a result of a noisy ionosphere - Janssen et al, 2001 - precluded the use of this data.) Only the L1

measurements were processed using the UNSW Baseline software for a 17-day time series of 1-hour data sessions. The effect of the ionosphere was ignored for such a short baseline in a mid-latitude location. The standard Saastamoinen troposphere delay model was applied to both ends of the baseline. It can be clearly seen that the variability in the up component, compared to the easting and northing, is much larger (Fig 5.1). The standard deviation in the easting, northing and up components is 7, 11 & 41mm respectively.

For a volcano monitoring application this is problematic, as the most likely signal indicating some pending activity should be in the vertical component. It is important to reduce this solution variability, and thereby increase the accuracy and effectiveness of the forecasting and prediction of pending volcanic activity. In this chapter meteorological concepts are introduced, and the results of testing in equatorial regions using radiosonde data are presented. The scientific literature recommends the use of the Saastamoinen model for most applications, and its performance is compared using standard and local meteorological measures. It is concluded that parameter estimation is the best method for dealing with the differential troposphere, and consequently this approach is described in some detail. The specific aim of this research is to reduce the variability in the up component for regional equatorial, low-cost GPS-based volcano monitoring systems.

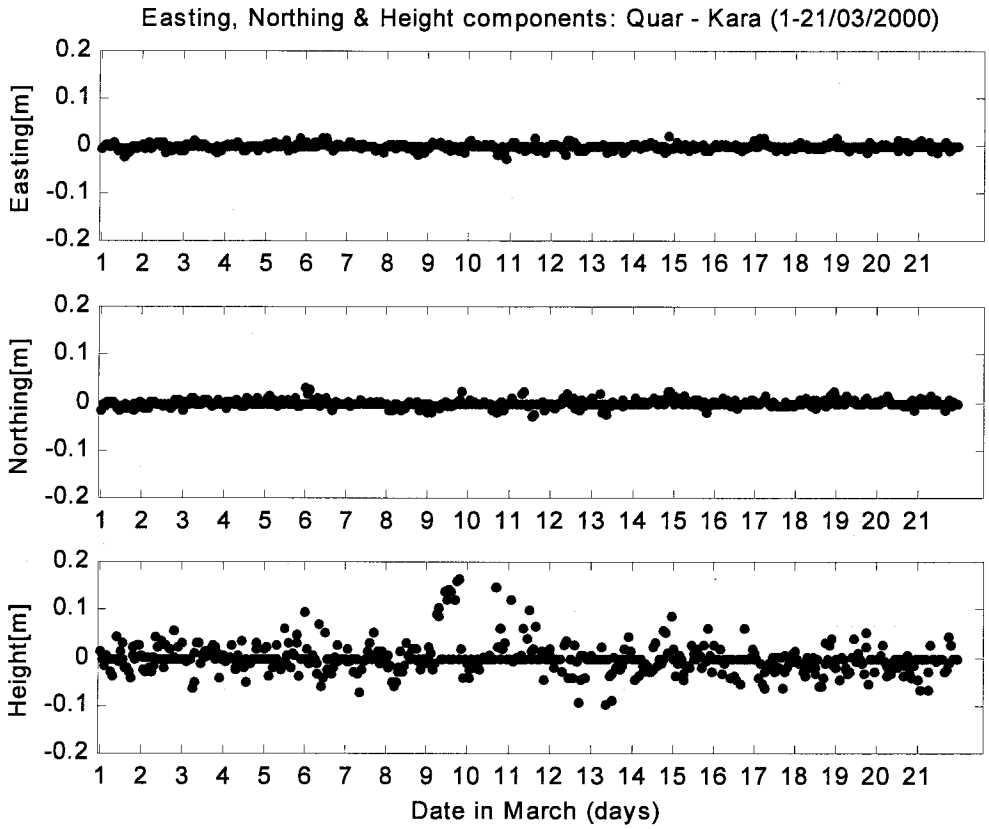

Figure 5.1 - *Time series of 1-hour baselines from SAGE-NZ network.*

5.2 Fundamentals of Tropospheric Modelling

In order to better understand the challenge of tropospheric modelling it is necessary to know something of the composition of the atmosphere and how it influences GPS signal propagation. The following discussion will focus on the non-ionised, neutral part of the atmosphere. Some meteorological terminology and concepts will be introduced, followed by a discussion of two widely used tropospheric delay models.

5.2.1 Standard Atmospheres

Mendes (1999) provides an excellent description of the composition and physics of the earth's atmosphere as well as introducing terminology relating to radio meteorology. The earth's atmosphere is very nearly in a state of hydrostatic equilibrium (ie the constituent gases which make up the dry part of the atmosphere are evenly mixed, up to about 80km altitude). This allows very accurate prediction of the electrical path (ie for a GPS signal) in the zenith direction based on surface pressure only, regardless of the

actual temperature structure (Saastamoinen, 1973; Davis, 1986). Indeed this is the assumption that is made for all tropospheric models with regard to the hydrostatic part of the tropospheric delay.

Figure 3.9 showed the various layers that make up the atmosphere. The earth's atmosphere can be approximated by model or standard atmospheres. Standard atmospheres were first developed in the 1920s under the assumption that the air is free of moisture, in a state of hydrostatic equilibrium, and behaves as a perfect gas. Details of these historic atmospheres can be found in List (1958).

A standard atmosphere, for the neutral atmosphere layer, should contain pressure, temperature and water vapour profiles with respect to height, as well as some information on seasonal and latitudinal variations. The U.S. Standard Atmosphere USSA66 (ESSA/NASA/USAF, 1966) provides for these conditions and has been identified as the most appropriate model for radio propagation studies (Mendes, 1999). The U.S. Standard Atmosphere Supplements (NOAA/NASA/USAF, 1976) provide a set of 9 additional atmospheres located at 15° latitude bands ranging from the equator to the pole, for both hemispheres. Additionally, within these bands the seasonal variability is taken into account by considering different conditions for July and January (except for the equatorial 30° band which is considered to have a negligible seasonal variability). Relative humidity is used to account for the moisture content of the atmosphere. Data for these models is empirically derived from radiosonde soundings (see section 5.2.2).

Commercial GPS baseline processing software such as Leica's SKI software and Trimble's Geomatics Office use values derived from these standard atmospheres to model the tropospheric bias. Scientific softwares, such as Bernese and GAMIT, go a step further and use a-priori values derived from these models, and estimate corrections.

5.2.2 Radiosondes

A radiosonde consists of a large weather balloon with a microprocessor and some form of radio link, carrying meteorological sensors to measure temperature, pressure and humidity at time intervals of a few seconds as it rises through the atmosphere. This

system is relatively inexpensive with about one thousand radiosonde stations operating twice daily for weather forecasting all over the world.

Bean et al (1966) have produced, "A World Atlas of Atmospheric Radio Refractivity", compiled exclusively from radiosonde soundings, and present world maps and graphs of upper-air radio refractivity (see section 5.2.4). It is these data which form the basis of the standard atmospheres mentioned in section 5.2.1. These data provide a vertical profile of the atmosphere which can be used to empirically derive inversion height, tropopause height and the temperature lapse rate (section 5.2.3) at points evenly distributed all over the earth. These data are also available for scientific use.

There are, however, some deficiencies with radiosonde data. Baby et al (1988) report, "...that radio soundings suffer from poor time resolution. It takes the radiosonde several hours to reach its maximum altitude. Therefore the obtained profiles are not representative of an instantaneous situation." Also there is a relatively slow response time of the radiosonde temperature and humidity sensors, which tends to bias the refractivity profiles. Another major problem is the spatial effect as the radiosonde drifts away from the release point. The planetary boundary layer[1] affects the refractivity profiles determined by the radio soundings up to about 1-km above the surface. Values of 3 km and above show no such problems (Bean et al, 1966).

Despite these disadvantages radiosonde data still plays a crucial role in meteorology. Mendes (1999) used data from 100 radiosonde stations in an effort to test zenith delay models and mapping functions for a number of existing tropospheric delay models. In order to derive these zenith delay models he first had to derive accurate global values for the tropopause height, inversion height and temperature lapse rate (see section 5.2.3 & 5.3). Prior to this work, interpolation of mean value tables for certain locations and seasons was the only method of providing global estimates of these parameters.

[1] The Planetary Boundary Layer is the lowest part of the atmosphere which forms as a consequence of the interactions between the atmosphere and the underlying surface (land or sea) over time scales of one day

5.2.3 Temperature Lapse Rate

Temperature decreases with height. In general this temperature gradient or temperature lapse rate is considered constant or linear with height up to a layer called the *tropopause* which defines the upper surface of the troposphere. Bean et al (1966) describe the tropopause as the altitude of the base of the first layer (or layers) which have a total thickness of at least 2 km and a temperature lapse rate of less than -2°K/km.

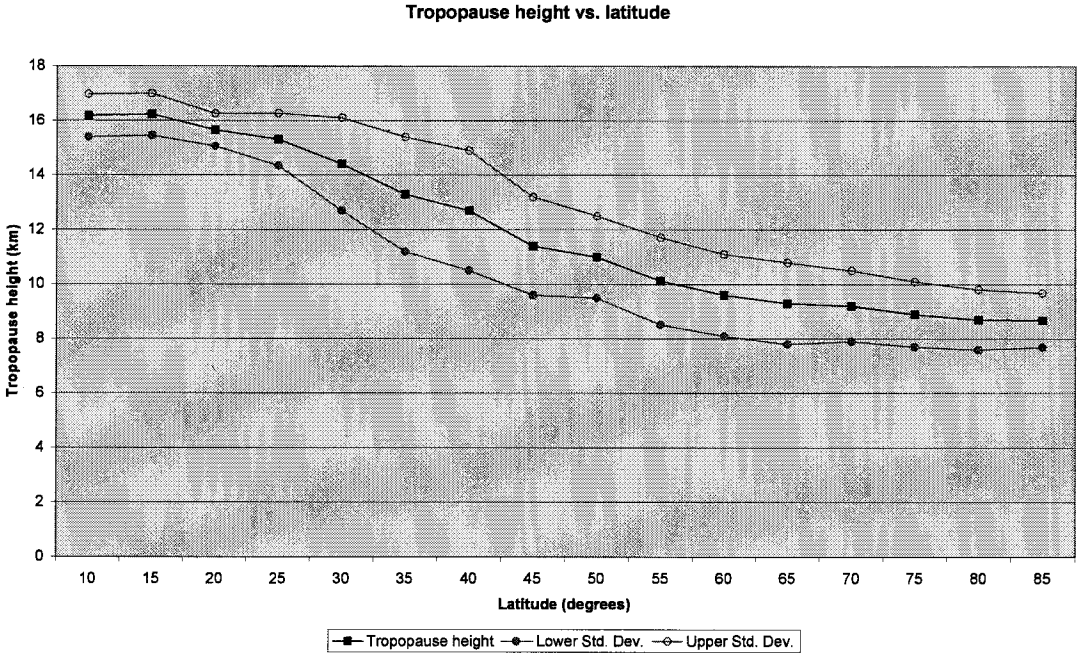

Figure 5.2 - *Height of tropopause (Based on data from Mendes, 1999).*

The height of the tropopause varies with location and season. The seasonal variations are more conspicuous for mid-latitude stations as compared to polar or equatorial stations (Mendes, 1999). Figure 5.2 illustrates the global tropopause height with respect to latitude and includes the seasonal variations in these values. Data is derived from over 100 radiosonde stations distributed globally.

An average value of the temperature lapse rate is defined as the rate of change of temperature with height between the top of an *inversion layer* and the tropopause (Bean et al, 1966). An inversion layer, instead of having decreasing temperature with height,

---

or less. In this layer, the effects of the surface roughness, temperature and other properties are directly transmitted through the mechanism of turbulent mixing.

causes the temperature above the ground surface to *increase* up to a certain height. An inversion layer is caused either by solar radiation from the ground surface, or due to adiabatic heating of a sinking layer of air. Radiation inversions are considered the most common form of inversion and the most straightforward to model. Such inversion layers are dependent on the length of the night and the surface temperature. The thickness of these layers ranges from only a few hundred metres for low and mid-latitude stations up to more than 2 km for polar stations. Given that both tropopause height and inversion height both vary with location and season, the temperature lapse rate therefore varies significantly.

The USSA66 model (section 5.2.2) is used in standard tropospheric modelling and the mean global value adopted for the temperature lapse rate is –6.50°K/km, and temperature is expressed as:

$$T = T_s - 0.0065 * (h - h_s) \qquad \text{- (5.1)}$$

where;

T_s - Temperature (°K) at sea level,
h_s - Height (m) at sea level.

Subscript *s* represents values at sea level.

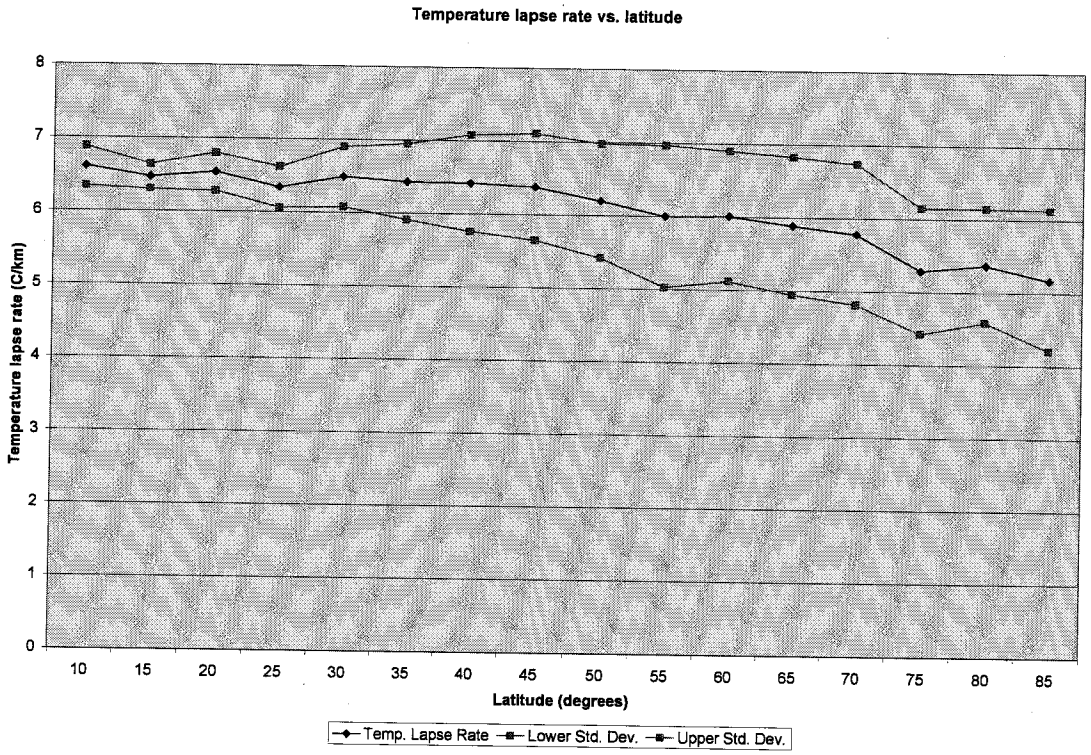

Figure 5.3 - *Temperature Lapse Rate (Based on data from Mendes, 1999).*

The highest lapse rates occur in tropical and mid-latitude arid regions with values of up to -8 °C/km. Seasonal variations are smallest in tropical regions (Bean et al, 1966).

The mean annual temperature lapse rate varies from -6.61°K/km at the equator down to -5.17°K/km at the poles (Fig 5.3). An average mean global value of -6.10°K/km is generally adopted. Figure 5.3 therefore shows that a global lapse rate of -6.10°K/km is adequate for all latitudes except the poles, as a first approximation. Appendix C shows that this discrepancy between the USSA66 value and that computed by Mendes (1999) can be considered negligible when computing the total zenith tropospheric delay using the Saastamoinen model.

5.2.4 Refractive Index

The propagation velocity of electromagnetic radiation in a vacuum adopted as a primary constant is c = 2.997922458 x 10^8 m/s (McCarthy, 1989). The propagation velocity of the GPS signals will be influenced by the earth's atmosphere and is characterised by the refractive index. The refractive index *n* is defined as the ratio of the (phase) velocity of

propagation of an electromagnetic wave in a vacuum to the (phase) velocity of propagation in the medium v.

$$n = \frac{c}{v} \qquad \text{- (5.2)}$$

The difference between actual refractive index and unity is of the order of 0.00027 greater than unity at sea level, and varies with altitude, latitude and various meteorological conditions (Parkinson & Spilker, chapter 13, 1996). This causes an excess path delay. As this value is very close to 1, it is considered more convenient to use the refractivity N:

$$N = (n-1)*10^{-6} \qquad \text{- (5.3)}$$

Atmospheric delay is defined as the integral of the refractivity over the ray path (MacMillan, 1995). At L-band frequencies (ie for GPS signals), the refractive index remains constant with frequency (Parkinson & Spilker, 1996). This characteristic defines a non-dispersive medium. The group refractive index (ie average refractive index when considering all constituents of the medium) and phase refractive index are equivalent. Hence the group velocity and the phase velocity are likewise identical. This is why tropospheric delay on the L1 and L2 frequencies is the same (as distinct from the ionospheric delay - section 3.2.4).

The tropospheric path delay can be defined in terms of refractive index integrated along the signal ray path:

$$d_{trop} = 10^{-6} \int N_{trop} ds = \int (n-1) ds \qquad \text{- (5.4)}$$

where;

N_{trop} is the refractivity of the troposphere from the ground up to the top of the tropopause.

Hopfield (1969) and Saastamoinen (1973) separate the tropospheric delay into a dry (or hydrostatic) and a wet (or non-hydrostatic) part, so that the total delay can be written as:

$$d_{trop} = 10^{-6} \int N_{dry} ds + 10^{-6} \int N_{wet} ds \qquad \text{- (5.5)}$$

Models for the refractivities are substituted into equation (5.5), and numerical methods are used to solve the integration. This results in simplified models which can easily be implemented in GPS baseline processing software.

Analytical integration along the ray path is theoretically impossible because the refractivity profile along the ray path must be well known, as well as the elevation angle of the ray at the reception site. The refractivity can be approximated in the zenith direction only under the assumption of no ray bending in the zenith and a spherically symmetrical atmosphere. More specifically this assumes that the integration step sums a series of thin spherical shells in which the refractive index does not change significantly within the signal's wavelength and the fractional refractivity changes between neighbouring shells are small within a wavelength (Mendes, 1999).

This representation can be further separated into the zenith hydrostatic and the zenith non-hydrostatic delay (or dry and wet zenith delay). Multiplying by an appropriate mapping function (see section 5.2.6) can accommodate all other elevation angles.

The actual path of a signal propagating through the atmosphere is curved due to changes in the refractive index with height. Therefore the actual path length of the signal is longer. The quantity of primary interest is the excess delay caused by the neutral atmosphere, and more specifically the troposphere. The error caused by the neglect of path curvature is less than 3mm for elevation cut-off angles larger than 20°, and 2cm for a cut-off of 10° (Davis, 1986), and is therefore not considered further.

Physicists have been investigating the refractive index of EDM and light waves as well as radio waves since the 1930s. Smith & Weintraub (1953) and Boudouris (1963) provide a general expression for refractivity (N):

$$N = K_1 \frac{P_d}{T} + K_2 \frac{P_w}{T} + K_3 \frac{P_w}{T^2} \qquad \text{- (5.6)}$$

where;

P_d - Partial pressure due to the hydrostatic component including CO_2 (hPa),

T - Temperature (^oK),

P_w - Partial pressure of water vapour due to the non-hydrostatic component (hPa),

K - terms represent the refractivity constants where K_3 is a second order effect.

As the first term on the right hand side of equation (5.6) does not depend on water vapour it is called the dry component of the refractivity, while the remaining two terms constitute the wet component of the refractivity.

The refractivity constants K are determined empirically in laboratory conditions. The following formulae show some of the different constants adopted by geodesists.

Essen 1951: $$N = (n-1).10^{-6} = 77.624\frac{P_d}{T} - 12.92\frac{P_w}{T} + 371900\frac{P_w}{T^2} \qquad \text{- (5.7)}$$

Liebe 1977: $$N = (n-1).10^{-6} = 77.676\frac{P_d}{T} + 71.631\frac{P_w}{T} + 374656\frac{P_w}{T^2} \qquad \text{- (5.8)}$$

Boudouris 1963: $$N = (n-1).10^{-6} = 77.594\frac{P_d}{T} + 72.0\frac{P_w}{T} + 375400\frac{P_w}{T^2} \qquad \text{- (5.9)}$$

The above formulae assume T is in units of ^oK, and P_d and P_w are in millibars. The well known Essen & Froome formula can be derived by rearranging the Essen formula (5.7) and expressing the pressure as millimetres of mercury (Laurila, 1976):

Essen & Froome 1951: $$N = \frac{103.49}{T}(P_d - P_w) + \frac{86.26}{T}\left(1 + \frac{5748}{T}\right)P_w \qquad \text{- (5.10)}$$

The International Union of Geodesy and Geophysics (IUGG, 1963) resolution concerning the refractive index for radio waves recommended that the Essen-Froome

formula be used. This convention is still followed today, but it is recognised that the empirically derived constants by Essen & Froome (1951) are no longer the best available. The International Association of Geodesy (1993) working paper on "Refractive Index of Air for Radio Waves – Issues and Questions", recommend using the values derived by Boudouris (1963) or Liebe & Hopponen (1977) (Rueger, 1999, personal communication).

In practice, either set of refractivity constants could be used without an appreciable change in the tropospheric delay results.

5.2.5 Troposphere Models

The Hopfield and Saastamoinen models, two of the more popular and well-known tropospheric models, are discussed here. These models illustrate two different approaches adopted for tropospheric delay modelling (also using different refractivity constants).

Hopfield model

Hopfield (1969) has used data covering the whole earth and empirically derived a representation of the dry refractivity as a function of station height above the surface of the earth. She assumes a single polytropic[2] layer h_d describing the height of the dry component of the neutral atmosphere in metres related to the ground temperature. Hopfield based her model on the refractivity terms given by Smith & Weintraub (1953). Integrating along the signal ray path it is possible to compute the dry delay knowing only the station height and pressure. Hopfield has made the assumption that the functional model for the dry component can also be used for the wet and has simply adopted a mean value for the height of the polytropic layer describing the wet part of the neutral atmosphere, ie h_w = 11000m. A mapping function is introduced into the model to account for varying elevation angles (not shown). The zenith hydrostatic delay formulae are given below.

[2] Polytrope – A gaseous sphere in which the distribution is according to the law $P = k\rho\gamma$, P being pressure at a given point, ρ the density, γ and k arbitrary constants.

The integrand for the refractivity of the hydrostatic component is:

$$N_{dry} = N_{sdry} \frac{(h_d - h)^4}{(h_d)^4} \qquad \text{- (5.11)}$$

where;

N_{sdry} – refractivity of the dry component at the ground surface,
h – height of the observation site.

The single polytropic layer describing the height of the dry component of the neutral atmosphere is given as:

$$h_d = 40{,}136 + 148.72(T - 273.16) \qquad \text{- (5.12)}$$

where T is in ^oK.

The Hopfield zenith dry delay is:

$$d_{dry}^{zenith} = 77.64 \times 10^{-6} \frac{P_s}{T_s} . \frac{h_d}{5} \qquad \text{- (5.13)}$$

The Hopfield zenith wet delay is:

$$d_{wet}^{zenith} = 0.373 . \frac{e}{T_s^2} . \frac{h_w}{5} \qquad \text{- (5.14)}$$

The subscript s refers hereafter to surface observations, P is pressure in millibars, T is temperature in ^oK and e is the partial pressure of water vapour, also in millibars.

Note that the Hopfield model is expressed by a quartic model for the refractivity profile (equation (5.11)). It is interesting to note that this term was chosen in 1969 as a "good approximation" to the refractivity profiles and for computational convenience (Hopfield, 1969). The exponent *4* depends on a temperature lapse rate of -6.81°C/km,

which is a reasonable approximation of the actual atmosphere. With increased computing power and a better approximation of the global temperature lapse rate (ie – 6.61°C/km according to Mendes, 1999), perhaps a more precise non-integer value could be chosen for this exponent.

Saastamoinen Model

This model utilises the gas laws to deduce refractivity, and the tropospheric delay is therefore a function of zenith angle, pressure, temperature and the partial pressure of water vapour. Saastamoinen (1973) used the refractivity constant given by Essen & Froome (1951) for mid-latitudes and average conditions. The original model has subsequently been refined to include two correction terms: one for station height B and the other for height and zenith angle δR. Both can be determined from tables.

The total zenith delay is given by:

$$d_{total}^{zenith} = 0.002277\left[P_s + \left(\frac{1255}{T_s} + 0.05\right)e - B\tan^2 z\right] + \delta R \qquad \text{- (5.15)}$$

For comparison, the formula for the hydrostatic part of the Davis model (Davis et al, 1985) has been included to demonstrate the negligible difference as a result of using different values for the refractivity. Davis used the K_1 constant given by Thayer (1974), namely 77.60 (compare with equations (5.7), (5.8) & (5.9)) and reworked the Saastamoinen model giving:

$$d_{dry}^{zenith} = \frac{0.0022768P_s}{\left(1 - 0.0026\cos 2\varphi - 0.00028h_s\right)} \qquad \text{- (5.16)}$$

The corresponding formula for the zenith hydrostatic delay for the Saastamoinen model using the refractivity terms from Essen & Froome (1951) is:

$$d_{dry}^{zenith} = \frac{0.002277P_s}{\left(1 - 0.0026\cos 2\varphi - 0.00028h_s\right)} \qquad \text{- (5.17)}$$

This is clearly a negligible difference for all but the most precise applications. Brunner & Tregoning (1994b) provide an error analysis of the Saastamoinen model for determining the zenith wet delay with respect to errors in temperature and relative humidity.

Many other tropospheric models exist, which produce similar results to the Hopfield and Saastamoinen models. The variety of models is largely due to the different approaches to modelling the water vapour, and also the method of mapping the zenith delay for all elevation angles.

Mendes (1999) provides a comprehensive comparison of several tropospheric models, but recommends the Saastamoinen model be used in predicting the zenith hydrostatic and non-hydrostatic delay for most applications.

5.2.6 Mapping Functions

Following the construction of tropospheric delay model for the zenith direction, this zenith delay must be scaled by a 'mapping function' to give the delay for any arbitrary elevation angle. The simplest form of mapping function could be constructed by assuming a flat earth and constant refractivity. The tropospheric delay for any elevation angle is therefore:

$$d_{trop} = d_{trop}^{zenith} \cos ec(E) \qquad \text{- (5.18)}$$

where E is the elevation angle.

This over-simplified model is not representative of the actual neutral-atmosphere. The propagation delay does depend on the temperature and refractivity structure, water vapour and the local density, which vary both spatially and temporally (Davis, 1986). Therefore a mapping function can be further separated into its hydrostatic and non-hydrostatic parts:

$$d_{trop} = d_{dry}^{zenith} m_h(E) + d_{wet}^{zenith} m_{nh}(E) \qquad \text{- (5.19)}$$

where;

m_h & m_{nh} refer to the hydrostatic and non-hydrostatic mapping functions respectively.

The sophistication of mapping functions has developed as a result of high precision VLBI (Niell, 1996). Generally these mapping functions assume hydrostatic equilibrium and azimuthal symmetry. Mendes (1999) compares many mapping functions and categorises them into groups. The first group includes those that follow the quartic refractivity profile approach adopted by Hopfield (1969). Another group is based on the truncated form of a continued fraction first proposed by Marini & Murray (1973), and a smaller group develops the cosecant law (see equation (5.17)) and is used by Saastamoinen (1973).

The stability of the mapping function decreases as the elevation angle approaches the horizon. The uncertainties of the neutral atmosphere for tropospheric delay modelling are magnified as the radio signal propagates through a thicker layer at lower elevations. Mendes (1999) provides a comprehensive comparative study of existing mapping functions with ray tracing to determine their accuracy with respect to elevation angle. Mapping functions can therefore be appraised by the minimum elevation angle to which they are still accurate. Ibid (1999) concludes, "In the cases where no reliable meteorological measurements are available, we recommend the Niell mapping function (Niell, 1996) to be used in modelling the elevation dependence of the zenith delay." For most practical purposes, an elevation cut-off of down to 10° will not introduce errors due to the mapping function into the tropospheric estimation.

5.3 Tests with Radiosonde Data from Indonesia

Accepting the Mendes (1999) recommendations that the Saastamoinen model is the most suitable for tropospheric delay modelling, it is apparent that the configuration of radiosonde stations used to derive his conclusions is poorly represented by stations in equatorial regions.

Ibid (1999) uses data from 100 radiosonde stations in order to determine a better approximation for parameters such as tropopause height and temperature lapse rate, compared to standard model profiles. The distribution of radiosonde stations with latitude is illustrated in Figure 5.4. From Figure 5.4 it can be seen that only 2 of the 100 radiosonde stations are located in regions within 10° latitude of the equator!

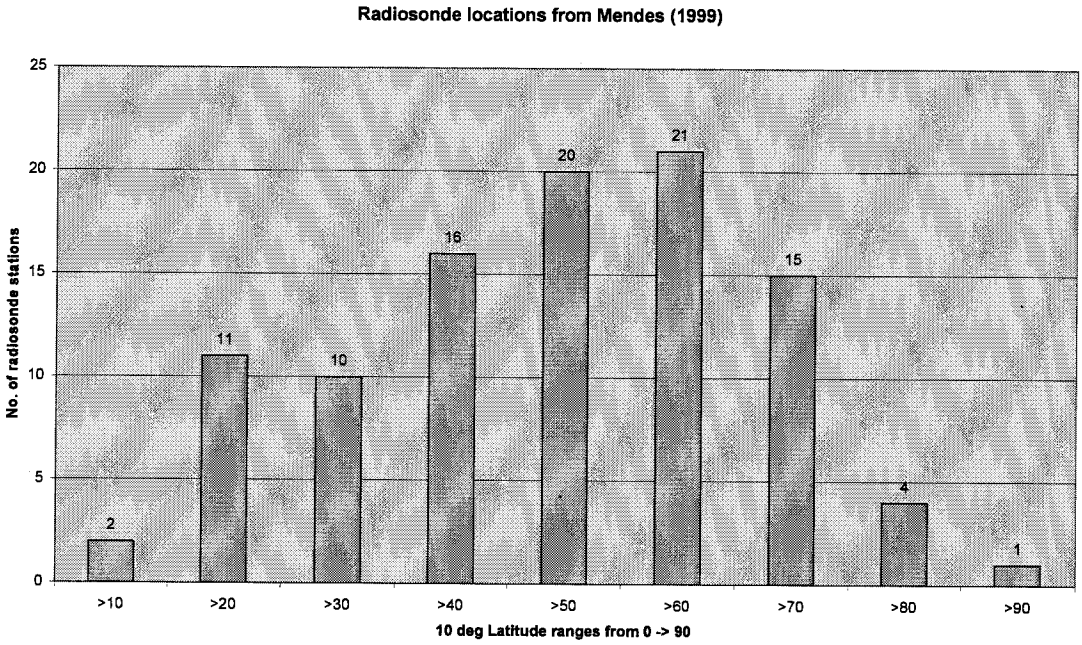

Figure 5.4 - *Location of radiosonde stations with respect to latitude (Based on data from Mendes, 1999).*

The focus of this study is differential troposphere modelling in equatorial regions. The temperature lapse rate derived for the USSA66 standard atmosphere, and later adopted by Mendes (section 5.2.3) are perhaps not representative of the local conditions experienced at Gunung Papandayan (latitude ≅ 7°S).

Three years of radiosonde data from two meteorological sites in Jakarta (latitude ≅ 6°S) and Surabaya (latitude ≅ 7°30'S) located on either side of Gunung Papandayan were kindly provided by the British Atmospheric Data Centre (1999). The data spans the period from December 1996 until November 1999. An example excerpt from the raw data file is given in Figure 5.5.

96749 19961217 00 -6.12 106.65 ******

PP(mb*100)	HT(m)	TT(°K)	TD(°K)	DD(°)	FF
100700.	10.	296.9	295.2	240.	1.5
100700.	-999999.	296.9	295.2	-999999.	-999999.
100000.	60.	296.9	295.0	240.	6.7
96000.	-999999.	296.9	294.0	-999999.	-999999.
92500.	750.	295.5	290.5	260.	17.0
85000.	1480.	292.7	281.7	275.	21.6
84600.	-999999.	292.5	280.5	-999999.	-999999.
80600.	-999999.	289.1	287.6	-999999.	-999999.
70000.	3130.	281.9	281.9	280.	13.9
69900.	-999999.	281.9	281.9	-999999.	-999999.
63500.	-999999.	276.7	274.9	-999999.	-999999.
61700.	-999999.	273.7	252.7	-999999.	-999999.
55600.	-999999.	273.1	268.1	-999999.	-999999.
52300.	-999999.	270.0	260.0	-999999.	-999999.
51500.	-999999.	270.0	268.0	-999999.	-999999.
50000.	5840.	268.8	266.3	265.	11.3
43600.	-999999.	263.4	258.4	-999999.	-999999.
40000.	7560.	259.2	251.2	270.	14.9
37100.	-999999.	255.6	244.6	-999999.	-999999.
33700.	-999999.	249.2	244.2	-999999.	-999999.
32400.	-999999.	248.6	237.6	-999999.	-999999.
30000.	9680.	244.0	233.0	190.	0.5
25000.	-999999.	233.0	223.0	-999999.	-999999.
25000.	10960.	233.0	223.0	295.	3.1
20000.	12420.	220.2	-999999.	40.	8.7
15000.	14230.	205.2	-999999.	55.	15.4
13700.	-999999.	200.6	-999999.	-999999.	-999999.
10700.	-999999.	-999999.	-999999.	-999999.	-999999.

Figure 5.5 - *Example radiosonde data set, Jakarta 17 Dec. 1996, 00 hrs UTC, where; PP = pressure, HT = height, TT = temperature, TD = dewpoint, DD = wind direction & FF = wind speed. (Data courtesy of Robert Wood, British Atmospheric Data Centre (1999), personal communication).*

Note: 96749 denotes the station name for Jakarta, 19961217 00 is the date and UTC time of observation, -999999. indicates no data was measured for this pressure level.

From this data the decreasing pressure and temperature are measured directly as the radiosonde balloon ascends the atmosphere. The dew point temperature, defined as the temperature at which air reaches 100 % relative humidity when cooled at constant pressure, is measured, from which *e,* the partial pressure of water vapour, can be computed using Buck's formula (Rüeger, 1996).

$$e = \left[1.0007 + \left(3.46 \times 10^{-6}.P\right)\right] 6.1121.\exp^{\left[\frac{17.502.T}{(240.97+T)}\right]} \qquad \text{- (5.20)}$$

It is clear from Figure 5.5 that many data gaps are present, particularly in the altimeter heights. Kahmen & Faig (1988) give a simplified formula for height (in metres) based on pressure (in mbar) only, and using Commission Internationale de Navigation Aerienne (CINA) norm values:

$$h_{na} = 44307.69 - 11874.31.P^{0.190259} \qquad \text{- (5.21)}$$

where subscript *na* refers to the neutral atmosphere only (ie both dry and wet terms used).

Using equation (5.21) for those measurements where both pressure *and* altimeter heights were given (ie nodal points) provides a check on the altimeter accuracy. Instead of resolving an identical value for the altimeter height using equation (5.21) at these nodal points, an approximate linear trend between the computed and the measured altimeter heights was detected. Assuming the altimeter heights to be correct, a double linear interpolation was carried out; first to correct to the altimeter heights and second to interpolate all the missing heights between the nodal points using equation (5.21). For radiosonde stations Jakarta and Surabaya, an equatorial tropopause height of 16,000 m was assumed. (Note: wind speed and direction data were not used.)

Table 5.1 lists the mean temperature lapse rates computed from the three years of data for 00 UTC, 12 UTC, and an average value.

Table 5.1 - *Temperature lapse rate from local radiosonde data.*
Note: values in parentheses refer to standard deviations.

Site	Time	TLR (°K/km)
Jakarta	00 UTC	6.275 (0.22)
Jakarta	12 UTC	6.532 (0.24)
Jakarta	Average	6.392 (0.26)
Surabaya	00 UTC	6.347 (0.26)
Surabaya	12 UTC	6.549 (0.19)
Surabaya	Average	6.408 (0.25)

The mean annual temperature lapse rate for 3 years of radiosonde data for stations Jakarta and Surabaya is 6.40°K/km (0.26). Mendes (1999) states a mean annual temperature lapse rate between 0° - 10° latitude of 6.61°K/km (0.27). So despite the weak distribution of radiosonde stations in equatorial latitudes (see Fig 5.4), the mean annual locational temperature lapse rate corresponds closely to the values computed from the two independent radiosonde sites surrounding Gunung Papandayan.

The effect of changing the temperature lapse rate value on tropospheric delay resolution is illustrated below for the Saastamoinen model. Equation (5.15) is the range correction using the Saastamoinen tropospheric path delay model. The temperature lapse rate appears in the hydrostatic equation for pressure:

$$P = P_s \cdot \left(\frac{T_s + \beta h}{T_s} \right)^{\frac{-Mg}{R\beta}} \qquad \text{- (5.22)}$$

And for the vertical gradient of temperature (see also equation (5.1)):

$$T = T_s - \beta (r - r_s) \qquad \text{- (5.23)}$$

Also for the partial pressure of water vapour:

$$e = e_s \cdot \left(\frac{T}{T_s} \right)^{\frac{-4Mg}{R\beta}} \qquad \text{- (5.24)}$$

Finally for the B correction term used in equation (5.15):

$$B = \frac{R}{r_s g} \left[\frac{P_s T_s - \left(\frac{R\beta}{g} \right) \cdot P^T T}{1 - \left(\frac{R\beta}{g} \right)} \right] \qquad \text{- (5.25)}$$

where:

P_s & T_s – pressure (hPa) and temperature (°K) on the earth's surface,

β - temperature lapse rate (°K/km),

h – height of the receiving station (m),

M – mean molar mass of air (subscript d – dry, w – wet),

g – local value of gravity at the centroid of the atmospheric column(m/s^2),

R – universal gas constant (J/kmol/K),

r_s – spatial vector from the centre of the earth to the receiving station (km),

e_s – partial pressure of water vapour on the earth's surface (hPa), and

P^T – pressure at the tropopause(hPa).

A change in the temperature lapse rate of -0.2°K/km introduces only minor changes to the resultant range correction (Appendix C).

Similarly, the diurnal change in temperature lapse rate, as indicated in Table 5.1, will have little effect on the range correction. Figure 5.6 shows a sample 17-month data set from radiosonde station Surabaya, indicating radiosonde soundings taken at 00 UTC and 12 UTC.

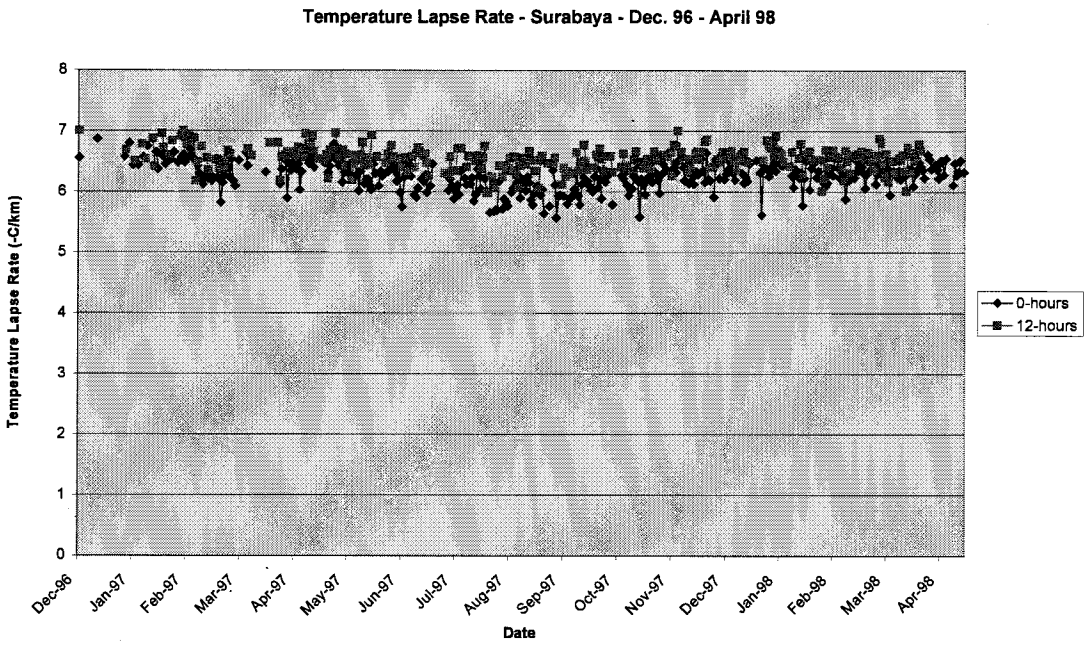

Figure 5.6 - *Temperature lapse rate data, Surabaya, Dec. 96 – April 98 (British Atmospheric Data Centre, 1999).*

Table 5.1 shows an average difference of -0.2°K/km diurnally between radiosonde soundings at 00 UTC and 12 UTC. This difference is negligible and will not be considered further as a possible error source in tropospheric delay modelling specific to regional equatorial networks.

5.4 Differential Troposphere

When two points in a small scale GPS network are separated by a large change in height, existing tropospheric models do not accurately account for the tropospheric delay between each site and therefore bias the baseline results, predominantly in the vertical component. Rizos (1997a) offers an elementary calculation. Given two receivers, one at sea level and another at an altitude of 3000m with an incident ray path elevation angle of 20°, the tropospheric refraction at sea level is computed to be 7.8m compared with 4.8m at 3000m. Most tropospheric models are scaled to account for different heights but it is the variation in the temperature and water vapour content that depart from those assumed by the models which introduce the cm level differential biases into the resultant baselines. Figure 5.1 illustrates this phenomenon.

It is well known that GPS is geometrically weak in the vertical component. Yunck (1993) states, "The large vertical effect of an atmospheric delay error is not simply a consequence of the geometric weakness in the vertical exhibited by all space geodetic techniques...but what might be called the atmosphere-induced weakness in the vertical can far surpass the inherent geometric weakness." He presents a co-variance analysis to substantiate his claim.

The large variation in the vertical component is mainly due to the presence of water vapour along the ray path. The amount of water vapour can vary significantly, both spatially and temporally, corrupting the standard troposphere models and causing errors in the height accuracy (Rühmnöβl et al, 1998; Yunck, 1993; Brunner & Tregoning, 1994a).

Relative troposphere errors are difficult to model for small regional networks (Rothacher et al, 1986). The zenith wet delay can be as much as 20 cm in tropical regions which is further exaggerated as this zenith delay is mapped onto the incident ray path of the GPS measurement (Beutler et al, 1990).

With regard to modelling this delay, temperature is critical (and to a lesser extent humidity) because a model must assume gradients in the atmosphere which were derived from empirical studies that may be invalid for the special case under consideration (Beutler et al, 1990; Davis, 1986). The high temperatures and highly variable water content experienced in tropical Indonesia exacerbate this bias further.

Hendy (1990) claims that up to 60% of the water vapour content in the atmosphere can be found in the first two kilometres above the ground surface based on radiosonde data. The next layer, up to 7.5 km above the ground surface, contains approximately a further 38% of the water vapour, with the remaining 2% above the 7.5km layer.

Attempts have been made to model the water vapour content in the atmosphere. Bean et al (1966) notes that the saturation vapour pressure is itself an exponential function of temperature (which generally decreases linearly with height). Therefore one of the best wet-term models is *probably* an exponential curve (Reitan, 1963; Dutton & Bean 1965).

Bean et al (1996) is careful to add that an exponential model of the wet term should be used with discretion because of the extreme variability of humidity, due to variations in the temperature within different air masses as well as terrain and land-water effects (ie ground proximity effects).

Janes et al (1991) notes that, "...where vertical elevation differences between stations are significant, careful measurement of surface meteorology is essential to proper modelling of the resulting differential delay." (Ibid 1991 adds that this procedure is only valid when the meteorological conditions between stations exceeds the accuracy to which these values can be measured. Also that ground proximity effects should be avoided; a difficult task indeed.) This would seem logical as tropospheric models are based on global average meteorological measures which may not be representative for a regional network. *Surely local measures of temperature, pressure and relative humidity would better model the local conditions?*

Empirical testing using local meterological measures in troposphere models

This hypothesis was tested on data from the SCIGN network in California and the SAGE network in New Zealand, firstly to see if there existed a correlation between the variation in the computed vertical component and the measured values of temperature or humidity, and secondly to test if using local meteorological values as compared to the standard models would reduce the variation in the vertical component.

Six sets of baselines were chosen to simulate the network configuration on Mt Papandayan. Two stations, JPLM and WLSN from the SCIGN network, are discussed below. The sites are 11.1 km apart and separated by a change in height of 1270m. Only the L1 data was used and 3 days of 1-hour session data was processed using the UNSW *Baseline* processing software. Double-differencing and the standard Saastamoinen troposphere model were applied. The effect of the ionosphere was ignored for such a short baseline. Additionally, the JPLM station was equipped with meteorological sensors (Paroscientific MET3) which gave temperature, pressure and relative humidity every 10 minutes to an accuracy of 0.5°C, 0.5mbar and 2% respectively. Figure 5.7 shows a time series of the vertical component vs. the temperature and relative humidity.

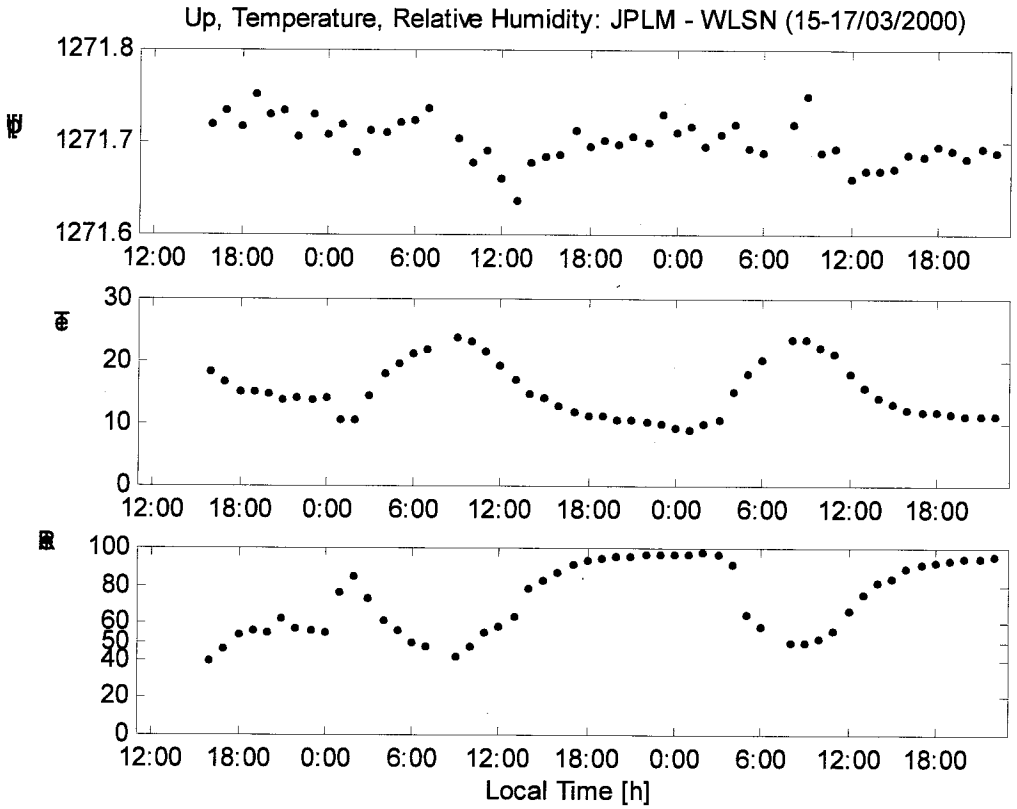

Figure 5.7 - *Time series of vertical component vs. Temperature and Relative Humidity for the baseline JPLM – WLSN, 15 – 17 March, 2000. Approximate baseline length 11.1km. Change in height 1270m.*

Visual inspection reveals a possible positive correlation between the vertical component and the temperature in Figure 5.7. However applying a cross-correlation function to these two data series results in a value of 0.05, indicating almost no correlation at all. The same software and processing regime was adopted for all six baselines. The cross-correlation function was then applied to all baselines.

Table 5.2 lists the length and change in height for each baseline, as well as the cross-correlation between the vertical component and temperature and relative humidity. The highest correlation appears for the baseline JPLM-CIT1, but this also is the baseline with the smallest change in height of the six considered in this study. In general, a cross-correlation value of at least 0.8 would indicate a similar trend between time series, and could be used as a basis for further investigation. From the results obtained for the six baselines investigated it can be concluded that there exists no correlation between surface meteorological values and the variation in the computed vertical component.

Table 5.2 - *Cross-correlation between vertical vs. Temperature and vertical vs. Relative Humidity for various short baselines with large vertical height differences.*

Baseline	Length (m)	Vertical (average) (m)	Std. Dev. (m)	X-corr (Vertical v Temp)	X-corr (Vertical v RH)
JPLM-CIT1	8665	-214.6	0.018	-0.73	0.70
DAM2-CMP9	2499	554.3	0.017	-0.17	-0.16
CSN1-OAT2	11112	841.5	0.003	0.07	-0.28
CSN1-CMP9	15165	858.7	0.026	0.25	-0.34
JPLM-WLSN	11142	1271.7	0.023	0.05	-0.27
QUAR-KARA	9233	1338.7	0.031	-0.32	-0.12

This conclusion confirms studies by Brunner & Tregoning (1994b), Mendes (1999), Davis (1986) and Zhang (1999), that the zenith wet delay (and therefore the variation in the vertical component) is only weakly related to the meteorological surface conditions, which are generally poor indicators of the humidity distribution above the receiver.

Based on this conclusion, only a limited sample of data was tested further. Twenty four one-hour sessions of data from the QUAR-KARA baseline from the SAGE New Zealand network were processed twice. First using the Saastamoinen model with standard meteorological values, and again using the Saastamoinen model but this time using local measured values. The results are presented in Figure 5.8. The mean and standard deviation of the vertical values using the standard model is 1338.740 and 0.024m, and when using the local meteorological values it is 1338.780 and 0.034m respectively.

Therefore using the local meteorological observations in the Saastamoinen model results in an accurate estimate for the vertical component but a larger standard deviation than that obtained using the standard model. Brunner & Tregoning (1994b) draw the same conclusions and attribute this counter-intuitive result to ground proximity effects.

Micro-meteorological variations occur in the first 50-100m above the ground and will obviously affect local meteorological observations. These biased observations then severely affect the wet refractivity profile computed using the models. Such ground proximity effects occur primarily as a result of solar radiation, either through the

ground's radiation loss at night (inversion) or due to rising thermals as the sun heats the ground during the day (convection). Ground proximity effects are therefore diurnal, so that averaging a daily (or weekly) time series of one-hour baseline results will provide an accurate mean value, but with a relatively poor repeatability (ie precision) as compared to using the standard Saastamoinen model.

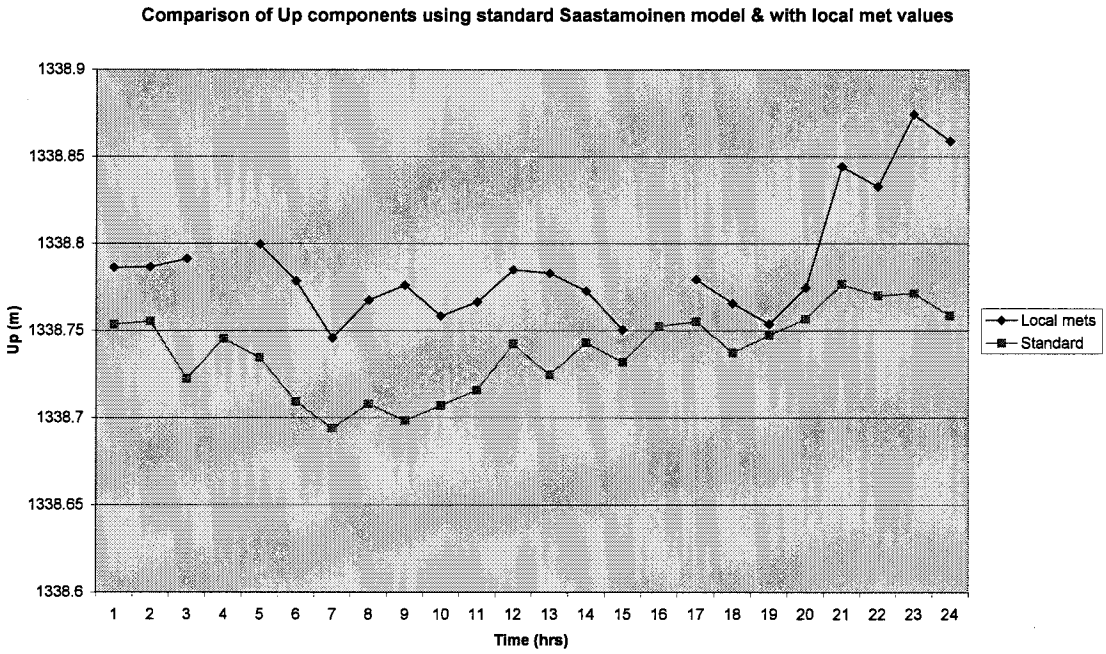

Figure 5.8 - *Time series of vertical component processed using the standard Saastamoinen model vs. Saastamoinen model using local meteorological measures for the baseline QUAR – KARA, 15 March, 2000. Approximate baseline length 9.2km. Change in height 1338m.*

The differential tropospheric bias contributes significantly to the relative vertical accuracy for small-scale GPS networks. Beutler et al (1990) claims that an error of 1°C in temperature difference between both ends of a baseline could produce a height bias of between 10 and 80mm! As stated previously, Gurtner et al (1989) suggest a 'rule of thumb' of 2-5mm per 100m height difference due to unmodelled conditions.

A differential tropospheric bias for a small-scale network can be problematic. A bias of 10 mm is 10 ppm on a 1km baseline, but only 0.01ppm on a 1000km baseline (Beutler et al, 1988). A differential tropospheric bias of 10 mm could introduce a 30 mm station

height bias, amplified as the zenith wet delay is projected to all elevation angles using a mapping function (Rothacher et al, 1996; Beutler et al, 1990).
The accurate measurement of local meteorological conditions, whilst avoiding ground proximity effects, is not feasible for the volcano monitoring system proposed in this thesis. Brunner & Tregoning (1994b) suggest that the best solution is simply to estimate the ground proximity effects as a residual relative zenith delay parameter.

5.5 Parameter Estimation

The volcano monitoring system proposed in this thesis has sought to demonstrate comparatively high accuracy using low-cost hardware. The sophistication of the software must therefore compensate for any losses due to the hardware. The conventional modelling technique to account for tropospheric effects has proven unsatisfactory. The δX_{trop} term from equation 3.1 (section 3.2) can be reduced using smarter software. Analysis of the quality of baseline data, particularly in the height component, requires that the software sophistication be enhanced to accommodate estimation of an additional residual troposphere parameter. It is recommended that estimating residual tropospheric parameters is only necessary for very high precision work (Davis, 1986; Brunner & McCluskey, 1991; Rizos, 1997a). The large differential height between stations necessitates the parameter estimation technique to also be adopted in the processing strategy for this volcano monitoring application.

This claim is also made by Abidin et al (1998). The processing of a campaign-style GPS survey of Gunung Guntur, Indonesia, with baseline lengths under 10 kms and a height difference of about 1500m demonstrated that parameter estimation is the best means of dealing with the effects of differential tropospheric delay. They conclude that when the volcano deformation signal is at the level of a few cms or less, scientific software[3] with tropospheric estimation capability is essential.

The addition of an extra residual troposphere parameter into the least squares estimation process requires some explanation. The method of GPS baseline processing adopted so far in this thesis uses double-differenced data. The coordinate of the base station is held

[3] Bernese 4.0 was used by Abidin et al (1998).

fixed and the coordinate differences ΔX, ΔY & ΔZ to the slave station and the double-differenced ambiguity term N for a satellite pair are estimated. The number of satellite pairs will determine the number of ambiguity parameters. Rizos (1997a) provides a thorough description of this procedure.

The fundamental equation for GPS baseline processing is the one-way phase model. This is the functional model (or mathematical model) which relates the distance between one satellite and one receiver to a number of biases and the measurement (see equation (5.26)).

$$\Phi_i^j(t) = \frac{1}{\lambda}.\rho_i^j(t) + N_i^j + f^j \Delta\delta_i^j(t) + \varepsilon \qquad \text{- (5.26)}$$

where:

$\Phi^j{}_i(t)$ - measured carrier phase at epoch t,

λ - wavelength of the carrier,

$N^j{}_i$ - time dependent phase ambiguity,

f^j - frequency of the satellite signal,

$\rho^j{}_i(t)$- geometric distance between the satellite and observing point,

$\Delta\delta^j{}_i$ (t) - the combined satellite and receiver clock error, and

ε - measurement noise.

Also:

$$\rho_i^j(t) = \sqrt{(X^j(t) - X_i)^2 + (Y^j(t) - Y_i)^2 + (Z^j(t) - Z_i)^2} \qquad \text{- (5.27)}$$

where;

$X^j(t)$, $Y^j(t)$, $Z^j(t)$ – are the components of the geocentric position vector of the satellite for epoch *t* and,

X_i, Y_i, Z_i – are the three unknown coordinates of the observing site in the WGS84 (or similar) datum.

And;

$$\Delta\delta_i^j(t) = \delta^j(t) - \delta_i(t) \qquad \text{- (5.28)}$$

where;

$\delta^j(t)$ - is the satellite clock bias,

$\delta_i(t)$ - is the receiver clock bias.

Information concerning the satellite clock is known and transmitted via the broadcast message in the form of three polynomial coefficients a_0, a_1 and a_2:

$$\delta^j(t) = a_0 + a_1(t - t_0) + a_2(t - t_0)^2 \qquad \text{- (5.29)}$$

This enables the calculation of the satellite clock bias for epoch *t*. The polynomial removes the major part of the satellite clock bias, but a residual error remains.

Equation (5.26) can be augmented with an extra term to account for the residual effect of the troposphere:

$$\Phi_i^j(t) = \frac{1}{\lambda}.\rho_i^j(t) + N_i^j + f^j \Delta\delta_i^j(t) + Trop_i^j(t) + \varepsilon \qquad \text{- (5.30)}$$

where;

$Trop^j{}_i(t)$ – is a time dependent tropospheric delay term.

Previously, the tropospheric delay has simply been subtracted from the observation using a standard model (usually Saastamoinen, equation (5.15)) and a corrected one-way phase observation was then differenced. Differencing still takes place but now with the addition of this extra troposphere term which is carried through all the operations. This term may simply be the Saastamoinen model (equation (5.15)), or any other model that the user may wish to use.

Between-station differencing, which removes the effect of the satellite clock bias, would result in the single-difference equation:

$$\Phi^{j}_{AB}(t) = \frac{1}{\lambda}\left(\rho^{j}_{B}(t) - \rho^{j}_{A}(t)\right) + \left(N^{j}_{B} - N^{j}_{A}\right) - \left(f^{j}\delta_{B}(t) + f^{j}\delta_{A}(t)\right) + \left(Trop^{j}_{B}(t) - Trop^{j}_{A}(t)\right) + \varepsilon \quad \text{- (5.31)}$$

where;

subscripts A & B refer to ground stations.

Note that the troposphere term is now complicated by differencing between the two ground stations. Differencing again for another satellite k, between ground stations A and B, will result in the following double-difference equation:

$$\Phi^{jk}_{AB}(t) = \frac{1}{\lambda}\left(\rho^{j}_{B}(t) - \rho^{j}_{A}(t) - \rho^{k}_{B}(t) + \rho^{k}_{A}(t)\right) + \left(N^{j}_{B} - N^{j}_{A} - N^{k}_{B} + N^{k}_{A}\right) + \left(Trop^{j}_{B}(t) - Trop^{j}_{A}(t) - Trop^{k}_{B}(t) + Trop^{k}_{A}(t)\right) + \varepsilon \quad \text{- (5.32)}$$

(Note that it is assumed that $f^{j} = f^{k}$ to eliminate the receiver clock bias.) After double-differencing the troposphere term is further complicated, consisting of four terms from each of the one-way phase observations.

The double-differencing technique is used to eliminate the largest biases, namely the clock errors, and is the input for the following observation equation:

$$\Phi^{jk}_{AB}(t) = \frac{1}{\lambda}\rho^{jk}_{AB}(t) + N^{jk}_{AB} + Trop^{jk}_{AB}(t) + \varepsilon \quad \text{- (5.33)}$$

The troposphere term from equation (5.33) is:

$$Trop^{jk}_{AB}(t) = Trop^{j}_{B}(t) - Trop^{j}_{A}(t) - Trop^{k}_{B}(t) + Trop^{k}_{A}(t) \quad \text{- (5.34)}$$

Mapping the zenith delay for all elevation angles results in:

$$Trop_{AB}^{jk}(t) = Trop_A^Z(m_A^j - m_A^k) - Trop_B^Z(m_B^j - m_B^k) \qquad \text{- (5.35)}$$

where the superscript Z refers to the zenith delay. Assuming that for short baselines the mapping function at A is equivalent to that at B, then:

$$Trop_{AB}^{jk}(t) = (Trop_A^Z - Trop_B^Z)(m_A^j - m_A^k) \qquad \text{- (5.36)}$$

The basic equation (5.26) refers to the true value of the phase measurement. The true value comprises the computed values and corrections to these computations as shown in equation (5.37) in simplified form:

$$\Phi = \frac{\rho(\overline{X},\overline{Y},\overline{Z})}{\lambda} + \overline{N} + \overline{Trop} + \frac{1}{\lambda}.\frac{\partial\rho}{\partial X}\delta X + \frac{1}{\lambda}.\frac{\partial\rho}{\partial Y}\delta Y + \frac{1}{\lambda}.\frac{\partial\rho}{\partial Z}\delta Z + \frac{\partial N}{\partial N}\delta N + \frac{\partial Trop}{\partial \delta z}\delta z + \varepsilon \qquad \text{- (5.37)}$$

The first three terms of equation (5.37) are the computed part of the observation equation, and are denoted with a bar over these terms. The next five terms define the corrections, and it is these corrections which relate to the design matrix of the least squares estimation procedure (see equation (5.38)). This is the crucial step for residual tropospheric parameter estimation.

The δz term refers to the relative zenith delay term for the two stations. It is difficult to describe its physical meaning. Essentially the correction to the relative estimate of the mis-modelling of the troposphere between the two stations is sought using this term. Brunner & Tregoning (1994b) define residual zenith delay as the difference between the actual zenith delay and that calculated from a standard model.

Zhang (1999) states that this residual tropospheric delay is mostly due to the wet component, as the dry component can be well modelled using the standard values of surface pressure. In addition, the ionosphere-free combination of GPS carrier phase

observations provides a good measurement for this residual tropospheric delay (Ibid, 1999). This approach is not suitable for this study as only L1 data was used.

The fundamental double-differenced observation equations are the basis of the design matrix. The design matrix is constructed as:

$$\begin{bmatrix} \frac{\partial\Phi}{\partial X} & \frac{\partial\Phi}{\partial Y} & \frac{\partial\Phi}{\partial Z} & 1 & . & . & \frac{\partial\Phi}{\partial \delta z} \\ \frac{\partial\Phi}{\partial X} & \frac{\partial\Phi}{\partial Y} & \frac{\partial\Phi}{\partial Z} & . & 1 & . & \frac{\partial\Phi}{\partial \delta z} \\ . & . & . & . & . & . & . \\ . & & & & & & \\ . & & & & & & \end{bmatrix} \quad \text{- (5.38)}$$

where unity refers to the partial derivative of the ambiguity terms. The double-differenced residual troposphere parameter is partially differentiated with respect to the relative zenith delay between the ground stations (Tsujii et al, 2000), giving:

$$\frac{\partial\Phi}{\partial \delta z} = \left(m^j - m^k\right) \quad \text{- (5.39)}$$

the difference between the mapping functions.

Alternatively, equation (5.36) could be written as:

$$Trop_{AB}^{jk}(t) = ((Trop_A^Z - Trop_B^Z)(m_A^j - m_A^k)).(1+s) \quad \text{- (5.40)}$$

where s refers to a scale factor term. Now partial differentiation with respect to the scale factor generates the appropriate troposphere parameter in the design matrix:

$$\frac{\partial\Phi}{\partial s} = (Trop_A^Z - Trop_B^Z)(m^j - m^k) \quad \text{- (5.41)}$$

Equations (5.39) and (5.41) illustrate two different approaches to troposphere parameter estimation. The relative zenith delay method in equation (5.39) is best suited for

networks where the relative station height between stations is small. The Trop terms in equation (5.41) include height information, therefore this procedure is more suited to the work presented in this thesis.

The design matrix estimates corrections to the computed values in an effort to resolve the true value. The residuals of the computation reflect the quality of the least squares estimation. The residuals may contain mis-modelled and imprecisely estimated tropospheric effects as well as biases from the ionosphere, multipath and instrument noise. Introducing extra parameters into the observation equations can help to minimise the residuals, however it may be unclear whether the new parameters are "soaking up" the unmodelled effects. Beutler et al (1988) claims that estimating too many parameters will weaken the solution considerably. For this reason, it is recommended that only one extra residual tropospheric parameter per session should be estimated, together with the slave station coordinates and the double-differenced ambiguity terms.

Two basic solution strategies exist (Brunner & McCluskey, 1991):

- Solve for the delay at all n stations within a network or,
- Solve for the relative delay at (n-1) stations (except at the reference station).

It is recommended that for short baselines and small networks, that the relative delay (site minus reference station) technique should be used. Rothacher & Mervart (2000) state, "In local campaigns it is recommended to estimate troposphere parameters for all but one station (due to strong correlations between the troposphere parameters of the sites included)."

Examining this troposphere parameter more closely, other considerations arise. There exists a correlation between the station height and the estimated troposphere parameter which can be difficult to distinguish (Rothacher et al, 1998b; Santerre 1991; Rühmöβl et al, 1998). A decorrelation of the physical effects of orbit error and atmospheric delay will tend to occur as the inter-station distances (and the height between points) becomes larger (Rizos, 1997a). Therefore as the baseline length increases, a troposphere parameter for all *n* stations should be estimated.

Additionally, Yunck (1993) cautions that elevation-dependant influences can be falsely interpreted as changes in height, and the repeatability in the height estimate can actually deteriorate. Although low elevation satellites provide noisier measurements, these are essential for parameter estimation. Brunner & McCluskey (1991) propose the use of low elevation satellites to prevent ill conditioning of the normal equations. Yunck (1993) investigates this further and concludes that, "...low elevation data are harmful if a fixed zenith delay error is present and helpful if the delay is adjusted in the solution, provided the mapping function remains valid."

Rothacher & Mervart (2000) have addressed this problem in the Bernese 4.2 software, where an elevation-dependent weighting of the observations is introduced to improve the accuracy of the height component. Despite the higher tropospheric refraction and increased multipath, using low elevation observations improves the height component of the station solution. A primary motivation for introducing these new strategies is to gain a better decorrelation between the estimated height and the troposphere delay parameters (Rothacher & Beutler, 1998).

The Bernese 4.2 draft documentation also highlights the inadequacies of the Saastamoinen and Hopfield mapping functions for low elevation satellites, and advocates the use of the superior Niell mapping function. However, in order to implement this new approach, rather than estimating corrections to an a-priori model, they recommend estimating the full delay using the dry Niell mapping function. This approach is more suited to larger networks.

The Saastamoinen model using the cos(z) mapping function is considered accurate to an elevation angle of 10° (Mendes, 1999); the elevation cut-off angle used in this system.

Tilting of the tropospheric layers or *tropospheric gradients* are now considered in the Bernese V4.2 software. Estimation of tropospheric gradients account for azimuthal asymmetries, thereby improving the horizontal station coordinates and the repeatability in the height (providing elevation-dependent weighting of observations is also implemented) (Rothacher et al, 1998). However it is recommended not to implement this parameter in the case of small-area networks or individually processed baselines, such as is the case in this application. This is because an individual baseline has no data

distribution in order to sense tropospheric gradients and the introduction of an extra parameter for L1 only data may compromise accuracy.

The Bernese 4.2 software also provides a local troposphere model technique that is recommended for use in local campaigns with large height differences (Rothacher & Mervart, 2000). This procedure is investigated in chapter 6.
Equations (5.39) and (5.41) define the two partial derivatives that are used in the design matrix for the relative zenith delay and scale factor approaches respectively. However these parameters, unlike the observing station coordinates and ambiguity parameters, have no physical meaning. Tsujii et al, (2000) has proposed a different approach for positioning stratospheric airships (ie with extreme height differences). The double-differenced tropospheric delay can be written as a function explicitly dependent on the height difference. The tropospheric parameter therefore becomes the estimate of the surface pressure assuming the temperature lapse rate and surface temperature are correct. A parameter for the water vapour pressure is also included. This approach requires measurement of some meteorological values and is therefore not suitable for a low-cost volcano monitoring system.

Historically, the Trimble software TRIMVEC^{TM} from the early 1990s offered the option to solve for a *baseline tropospheric scale parameter* but it is generally conceded that this is ineffectual (Rizos, 1997a).

The parameter estimation approach is generally used for high precision large-scale networks. The addition of an extra troposphere parameter into the least squares process necessitates more observations in order to guarantee reliable ambiguity resolution and baseline accuracy. Various researchers (Gurtner et al, 1989; Tralli & Lichten, 1990; Abidin et al, 1998) have recommended a session length of at least one hour or more. This puts into question the reliability of an RTK system providing single epoch, real-time, filtered results with a claimed accuracy at the sub-centimetre level.

As only L1 data is used on Gunung Papandayan, the session length can be extended to accommodate extra observations. Chapter 6 investigates the impact of session length on height repeatability using troposphere parameter estimation.

It is interesting to compare a low-cost hardware system to a very precise rigorous system such as the Automated GPS Network Switzerland (AGNES) recently deployed to monitor and maintain the Swiss first-order network. One zenith delay parameter per hour per station is estimated for this network (baseline length up to 190km, differential height up to 3600m). Tropospheric refraction is recognised as the ultimate limiting factor and it is claimed that (sub-) cm accuracy in horizontal baseline components and 3-5 cm accuracy for the vertical component is achievable (Schaer et al, 1999).

Recommendations

This chapter has identified the tropospheric bias as a major measurement bias to be considered for small scale, GPS-based volcano monitoring systems, and in particular has discussed how to best account for the troposphere in order to improve the accuracy of the height component. Several recommendations can be made:

1. Standard troposphere modelling, as used in commercial software packages, is not appropriate to achieve centimetre level repeatability for small-scale networks with large changes in station elevation.

2. Measuring local meteorological values and modelling provides no improvement to the accuracy or precision of the estimated height component.

3. Radiosonde data offers no extra information to enhance the local modelling of the troposphere at Gunung Papandayan, Indonesia. This is likely to apply to most sites/stations where there is no radiosonde program.

4. Estimation of an additional residual troposphere parameter is necessary to satisfy the accuracy requirement of the volcano monitoring system.

5. The Saastamoinen troposphere model and mapping function are considered to be at the best accuracy as an a-priori troposphere model.

6. It is recommended that estimated parameters for this thesis will comprise X, Y, Z, N and one extra residual relative zenith troposphere parameter per session.

7. Elevation-dependent weighting and tropospheric gradients are not considered to be appropriate techniques for this thesis.

8. Meteorological measurements are not recorded as the low-cost nature of the system precludes the measurement of pressure or water vapour pressure.

9. To ensure correct ambiguity resolution for L1-only data, the session length should be no shorter than 1 hour. Conversely, to ensure the troposphere parameter is regularly estimated, the session length should be no greater than about four hours.

The recommendations presented here are tested in chapter 6 using a 24-hour data set from the SAGE-NZ network initially and later extended to a 21-day time series. A 21-day time series from the Papandayan network collected in July 2001 is compared to the SAGE-NZ network.

Chapter 6
DATA PROCESSING AND ANALYSIS

6.1 Introduction

The recommendations made in chapter 5 will be implemented in chapter 6 using data from the SAGE network in New Zealand[1]. It is assumed that the points QUAR and KARA are stationary during the period of observation, and that any departure of the time series results from a mean value is due to a systematic bias, not a geophysical phenomenon. Initially tests on a 24-hour segment of the 21-day time series are performed to determine the best analysis strategy before processing the entire data set. Digital signal processing techniques are employed in order to analyse the full time series for repeatable geophysical signals or systematic biases present in the data. Multipath is detected and a simple filtering of the data will seek to reduce the variability of the height component. The Allan variance of the height component is computed to indicate an upper boundary of the systematic biases at different time intervals. Measures outside this upper boundary, when not identified as outliers, would be considered meaningful movements of the receiver(s). Similar time series analyses are also performed on data from the low-cost network on Gunung Papandayan collected in July 2001.

6.2 Investigating Processing Strategies

6.2.1 Baseline vs. Bernese

The custom written UNSW GPS processing software Baseline is compared with the scientific software Bernese to ensure both softwares are compatible. The primary recommendation of chapter 5 is that estimation of an additional residual relative

---

1

Data from the Gunung Papandayan 2000 campaign was not suitable to investigate the effects of differential troposphere as the time series was not continuous. In addition, this data was corrupted by ionospheric noise (Janssen et al, 2001), as well as probable multipath, which masks the differential tropospheric signal in the data. The SAGE network is located well away from the equator to avoid ionospheric noise, and the time series was chosen to be the same period as the Papandayan 2000 data.

troposphere parameter is necessary in order to satisfy the accuracy requirements of the proposed system. The UNSW baseline software does not currently accommodate such an approach (Rizos et al, 2000), hence the Bernese V4.2 software package was used. In order to ensure that both softwares were compatible, the same data, using identical starting coordinates (and all other parameters and conditions set the same), were processed and compared for a 24-hour test data set (Fig 6.1).

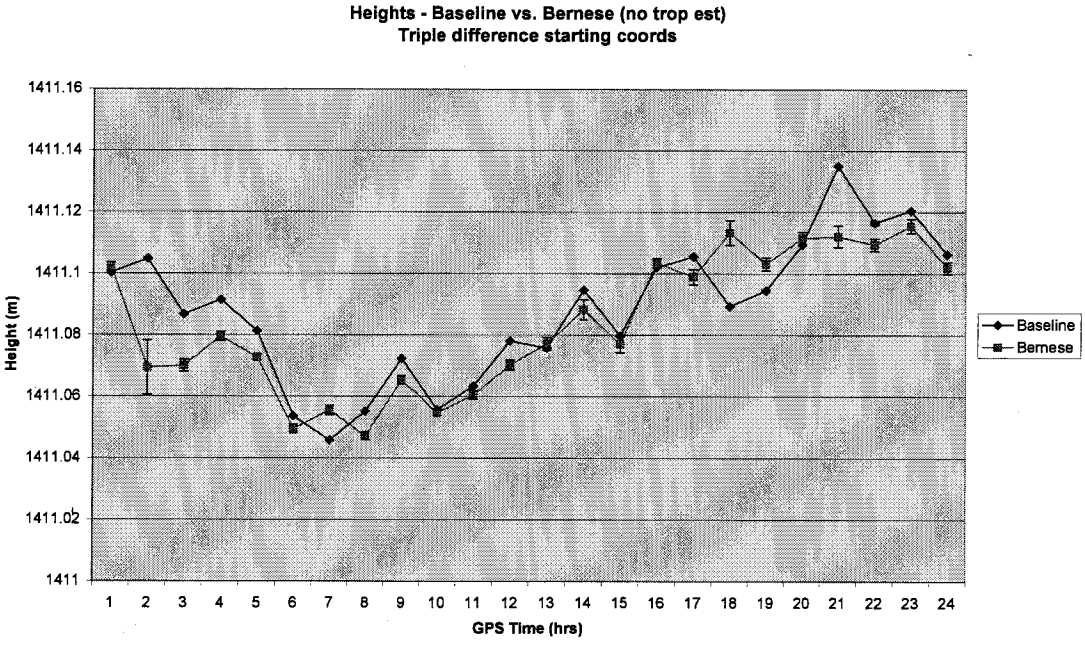

Figure 6.1 – *Results of 24 1-hour sessions of data processing using Baseline vs. Bernese and standard Saastamoinen troposphere modelling for the baseline QUAR – KARA from the SAGE-NZ network on 15/3/2000.*

The computed ambiguities were manually checked and found to be identical. Differences in the height component arise from different base satellites being used for the double-differencing, the occasional use of less satellites by either software package, and minor differences in the implementation of the algorithms. The error bars for the Bernese results in Figure 6.1 relate specifically to the height component. Equivalent error bars from Baseline were unavailable.

Table 6.1 – *Comparison of average height and distance values for 24 1-hour sessions of data processing using Baseline vs. Bernese and standard Saastamoinen troposphere modelling for the baseline QUAR – KARA from the SAGE-NZ network on 15/3/2000.*

	Baseline		**Bernese**	
	Height	Distance	Height	Distance
QUAR - KARA	1411.0878	9233.1881	1411.0829	9233.1855
15 May 2000	(0.0234)	(0.0096)	(0.0226)	(0.0087)

Table 6.1 confirms that the baseline computations from the Baseline and Bernese software packages can be considered equivalent. Further research in this chapter will therefore compare results from a modelling approach using Baseline versus parameter estimation using Bernese, with some confidence. Note the height values shown are the absolute heights of the observing station KARA with respect to the fixed base station QUAR. This convention will be adopted throughout this chapter.

6.2.2 Modelling vs. Estimation using Bernese

Using the Bernese software, it is possible to compare the same 24-hour time series using troposphere modelling versus estimating 1 troposphere parameter per 1-hour baseline. Note that the same starting coordinate for base station QUAR is used for both processing runs.

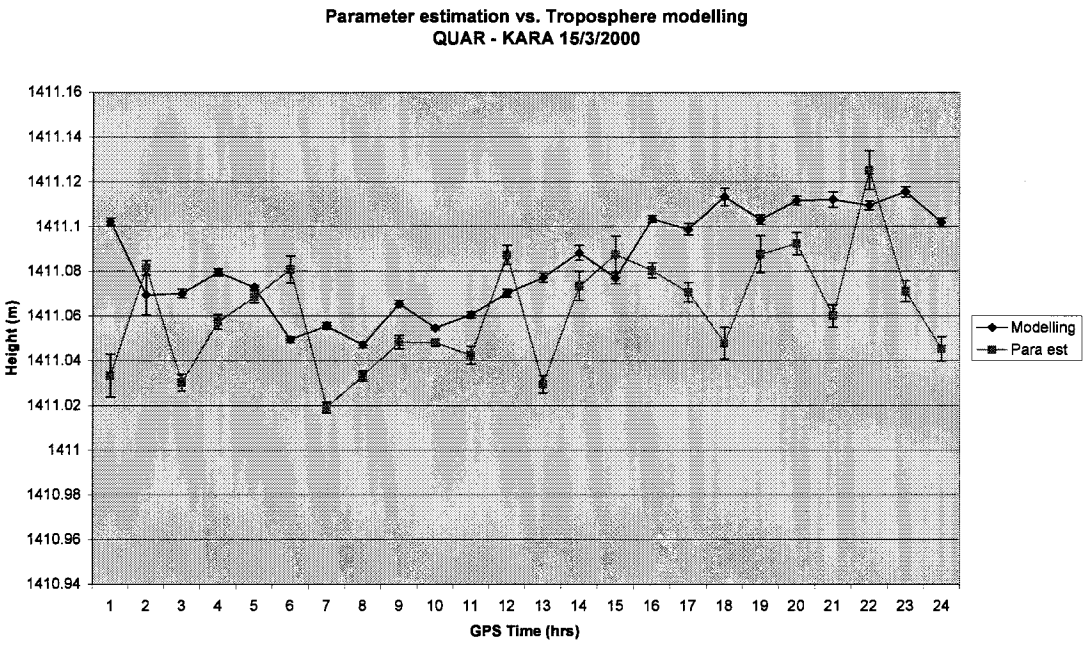

Figure 6.2 – *Comparison of time series height data using Bernese processing with standard troposphere modelling (Saastamoinen) vs. Bernese and estimating 1 troposphere parameter per 1-hour baseline. Starting coords from triple differencing.*

It appears from Figure 6.2 that the scatter of the height estimates using parameter estimation is larger, and there seems to be a bias in the height between the two approaches. This larger scatter is due to the paucity of data available for one session (see section 6.2.5). Note from Table 6.2 that the average height value computed using modelling is slightly higher than that from parameter estimation, yet the standard deviations are similar. This characteristic is also evident in Table 6.5 for the full 21-day time series.

Table 6.2 – *Comparison of average height and distance values for 24 1-hour sessions of data processing using Bernese (modelling) vs. Bernese (1 troposphere parameter) for the baseline QUAR – KARA from the SAGE-NZ network on 15/3/2000.*

	Bernese (modelling)		**Bernese (estimation)**	
	Height	Distance	Height	Distance
QUAR - KARA	1411.0829	9233.1855	1411.0639	9233.1839
15 May 2000	(0.0226)	(0.0087)	(0.0254)	(0.0100)

Also note that when using troposphere modelling there appears to be a diurnal trend in the data which is not apparent when using the parameter estimation approach. It

therefore appears that standard troposphere modelling introduces a synthetic temporal signal into the height component. From Table 6.2 the standard deviation of the results using troposphere modelling is less than that when the parameter estimation approach is used (ie 0.0226 vs 0.0254). However, if the time series resulting from processing with troposphere modelling suggests that the point KARA is moving, when it clearly is not, then it puts into question the validity of this processing methodology. This limited test confirms the conclusions of chapter 5, and of the literature, that standard troposphere modelling for baselines separated by large changes in height is not recommended (Brunner & Tregoning, 1994b; Beutler et al, 1990; Gurtner et al, 1989).

Also note that the variation in coordinate results between epochs appears to be quite smooth for the troposphere modelling approach compared to the estimation approach, which appears quite scattered, yet the standard deviations of both time series' are very similar. This is because the standard deviation is computed on a single mean value assuming that the point KARA is not moving. However, the time series resulting from the troposphere modelling approach indicates an upward trend in the height component. The hypothesis that the points QUAR and KARA are not moving has therefore exposed the problem with the troposphere modelling approach for baselines with large differential height.

6.2.3 Starting Coordinates

For any deformation monitoring network the fixed coordinate of a base station to which all antenna movements are referred is crucial (see section 3.2.6). The WGS84 coordinates in the RINEX header file of the QUAR and KARA stations for instance were derived from a navigation solution provided by the field engineer during installation of the site (UNAVCO, 2000). The Bernese software was used to provide a single point position (SPP) solution. The KARA site coordinates were derived relative to the SPP-fixed QUAR site, using the Bernese software. This was adopted as an initial coordinate for subsequent processing. It should be noted therefore that the absolute position of QUAR and KARA is only known at the 5-10 metre accuracy level due to the SPP processing (Rizos, 1997a).

A better estimate of the initial starting coordinate can be derived by computing a regional solution using fixed stations connected to the IGS global network (see method (2) section 3.2.6). Section 4.6.6 details the computation of the base station coordinate for the single-frequency network on Gunung Papandayan. The SAGE network data is presented only to illustrate different processing strategies, and therefore the single point positioning result is considered sufficient.

Although investigations in this thesis focus on single-frequency GPS networks, dual-frequency data is available in the SAGE network. A more rigorous 24-hour solution using dual-frequency data, with six troposphere parameter estimates, was performed to improve the initial coordinates for the KARA observing station. The fixed coordinate for QUAR was preserved during this step. Table 6.3 summarises the improvements to the starting coordinates, which is also reflected in the computed distance between coordinate estimates.

Table 6.3 – *Comparison of starting coordinate values, used for baseline computations QUAR – KARA from the SAGE-NZ network.*

QUAR	X	Y	Z	
RINEX header	-4558537.1502	818912.5887	-4370555.8018	
Triple diff soln	-4558543.2147	818913.5094	-4370560.6275	
Dual freq soln	-4558543.2147	818913.5094	-4370560.6275	
KARA	**X**	**Y**	**Z**	**Join distance**
RINEX header	-4553134.0536	821272.8693	-4377657.9327	9230.6360
Triple diff soln	-4553138.6920	821278.1159	-4377663.5453	9233.1831
Dual freq soln	-4553138.6235	821278.1070	-4377663.4990	9233.1853

Table 6.3 indicates a 3-metre improvement in the distance between the navigation solution and the triple-difference coordinates. The difference in the distance between the single-frequency triple-differenced solution, and the more rigorous 24-hour dual-frequency solution, is only a few mm's. Therefore it can be concluded that the single-frequency triple-differenced results are sufficiently accurate as initial coordinates for subsequent baseline processing.

This assertion was further tested by processing the 24-hour sample data set using the triple-differenced approach and the dual-frequency starting coordinates (Table 6.3), and comparing the height results (the component of interest in this thesis), as shown in Figure 6.3.

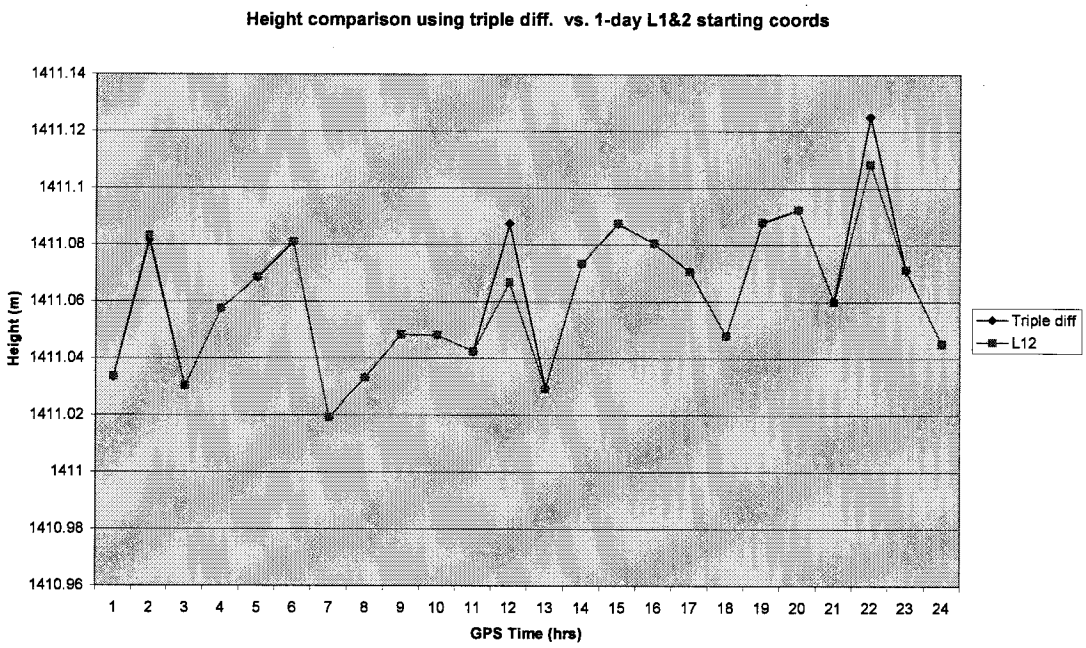

Figure 6.3 – *Comparison of time series of the height component using starting coordinates from L1 Triple-differencing vs. 24-hour dual-frequency processing (L1&2). 1-hour baselines are compared using the Bernese software and estimating 1 troposphere parameter per 1-hour data set.*

For both runs, 24 1-hour sessions were processed using the Search AR technique, L1-only data and estimating one troposphere parameter per session. The differences at the 12 and 22-hour sessions can be attributed to slightly different constellations of satellites used during processing between the two runs. Figure 6.3 illustrates that for slightly different starting coordinates for the observing station, the difference in the resulting height component is negligible.

6.2.4 Ionosphere

The effect of the ionosphere has been ignored by assuming that for short baselines its influence is inconsequential. The data collected is single-frequency only, therefore the

ionosphere-free linear combination cannot be used to eliminate this effect. The Bernese Manual V4.0 states, "For very small high-precision networks (with a maximum extent of about 10km), we recommend to use – even if dual-band data is available – L1 data only together with an ionosphere model (Beutler et al, 1995)."

The Bernese software also offers a means of computing regional and local ionosphere models, however these can only be done using dual-frequency data. This leaves only empirical models such as the Klobuchar ionospheric correction model, broadcast with the navigation message, able to remove approximately 50% of the delay. Other options include the Bent ionospheric model and a daily global average model provided by the International Earth Rotation Service (IERS), however both of these models are considered to be of comparable quality to the broadcast model (Wild, 1994; Langley, 2000). Several baselines from the Gunung Papandayan network were processed with and without using the Klobuchar ionosphere model. The comparison revealed almost identical results.

Time series data has therefore been processed ignoring the effect of the ionosphere. Data analysis using digital signal processing techniques did not detect a significant signal due to unmodelled ionospheric effects. Section 6.5 shows a negligible change in baseline components when processing with and without the global ionospheric models provided by the IERS for the Papandayan 2001 time series.

6.2.5 Session Length

It had been proposed that 1-hour data sessions would be processed to detect possible ground deformation signals. The data sample rate is set at 30 seconds for the SAGE-NZ network, providing 120 epochs of data per session for (correct) ambiguity resolution, the estimation of the slave station coordinate and an additional tropospheric parameter. L1-only carrier phase and pseudo range data is used, limiting the number of measurements. Extending the length of the sessions provides more data, thereby increasing the reliability of the results but decreasing the time resolution for ground deformation signals.

The 24-hour test data set has been processed four times using 1-hour, 2-hour, 3-hour and 4-hour sessions estimating one troposphere parameter per session. Table 6.4 compares the results for differing session lengths.

Table 6.4 – *Comparison of session lengths using a 24-hour time series QUAR – KARA from the SAGE -NZ network March 15, 2000.*

Session length	Height	Baseline length	RMS (length)
1-hour	1411.0612	9233.1813	0.0047
	(0.0235)	(0.0187)	(0.0020)
2-hour	1411.0618	9233.1816	0.0034
	(0.0257)	(0.0117)	(0.0018)
3-hour	1411.0521	9233.1811	0.0026
	(0.0201)	(0.0099)	(0.0006)
4-hour	1411.0533	9233.1813	0.0022
	(0.0209)	(0.0109)	(0.0005)

From Table 6.4 it can be seen that as the observation session length increases from two to three hours, the average value of the height component displays a jump. This is possibly due to the smaller data quantity and the unstable nature of GPS height determination. A longer session length guarantees a better satellite geometry to avoid this effect. The average of the baseline length shows no such jump, and as expected the rms of the processing solution decreases steadily with observation session length. Figure 6.4 illustrates the effect of different session lengths on the estimated height component.

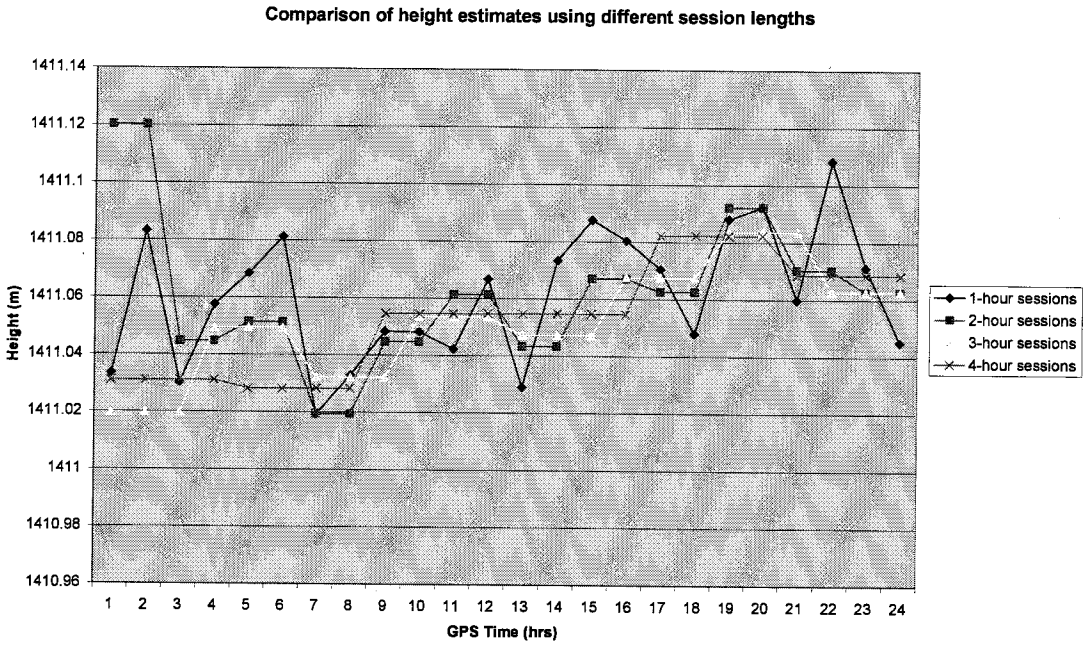

Figure 6.4 – *Time series of estimated height component vs. session length for the baseline QUAR – KARA 15/3/2000.*

The standard deviation of the estimated baseline length remains approximately the same regardless of session length, although from Figure 6.4 there appears to be a discrepancy during the first few hours of the time series for the 1 and 2-hour cases. This is due to a lack of data and/or a bad satellite corrupting the processing. Eliminating these anomalous session results from the average computation gives a standard deviation of the baseline length component that is commensurate with those for the longer observation sessions.

The ease of processing greatly increased for baselines of 2-hour length or greater. There was no requirement to eliminate a satellite from the processing in order that the ambiguities were resolved. Obviously a 1-hour session is less stable than a 2-hour or longer session when processing L1-only data. This could be an important consideration for a system which is required to automatically process baseline data.

Temporal variations in the tropospheric effect requires frequent recomputation. In addition, sudden movements of a deforming body can remain undetected if the session length is made too long.

Although a parameter estimation approach is used for this test data, Figure 6.4 seems to indicate a temporal trend in the height component. The point KARA is assumed to be stationary, therefore this trend is an artefact of the processing. Perhaps the troposphere parameter has absorbed effects other than just the unmodelled troposphere in the least squares estimation (see Fig 6.10 and discussion).

Another way to examine this data is to process the whole 24-hour session four times and estimate 24, 12, 8 and 6 troposphere zenith parameters corresponding to 1, 2, 3 and 4-hour sessions respectively. Results of processing using L1-only data and a 10-degree elevation cut-off angle are shown in Figure 6.5.

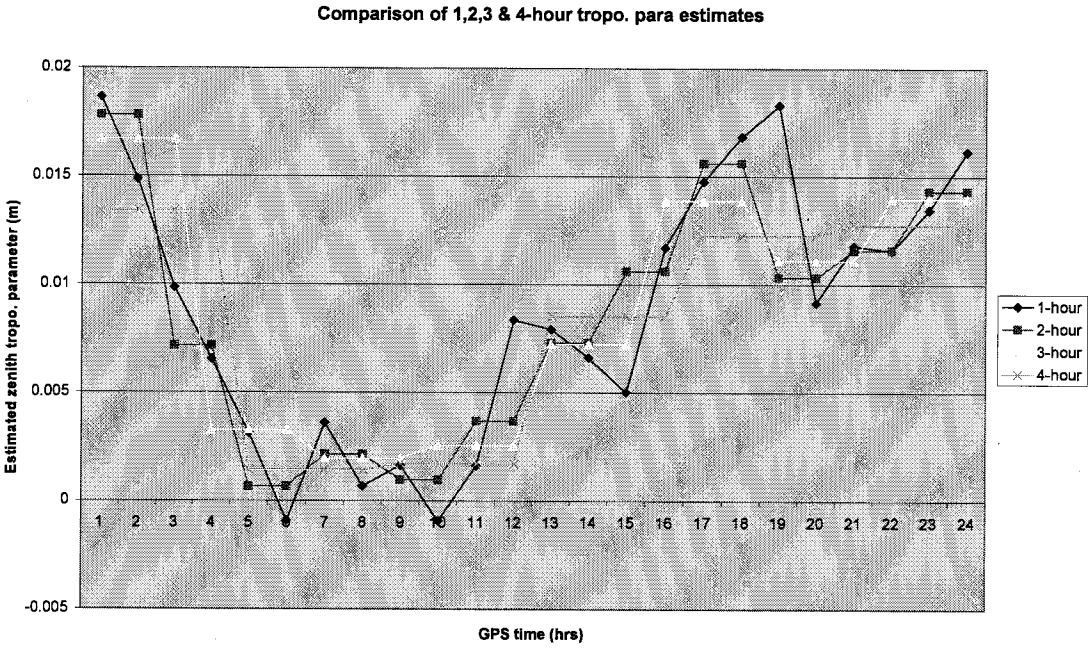

Figure 6.5 – *Comparison of 1, 2, 3 & 4-hour residual relative troposphere zenith delay parameter estimates.*

It should be pointed out that the residual relative zenith troposphere delay parameter is the composite of four separate troposphere estimates using a double-differencing strategy. These estimates therefore have no physical meaning and negative values are results of differencing and do not indicate negative tropospheric delay.

Using the full 24-hour data series is counter productive for a monitoring system, as a 24-hour time delay is introduced into the resulting coordinate estimates used for

detection. A 24-hour data set leads to more reliable estimates of the ambiguities, and the resultant troposphere parameter estimates should be more stable. This can be easily illustrated by comparing the magnitude of the troposphere parameter estimates for the 1-hour session case vs. the 24-hour session and estimating 24 1-hour parameters. Figure 6.6 illustrates this comparison.

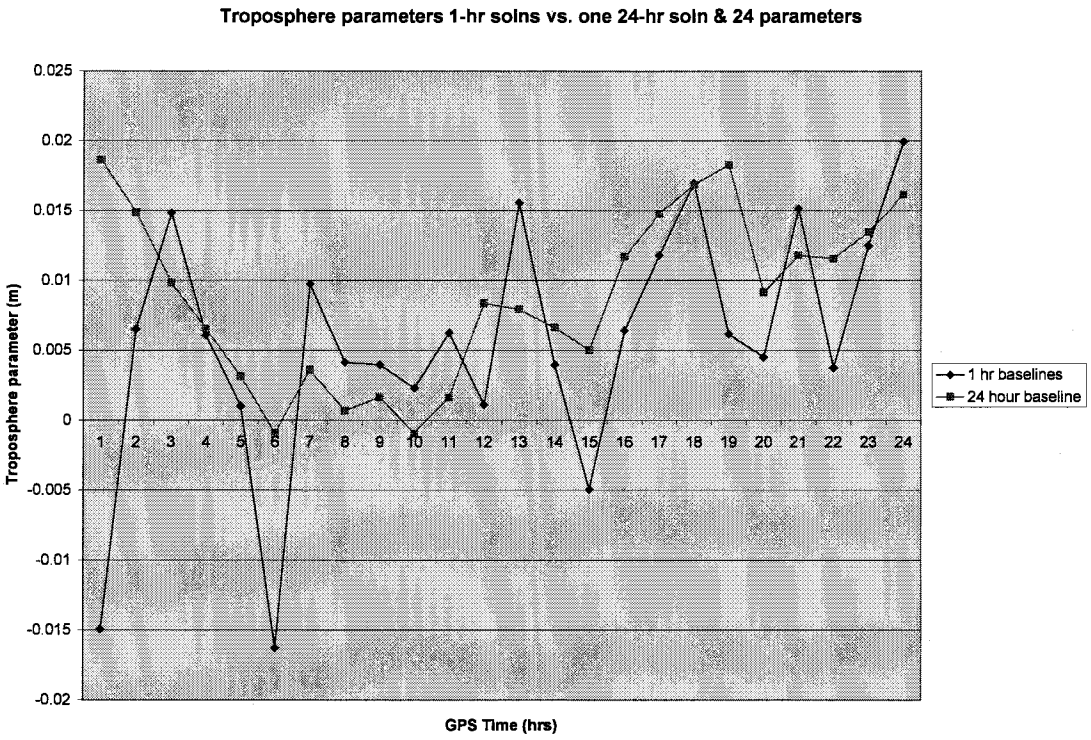

Figure 6.6 – *Troposphere parameter estimates for 1-hour solutions vs. 24 estimates for one 24-hour solution.*

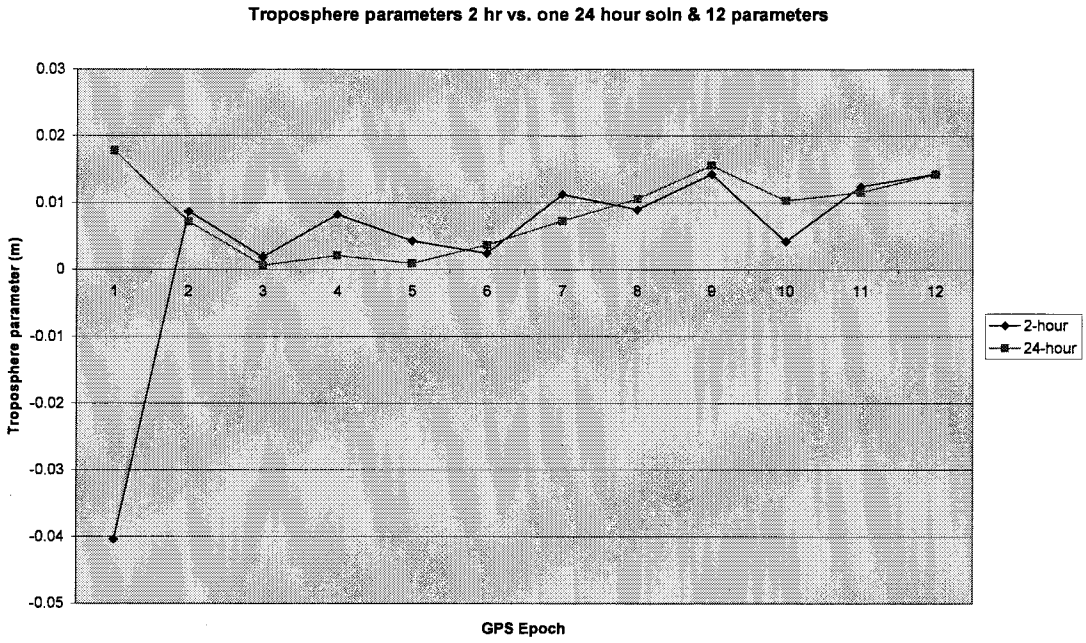

Figure 6.7 – *Troposphere parameter estimates for 2-hour solutions vs. 12 estimates for one 24-hour solution.*

Clearly, estimating 24 parameters from a full day of data produces more stable results. Figure 6.7 illustrates the same comparison for 2-hour sessions vs. 12 estimates from the full 24 hours of data.

While still more erratic, the 2-hour sessions are much more stable than the corresponding 1-hour sessions shown in Figure 6.6. The 3-hour and 4-hour session cases are still more convincing (see Figs 6.8 and 6.9)

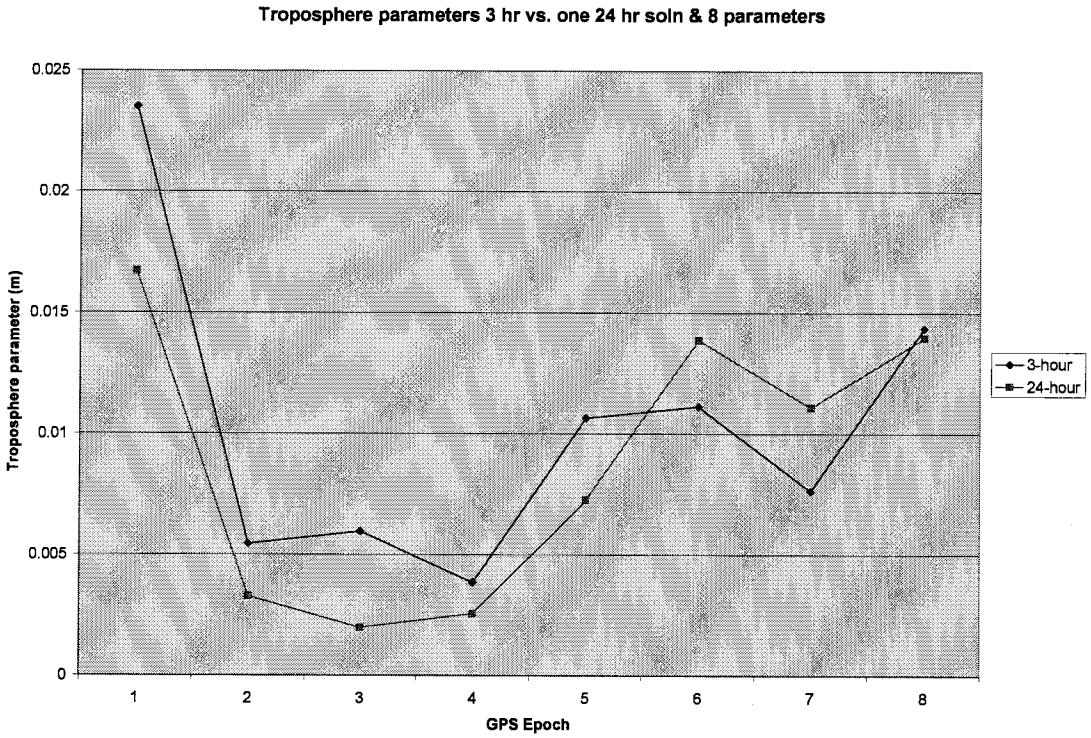

Figure 6.8 – *Troposphere parameter estimates for 3-hour solutions vs. 8 estimates for one 24-hour solution.*

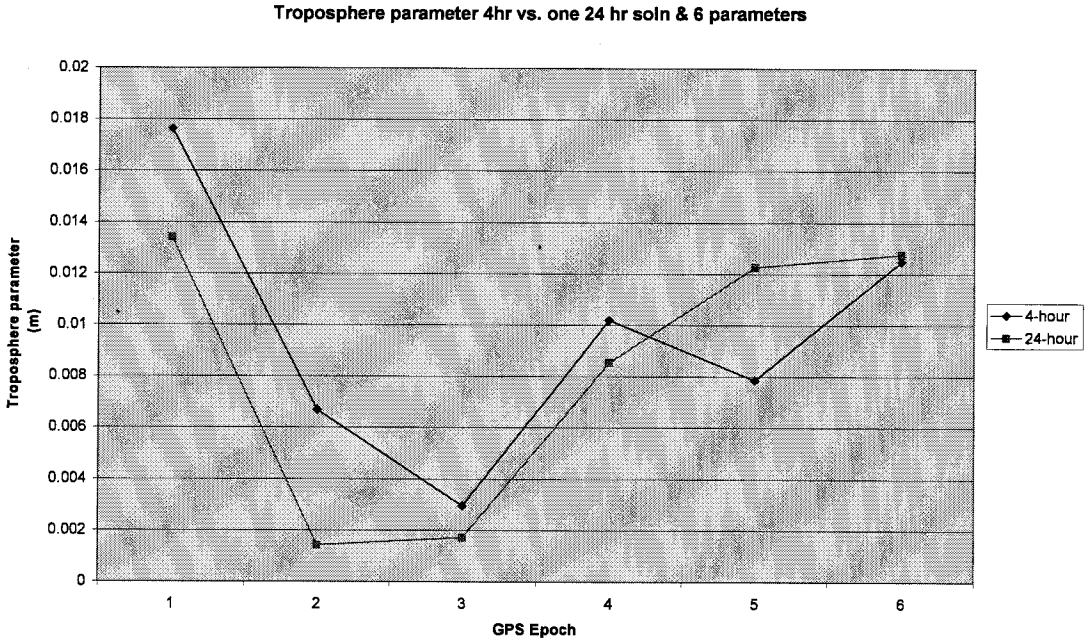

Figure 6.9 – *Troposphere parameter estimates for 4-hour solutions vs. 6 estimates for one 24-hour solution.*

Note that the corrupted sessions in the first few hours of this test data series destabilise the solution for the shorter sessions but are absorbed in the case of increasing session length (ie Figs 6.8 and 6.9).

The residual relative troposphere zenith delay parameter is intended to absorb mis-modelled tropospheric effects, however it may also soak up other mis-modelled effects such as ionospheric effects, multipath and/or instrument noise. Chapter 5 recommends estimating just one extra parameter as too many extra parameters will weaken the solution (see also Beutler et al, 1988) and require longer session lengths. Because a correlation exists between the receiver station height and the estimated troposphere parameter, this correlation could be used to assess the quality of the parameter estimate. Figure 6.10 displays the height results for the 1-hour session case versus the magnitude of the estimated troposphere parameter. These two time series are then compared using the cross-correlation function, to indicate any similarities.

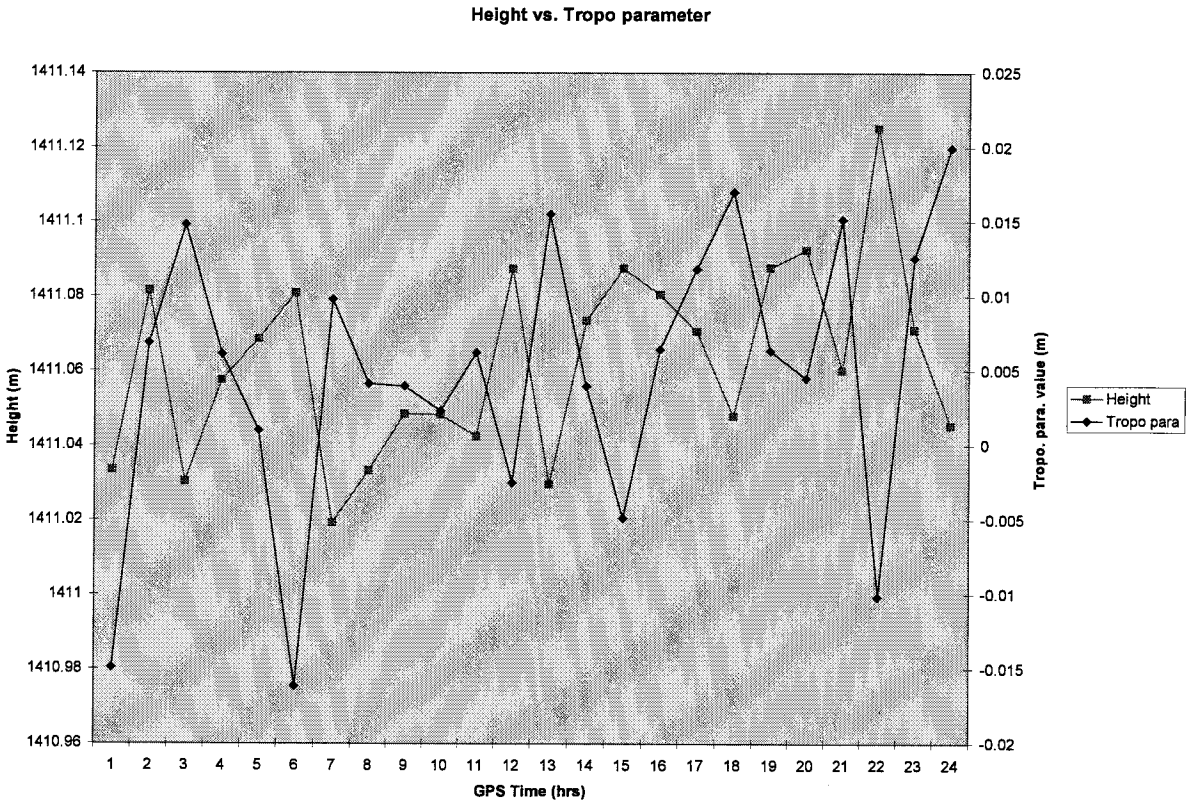

Figure 6.10 – *Height component vs. magnitude of the estimated troposphere parameter for 1-hour sessions.*

An inspection of Figure 6.10 suggests a negative correlation between the two time series (note that the first session again is a corrupted baseline). The cross-correlation value of these two lines (excluding the first session) is –0.6. While this is not a very strong correlation, it is encouraging. This cross-correlation measure could be used as a measure of the validity of a particular troposphere parameter estimate.

6.2.6 Troposphere Parameter Estimation

The Bernese V4.2 software offers several different parameter estimation options. The analyst can choose from the residual relative zenith delay approach (as shown above), using either the Saastamoinen or the Hopfield model. In addition, the Essen-Froome approach is provided as an option, as well as a local troposphere estimation procedure.

The residual relative zenith delay procedure is described in chapter 5 and uses the Saastamoinen a-priori model and a mapping function. The Bernese V4.2 software offers the superior Niell mapping function as an alternative to the Saastamoinen or Hopfield mapping functions. Although Mendes (1999) recommends the Niell mapping function as the most reliable for elevation angles below 6°, he also claims it is equivalent to the Saastamoinen model to a cut-off angle of 10°.

The Essen-Froome model is applied to the atmospheric layer between the lowest and highest site. The tropospheric delay above the highest site is determined using the Saastamoinen model (Rothacher & Mervart, 1996). This is a slight departure from the residual relative zenith delay in that the differential troposphere between the lowest and highest sites is dealt with explicitly. There is a negligible difference in the resulting height component between these two approaches (Schaer 2001, personal communication). The 24-hour test data series was processed using the Essen-Froome approach for the entire 24-hour session, while estimating 6 parameters (ie 4-hour sessions). The average height and baseline length differences were at the millimetre level, confirming this assertion.

The Bernese V4.2 software also offers a local troposphere model option which is recommended for local campaigns with small baseline lengths and large height differences. Details of this technique are given in the Draft Bernese V4.2 User Manual,

section 12.5.1. This approach is most effective with four or more stations. It models the residual zenith troposphere delay correction using a polynomial representation of degree n as a function of the station height (assuming no correction with respect to the a priori model at a given reference height). Schaer (2001, personal communication) suggests a polynomial degree of n=2 is a reasonable setting, as used during analyses for the Turtmann network (Beutler et al, 1995). The value n should be smaller than the number of stations involved in the network. Using only two stations is equivalent to the residual relative zenith delay approach described in chapter 5.

As this thesis compares example data from the SAGE-NZ network, comprising just two nearby stations, with data from 2 stations of the Papandayan network (section 6.4), then the local troposphere model approach is not appropriate for these studies.

Using other parameter estimates will therefore not yield appreciable differences and it is recommended to process using the relative residual zenith delay parameter approach (Peter Morgan 2001, personal communication).

6.3 Data Processing of the SAGE-NZ Time Series

6.3.1 Processing for 21 days of Data using Standard Troposphere Modelling

Results presented in section 6.2 have dealt with one 24-hour segment of data which may not be representative of a longer time series. Figure 6.11 shows the 21-day data set of the baseline QUAR – KARA, from 1 – 21 March 2000 (see also Fig 5.1). The easting, northing and height components are shown for demonstrative purposes only. This time series was processed using the Baseline software and the standard Saastamoinen model for 1-hour sessions with an elevation cut-off angle of 10°. Despite the recommendations of chapter 5, the whole 21-day time series was processed using the Baseline software to confirm that the effects described in section 6.2 are not restricted to the 24-hour segment of test data. Although the points are assumed stationary, a change of up to 20 cm in the height component can be observed due to the mis-modelling of the differential troposphere using the standard Saastamoinen model.

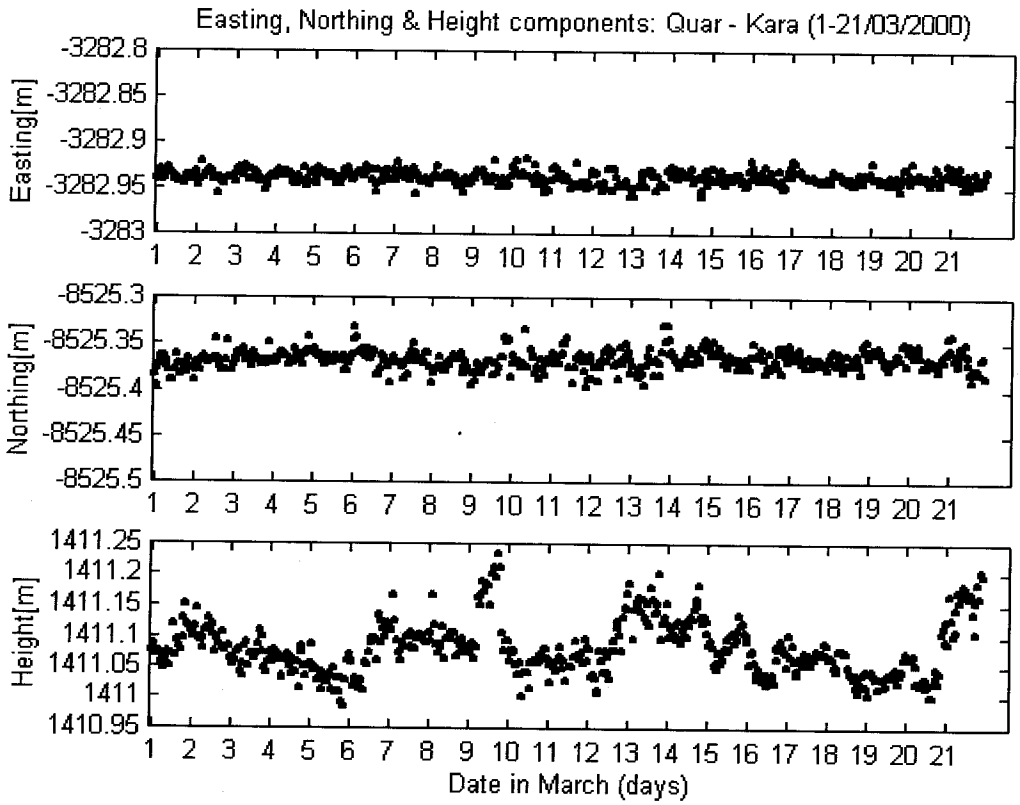

Figure 6.11 – *Coordinate time series of 1-hour sessions from Baseline with standard Saastamoinen troposphere modelling QUAR – KARA, 1 – 21/03/2000 easting, northing and heights.*

In general, the troposphere exhibits a 4 – 5 day correlation period relating directly to changing weather conditions (Peter Morgan 2001, personal communication). The height component in Figure 6.11 reflects this characteristic. There is a downward trend in the height between days 2 and 6, followed by a steadying in the height, and some more erratic behaviour between days 13 and 16 and then an upward trend in the last few days. This further confirms the statement made in section 6.2 (Modelling vs. Estimation using Bernese) that the troposphere modelling approach introduces an artificial temporal signal into the estimated height component for small scale networks with a large change in height.

The same time series was processed using the Baseline software, with 3-hour sessions, Saastamoinen modelling and 10° elevation cut-off (see Fig 6.12). Again, the temporal trend due to a mis-modelled troposphere is obvious.

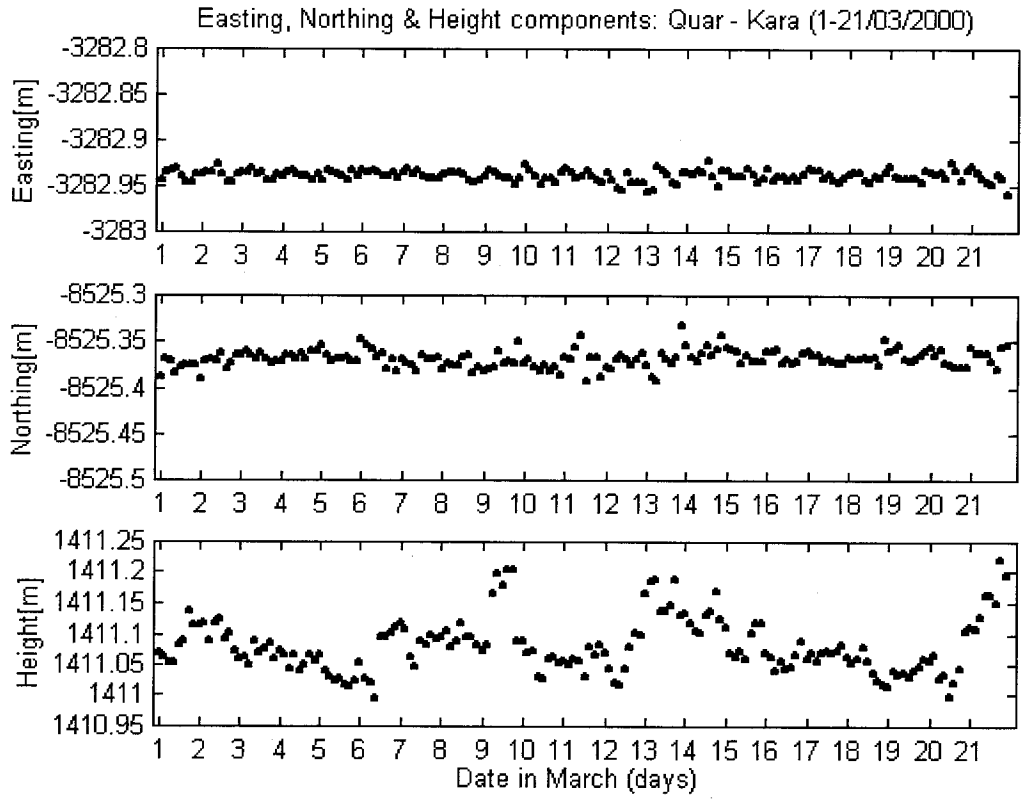

Figure 6.12 – *Coordinate time series of 3-hour sessions from Baseline with standard Saastamoinen troposphere modelling. QUAR – KARA 1 – 21/03/2000 easting, northing and heights.*

6.3.2 Processing for 21 days of Data using Troposphere Parameter Estimation

The same 21-day data series was processed using the Bernese software to generate L1-only solutions. Identical starting coordinates were used and one residual relative zenith troposphere delay parameter was estimated, with a simple cosine (zenith) mapping function. The intention of this processing was to study the difference in the results obtained by troposphere modelling versus troposphere parameter estimation. One-hour sessions (Fig 6.13) and three-hour sessions (Fig 6.14) were processed for the entire time series for direct comparison with the troposphere modelling shown above.

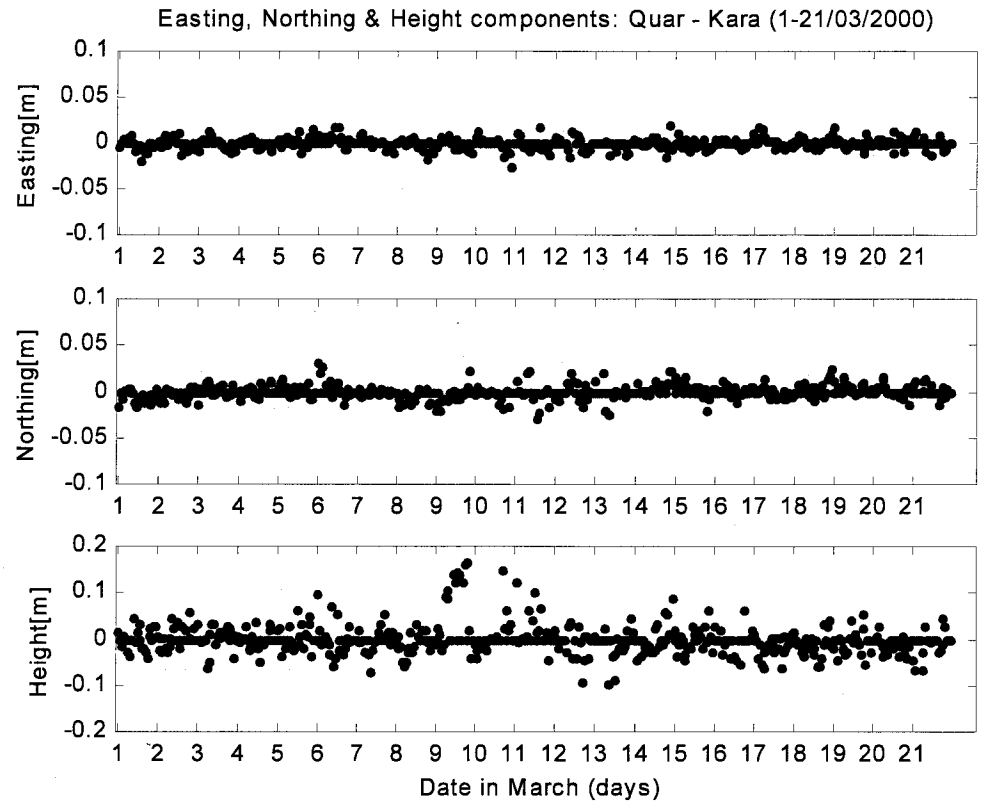

Figure 6.13 – *Coordinate time series of 1-hour sessions from Bernese processing with Saastamoinen parameter estimation cos(z) mapping function. QUAR – KARA, 1 – 21/03/2000 easting, northing and heights.*

Easting, northing and height components in Figures 6.13 and 6.14 are presented as zero mean values. The boundary lines represent two standard deviations of the mean. This data series does not exhibit a diurnal trend, as was the case for results from the troposphere modelling approach. This suggests that the troposphere parameter estimation approach is perhaps immune to atmospheric changes; a very desirable characteristic for a GPS-based monitoring system.

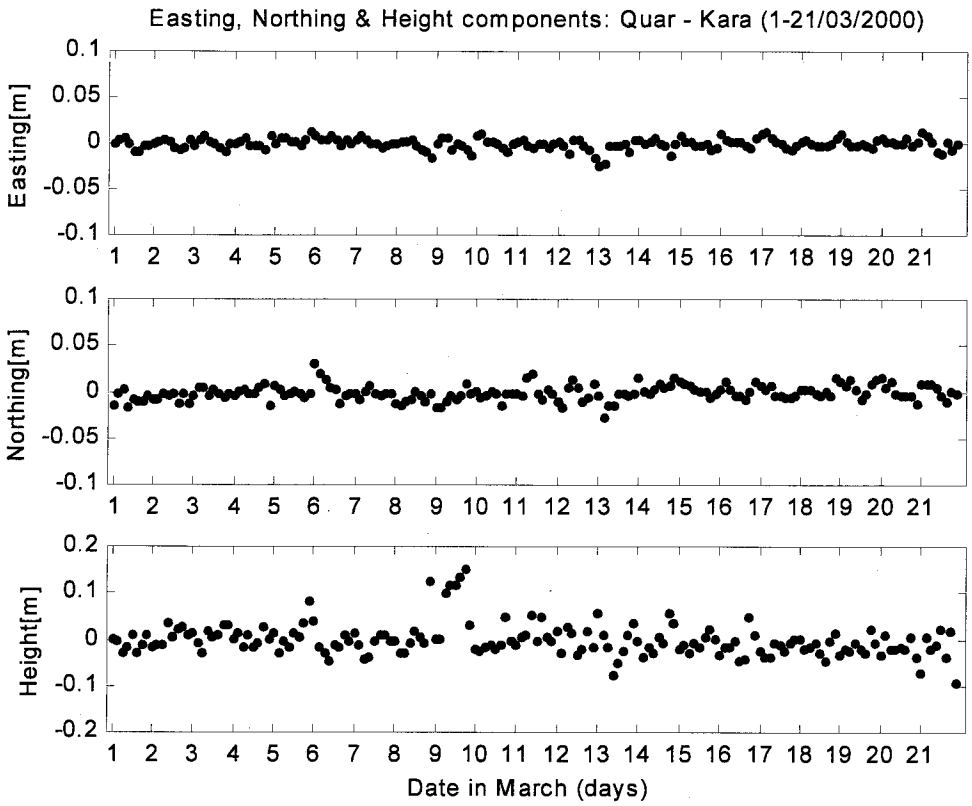

Figure 6.14 – *Coordinate time series of 3-hour sessions from Bernese processing with Saastamoinen parameter estimation and cos(z) mapping function. QUAR – KARA, 1 – 21/03/2000 easting, northing and heights.*

Table 6.5 - *Average values and standard deviations for 1-hour & 3-hour sessions using the Baseline and Bernese software packages.*

	EAST	NORTH	HEIGHT	DISTANCE
1-hr sessions	-3282.9382	8525.3676	1411.0797	9233.1885
Baseline	(0.0068)	(0.0103)	(0.0432)	(0.0126)
3-hr sessions	-3282.9385	8525.3684	1411.0811	9233.1895
Baseline	(0.0059)	(0.0094)	(0.0450)	(0.0115)
1-hr sessions	-3282.9375	8525.3676	1411.0623	9233.1856
Bernese	(0.0067)	(0.0087)	(0.0324)	(0.0111)
3-hr sessions	-3282.9375	8525.3679	1411.0616	9233.1854
Bernese	(0.0061)	(0.0086)	(0.0351)	(0.0102)

From Table 6.5 it can be seen that the standard deviation for the estimated height component using the troposphere parameter estimation approach is smaller than for the case of tropospheric delay modelling. There is a slight improvement in all components (except the height component) when a longer session length is used. This is to be

expected as the amount of observation data is increased, improving the chances of correct ambiguity resolution, and more reliable estimation of the residual relative troposphere delay. Various researchers (Gurtner et al, 1989; Tralli & Lichten, 1990; Abidin et al, 1998a) have recommended a minimum observation session length of about one hour, preferably more, especially in the case of single-frequency GPS data processing.

6.3.3 Discussion of Processing Results

The processing of this data was an arduous task, jeopardising the concept of automatic baseline processing using the Baseline software. For any one-day of data (using 1-hour sessions), perhaps 10 baselines could not be processed automatically and required some manual attention. This could entail either deleting one or more satellites, reducing the length of the session (to avoid some noisy data) or, less frequently, changing the base satellite in the double-differencing strategy in order to ensure correct ambiguity resolution. There seemed to be no pattern that could be accounted for by filtering or in some additional automatic routine. This data was taken from a high quality network of dual-frequency GPS receivers using geodetic quality antennas, and located in the mid-latitudes to avoid excessive disturbance from the ionosphere. Automatic data processing using the Baseline software, collected by a low-cost system in an equatorial region, is therefore not feasible at this stage.

In contrast to the processing using the Baseline software, the processing using the Bernese software was successful for every run, without the need for any extra manual attention. This was fortunate, as manual attention using the Bernese software can be cumbersome. In truth, the Bernese software is far too sophisticated for the task at hand. However, it was the only software available to the author to demonstrate troposphere parameter estimation. It is also this sophistication which permitted a solution at every program run, compared to the manual attention demanded when using the Baseline software. However, on closer inspection it could be seen that for many of the Bernese solutions only a float solution was obtained. For a one hour baseline only 120 epochs of data is available. Given that the least squares solution needs to find the X, Y, Z coordinates of the roving station as well as a troposphere parameter, then perhaps a longer session length would yield results that are more reliable. This in fact was the

case. For the one-hour session case, from 504 baselines, 147 float solutions were obtained (29.2%). However, for the three-hour session case, from 168 baselines, in only 6 solutions was it not possible to fix ambiguities (3.6%). A dramatic improvement!

Despite this improvement there still remained some outliers in the data which had to be manually removed. For an automatic baseline processing system, some form of filtering needs to be implemented to identify these outliers.

6.3.4 Data Analysis

The height components of the four derived time series (Table 6.5) were analysed using digital signal processing techniques to try to detect any repeatable signal present in the data. This could indicate either diurnal movement or an unidentified systematic bias in the system. Welch's averaged, modified periodogram method was used to produce power spectral density (PSD) estimates of the discrete-time signal of estimated heights. The application of an overlapping Hanning window in the PSD computation improved the readability of the frequency domain plots (Mathworks, 1998). Figures 6.15 and 6.16 show the PSD analysis for the 1-hour and 3-hour sessions resulting from processing using the Baseline software and tropospheric modelling, and Figures 6.17 and 6.18 show the corresponding analysis from the Bernese software processing and troposphere parameter estimation.

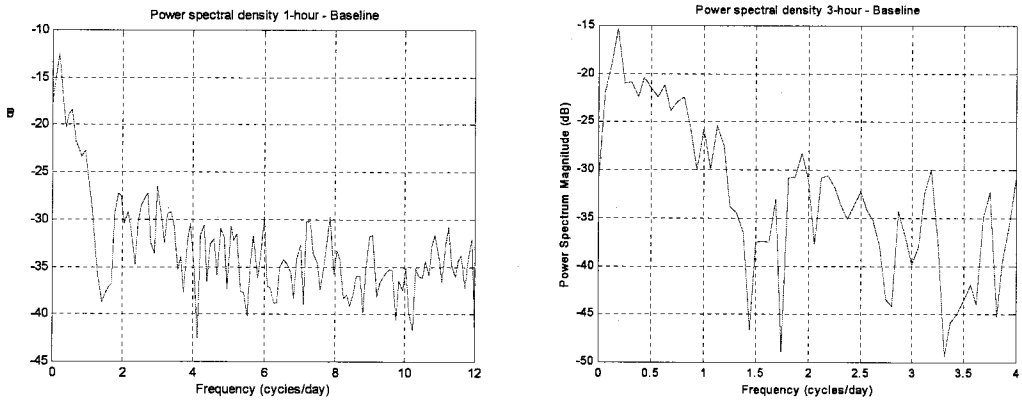

Figure 6.15 and 6.16 - *Power spectral density graphs for the Baseline results using troposphere modelling for the 1-hour (left) and 3-hour sessions (right).*

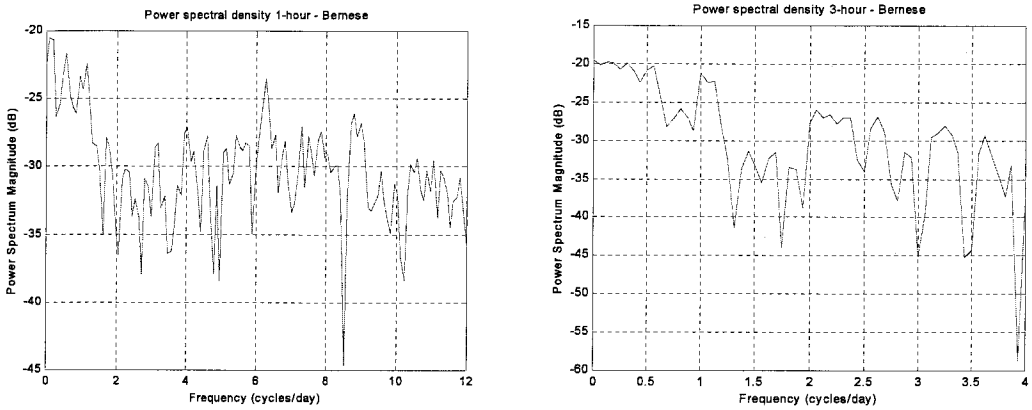

Figure 6.17 and 6.18 - *Power spectral density graphs for the Bernese results using troposphere parameter estimation for the 1-hour (left) and 3-hour sessions (right). The peak corresponds to a 24-hour repeat period.*

The frequency axis is in units of cycles/day. In the figures, low frequency information to the left grades to higher frequency to the right. The peak value around less than one cycle/day is referred to as "red noise" and is a typical signal present in geophysical data. The objective of stochastic modelling in GPS data analysis is to reduce this red noise (Peter Morgan 2001, personal communication). In Figures 6.15 and 6.16, perhaps another peak can be seen at around 2 cycles/day (or every 12 hours) but this is a far less significant signal than that of the red noise.

Figures 6.17 and 6.18 also show this red noise effect but there appears to be a clearer signal at 1 cycle/day. Figure 6.17 shows a peak at 6 cycles/day (or every 4 hours) but this is not detectable (and therefore cannot be verified) from Figure 6.18 due to the sampling frequency of 3-hours (ie session length). From the Nyquist's sampling theorem (Bateman & Yates, 1989), the minimum detectable signal must be at least twice the sampling frequency.

For clarity both power spectral density plots (for the Baseline and Bernese software approaches) are plotted on the same axes. This highlights the agreement between the processing for the 1-hour and 3-hour session cases (Figs 6.19 and 6.20).

The plots of results using the Baseline software have no recognisable signal apart from the red noise mentioned earlier. However, the plots of results using the Bernese software show a definite peak, for both the 1-hour and 3-hour session processing, at 1

cycle/day (or every 24 hours). This peak corresponds to a multipath signal (see section 4.6.2) repeating every sidereal day.

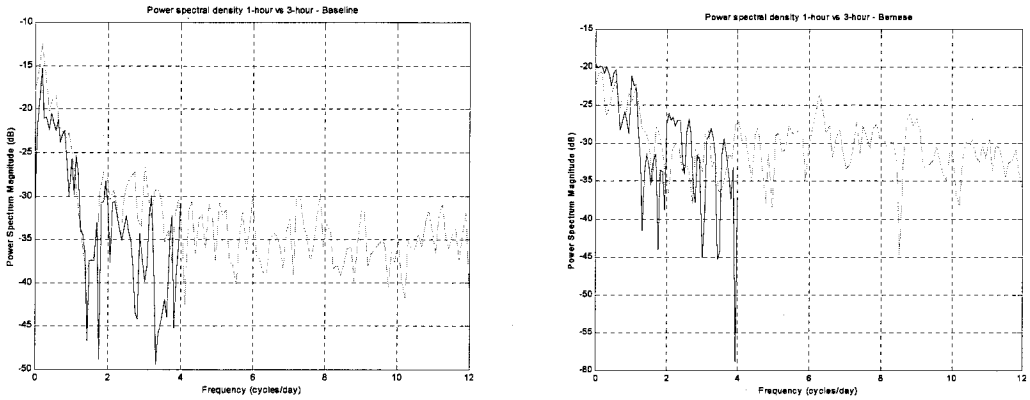

Figure 6.19 and 6.20 - *Comparison of power spectral density graphs for Baseline (left) & Bernese (right) results for 1 (light) & 3-hour (dark) sessions.*

Also note that the power of the 2-cycles/day peak in Figure 6.19 is around –28dB, whereas the power of the distinct multipath peak in Figure 6.20 is around –22dB. The troposphere estimation approach technique therefore results in a significantly greater peak value. This further reinforces the use of this approach as systematic biases can be detected, whereas troposphere modelling tends to blur this signal into the noise.

The multipath effect is eliminated from the time series data using simple FFT filtering in the frequency domain and converting back into the time domain. The standard deviation of the time series is decreased indicating a slight improvement due to filtering (see Table 6.6).

Table 6.6 – *Improvement in standard deviation of time series height data before and after FFT filtering for the Bernese 1-hour and 3-hour cases.*

Standard Deviation	Before filtering	After filtering
Bernese 1-hour	0.0324	0.0308
Bernese 3-hour	0.0351	0.0321

6.3.5 Allan Variance of Time Series Data for Deformation Monitoring

The time series of height results shown in Figures 6.13 and 6.14 indicate a repeatability between sessions which has been measured using the standard deviation of an adopted mean value under the assumption that the points QUAR and KARA are not moving. *How then is it possible to separate a possible movement of a volcanic edifice from a systematic bias of the GPS system monitoring it?*

Section 2.3 suggests three different types of movements namely; a constant movement with time, a varying movement with time or a sudden movement. A slow movement at the millimetre level will not be detected by comparing consecutive session solutions. However, comparisons over several sessions, or days, or weeks, could highlight slow consistent changes. The Allan variance (see 2.4.3.2) is introduced as a means of characterising an upper boundary of sensitivity of a deformation monitoring system.

Hellwig (1977) used the Allan variance to test the performance of frequency standards for scientific instrumentation. He states, "A good reproducibility is an asset in applications where it is of importance to rely on some degree of conformity of the output frequency of several devices such as a factory-guaranteed frequency value." This same logic is applied to the stability of new baseline components from a deformation monitoring system.

A standard F-test can be applied to provide a statistical limit above which a new measurement must not breach. The F-test checks if the variability of two processes are statistically similar. In this case if a new measurement with a specified data interval τ differs from the Allan variance representation.

The null hypothesis:

H_0: $\sigma_{new}^2 = \sigma_{Allan}^2$

H_1: $\sigma_{new}^2 \neq \sigma_{Allan}^2$

The purpose of this work is to identify a new measurement which may indicate a movement of the volcano edifice therefore a single-sided case shall be utilised.

$F > f_{\alpha}(V_1V_2)$ for alternative $\sigma_{new}^2 > \sigma_{Allan}^2$

In this case, the degrees of freedom (V_1V_2) for the first observation will be 503 and 167 for the 1-hour and 3-hour cases respectively. Therefore V_2 is sufficiently close to ∞. Using a standard F-ratio table it is therefore possible to apply a statistical upper limit to the Allan variance to a desired confidence level.

Using equation (2.5), Allan variance representations of the Bernese processed 1-hour time series from the QUAR-KARA baseline is presented in Figure 6.21. The lower line represents the Allan variance representation of the data. A 1-day (ie τ = 24 hours) F-ratio statistic at a 95% confidence level is represented by the upper line.

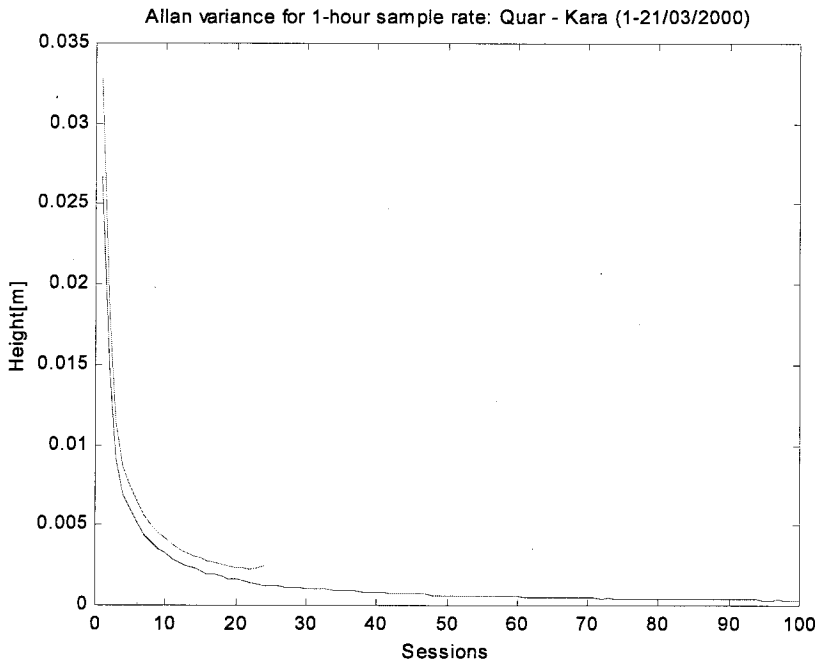

Figure 6.21 – *Allan variance plot of 1-hour time series QUAR-KARA 1-21/03/2000 and a 1-day F-ratio statistic (95% confidence level).*

The Allan variance representation of this time series peaks at 0.026m after the first session for τ = 1-day. The corresponding F-ratio is at 0.033m. This means that a new measurement must be over 0.033m to be considered statistically dissimilar from the base SAGE-NZ data for a 24-hour time window. Any time interval τ can be applied to the data for any confidence interval (in this case 24-hours). Note the upper line curls up

in the last few sessions due to the increasing F-ratio values as the degrees of freedom approach one. This Allan variance approach gives a user the opportunity to statistically assess historical time series data and perhaps determine a hidden trend. Roberts et al (2002a) provides a more detailed description of Allan variance and its application to deformation monitoring.

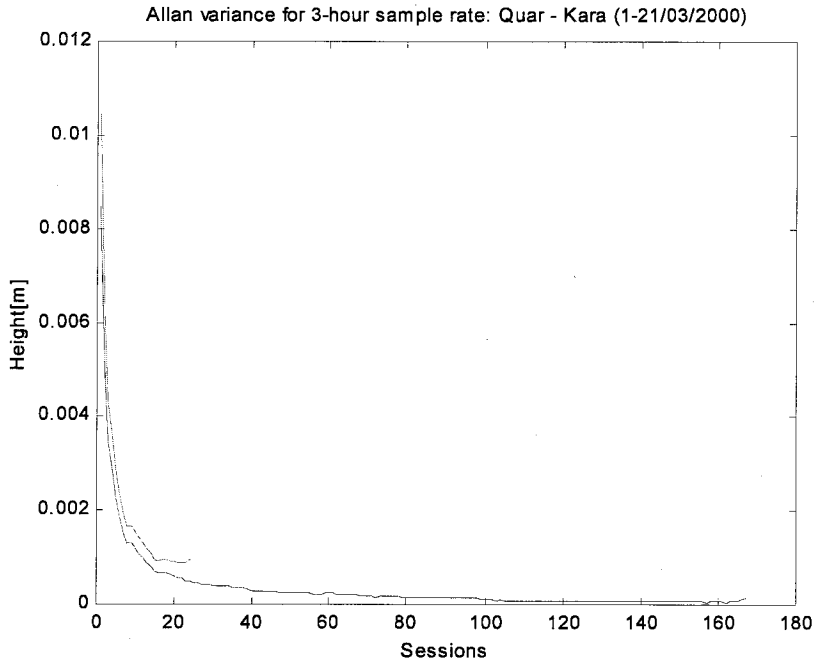

Figure 6.22 – *Allan variance plot of 3-hour time series QUAR-KARA 1-21/03/2000 and a 1-day F-ratio statistic (95% confidence level).*

Note in Figure 6.22 that the data values are one third that of Figure 6.21 reflecting the 3-hr session length (see equation 2.4).

6.4 Data Processing of the Gunung Papandayan Time Series

During the March 2000 campaign on Gunung Papandayan only three days of continuous data was collected due to several hardware and software problems. Another campaign in July 2001 collected 21 days of continuous L1-only data. The limited data-set from March 2000 was processed using the Baseline software with troposphere modelling. As stated above (section 6.3 - *discussion of processing*), the data was extremely noisy and very difficult to process. On several occasions no meaningful baseline result could be obtained. Janssen et al (2001) suggests that the noisy data is a

result of the solar cycle (no. 23) creating high ionospheric noise. This effect is exacerbated by the equatorial location of the Papandayan network. Figure 6.23 illustrates the present solar maximum. Examining this plot more carefully, for March 2000 the solar activity was around sunspot number 140, and for July 2001 the value is approximately 80. Ibid (2001) shows a pattern of unresolved baselines between sunset and sunrise (local time) and suggests that this is the result of phase scintillations. This suggestion is reinforced by ionospheric correction terms processed at this time displaying unusually large magnitudes.

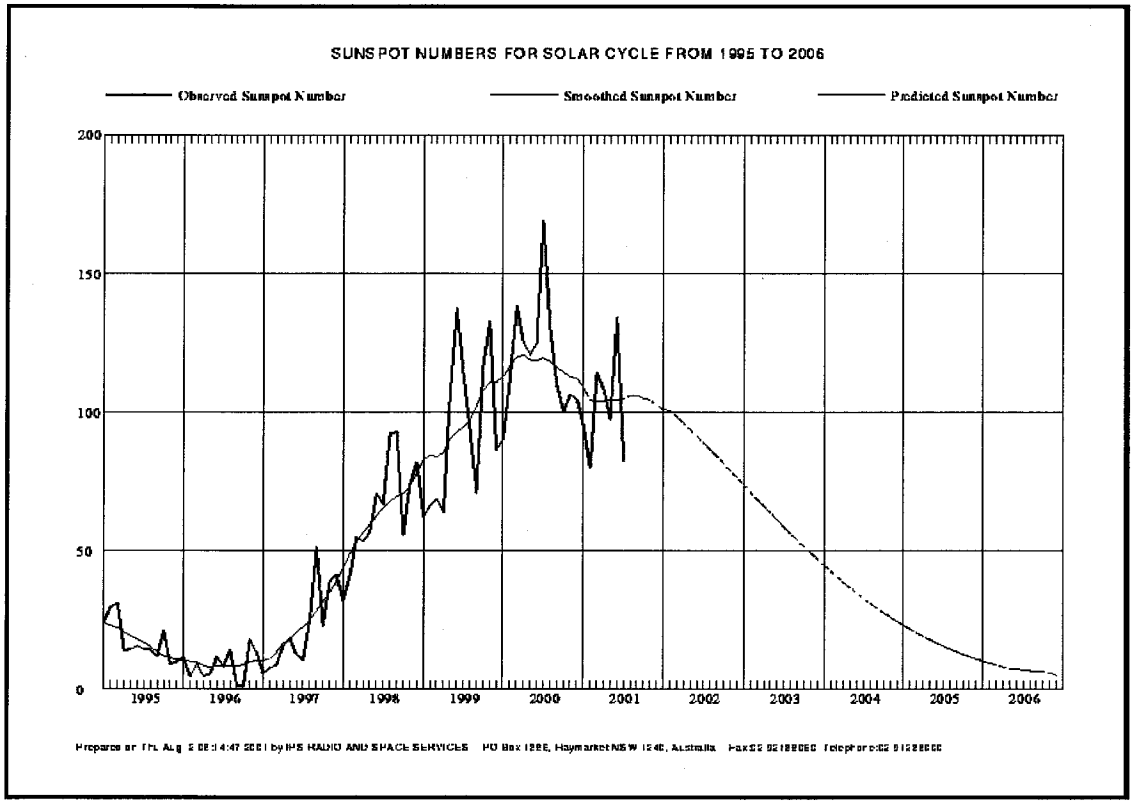

Figure 6.23 - *Monthly, smoothed and predicted sunspot numbers for solar cycle from 1995 to 2006 (IPS, 2001).*

Given that the solar activity seems to have abated[2] during the July 2001 campaign, it is expected that the processing will be less troublesome.

[2] The solar maximum has abated relative to the March 2000 peak. Actually July 2001 remains on the cusp of the solar maximum.

Data Processing

L1-only data from 11-31 July, 2001 was collected continuously using the UNSW volcano deformation monitoring system installed on Gunung Papandayan. The time series was processed using the Bernese software, with 3-hour sessions, 10° elevation cut-off angle and one residual relative zenith troposphere delay parameter estimated per session. The starting coordinates computed previously in section 4.6.6 were adopted. The result of this data processing is compared with the SAGE-NZ time series. Figure 6.24 displays the easting, northing and height components for the 168 baselines processed.

The first comment to be made is that it was possible to process all baselines. Compared to the data from March 2000, where it was not possible to process many of the baselines at all, this is a significant achievement! This reinforces the statement made above regarding the decreased solar activity during the most recent measurement campaign. The quality of the estimated baselines, however, must be questioned.

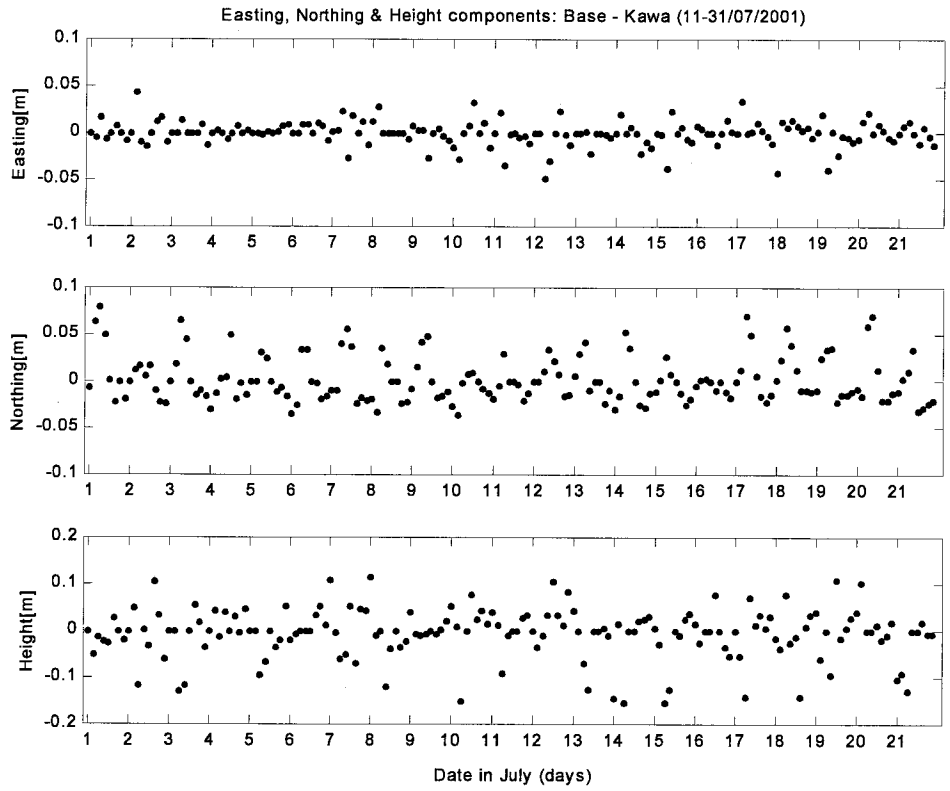

Figure 6.24 – *Time series of 3-hour sessions from Bernese with Saastamoinen parameter estimation cos(z) mapping function. BASE – KAWA, 11 – 31/07/2001 easting, northing and heights.*

From Figure 6.24 note that the height component scale is twice that of the easting and northing scales. Comparing this time series result with the SAGE-NZ network (Fig 6.14), the scatter in all components is significantly more, as is the number of float solutions and outliers. For the Papandayan 2001 time series, 14 epochs were float solutions, corresponding to 8% of the baselines. These observations were removed from the time series, however many outliers still remained.

A visual inspection of the data series identified the major outliers. These were deleted. For the easting component 29 epochs were eliminated; for the northing component 8 were deleted, and for the height component 22 outliers were removed from the time series. Outliers were those with values farthest from the sample mean value (under the assumption that the volcano edifice is stationary) and those measurements with an unusually large a-posteriori sigma of unit weight.

The number of outliers and float solutions eliminated from the time series is a reflection of the poor quality of the data solutions. This is due to the more active ionospheric conditions experienced in Indonesia at this time (Janssen et al, 2001). In total 28%, 13% and 21% of solutions were eliminated from the time series of the easting, nothing and height components respectively. Nevertheless, the standard deviations of the sample means for each component for the Papandayan 2001 time series were still at least twice those of the SAGE-NZ network (see Table 6.7).

Table 6.7 – *Comparison of Bernese 3-hour session results for the 21-day time series from SAGE-NZ vs. Papandayan 2001.*

	EAST	NORTH	HEIGHT	DISTANCE
SAGE-NZ	3282.9375	8525.3679	1411.0616	9233.1854
3-hr sessions	(0.0061)	(0.0086)	(0.0351)	(0.0102)
PAPANDAYAN	6331.7330	4268.1147	2197.8689	7707.3403
3-hr sessions	(0.0154)	(0.0264)	(0.0609)	(0.0282)

Data Analysis

Figure 4.8 shows the GPS antenna at the Kawah observing station surrounded by a barbed wire fence, and in close proximity to a mounted solar panel. This is far from a multipath-free environment. Power spectral density analysis of the time series should therefore indicate a multipath signal. Figure 6.25 illustrates the results of this analysis.

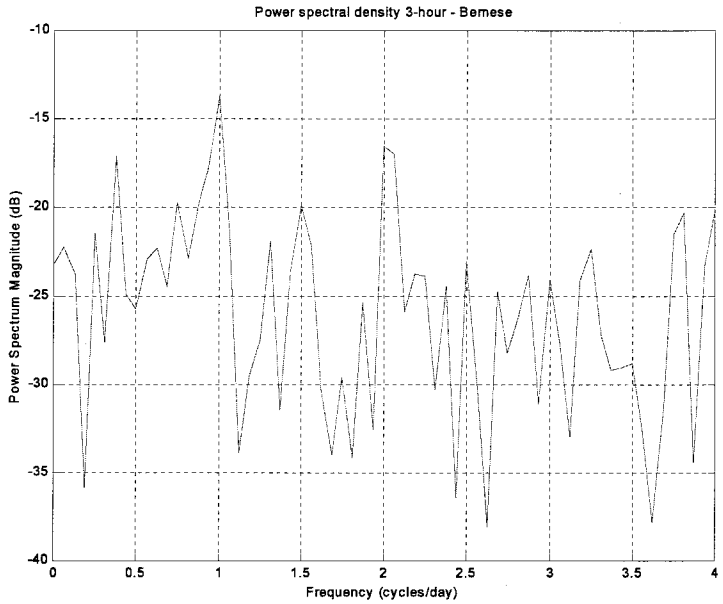

Figure 6.25 – *Power spectral density graphs for the Bernese results (using troposphere parameter estimation) for 3-hour sessions.*

It is clear from Figure 6.25 that a significant peak exists at 1-cycle/day corresponding to a multipath signal. As for the SAGE-NZ data, this signal is filtered out using a simple FFT filter. The standard deviation of the height component within the time series is therefore reduced from 0.0609 to 0.0501m. The Allan variance for the 3-hour session time series is presented in Figure 6.26.

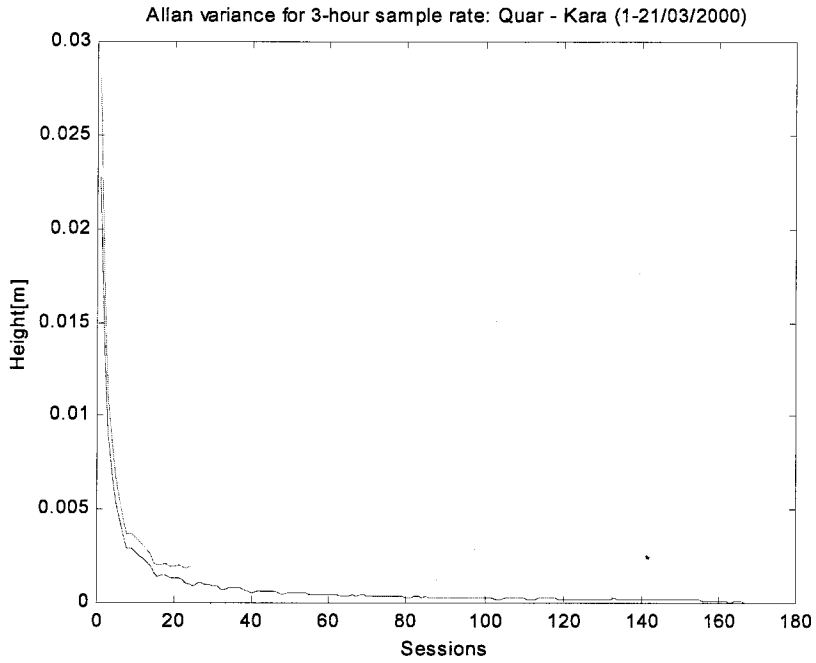

Figure 6.26 – *Allan variance plot of 3-hour time series BASE - KAWA 11-31/07/2001, Papandayan 2001 and a 1-day F-ratio statistic (95% confidence level).*

The Allan variance representation of this time series peaks at 0.023m after the first session. This is more than twice that of the SAGE-NZ data and indicates the much larger variability of this time series. The UNSW-designed GPS monitoring system is therefore a significantly less sensitive system than that for the SAGE-NZ network (section 6.3).

6.5 Concluding Remarks and Further Investigation

It must be remembered that the data used to produce the Allan variance representation shown in Figure 6.26 for the height component is derived from 3-hour sessions, Bernese processing with troposphere parameter estimation, and after discarding a significant number of epochs as outliers. Despite this, the height component still displays an erratic behaviour, even after multipath is filtered from the signal.

During the Papandayan 2001 campaign a Leica SR9500, dual-frequency GPS receiver was set up to collect 24-hour sessions of data (day 190) in close proximity to the base station and Bukit Maung sites respectively (actually the ITB GPS repeat survey campaign sites were used). The purpose of this survey was to compare the quality of the

carrier tracking loops of the single-frequency CMC receiver and a high quality, dual-frequency GPS receiver. Although identical sites were not occupied, the repeatability of segments of this data would indicate the relative quality of the tracking loop performance.

Unfortunately the CMC and Leica receivers were not operating simultaneously so identical atmospheric conditions could not be compared. L1-only data from the Leica receiver was processed using the Bernese software, with 3-hour sessions, 10° elevation cut-off angle and one residual relative zenith troposphere delay parameter estimated as before. The results derived from the Leica data were similarly erratic to those of the CMC, which reaffirms the carrier tracking loops for both receivers are comparable. Additionally, the rms of the triple-differenced solutions for both CMC and Leica receivers was at the mm level, indicating good quality phase measurements. This empirical test reaffirms initial tests carried out when designing the GPS/PC module (see section 4.2.2) that the CMC receiver hardware was of geodetic quality.

So why is the time series resolution so poor for the Papandayan 2001 data?

As stated above (section 6.2 – Ionosphere), the Bernese V4.0 manual recommends using a global ionosphere model to improve results for small scale, L1-only networks. The University of Berne global models (Schaer et al, 1996) were included in the single-frequency processing of the CMC data for day 192 of the Papandayan 2001 data series. These models are global estimates and can only approximate local conditions. Figure 6.27 shows a comparison between the day 192 easting, northing, height, and distance results, with and without the application of these global models for 3-hour sessions.

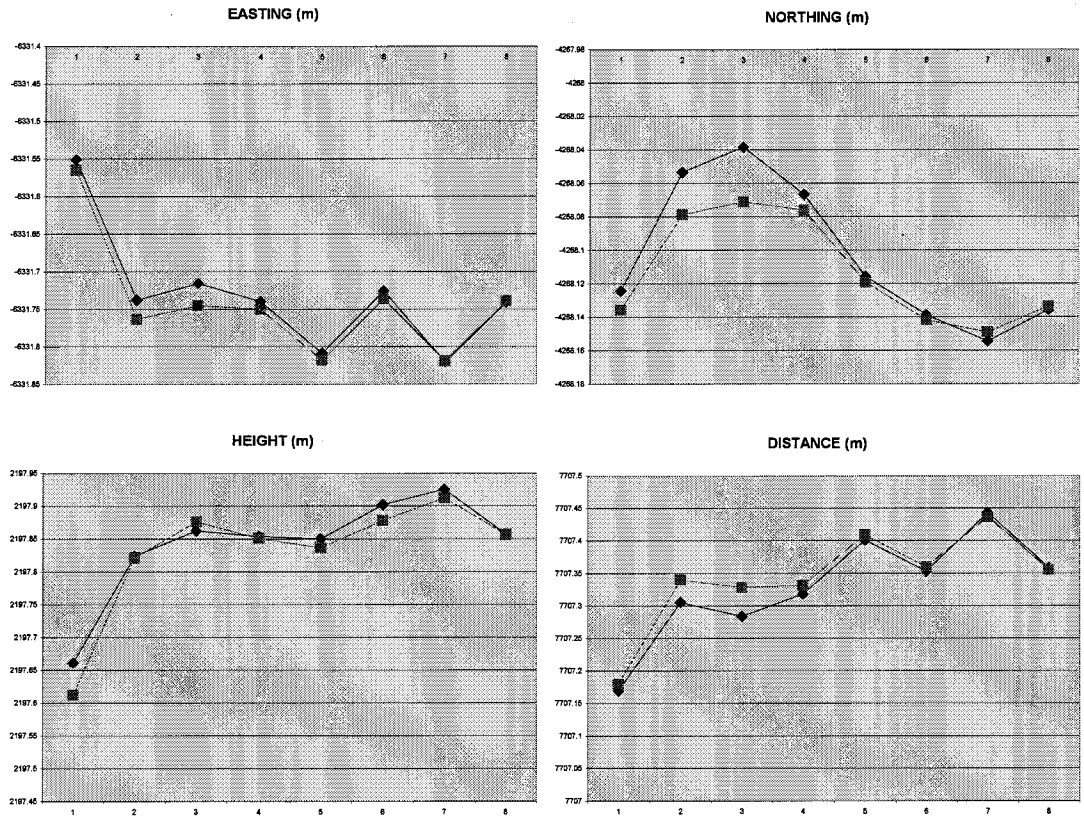

Figure 6.27 – *CMC baseline BASE – KAWA, day 192 processed with (denoted by +) and without (denoted by 6) global ionospheric models for the easting, northing, height and distance components.*

Figure 6.27 indicates that using the global ionosphere models results in only a minor difference to the baseline results, and does not improve the time series repeatability.

The investigations into the carrier tracking loop stability serendipitously provided Leica dual-frequency data in close proximity to the L1-only network. This allowed an ionosphere-free solution to be processed and compared with the single-frequency result. Seven 3-hour sessions were processed using this dual-frequency data set, and the Quasi-Ionosphere Free (QIF) baseline processing option within the Bernese software. All other parameters were set as before for direct comparison. Figure 6.28 illustrates the comparison between the L1-only and the dual-frequency solutions for the easting, northing, height, and distance components.

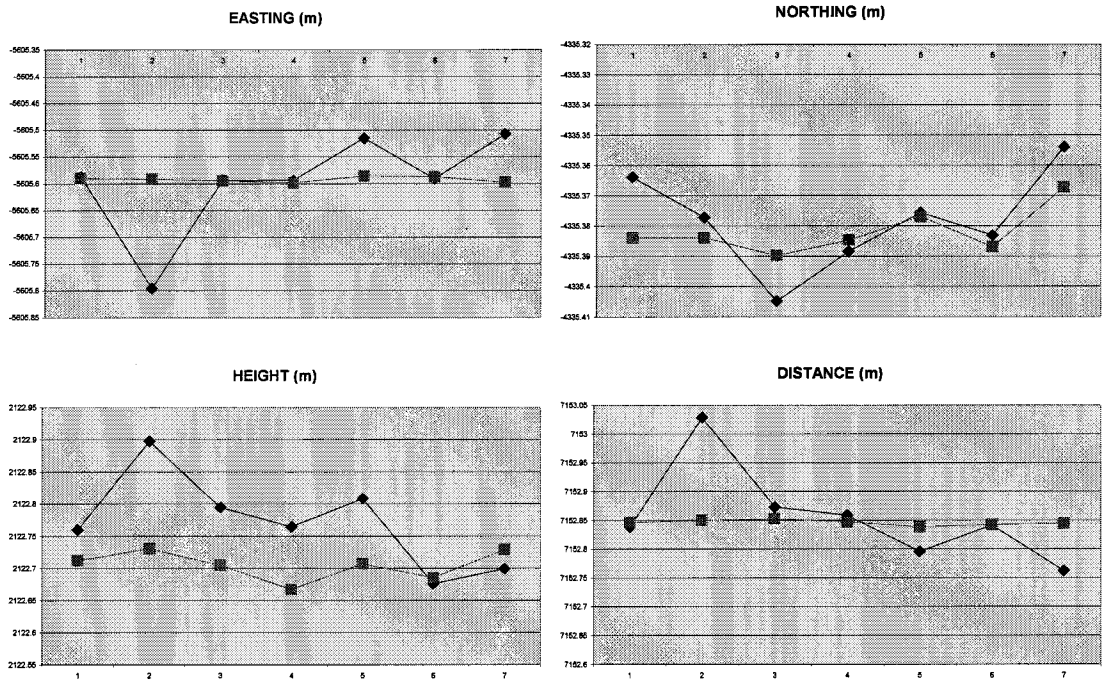

Figure 6.28 – *Comparison for seven 3-hour sessions between Leica L1 data (denoted by 6) vs. Leica dual-frequency data (denoted by +) processed using the QIF strategy, day 190.*

From this limited data set it is clear that the variability in all components is far less using dual-frequency data. The difference between the single and dual frequency approaches highlights the significant impact the ionosphere has on GPS signals even over distances as short as 7-8 km in this region. Table 6.8 compares the results of Figure 6.28 with previous results from the SAGE-NZ and Papandayan 2001 time series.

Table 6.8 – *Comparison of seven 3-hour sessions using Leica dual-frequency data with the 3-hour session results for the 21-day time series' from SAGE-NZ and Papandayan 2001.*

	EAST	NORTH	HEIGHT	DISTANCE
SAGE-NZ	3282.9375	8525.3679	1411.0616	9233.1854
168 sessions	(0.0061)	(0.0086)	(0.0351)	(0.0102)
PAPANDAYAN	6331.7330	4268.1147	2197.8689	7707.3403
168 sessions	(0.0154)	(0.0264)	(0.0609)	(0.0282)
LEICA (L1&2)	5605.5918	4335.3818	2122.7053	7152.8460
7 sessions	(0.0049)	(0.0075)	(0.0226)	(0.0048)

Note the comparisons of the standard deviations (in brackets). (The component values are included for completeness.) PAPANDAYAN sessions refer to the BASE – KAWA baseline. The LEICA (L1&2) results refer to the ITB network points located close to the BASE and Bukit Maung sites (hence the component differences for PAPANDAYAN and LEICA (LI&2)).

The standard deviation for the LEICA (L1&2) baselines is lower than the SAGE-NZ results, and significantly lower than the Papandayan 2001 results. The essential difference between processing using L1-only data and dual-frequency data is the elimination of ionospheric biases (section 3.2.4). Although the LC combination produces a higher noise level, the standard deviation of the results was still far smaller than that for the L1 only solution. Chen et al (2001) demonstrated high quality, single-frequency receiver densification of existing dual-frequency networks at three different locations in *mid-latitude regions*. Investigations from the Papandayan 2001 network indicate that the increased ionospheric activity in *equatorial regions* precludes such low-cost densification without some consideration of the ionosphere, even for short baselines.

Additionally, it was expected that more multipath will be experienced for the Leica data as compared to the SAGE-NZ data. The AT303 antenna used for the Leica observations includes no external groundplane, whereas the SAGE-NZ network uses a Trimble L1/L2 antenna with groundplane. Also the Leica data was collected using tripods as compared to stable pillars. Despite these factors it appears that the dual-frequency Leica data are more precise than the L1-only results.

The Papandayan 2001 network comprised four single-frequency CMC low-cost GPS/PC modules, girt by an outer fiducial network of dual-frequency Leica CRS1000 GPS receivers. This fiducial network will provide post-processed ionospheric correction terms (see section 4.6.4) to the single-frequency baselines, thereby improving the precision to a level comparable to that of dual-frequency baselines.

Recommendations

As a result of the processing of the SAGE-NZ and Papandayan 2001 networks, the following recommendations are made:

1. A 3-hour session length provides a good compromise between reliability and resolution of a geophysical signal using single-frequency GPS data at the cm-level.

2. The cross-correlation coefficient between the resultant height component and the magnitude of the troposphere parameter estimate, can provide a useful indicator of the quality of the baseline estimation procedure.

3. The estimation of the relative residual zenith delay parameter is considered the best strategy for dealing with the troposphere for these studies. The local troposphere estimation procedure should be used for networks comprising four or more GPS stations.

4. Groundplanes on GPS antennas should be used where possible to reduce multipath.

5. Power spectral density analysis of time series data indicates multipath signals that can be subsequently filtered to improve repeatability.

6. The fact that no discernible multipath signal is evident from power spectral density analysis in the time series data from troposphere modelling, is further evidence that troposphere modelling is inappropriate for small scale networks with large differential receiver heights.

7. The Allan variance representation of a time series provides a good temporal measure of the upper limit of the sensitivity of a deformation monitoring system.

8. The carrier tracking loops of the CMC receiver appear to have similar performance to geodetic quality, dual frequency GPS receivers.

9. Global ionospheric models contribute very little to improving the repeatability of baseline resolution in equatorial regions during a solar maximum.

10. Single-frequency data is not suitable for high precision, small scale networks in equatorial regions due to ionospheric effects during a solar maximum. Ionospheric biases must be either eliminated using an ionosphere-free linear combination and dual-frequency data, or corrected using data from an external, fiducial network.

Chapter 7
SUMMARY AND CONCLUSIONS

Ground deformation of a volcano is considered a sure indicator of impending eruptive activity. GPS is ideally suited to monitor this deformation. However, the use of expensive, geodetic quality systems is often not feasible. This thesis has proposed a low-cost, GPS-based deformation monitoring technique to assist volcano hazard mitigation. The system was designed, tested and deployed on Gunung Papandayan in Indonesia. Data processing of a similar system from the SAGE-NZ network, located in mid-latitudes, permitted algorithm testing. The use of the single-frequency approach was found unsuitable for volcano monitoring (at this stage) due to high ionospheric noise during the current solar maximum in equatorial regions.

7.1 Hardware and System Design

This project designed, tested and deployed the first low-cost, continuous GPS-based volcano monitoring system in Indonesia. The innovations and modifications required by this project are summarised below.

Initial testing of several GPS OEM boards found the oscillator of the CMC Allstar 12 to be the most stable available. The clock stability impacts on the quality of the pseudo-range and carrier phase measurements. UNAVCO engineers confirmed the quality of the CMC boards independently, and claimed that the CMC receiver is capable of mm-level carrier phase measurements.

The magnitude of the antenna phase centre variations of a very low-cost vehicle tracking antenna and a single-frequency surveying standard antenna were compared. Rotation tests confirmed that the vehicle tracking antenna was too unstable with respect to APCV and therefore unsuitable for a monitoring application. This was the impetus for the computation of the antenna phase centre variation tables, conducted by the NGS, for the MicroPulse L1 survey antenna. The antennas were not equipped with additional external ground planes.

The GPS antennas were mounted on 1.5m high fibreglass poles. The fibreglass was used to resist corrosion from sulphur gas, and the 1.5m height was considered optimal to reduce multipath effects. The poles were connected to relatively low-cost, stable monuments emplaced at locations designed to detect possible volcanic deformations.

A power budget for the remote slave stations was computed and the appropriate-sized solar panel array was mounted at each station. The solar panels were fixed onto aluminium frames to avoid sulphur gas attack. A continuous power system for the base station was custom-designed to supply uninterrupted power to all components.

An off-the-shelf radio telemetry system was extensively tested in Australia before deployment in Indonesia.

The software sub-system written to control the monitoring system is in two parts; the slave station software and the base station software. The slave station software dealt with binary GPS data logging, file management and radio transmission to the base station. The base station software also logged binary data from the base GPS receiver as well as receiving all remote station binary files, converting data to RINEX format, and archiving the data. Another version of the base station software was capable of automatic baseline processing using the UNSW Baseline software, but this was not implemented due to the extraordinary data noise experienced in Indonesia, which corrupted baseline processing.

At the slave stations, the GPS/PC module, radio and battery bank were housed initially inside a steel drum on a concrete slab, and later within a plastic drum to avoid corrosion. PVC pipe and electrical tape was found to adequately protect components exposed to harsh, corrosive gases. Those components composed of fibreglass or aluminium were relatively unaffected by the sulphur gas. Caustic soda was placed inside the drum to help negate the sulphurous environment.

7.2 Data Processing and Analysis

The data processing and analysis investigated ways to improve the time series repeatability (or accuracy), particularly in the height component. Differential troposphere was identified as a significant error source for small scale, low-cost GPS volcano monitoring systems due to irregular conditions brought about by the large change in height between monitoring stations. The extreme ionospheric noise and lack of continuous data from the Papandayan 2000 campaign required data from the mid-latitude SAGE-NZ network to be used for initial investigations. Subsequent data from the Papandayan 2001 campaign was then compared to the SAGE-NZ results. Effects of the differential troposphere are best mitigated by estimating an extra tropospheric parameter during the least squares procedure. Despite the small scale of the network, dual-frequency data is required to account for the ionosphere and in order to provide a reliable, centimetre-level accuracy monitoring system in equatorial regions, especially during a solar maximum.

7.2.1 Mitigating the Effects of Differential Troposphere

Standard troposphere models, as used in commercial software packages, are not appropriate to achieve centimetre-level accuracy in the height component because anomalies in the local meteorological conditions between stations are not accounted for.

Local meteorological measurements, replacing the standard model values, appear to provide no improvement to the accuracy of the estimated height component. This is because it is very difficult to measure meteorological values accurately due to ground proximity effects. Moreover, the cost of meteorological sensors at each GPS station would be prohibitive.

The global estimate for the temperature lapse rate used in standard troposphere models is sufficiently accurate for centimetre-level applications. A local temperature lapse rate value was computed for the island of Java from three years of radiosonde data, but these new values made only a negligible difference to the results generated using standard

troposphere models. Radiosonde data appears to offer no extra information to enhance the local modelling of the troposphere at Gunung Papandayan.

This thesis has demonstrated that for small-scale networks with large changes in height between stations, processing using the conventional short-baseline modelling approach produces unreliable results. Estimating a residual relative tropospheric delay parameter improves the reliability of the processing (small standard deviation of the time series), and the results cluster around a mean value. This was demonstrated with data from the SAGE-NZ network and Papandayan 2001, under the assumption that the GPS points are stationary.

It was found that changes in the weather affected the height component using the troposphere modelling approach, however the height resolution using parameter estimation is immune to weather changes. It was also recognised that modelling introduced a bias, usually resulting in a slightly higher average height component, compared to the parameter estimation technique.

The Saastamoinen troposphere model and mapping function are considered to be of sufficient accuracy as an a-priori troposphere parameter estimate. Other a-priori models were tested but, in the absence of any other meteorological measurements, the difference between models was negligible.

It is recommended that the estimated parameters be X, Y, Z, N (ambiguity) and one extra residual relative zenith troposphere parameter per session, where the session length should range between 1 - 4 hours depending on the geophysical signal sought. The elevation-dependent weighting and tropospheric gradient techniques offer no improvements in accuracy.

7.2.2 Other Considerations for Data Processing

To ensure correct ambiguity resolution for L1-only data (ie a reduced number of measurements), the session length should be no shorter than 1 hour. Conversely, to ensure the troposphere is regularly estimated, the session length should be no greater

than four hours. A 3-hour session length provides a good compromise between reliability and resolution of a geophysical signal estimated from single-frequency data. The estimated troposphere parameter is designed to absorb anomalous effects not accounted for by the a-priori models. Therefore, the value of the resultant height component should follow the same trend as the value of the troposphere estimate over time. It is proposed that the correlation coefficient between these time series be used as a means of testing the validity of a particular troposphere estimate. The correlation coefficient will therefore indicate the degree to which other error sources have corrupted the intended troposphere estimate.

Automatic baseline processing is not considered feasible for the low-cost Papandayan network at this stage. The high ionospheric activity precludes reliable ambiguity resolution for the single-frequency baselines. Even the high-quality Bernese scientific software could only resolve dubious float solutions on many occasions. Processed time series baseline components contain a disappointing number of outliers.

In comparison to the Papandayan network, data from the SAGE-NZ network is of a high quality, using top-of-the-range GPS receivers, choke ring antennas, stable monuments, and, significantly, it is located in a mid-latitude region experiencing lower ionospheric noise. Automatic processing of the L1-only data using the Bernese software and 3-hour session lengths would be feasible for this network.

7.2.3 Data Analysis

The time series baseline results were analysed using digital signal processing techniques. Power spectral density analysis of the time series data generated using the parameter estimation technique detected a distinct multipath signal. This was not the case for the more erratic time series produced using tropospheric modelling. The fact that no discernible multipath signal is evident from power spectral density analysis of the time series data generated from tropospheric modelling is further evidence that such modelling is inappropriate for small scale networks with large differential heights.

A simple FFT filter eliminated the multipath effects and therefore reduced the variability (and standard deviation) of the time series. Although DSP techniques are

proposed to account for multipath effects, and have proven to be successful, subsequent systems should accommodate ground planes on GPS antennas to reduce multipath at the source. This is a relatively low-cost modification.

The Allan Variance representation of a time series provides a temporal measure of the upper limit of the accuracy of a particular deformation monitoring system. It is a novel way of indicating the systematic error inherent in a monitoring system for increasing measurement periods. Any measure outside this limit should be flagged as a possible geophysical movement. Such a methodology could be a useful addition to any existing deformation monitoring system in order to indicate its quality.

Investigations into the quality of the carrier phase tracking loops of the CMC GPS receiver revealed no appreciable difference when compared with geodetic standard, dual-frequency GPS receivers. The dual-frequency data collected during the course of these investigations were subsequently processed using an ionosphere-free linear combination. The limited time series of 3-hour sessions (ie less than 24-hours of data) showed a very low variability, indicating that the ionospheric effects were indeed the major accuracy limiting factor for the Papandayan single-frequency network. It should also be noted that global ionospheric models, provided by the IGS, contributed very little to improving the quality of the baseline solutions using single-frequency data.

Data from the SAGE-NZ network was initially compared with data from the Papandayan 2000 campaign, for the same period. The data quality of the SAGE-NZ was far superior to that of the Papandayan 2000 campaign. This confirmed the hypothesis that by retreating to a mid-latitude location, the extreme effects of the ionosphere could be significantly reduced. Subsequent comparisons were undertaken between the same SAGE-NZ data series and the Papandayan 2001 campaign data, when the sunspot activity was lower (see Figure 6.25). Nevertheless, the Papandayan 2001 data were still noisier due to its equatorial proximity.

It is concluded therefore that single-frequency data, alone were not suitable for high precision, small scale networks (ie less than 10km) in equatorial regions. Ionospheric biases must be either eliminated using an ionosphere-free linear combination (ie dual frequency data) or corrected using information derived from an external, fiducial

network of dual-frequency receivers. Even for baselines as short as 2km in length, ionospheric scintillations could still adversely affect baseline determinations, particularly during a solar maximum (see section 3.2.4.1).

7.3 Suggestions and Recommendations for Further Research

The Papandayan 2000 and 2001 campaigns deployed a fiducial network of dual-frequency, geodetic standard GPS receivers in a triangular network surrounding the internal single-frequency network. The purpose of this network was to map the ionospheric and tropospheric biases in the region and to generate corrections for these biases to the inner network. This work follows the algorithms proposed by Han & Rizos (1996a) and implemented in Chen et al (1999).

The ionospheric corrections for this equatorial network were generated in the post-processed mode and applied to the Papandayan single-frequency network. Improvements in the satellite orbit bias, tropospheric delay, multipath and observation noise can also be gained using this approach (Han, 1997). It is therefore anticipated that the baseline accuracy will be improved. Chen et al (1999) has demonstrated this at three mid-latitude networks, but has not been demonstrated at an equatorial location, particularly during a solar maximum.

Data from the Papandayan 2001 network will be processed to test the correction algorithm under these more extreme ionospheric conditions. If shown to be reliable, automatic baseline processing of the single-frequency network, with the addition of network generated corrections could be implemented. The resultant baseline data must be presented such that a non-geodesist can understand and use this information for assessment of the hazards presented by a volcano.

The external fiducial network is an expensive addition. However, due to the close proximity of active volcanoes in Indonesia, a sparse fiducial network could be established to encompass more than one active volcano, and therefore provide corrections for several single-frequency volcano networks. For example, one fiducial network could cover the Papandayan, Guntur and Galunggung volcanoes in West Java.

As the current solar maximum abates, and the ionospheric noise decreases, the session length could be reduced without affecting the quality of the time series. This needs to be verified using more data.

The GPS/PC modules used for this low-cost system are restricted due to the DOS operating system. DOS is not designed for real-time applications and the software must be carefully written to avoid problems with memory allocation. Much time was lost during this work for this reason. Subsequent versions of the GPS stations will use micro-controllers integrated with GPS OEM boards. This is expected to be a more reliable, robust solution.

The radio telemetry system is also quite elementary, and the number of slave stations in a network is restricted by the radio polling methodology used. The radios can also be set to an asynchronous mode, and unique addresses of each radio can be used. In such a mode, data can be sent continuously, from all remote slave stations and received data is sorted by the base. This allows a larger number of slave stations in any one network, and the possibility of switching to an RTK mode if some deformation activity is detected.

REFERENCES

Abidin, H.Z., & Tjetjep, W.S. (1996) GPS-based volcano deformation monitoring in Indonesia. ***GIS Asia Pacific***, 2(5), 30-33.

Abidin, H.Z., Meilano, I., Suganda, O.K., Kusuma, M.A., Muhardi, D., Yolanda, O., Setyadji, B., Sukhyar, R., Kahar, J., & Tanaka, T. (1998a) Monitoring the deformation of Guntur Volcano using repeated GPS survey method. *FIG '98, XXI Int. Conf.*, Brighton, UK, 19-25 July.

Abidin, H.Z. (1998b) Some aspects of volcano deformation monitoring using repeated GPS surveys, *Int. Conf. of Spatial Information Science & Technology, Wuhan, China,* 13 – 16 Dec., 92 –109.

Abidin, H.Z., Darmawan, D., Suganda, O.K., Kusuma, M.A., Meilano, I., Anthony, F., Gamal, M., & Wirakusumah, A.D. (2000) Studying the deformation of Papandayan volcano, Indonesia, using repeated GPS survey method. *IAVCEI General Assembly*, Bali, Indonesia, 18 – 22, July.

Allan, D.W., Gray, J.E., Machlan, H.E. (1974) The National Bureau of Standards Atomic Time Scale: Generation, stability, accuracy and accessibility, ***NBS Monograph 140, Time and Frequency: Theory and Fundamentals***, 205 – 231.

Baarda, W. (1968) A testing procedure for use in Geodetic Networks, *Net. Geod. Comm.* Vol 2, No. 5.

Baby, H.B., Golé, P., & Lavergnat, J. (1988) A model for the tropospheric excess path length of radio waves from surface meteorological measurements. ***Radio Science, 23,*** 1023 – 1038.

Bateman, A., & Yates, W. (1989) ***Digital signal processing design***, Computer science press, New York, USA, 385pp.

Bean, B.R., Cahoon, B.A., Samson, C.A., & Thayer, G.D. (1966) A world atlas of atmospheric radio refractivity. *ESSA Monograph 1.*

Berntsen (2001) www.berntsen.com

Beutler, G., Bauerisma, I., Gurtner, W., Rothacher, Schildknecht, T., & Geiger, A. (1988) Atmospheric refraction and other important biases in GPS carrier phase observations. In Atmospheric Effects on Geodetic Space Measurements, Monograph 12, School of Surveying, University of New South Wales, Kensington, NSW, Australia, 15 – 43.

Beutler, G., Gurtner, W., Rothacher, M., Wild, U., & Frei, E. (1990) Relative static positioning with the Global Positioning System: Basic technical considerations. In Global Positioning System: An Overview, the proceedings of International Association of Geodesy Symposium No. 102, Edinburgh, Scotland, 7 – 8 August, 1991, Springer-Verlag, New York, 1 – 23.

Beutler, G., Geiger, A., Rothacher, M., Schaer, S., Schneider, D., & Wiget, A. (1995) Dreidimensionales testnetz Turtmann 1985-1993, Teil II (GPS-Netz), Geodätisch-geophysikalische Arbeiten in der Schweiz, Band 51.

Bifrost Project (1996) GPS measurements to constrain geodynamic processes in Fennoscandia. ***EOS: Trans. AGU,*** *77(35).*

Bilitza, D. (ed.) (1990) *International Reference Ionosphere 1990*, NSSDC 90-22, Greenbelt, Maryland.

Bissell, A.F. (1984) ***An Introduction to Cusum Charts,*** The Institute of Statisticians, Bury St. Edmunds, Suffolk.

Blewitt, G., Heflin, M.B., Webb, F.H., Lindqwister, U.J., & Malla, R.P. (1992) Global coordinates with centimetre accuracy in the International Terrestrial Reference Frame using GPS, ***Geophys. Res. Let., 19,*** 853 – 856.

Blong, R.J. (1984) ***Volcanic Hazards: A sourcebook on the effects of eruptions.*** Academic Press, Australia.

Blong, R.J. (1999) Volcanic hazards and risk management. In: Encyclopedia of Volcanoes, Ed. Harald Sigurdsson, Academic Press, 1999, 1215 – 1227.

Bock, Y., Wdowinski, S., Fang, P., Zhang, J., Williams, S., Johnson, H., Behr, J., Genrich, J., Dean, J., van Domselaar, M., Agnew, D., Wyatt, F., Stark, K., Oral, B., Hudnut, K., King, R., Herring, T., Dinardo, S., Young, W., Jackson, D., & Gurtner, W. (1997) Southern California permanent GPS geodetic array: Continuous measurements of regional crustal deformation between the 1992 Landers and 1994 Northridge earthquakes. ***J. Geophys Res,*** 102, B8, 18013 - 18033.

Boudouris, G. (1963) On the basic index of refraction of air, the absorption and dispersion of centimetre waves by gases. ***J. of Res. of the Nat. Bureau of Standards – D. Radio Propagation***, 67D(6), 631 – 661+.

Braun, J., Stephens, B., Ruud, O., & Meertens, C. (1997) The effect of antenna covers on GPS baseline solutions, www.unavco.ucar.edu/dev_test/publications/dome_report/domeX5Freport-1.html

British Atmospheric Data Centre (1999) Robert Wood, personal communication.

Brunner, F.K. & McCluskey, S. (1991) Tropospheric zenith delay parameters: How many should be estimated in GPS processing? ***Aust. J. Geod. Photogram. Surv.,*** *55,* 67-75.

Brunner, F.K. & Welsch, W.M. (1993) Effect of the troposphere on GPS measurements. ***GPS World,*** 4(1), 42-51.

Brunner, F.K. & Tregoning, P. (1994a) Investigation of height repeatability from GPS measurements. ***Aust. J. Geod. Photogram. Surv.,*** *60,* 33-48.

Brunner, F.K. & Tregoning, P. (1994b) Tropospheric propagation effects in GPS height results using meteorological observations ***Aust. J. Geod. Photogram. Surv.,*** *60*, 49-65.

Campbell, J.H., Cloppenburg, F.-J., & Lohmar (1984) Estimating the ionospheric refraction effect on interferometric GPS-measurements. ***Proc. Int. Symp. Space Techniques for Geodynamics, Vol. 2***, Sopron, Hungary, 196 - 206.

Chen, H-Y., Rizos, C., & Han, S. (1999) Rapid static, medium-range GPS positioning techniques for geodynamic applications, *4th Aust. Symp. on Sat. Nav. Tech., Brisbane, Australia, 20-23 July.*

Chen, H.Y., Rizos, C., & Han, S. (2001) From simulation to implementation: Low-cost densification of permanent GPS networks in support of geodetic applications. ***Journal of Geodesy,*** *75(9/10), 515-526.*

Clark, T.A., & Schupler, B.R. (1996) What are phase-center variations and why should I worry? *IGS meeting*, Silver Springs, MD, USA, 19-21 March.

Collins, J. P., & Langley, R. B. (1997) Estimating the residual tropospheric delay for airborne differential GPS positioning. *10th Int. Tech. Meeting of the Satellite Division of the US Inst. of Navigation*, Kansas City, Missouri, 16-19 Sept., 1197 – 1206.

Condor (2000) Condor 3-D real-time monitoring software. http://www.3d-gps.com

Cross, P.A. (1983) Advanced least squares applied to position fixing. *Working Papers, North East London Polytechnic*. Dept. of Land Surveying, pp 205.

Cross. P.A. (1999) Trends in estimation techniques: Modern least squares for surveyors, *Directions in GPS Lecture Series, 8-9 April, 1999*, University of New South Wales, Sydney, Australia.

Davis, J.L., Herring, T.A., Shapiro, I.I., Rogers, A.E., & Elgered, G. (1985) Geodesy by radio interferometry: Effects of atmospheric modelling errors on estimates of baseline length. ***Radio Science***, *20*, 1593 - 1607.

Davis, J.L. (1986) Atmospheric propagation effects on radio interferometry. AFGL Technical Report 86-0243, US Air Force Geophysical Laboratory, Hanscomb AFB, Mass.

Decker, R. W., & Decker, B. (1997) ***Volcanoes, third edition.*** W. H. Freeman and Co., USA.

Dutton, E.J., & Bean, B.R. (1965) The bi-exponential nature of tropospheric gaseous absorption of radio waves, ***Radio Sci. J. Res.***, NBS 69D, No. 6, 885-892.

Dvorak, J., & Dzurisin, D. (1997) Volcano Geodesy: The search for magma reservoirs and the formation of eruptive events. ***Rev. Geophys.***, 35(3), 343 - 384.

Dzurisin, D. (1996) USGS website,
http://vulcan.wr.usgs.gov/Projects/Deformation/Alaska/Augustine

Environmental Science Services Administration, National Aeronautics and Space Administration, and the United States Air Force (1966) U.S. standard atmosphere supplements, 1966. US Government Printing Office, Washington, DC, 290 pp.

Essen, L., & Froome, K.D. (1951) The refractive indices and dielectric constants of air and its principal constituents at 24000 Mc/s, ***Proc. of Physical Society***, *64(B)*, 862 – 875.

Ewert, J.W. & Swanson, D.A. (eds) (1992) *United States Geological Survey Bulletin 1966*, Monitoring volcanoes: Techniques and strategies used by staff of the Cascades volcano observatory 1980-90. Washington DC: United States Government Printing Office.

Fiske, R. S., (1984) Vulcanologists, journalists and the concerned local public: A tale of two crises in the eastern Caribbean. In *Explosive volcanism: inception, evolution and hazards*, Geophysics Study Committee (National Research Council), 170 – 176. Washington DC: National Academy Press.

Fu, W. X., & Rizos, C. (1997) The applications of wavelets to GPS signal processing, *10th Int. Tech. Meeting of the Satellite Division of the US Inst. of Navigation*, Kansas City, Missouri, 16-19 September, 1385-1388.

Ge, L., Chen, H.Y., Han, S., & Rizos, C. (2000) Adaptive filtering of continuous GPS results. ***Journal of Geodesy***, 4(7/8), 572-580.

GSI (2001), Geographical Survey Institute website, Japan, http://www.gsi.go.jp/ENGLISH/ABOUT/about.html

Gurtner, W., Beutler, G., Botton, S., Rothacher, M., Geiger, A., Kahle, H.-G., Schneider, D., & Wiget, A. (1989) The use of the Global Positioning System in mountainous areas. ***Manuscripta Geodetica,*** *14*, 53 - 60.

Gurtner, W., & Mader, G. (1990) Receiver independent exchange format version 2. *GPS Bulletin*, 3(3), 1-8.

Han, S., & Rizos, C. (1996a) GPS network design and error mitigation for real-time continuous array monitoring systems. *9th Int. Tech. Meeting of the Satellite Division of the US Inst. of Navigation*, Kansas City, Missouri, 17 - 20 Sept., 1827 – 1836.

Han, S., & Rizos, C. (1996b) Comparison of GPS ambiguity resolution techniques. *Int. Symp. Geo-Informatics'96*, Wuhan, 16 - 19 Oct., 136 - 146. CHAPT2

Han, S., & Rizos, C. (1997) Multipath effects on GPS in mine environments, Xth International Congress on the International Society for Mine Surveying, Fremantle, Australia, 2-6 Nov., 447-457.

Harvey, B. R. (1994) ***Practical Least Squares for Surveyors***, The School of Surveying, University of New South Wales, Sydney, Australia.

Hedling, G., & Jonsson, B. (1996) New developments in the SWEPOS network, *National Land Survey of Sweden*, Gävle, Sweden.

Heflin, M., Bertiger, W., Blewitt, G., Freedman, A., Hurst, K., Lichten, S., Lindqwister, U., Vigue, Y., Webb, F., Yunck, T., & Zumberge, J. (1992) Global geodesy using GPS without fiducials, ***Geophys. Res. Let., 19***, 131 – 134.

Hellwig, H. (1977) Frequency standards and clocks: A tutorial introduction, ***NBS Technical Note 616 (2d Rev),*** US Dept of Commerce, National Bureau of Standards.

Hendy, M.R. (1990) Models for the tropospheric zenith delay of microwaves. *Masters Thesis, University of New South Wales, Sydney, Australia.*

Hoblitt, R.P., Miller, C.D., & Vallance, J.W. (1981) Origin and stratigraphy of the deposit produced by the May 18 directed blast, *in Lipman P.W. and Mullineaux, D.R.(eds.) The 1980 eruptions of Mount St. Helens, Washington,* US Geological Survey Professional Paper, 1250, 401-419.

Hofmann-Wellenhof, B., Lichtenegger, H., & Collins, J. (1994) ***GPS Theory and Practice.*** Third revision, Springer-Verlag, Wien New York, 355pp.

Hopfield, H.S. (1969) Two-quartic tropospheric refractivity profile for correcting satellite data. ***J. Geophys Res***, *74*, 4487 - 4499.

Hudnut, K. (1996) The fixed-mount rock pin: Site selection, design and installation. http://www-socal.wr.usgs.gov/hudnut/hudnut/rock_pin.html

IGS (2001) International GPS Service website,
http://igscb.jpl.nasa.gov

International Union of Geodesy and Geophysics (1963) Resolution from General Assembly XIII – Berkeley, California. ***Bulletin Géodésique***, *70*, 390pp.

International Association of Geodesy (1993) Working paper on refractive index of air for radio waves – issues and questions. *Ad Hoc Working Group on Refractive Indices of Light, Infrarred and Radio Waves in the Atmosphere*. IAG SC3 – Fundamental constants.

Ionospheric Prediction Service (2001) http://www.ips.gov.au/asfc/current/sunspot

Jaldehag, R. T. K., Johansson, J. M., Rönnäng, B.O., Elósegui, P., Davis, J.L., Shapiro, I.I., & Niell, A.E. (1996) Geodesy using the Swedish permanent GPS network: Effects of signal scattering on estimates of relative site positions. ***J. Geophys Res***, 101, B8, 17,841 – 17860.

Janes, H.W., Langley, R.B., & Newby, S.P. (1991) Analysis of tropospheric delay prediction models: Comparisons with ray-tracing and implications for GPS relative positioning. ***Bulletin Géodésique***, *65*, 151 - 161.

Janssen, V., Roberts, C., Rizos, C., & Abidin, H. (2001) Experiences with a mixed-mode GPS-based volcano monitoring system at Mt. Papandayan, Indonesia, ***Geomatics Research Australasia***, *74,* June, 43-58.

Johnson, H., & Wyatt, F. (1994) Geodetic network design for fault mechanics studies. ***Manuscripta Geodetica,*** *19*, 309 - 323.

Johnson, J., Braun, J., Rocken, C. & Vanhove, T. (1995) The role of multipath in antenna height tests at Table Mountain, UNAVCO website, July 1995, http://www.unavco.ucar.edu/science_tech/technology/publications/tblmtn/tblmtn2.html

Juran, J. M., & Blanton-Godfrey, A. (1999) ***Juran's Quality Control Handbook***, 5th Edition, McGraw-Hill, New York.

Kahmen, H., & Faig, W. (1988) ***Surveying.*** De Gruyter, Berlin, New York, 578pp.

Kälber, S., Jäger, R., & Schwäble, R. (2000) A GPS-based online control and alarm system, ***GPS Solutions***, *3(3), 19 – 25.*

Kato, T., El-Fiky, G.S., Oware, E.N., & Miyazaki, S. (1998) Crustal strain in Japanese islands as deduced from dense GPS array, ***Geophys. Res. Let., 25***, 3445- 3448.

Kelley, M.C., Kotsikopoulos, D., Beach, T., Hysell, D., & Musman, S. (1996) Simultaneous GPS and Radar observations of equatorial spread F at Kwajalein, ***J. Geophys Res***, *101*, 2333 - 2342.

Kimberly, P., Siebert, L., Luhr, J.F., & Simkin, T. (1998) Volcanoes of Indonesia, V.1.0 (CD-ROM). *Smithsonian Institution, Global Volcanism Program*, Digital Information Series, GVP-1.

Klobuchar, J.A. (1987) Ionospheric time-delay algorithm for single-frequency GPS uses. *IEEE Transactions on Aerospace and Electronic Systems*, Vol. AES-23, No.2.

Klobuchar, J.A. (1991) Ionospheric effects on GPS. ***GPS World***, 2(4), 48-51.

Knight, M., & Finn, A. (1996) The impact of ionospheric scintillations on GPS performance. *9th Int. Tech. Meeting of the Satellite Division of the US Inst. of Navigation*, Kansas City, Missouri, 17 - 20 Sept., 555 - 564.

Kondo, H., & Cannon, M. E. (1995) Real-time landslide detection system using precise carrier phase GPS. *8th Int. Tech. Meeting of the Satellite Division of the US Inst. of Navigation*, Palm Springs, California, 12 -15 Sept., 1877 - 1884.

Langbein, J., Wyatt, F., Johnson, H., Hamann, D., & Zimmer, P. (1995) Improved stability of a deeply anchored geodetic monument for deformation monitoring. ***Geophys. Res. Let., 22,*** 3533 - 3536.

Langley, R.B. (1998) A primer on GPS antennas. ***GPS World,*** 9(7), 50-54.

Langley, R.B. (2000) GPS, the ionosphere, and the solar maximum. ***GPS World***, 11(7), 44-49.

Laurila, S.H. (1976) ***Electronic Surveying and Navigation***. John Wiley & sons, Inc. USA, 545pp.

Leick, A. (1995) ***GPS Satellite Surveying.*** Second Edition, John Wiley & Sons, Inc.,560pp.

Liebe, H.J., & Hopponen, J.D. (1977) Variability of EHF air refractivity with respect to temperature, pressure and frequency. *IEEE Trans. on Antennas and Propagation*, AP-25(3), 336-345.

List, R.J. (1958) Smithsonian meteorological tables, 204. *Smithsonian Institute*, Washington, D.C.

Lowry, A., & MacLeod, R. (1997) Pmos – a real-time precise DGPS continuous deformation monitoring system. *10th Int. Tech. Meeting of the Satellite Division of the US Inst. of Navigation*, Kansas City, Missouri, 16-19 Sept., 923 – 927.

MacMillan, D.S. (1995) Atmospheric gradients from very long baseline interferometry observations. ***Geophys. Res. Let., 22,*** 1041 - 1045.

Mader, G.L., & MacKay, R.J. (1996) Calibration of GPS antennas. *IGS meeting, Silver Springs, MD, USA*, 19 – 21 March, 81 - 105.

Marini, J.W., & Murray, C.W. (1973) Correction of laser range tracking data for atmospheric refractions at elevations above 10 degrees. *NASA-TM-X-70555*, Goddard Space Flight Center, Greenbelt, MD, USA.

McCarthy, D.D. (1989) (ed.) IERS Standards (1989). *IERS Technical Note 3,* Paris.

McGuire, W.J., Kilburn, C.R.J., & Murray, J. (1995) ***Monitoring Active Volcanoes.*** London, UK. UCL Press.

Meertens, C., Alber, C., Braun, J., Rocken, C., Stephens, B., Ware, R., Exner, M., & Kolesnikoff, P. (1996) Field and anechoic chamber tests of GPS antennas. *IGS meeting*, Silver Springs, MD, USA, 19 – 21 March 19-21, 107 - 118.

Meertens, C. (1997) Development of an L1-phase GPS volcano monitoring system, http://www.unavco.ucar.edu/dev_test/l1/status_l1_11_97.pdf

Meertens, C. (1998) Development of an L1-phase GPS volcano monitoring system, http://www.unavco.ucar.edu/dev_test/l1/status_l1_8_98.pdf

Mendes, V.B. (1999) Modelling the neutral-atmosphere propagation delay in radiometric space techniques. *PhD dissertation, Dept. of Geodesy and Geomatics Engineering Technical Report No. 199*, University of New Brunswick, Fredericton, New Brunswick, Canada, 353 pp.

Mertikas, S.P., & Rizos, C. (1997) On-line detection of abrupt changes in the carrier-phase measurements of GPS, ***Journal of Geodesy***, 71, 469-482.

Mogi, K. (1958) Relations between the eruptions of various volcanoes and the deformation of the ground surface around them. ***Bull. Earth Res. Inst. Univ. Tokyo***, 36, 99 - 134.

Murray, J.B., Rymer, H., & Locke. C. (1999) Ground deformation, gravity and magnetics. In: *Encyclopedia of Volcanoes*, Ed. Harald Sigurdsson, Academic Press, 1121 – 1140.

NASA (2001) http://liftoff/msfc.nasa.gov/academy/space/atmosphere.html

National Oceanic and Atmospheric Administration, National Aeronautics and Space Administration, and United States Air Force (1976) U.S. Standard Atmosphere, 1976. U.S. Government Printing Office, Washington, D.C., NOAA-S/T 76-1562, 227pp.

Newhall, C.G., & Self, S. (1982) The volcanic explosivity index (VEI): An estimate of explosive magnitude for historical volcanism. ***J. Geophys Res***, 87, 1231-1238.

Niell, A.E. (1996) Global mapping functions for the atmosphere delay at radio wavelengths. ***J. Geophys Res***, *101,* 3,227 - 3,246.

NGS Website (1998) http://www.ngs.noaa.gov/ANTCAL/Models

NGS (2001) http://www.ngs.noaa.gov/ANTCAL/Models

Ogaja, C. (2001) On-line GPS integrity monitoring and deformation analysis for structural monitoring applications, *Proceedings of the 14th International Technical Meeting of the Satellite Division of the Institute of Navigation, ION GPS-2001*, Salt Lake City, Utah, 11-14 September.

Omori, F. (1914) The Sakur-jima eruptions and earthquakes. *Bulletin of the Imperial Earthquake Investigation Committee* 8, Nos 1-6, 525.

Owen, S. (2000) http://pangea.stanford.edu/~owen/kilauea.html

Parkinson, B. W., & Spilker, J.J. (eds) (1996) ***Global Positioning System: Theory and Applications Vol. 1 & 2***, Vol. 163 progress in Astronautics and Aeronautics, USA, 793pp & 643pp.

Peng, S.Y. (1996) Review paper on designs of GPS antennas. *Int. Conf. on GPS*, Taipei, Taiwan, 12- 16 June.

Proakis, J.G., & Manolakis, D.G. (1996) ***Digital Signal Processing: Principles, Algorithms and Applications.*** Upper Saddle River, N.J: Prentice Hall.

Reitan, C.H. (1963) Surface dew point and water vapour aloft, ***J. Appl. Meteorol.*** *2(6),* 776-779.

Remondi, B. W., & Hofmann-Wellenhof, B. (1989) Accuracy of Global Positioning System broadcast orbits for relative surveys. *National Information Center*, Rockville, Maryland, *NOAA Technical Report NOS 132, NGS 45*.

Rizos, C., Galas, R., & Reigber, C. (1996) Design challenges in the development of a GPS-based volcano monitoring system. *8th International Symposium on Deformation Measurements*, Hong Kong. 25 - 28 June, 7 –15.

Rizos, C. (1997a) ***Principles and Practice of GPS Surveying,*** Monograph 17, School of Geomatic Engineering, The University of New South Wales, Sydney, Australia, 560pp.

Rizos, C., Han, S., Roberts, C., Galas, R., & Reigber, C. (1997b) Low-cost densification of permanent GPS networks for natural hazard mitigation. *GEODYSSEA Concluding Symposium*, 14 - 18 April, Penang, Malaysia.

Rizos, C., Han, S., & Roberts, C. (1997c) Permanent automatic low-cost GPS deformation monitoring systems: Error mitigation strategies and system architecture. *10th Int. Tech. Meeting of the Satellite Division of the US Inst. of Navigation*, Kansas City, Missouri, 16-19 Sept., 909 - 917.

Rizos, C., Han, S., Ge, L., Chen, H., Hatanaka, Y., & Abe, K. (2000) Low-cost densification of permanent GPS networks for natural hazard mitigation: first tests on GSI's GEONET network, *Earth, Planets and Space (EPS)*, Earth, Planets & Space, 52(10), 867-871.

Rizos, C., Han, S., Roberts, C., Han, X., Abidin, H.Z., Suganda, O.K., & Wirakusumah, A.D. (2000) Continuously operating GPS-based volcano deformation monitoring in Indonesia: Challenges and preliminary results In "Geodesy beyond 2000: The challenges of the first decade", Springer-Verlag, ISBN 3-540-67002-5, 361-366, *Proc. IAG General Assembly*, Birmingham, UK, 19-30 July, 1999.

Rizos, C. (2001) http://129.94.250.49/snap/gps/gps-survey/chap1

Roberts, C., Chen, H.Y., Han, S., & Rizos, C. (1998) Antenna phase centre variation: Cause for concern for precise GPS deformation monitoring applications, *Western Pacific Geophysics Meeting*, Taipei, Taiwan, 21 – 24 July.

Rocken, C. (1992) GPS antenna mixing problems. *UNAVCO Memo*, Nov. 12.

Rocken, C., Meertens, C., Braun, J., Exner, M., & Stephens, B. (1995) UNAVCO ARI antenna tests, http://www.unavco.ucar.edu/publications

Rocken, C., Sagiya, T., & Tsuji, H. (1997) Large permanent GPS networks in Japan. http://www.unavco.ucar.edu/community/activities/science_snap/rockenjapan-1.html

Rocken, C., Sagiya, T., & Tsuji, H. (1999) Large permanent GPS networks in Japan, ***UNAVCO website***, http://www.unavco.ucar.edu/community/activities/science_snap

Rocken, C., Johnson, J., Braun, J., Kawawa, H., Hatanaka, Y., & Imakiire, T. (2000) Improving GPS surveying with modelled ionospheric corrections, ***Geophys. Res. Let., 27***, 3821 - 3824.

Rothacher, M, Beutler, G., Gurtner, W., Geiger, A., Kahle, H.-G., & Schneider, D. (1986) The 1985 Swiss GPS-campaign, *Proc. 4th Int. Sat. Positioning Symp.*, Austin, TX, USA, 28 April – 2 May, 979-991.

Rothacher, M., Schaer, S., Mervart, L., & Beutler, G. (1995) Determination of antenna phase centre variations using GPS data. *IGS Workshop*, Potsdam, Germany, 15 – 17 May.

Rothacher, M., & Mervart, L. (eds) (1996a) ***Bernese GPS software Version 4.0***, Astronomical Institute of Berne, Switzerland.

Rothacher, M., Gurtner, W., Schaer, S., Weber, R., Schlueter, W., & Hase, H.O. (1996b) Azimuth- and elevation-dependent phase centre corrections for geodetic GPS antennas estimated from GPS calibration campaigns, *in IAG Symposium No. 115, edited by W.Torge*, Springer-Verlag, 335 – 339.

Rothacher, M., Springer, T.A., Schaer, S., & Beutler, G. (1998) Processing strategies for regional GPS networks. In: *Advances in Positioning and Reference Frames*, vol. 118, F.K. Brunner (ed.), 93-100.

Rothacher, M., & Beutler, G. (1998) The role of GPS in the study of global change. ***Phys. Chem. Earth***, *23(9-10),* 1029 – 1040.

Rothacher, M., & Mervart, L. (2000) ***The Bernese GPS software Version 4.2 Draft Manual.*** Chapter 12 - Troposphere modelling and estimation.

Rüeger, J.M. (1996) ***Electronic Distance Measurement: An Introduction.*** Springer Verlag. 4th Edition, Berlin, 276pp.

Rührnößl, H., Brunner, F.K., & Rothacher, M. (1998) Modellierung der troposphärischen korrektur für deformationsmessungen mit GPS im alpinen raum. *Allg. Verm. Nach., 1/98*, 14 – 20.

Saastamoinen, J. (1973) Contributions to the theory of atmospheric refraction. ***Bulletin Géodésique***, *107*, 13 - 34.

Sagiya, T., Yoshimura, A., Iwata, E., Abe, K., Kimura, I., Uemura, K., & Tada, T. (1997) Establishment of permanent GPS observation network and crustal deformation monitoring in the Southern Kanto and Tokai Areas. ***GSI Website***, http://www.gsi-mc.go.jp/ENGLISH/RESEARCH/BULLETIN/vol-41/gps.html

Santerre, R. (1991) Impact of GPS satellite sky distribution. ***Manuscripta Geodetica,*** *16*, 28 - 53.

Satirapod, C., Ogaja, C., Wang, J.L., & Rizos, C. (2001) GPS analysis with the aid of wavelets, *5th Australasian Symp. on Satellite Navigation Technology & Applications*, Canberra, Australia, 24-27 July, paper 35.

Schaer, S., Beutler, G., Rothacher, M., & Springer, T.A. (1996) Daily global ionosphere maps based on GPS carrier phase data routinely produced by the CODE analysis centre, *presented at the IGS Analysis Centre Workshop, NOAA, Silver Spring, MD, USA*, 19 – 21 March.

Schaer, S., Beutler, G., Rothacher, M., Brockmann, E., Wiget, A., & Wild, U. (1999) The impact of the atmosphere and other systematic errors on permanent GPS networks, *IAG Symposium on Positioning*, Birmingham, UK, 21 July 21.

Scheaffer, R.L., & McClave, J.T. (1990) ***Probability and Statistics for Engineers,*** Third Edition, PWS-Kent Publishing Company, Boston, USA.

Schupler, B.R., Allhouse, R.L., & Clark, T.A. (1994) Signal characteristics of GPS user antennas. ***Navigation,*** *41(3), 277 – 296.*

Seeber, G. (1993) ***Satellite Geodesy: Foundations, Methods and Applications.*** Walter de Gruyter, Berlin New York, 531 pp.

Shepherd, J.B., Aspinall, W.P., Rowley, K.C., Pereira, J., Sigurdsson, H., Fiske, R.S., & Tomblin, J.F. (1979) The eruption of Soufrière volcano, St. Vincent, April – June, ***Nature***, 282, 24 – 28.

Shimada, S., Fujinawa, Y., Sekiguchi, S., Ohmi, S., Eguchi, T., & Okada, Y. (1990) Detection of a volcanic fracture opening in Japan using Global Positioning System measurements. ***Nature***, 343, 631 - 633.

Sigurdsson, H. (1999) The history of volcanology. In: ***Encyclopedia of Volcanoes***, Ed. Harald Sigurdsson, Academic Press, 15 – 37.

Simkin, T., Siebert, L., McClelland, L., Bridge, D., Newhall, C., & Latter, J. H. (1994) ***Volcanoes of the World.*** Second edition, Smithsonian Institution.

Simkin, T., & Siebert, L. (1999) Earth's volcanoes and eruptions: An overview. In: ***Encyclopedia of Volcanoes***, Ed. Harald Sigurdsson, Academic Press, 249 – 261.

Smith, E.K., Jr., & Weintraub, S. (1953) The constants in the equation for atmospheric refractive index at radio frequencies, *Proc. of IRE, 41*, 1035 – 1037.

Solheim, F. (1993) Use of pointed water vapour radiometers to improve GPS surveying accuracy, *PhD Thesis*, Univ. Colorado, Dec.

Solheim, F., Alber, C., Exner, M., Rocken, C., Meertens, C., & Johnson, J. (1996) An improved GPS geodetic antenna, www.unavco.ucar.edu/dev_test/publications

Suganda, O.K. (1993) Analysis of EDM data in association with the 1992 eruption at Merapi Volcano, Indonesia. *Masters Thesis,* Department of Geophysics, Kyoto University, Japan.

Swanson, D., Casadevall, T.J., Dzurisin, D., Malone, S.D., Newhall, C.G., & Weaver, C.S. (1983) Predicting eruptions at Mount St. Helens, June 1980 through December 1982. ***Science,*** *221*, 1369 – 76.

Swanson, D., Casadevall, T.J., Dzurisin, D., Holcomb, C. G., Newhall, C.G., Malone, S.D., & Weaver, C.S. (1985) Forecasts and predictions of eruptive activity at Mount St. Helens, USA: 1975 – 1984. ***Journal of Geodynamics,*** *3*, 397 – 423.

SWEPOS (2001) http://swepos.lmv.lm.se/index_swep.htm

Thayer, G.D. (1974) An improved equation for the radio refractive index of air. ***Radio Science***, *9(10)*, 803 – 807.

The Mathworks (1998) *Signal Processing Toolbox.*

The Mathworks (2000) *Wavelet Toolbox.*

Tralli, D., & Lichten, S. (1990) Stochastic estimation of tropospheric path delays in Global Positioning System geodetic measurements. ***Bulletin Géodésique***, 64, 127 - 159.

Tsuji, H., Hatanaka, Y., Sagiya, T., & Hashimoto, M. (1995) Coseismic crustal deformation from the 1994 Hokkaido-Toho-Oki earthquake monitored by a nationwide continuous GPS array in Japan. ***Geophys. Res. Let.,*** ***22,*** 1,669 - 1,672.

Tsujii, T., Wang, J., Rizos, C., Harigae, M., & Inagaki, T. (2000) Estimation of residual tropospheric delay for high-altitude vehicles: Towards precise positioning of a stratosphere airship. *13th Int. Tech. Meeting of the Satellite Division of the US Inst. of Navigation*, Salt Lake City, Utah, 19-22 September, 696-704.

UNAM (2000) (Universidad Nacional Autonoma de Mexico) http://charro.igeofcu.unam.mx

UNAM (2001a) (Universidad Nacional Autonoma de Mexico) http://charro.igeofcu.unam.mx/L1/PP03.html

UNAM (2001b) http://charro.igeofcu.unam.mx/photo_catalogs/catalog_GFZ_Popo

UNAVCO (1999) http://www.unavco.ucar.edu

UNAVCO (2000) Data archive, www.ucar.unavco.edu.au

UNAVCO (2001) http://www.unavco.ucar.edu/project_support/active_projects/popo/long1-1.gif

USGS (2000) United States Geological Survey website, http://vulcan.wr.usgs.gov/Projects/Deformation/Alaska/Augustine

USGS (2001a) http://volcanoes.usgs.gov/Hazards/What/hazards.html

USGS (2001b) http://quake.wr.usgs.gov/research/deformation/twocolor/lv_continuous_gps.html

Voight, B. (1990) The 1985 Nevado del Ruiz volcano catastrophe – anatomy and retrospection. ***Journal of Volcanology and Geothermal Research,*** *42*, 151 – 88.

Wanninger, L. (1995) Enhancing differential GPS using regional ionospheric error models. ***Bulletin Géodésique***, *69*, 283 - 291.

Wells, D. E., Beck, N., Delikaraoglou, D., Kleusberg, A., Krakiwsky, E.J., Lachapelle, G., Langley, R.B., Nakiboglu, M., Schwarz, K.P., Tranquilla, J.M. & Vanicek, P. (1987) ***Guide to GPS Positioning.*** Canadian GPS Associates, Fredericton, New Brunswick, Canada, 2nd ed., 600pp.

Wild, U. (1994) Ionosphere and geodetic satellite systems: Permanent GPS tracking data for modelling and monitoring. *Geodätisch-geophysikalische Arbeiten in der Schweiz, Bd. 48, SGK.*

Wilson, R.M. (1935) Ground surface movement at Kilauea volcano, Hawaii. *University of Hawaii Research Publication No. 10,* 1-56. Honolulu: University of Hawaii.

Wilton, D.J. (1988) ***Computations for Surveyors.*** 7th Printing, Goodwill Press, 275 pp.

Wolf, P.R., & Ghilani, C.D. (1997) ***Adjustment Computations: Statistics and Least Squares in Surveying and GIS***, John Wiley & Sons, Inc.

Wyatt, F. (1982) Displacement of surface monuments: Horizontal motion. ***J. Geophys Res***, *87,* 979 - 989.

Wyatt, F., Bolton, H., Bralla, S., & Agnew, D. (1989) New designs of geodetic monuments for use with GPS, (Abs.) ***EOS Trans***. *70,* pp 1054.

Yunck, T.P. (1993) Coping with the atmosphere and ionosphere in precise satellite and ground positioning, In Geophys. Monograph 73, Environmental Effects on Spacecraft Positioning and Trajectories, AGU, IUGG Volume 13, 1-16.

Zhang, J. (1999) Investigations into the estimation of residual tropospheric delays in a GPS network. *Masters Thesis,* Dept. of Geomatic Eng., Uni. Of Calgary, Canada.

Appendix A

DERIVATION OF THE GEOMETRIC RELATIONSHIP OF MULTIPATH AT THE RECEIVING ANTENNA

Consider the received signal, comprising direct and indirect components. The relative phase offsets and phase differences are proportional to the difference in the path lengths. The following derivation describes the amplitude and phase of the received signal from plane ground reflection as a function of the antenna height, satellite elevation and signal attenuation factor. The direct and indirect signals interfere with each other at the electrical phase centre of the antenna. The combined signal is the sum of the direct and indirect signals. The direct signal can expressed as:

$$V_d = A\cos\varphi \qquad \text{- (A1)}$$

and the indirect signal is:

$$V_i = \alpha A\cos(\varphi + \Delta\varphi) \qquad \text{- (A2)}$$

The measured signal at the antenna therefore is:

$$V_m = V_d + V_i = A_m\cos(\varphi + \Delta\varphi_m) \qquad \text{- (A3)}$$

Where:

φ = phase of the direct signal,

$\Delta\varphi$ = phase shift due to extra path length of the indirect signal,

$\Delta\varphi_m$ = multipath affected phase shift of the direct & indirect signal,

A = amplitude of the direct signal,

A_m = multipath affected amplitude (direct & indirect signal), and

α = attenuation factor of the indirect signal (depends on the reflecting surface, and ranges in value from 0 to 1).

A_m and $\Delta\varphi_m$ can be represented by:

$$A_m = A \bullet \sqrt{1+\alpha^2+2\alpha\cos(\Delta\varphi)} \qquad \text{- (A4)}$$

$$\Delta\varphi_m = \tan^{-1}\left(\frac{\alpha\sin(\Delta\varphi)}{1+\alpha\cos(\Delta\varphi)}\right) \qquad \text{- (A5)}$$

From equations A2, A4 & A5 it is clear that if $\alpha = 0$ this implies that the indirect signal has been completely absorbed, and no multipath occurs.

Also, for phase measurements, for $\Delta\varphi_m = 90° = 1/4$ cycle will be a maximum if $\alpha = 1$ and $\Delta\varphi = 180°$.

So if an expression for $\Delta\varphi$ can be found, then the multipath on the signal can be estimated.

Consider the case where the ground acts as the reflecting surface, as illustrated in Figure A-1.

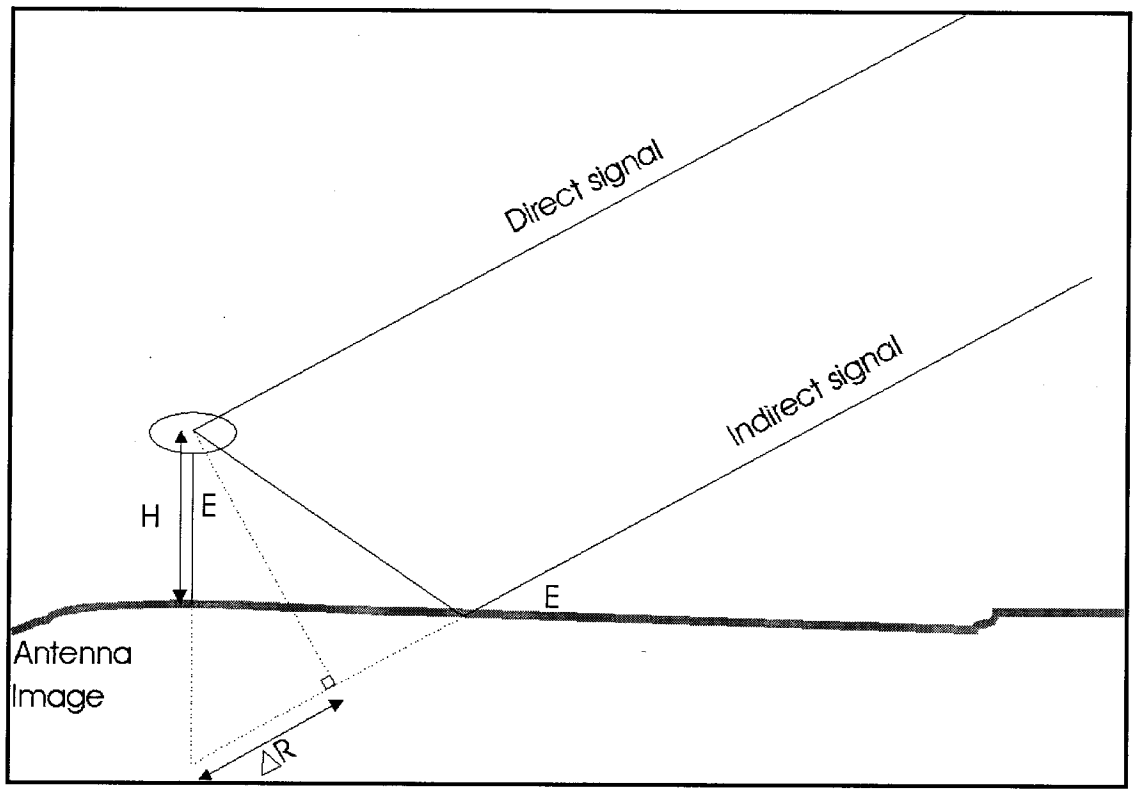

Figure A-1 – *Multipath from horizontal reflecting surface.*

E is the elevation angle of a satellite, H is the height of the antenna and Δ R is the extra path length travelled by the indirect signal compared to the direct signal.

From the diagram it can be shown that :

$$\sin E = \frac{\Delta R}{2H} \text{ or } \Delta R = 2H \sin E \qquad \text{- (A6)}$$

The extra path length in cycles is:

$$\Delta\varphi = \frac{\Delta R}{\lambda} 2\pi + \pi \qquad \text{- (A7)}$$

Hence:

$$\Delta\varphi = \frac{4\pi H \sin E}{\lambda} + \pi \qquad \text{- (A8)}$$

Where the extra π term represents the phase shift introduced after reflection. Therefore equation A8 can be substituted into equations A4 & A5. Equation A3 is the resulting multipath affected signal.

Now consider the case where a vertical object (eg a wall) acts as the reflecting surface, as illustrated in Figure A-2.

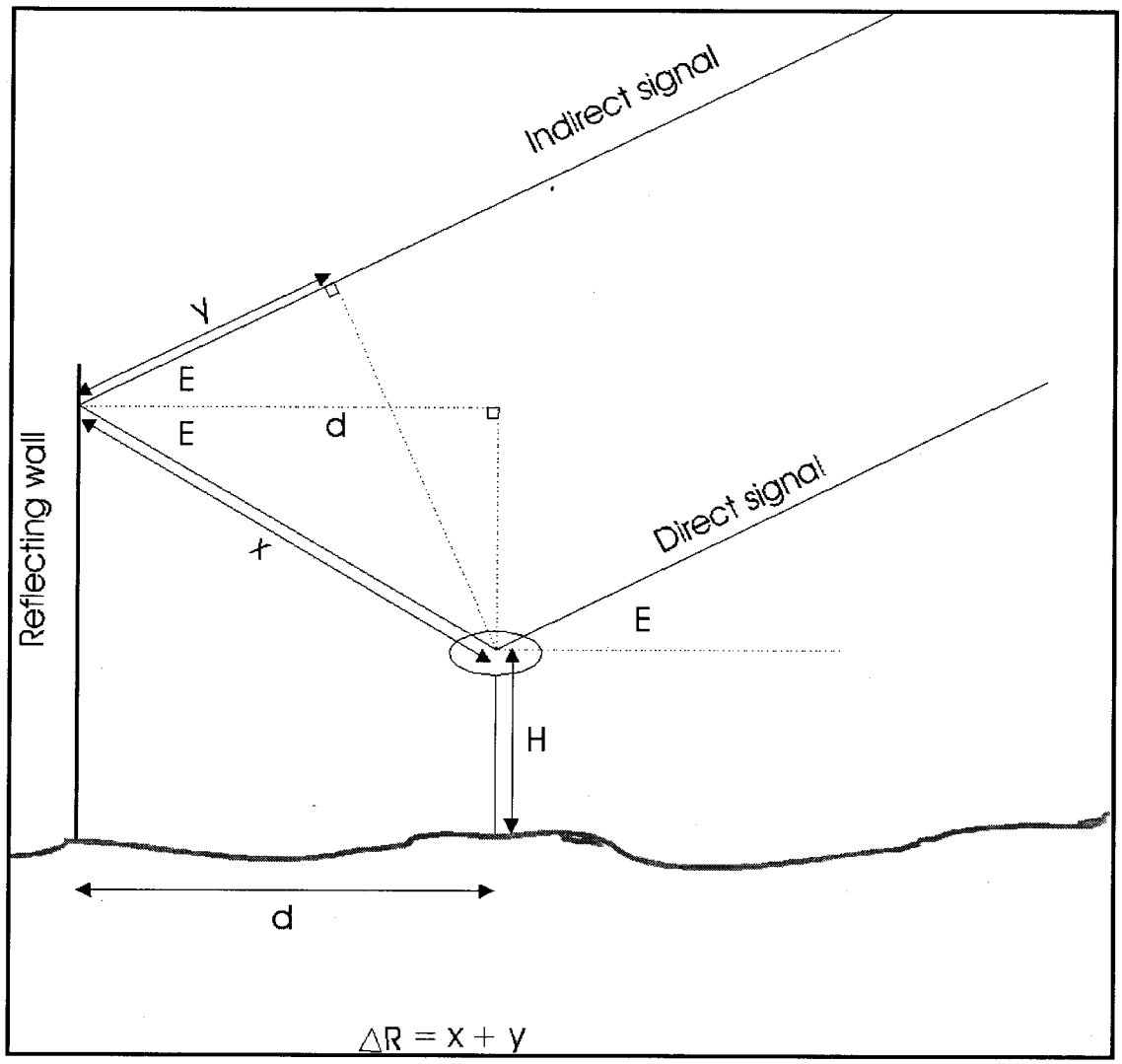

Figure A-2 – *Multipath from vertical reflecting surface.*

E is the elevation angle of a satellite, H is the height of the antenna, d is the distance between the antenna and the vertical reflecting surface, and ΔR is the extra path length (given here in 2 components: x + y) travelled by the indirect signal compared to the direct signal.

From the Figure A-2:

$$x = \frac{d}{\cos E} \qquad \text{- (A9)}$$

and :

$$y = x\cos 2E \text{ or } y = \frac{d}{\cos E}\cos 2E \qquad \text{- (A10)}$$

Hence:

$$\Delta R = x + y = \frac{d}{\cos E} + \frac{d}{\cos E}\cos 2E = \frac{d}{\cos 2E}(1 + \cos 2E) \qquad \text{- (A11)}$$

Using shows the trigonometric identity (Wilton, 1988):

$$\cos 2E = 2\cos^2 E - 1 \qquad \text{- (A12)}$$

$$\Delta R = \frac{d}{\cos E}\left(1 + 2\cos^2 E - 1\right) = 2d\cos E \qquad \text{- (A13)}$$

Therefore substituting into equation A7:

$$\Delta\varphi = \frac{4\pi d\cos E}{\lambda} + \pi \qquad \text{- (A14)}$$

Again the extra π term represents the phase shift introduced after reflection. Similarly equation A14 can be substituted into equations A4 & A5, and hence equation A3, to give the resulting multipath affected signal for the vertical reflection case.

Appendix B-1

INSTRUCTIONS FOR OPERATING THE CONTINUOUS GPS SYSTEM AT PAPANDAYAN

Written by Craig Roberts 12/7/1999
Updated 25/2/2000 & 12/7/2001

Overview

The following instructions describe the operation of the continuous GPS monitoring system installed at the VSI observatory, at Gunung Papandayan. The system comprises one base station located at the observatory (MA01), and three "slave" or "rover" stations located at Bukit Maung (MA02), Nangklak (MA03) and Kawah (MA04) respectively.

All stations consist of a single-frequency GPS receiver combined with a computer in a small aluminium box (hereafter called a GPS/PC module). This is connected to a radio, which is used to communicate between the base and slave stations. Power is supplied at the slave stations using a 12 V DC battery constantly charged by solar panels. Power at the base is supplied by AC power.

24 one-hour sessions are measured daily at all stations. The on-board computers control file creation. The base station radio routinely polls all the slave stations in sequence and stores their data files, as well as its own, on the hard disk. The following example describes the file naming convention:

MA02190c.99o – defines a file from Bukit Maung – "MA02" – on day-of-year "190" – "c" the third session for this day (ie the session from 2:00 – 2:59:45 UTC). Please note that these times are with respect to GPS time, which is 7 hours behind local time. The .99o is a standard RINEX file naming convention that defines the year 1999 and an observation file "o". (MA02190c.99n is the twin file of this session and contains the navigation data necessary for processing.)

Base Station

See Figure 4.10 for a diagram of the base station setup. Power is supplied to the base station system using AC power. However, the power source is unreliable. For this reason, an uninterruptable power supply (UPS) is connected between the AC power outlet and the base station system. The UPS regulates the power to guard against power spikes, and also automatically switches to its own on-board battery supply in the event of a power blackout. Unfortunately the on-board battery is only able to supply reserve power for about 20 minutes before it will be exhausted. At the observatory it is not unusual to experience 4 – 6 hour power blackouts. The small 7 Ah battery included in the UPS has been replaced by a larger battery bank. A 70 Ah and a 45 Ah 12 V wet lead acid battery have been included as part of the power system. Although the UPS includes a battery charger which constantly charges the backup battery, it is only designed for a 7 Ah battery. A powerful battery charger is included to more effectively charge the larger battery bank. Note that when the batteries are fully charged, the charger will stop operating.

From Figure 4.10 it can be seen that the monitor and a computer power supply are connected directly to the UPS. The computer power supply is used to power the hard disk. The GPS/PC module and radio receive power exclusively from the 12 V battery. The battery is continuously charged by a battery charger connected to the AC power. The battery charger will automatically trickle charge when the battery approaches a full charge. In the event of a power blackout, the 12 V battery should be able to continue to power the whole system for up to 2 days.

The UPS also powers the hard disk. Powering the hard disk however is more complicated. A hard disk requires both 12 V & 5 V DC, therefore the external PC power supply is used to power the hard disk. In the event of a power failure the UPS will quickly switch to the battery in order to continually power the system.

The GPS/PC module is connected to a monitor, keyboard, the GPS antenna and a data link to the radio. The radio is connected to an Omni dipole antenna mounted on the roof of the observatory.

The monitor is not crucial to the running of the system therefore it is recommended that when the system is operating reliably for a longer period, to simply switch off the power at the monitor. The monitor can be easily switched on again for status monitoring.

Operation of Base Station

1. To operate the base station first ensure that all components are correctly connected, as shown in Figure 4.10, before switching the power on. ***Note, do not connect the power to the GPS/PC module yet.***

2. Switch on the power at the wall and ensure that the UPS has started. The UPS will 'beep' and run through a boot up sequence (it checks if the backup battery can continuously supply power in the event of a blackout). The green light on the top left will then remain on. The monitor should also come on at this stage, but the hard disk will not begin to spin.

3. Now connect the white 12 V DC power cable to the GPS/PC module. If the hard disk does not start at this stage then simply press the button connected to the power supply. It should now start. The computer on the GPS/PC module will now go through its boot sequence, which will be visible on the monitor. Note that the hard disk is C:\ drive and is about 1.7 Gb in size. (D:\ contains about 6 Mb of Flash-PROM (Disk-on-Chip) and some useful software such as the laplink software LLPRO for transfer of data from the hard disk to another computer.)

4. To start the base station software go into directory C:\marconi2.

5. Execute BASE.EXE and wait. You will see some figures come up on the screen and eventually there will be one line on the screen with a time which will update every 15 secs. If you see this screen it means that the GPS receiver at the base station is operating correctly. Next to this time you will see something like:

12:34:45 10 of 10 -> 2 4 15 16 17 18 20 21 23 24

This indicates that 10 satellites are being tracked at epoch 12:34:45 and GPS SVs 2, 4, 15, 16, 17, 18, 20, 21, 23 & 24 are being tracked.

At 12:59:45 (for example) the current survey session will end and you will see the screen change. This is the software creating a new file and indeed it will show the new file name on the screen (in this case MA01190n.99o).

The base station communications software is smart. At 13:01:00 the base station radio will poll MA02 (Bukit Maung) and request data to be transmitted from this station. You can check to see if the lights on the radio flash intermittently, indicating that the radio is either receiving or transmitting data.

If the connection is successful, then data will appear on the screen starting with a header file stating MA02190m.99o, followed by the data which appears line by line starting at 12:00:00, and continuing for every 15 second epoch until all data is received. This process should continue for about 4 minutes until the last epoch for this station is sent. This is the GPS data from the first station (Bukit Maung) being sent to the base station. One 15 second epoch measurement is sent every second from the slave station, therefore 240 flashes per session should be seen at the base station. Navigation data is not sent from the slave stations because processing is carried out using the navigation files logged at the base station.

If the radio connection is good then and the radios should operate correctly. Data from the next station (MA03 or Nangklak) will be polled by the base station radio and sent at 13:08:30. At the completion of the transmission from Nangklak, the data from Kawah will be polled and sent at 13:15:30 (*See Trouble Shooting 4*).

This procedure is usually completed at around 13:20:30 (in this case) at which point the screen will simply revert back to the GPS epochs being logged at the base station, updating on the screen every 15 seconds until 13:59:45 when this whole procedure will begin again.

During the download of the data, the base station GPS/PC module continues to log GPS data for the present session, as do the slaves (whilst they are sending their data from the previous session).

If for some reason there is no radio connection, the base station will continually try to connect with the slave station until a certain time, at which point it will give up. The data file at the slave station will be deleted from the on-board computer at this time and the data will be lost. This feature guards against the limited Flash-PROM space on the slave station computers from filling up and simply stopping their data collection.

If the base station is unable to connect to any of the slaves, a worst case scenario, then the following messages will appear on the screen:

13:08:30 = quit =0, station = 2 force exit MA02

13:15:30 = quit =0, station = 3 force exit MA03

13:22:30 = quit =1, station = 4 force exit MA04

Note: the times indicate when the base station radio stops trying to connect to the respective slave station.

To stop the survey (although I hope this is not necessary) simply press CTRL-C. The data files already measured can only be viewed after stopping the survey.

Slave Station

See *Appendix B-3 & B-4* for an overview of the slave station design. The computer on-board the GPS/PC module at the slave station is much simpler than the 133 MHz Pentium-based PC used at the base station. It is only required to run rudimentary software which controls the file management of the GPS data files and the radio communications. The radios simply listen for polling from the base station. Once the slave stations are operating there is nothing more to be done.
See *Appendix B-3* for a diagram of the slave station connections.

Operation of Slave Station

1. Starting the survey at a slave station requires a laptop computer with the VTCOM.EXE software, and a laplink cable with a 10 pin Hirose connection for the GPS/PC module (*See Trouble Shooting 8*). Disconnect the power/data cable from COM1 of the slave station and connect the laplink cable.

2. Press D then K to change the file transfer option from Kermit to X-modem.

3. The following parameters should be set:
   baud rate to 9600
   databits to 8
   stop bit to 1
   parity to non
   duplex to full
   modem to com1 (or what you use)
   protocol is x modem.

4. Select option A for the communication screen.

5. Press CTRL-Z.

6. Power the GPS/PC module with the white power cable (*See Trouble Shooting 10*). You should see the boot sequence on the screen of the laptop. This is the computer inside the GPS/PC module starting up. I have written an autoexec.bat file to automatically start the survey. To stop this sequence, you must constantly press CTRL-C to exit out of this routine (*See Trouble Shooting 9*).

7. Press DIR and delete any extraneous .NOV files (*See Trouble Shooting 12*).

8. Execute the program 2_SLAVE1.EXE. A screen will scroll down and prompt *type any key to continue*. Do this and you've started the survey. After a few moments, some symbols such as this ♠ will appear on the screen every second. This indicates that the GPS receiver and PC are communicating with each other, and that GPS SVs are being tracked. (Note: 2_SLAVE1.EXE refers to Bukit Maung, 2_SLAVE2.EXE refers to Nangklak and 2_SLAVE3.EXE is for Kawah.)

9. Now disconnect the hirose connector from the GPS/PC module and connect the hirose connector from the radio, and the task of starting a slave station survey is complete. Note that when starting the survey manually, test data is sent every second for three minutes through the radio. After connecting the Hirose connector, it is therefore possible to check the operation of the slave station radios by checking that the transmit light is flashing every second.

10. Carefully place the plastic drum back over the slave station setup, being careful to not kink or trap any cables underneath the drum.

Trouble Shooting

The continuous monitoring system described in this document is very much a prototype and as such is susceptible to many problems which may stop the operation of the system. I have therefore written this trouble shooting guide to assist future users of the system to detect and solve any problems that may occur.

1) Base station will not start:

Check that the UPS is operating. Do you have 12 V DC coming through the white power cable to the GPS/PC module? Check all connections are tight and the configuration is the same as indicated in Figure 4.10.

2) Base station starts but I do not see the GPS time message with number of SVs tracked:

Is the monitor turned on (switch underneath RHS of screen)? Is the GPS antenna cable correctly connected? Check the continuity of the cable. If you have a separate GPS Rx, connect it to the antenna cable and run the CMC proprietary software GPSMON and check if the position is changing in real-time. Note: it is not enough to just see the time changing, you must see the position changing. Otherwise the GPSMON software is just running off an old almanac.

3) Radio receive light at the base station flashes intermittently:

This is probably just radio noise being detected by the base station antenna. The antenna is an omni dipole, meaning that it receives and transmits in all directions.

4) Can't see any lights flashing on the radios:

Check that the power to the radios is 12 V DC. Actually, of all the components at the slave stations, the radios use the most power when transmitting. If the power is sufficient, then the radios could somehow be broken. In my experience this is most unlikely. It is *not* recommended to unscrew the back of the radios as it is very easy to short circuit some internal connections even with static electricity from your hands. It is best to run the proprietary GLB software CMSW95 and check to see if you can read the settings in the radio. To run this software you will need a 12 V DC power supply, a

special RS232/power cable -> RS232 cable. Connect the power cables *first* to a battery and then connect the RS232 to the radio (important!!). Next connect the RS232 connection (without the power cables) to the computer. Start the CMSW95 software and click the "CMS Transceiver RS232C format" box and wait. Go to the pull down menu "Radio" and select "Read radio". You should see a box reading the settings inside the radio and counting up to 100. Now you can go to the first pull down menu and "Edit radio". Here you will see the settings of the radio. Below is a list of the most important settings that you should see:

Mode: Internal Modem
Preamble: 30 bytes
Preamble char: F0
Lookout time: 0 secs
Data format: GMSK
Serial port baud rate: 4800
Baud rate: 4800
Protocol: GLB CA mode
Channel switch position: 0 (Check the blue dial on the bottom of the radios)
Tx: 152.475 & Rx: 152.375 for the slave station radios
Tx: 152.375 & Rx: 152.475 for the base station radios.

If you see all these settings, and they are correct, then the radios should be operating correctly (Paul Simpson, personal communication, Feb. 2000, Bell-Pacific radios, distributor for GLB radio data systems, Sydney).

In my experience, however, it may still be necessary to check that the radios are really working by sending text data between two computers. Connect the radios as before for the CMSW95 test between two computers, and run the software "COMTEST4". Press Alt-B to change the baud rate to 4800. Now press any text character on one computer and see if it appears on the split screen on the other computer. You should also check that the lights on the radios flash as well. Note: Dummy load antennas (ie antennas with 50 Ohm resistors to decrease the power ouput of the radios) are required for this test and the radios should be separated by about 4 – 5 metres. If dummy load antennas are not

used, the huge power output can damage the receiving radio. (Analogous to reading a newspaper with a telescope (Graeme Hooper, 2001, personal communication)).

5) Base station operating fine but no data being received at the base station:
This could indicate any number of problems and will require a visit to the slave stations. It is worth checking the base station radio before doing so.

6) What do I check when I visit the slave stations?
You will need to check that the batteries have power at the slave station using a multimeter. Check that the solar regulator shows the same voltage as the multimeter. (The solar regulator runs through a continuous routine where 4 different screens constantly update the status of the solar panels and battery power.) Check that all connections are correct.

7) How do I check for a blown fuse in the slave station GPS/PC module?
Disconnect the antenna cable from the GPS/PC module, and check the voltage coming out of the antenna connection. Put the positive terminal of your multimeter inside the antenna connection and the negative on the outside on the screw thread. You should see 5 V (note 4.9 V is OK too). If this is correct, then it confirms that there are no blown fuses inside the GPS/PC module.

If, however, there is no voltage coming out of the antenna connection on the GPS/PC module, then you have blown a fuse. There are two surface mounted fuses in fuse holders inside the GPS/PC module. You will need to unscrew the 4 screws on the GPS/PC module in order to see these fuses. *Make sure that you have disconnected the power to the GPS/PC module before you open it up.* Try and get in the habit of opening the screws with the power connection on your RHS. This ensures that when you open the box away from, you avoid damaging the internal cables. The first fuse is a 2A fuse next to the power inlet. Check the continuity across this fuse with your multimeter. This fuse guards against too much power coming into the GPS/PC module and destroying the PC. The second fuse is on the opposite side of the board and protects the GPS Rx from receiving too much power from the antenna. It is a 125 mA fuse. (Note: at slave 3 this fuse often blows and I am currently using a 500 mA fuse for this GPS/PC module). You

can replace the fuse simply by pulling out the old one with a pair of tweezers and replacing it with a new one.

If you can see the PC using the VTCOM terminal software (*See Operation of Slave Stations*), but there is no voltage coming out of the antenna cable, then you know that the 125 mA fuse is blown.

If you cannot see the PC using VTCOM, then either the 2A fuse (or both fuses) have blown.

8) How do I read the PC inside the GPS/PC module?

You will need a laplink cable, an RS232 – 10 pin Hirose connection and a male/male 'gender bender'. Connect the laplink cable to the serial port of the computer, then the 'gender bender', and then the RS232-Hirose connector to the COM1 Hirose connection of the GPS/PC module. Start VTCOM.EXE and follow the steps set out in the *Operation of the Slave Station* description. Once connected to the PC, simply use standard DOS commands to access the computer.

9) What about the AUTOEXEC.BAT file?

In case the power accidentally goes off in the GPS/PC module, and then restarts, I have written an AUTOEXEC.BAT file to automatically restart the survey, delete any extraneous .NOV files, and record the time of the new power up. The contents of the AUTOEXEC.BAT file for SLAVE 1 is as follows:

```
break on
del *.nov
time < cr >> log.txt
2_slave1.exe
cr
```

Where cr is an extra file containing a 'carriage return' only.

The break on command will stop the AUTOEXEC.BAT if CTRL-C is pressed during the boot-up sequence.

10) How do I avoid blowing fuses?

The GPS/PC modules seem to be quite vulnerable to power surges, resulting in a blown fuse. I therefore suggest that when "powering up" the GPS/PC modules to always make sure that all cables are connected before powering up. I power up (by connecting the white cable) as the last step. Also when stopping the survey, disconnect the power as the first step.

11) How do I upload new software to the GPS/PC modules?

Using the same cable configuration as for VTCOM.EXE (*See Trouble Shooting 8*), type:

transfer /r <filename>
<enter>
Use the mouse to go to the transfer pull down menu and select "send data"
Browse file
Select file
Send
Hit F5
You should see the data being sent.

12) Check the .NOV files:

When the GPS Rx is operating, it copies the data to a binary file with some filename and the .NOV extension. Because the PCs in the GPS/PC modules are only 8086 PCs with 240 Kb of Flash-PROM, then it will quickly fill up. If the Flash-PROM fills up, then the data collection will stop. The software at the slave stations has been written to avoid this, but it could still happen. Power up the PCs with VTCOM and check that there are bytes free on the Flash-PROM using the dos command DIR.

13) How do I change the baud rate of the PCs inside the GPS/PC module?

Using VTCOM set to the same baud rate as the PCs, power up holding down the CTRL-Z key at the same time on the keyboard. You will now go into the BIOS settings for the PC. Use the Tab key to go to the Serial and Parallel Ports set up. Follow the prompts to change to 4800 baud rate. Save to CMOS and exit. You can now check again using VTCOM set to 4800-8-n-1.

14) Why do I use different software for the different slave stations?

Firstly due to the sequence of the radio polling for communications. More importantly, you will notice the names of the files for the three GPS/PC modules are as follows:

MA02 – Bukit Maung – 2_SLAVE1.EXE

MA03 – Nangklak – 2_SLAVE2.EXE

MA04 – Kawah – 2_SLAVE3.EXE

The baud rates differ between GPS/PC modules. 9600 is used for one slave between the GPS Rx and the PC, and 19200 for the other two GPS/PC modules. The GPS boards are a little different, and consequently different software was written for each slave unit. Keeping the correct software, with the correct units, will eliminate any incompatible baud rate problems.

15) How do I check which baud rates the GPS Rxs operate at?

Two small software packages have been written: CMC_19200.EXE and CMC_9600.EXE. Simply load these into the GPS/PC modules using VTCOM, and execute them. If it is the correct software, you will see some characters (which don't make any sense) appearing on the screen. These characters indicate that the correct baud rate has been selected. If you see nothing, then it is not the correct software. Try the other one. Delete this software and load the appropriate slave software into the GPS/PC module. This procedure could be necessary if GPS/PC modules are moved to other slave station sites, or if the hardware is changed in the field.

16) I see a flashing system light on the radio:

I noticed this one time at Kawah. The system light would flash 10 times followed by a pause and then it would flash again 10 times. I checked the radio using the CMSW95 software (*See Trouble Shooting 4*) and it worked fine. I simply restarted the whole system and it operated fine after that. I don't know what this means.

17) The size of the Flash-PROM on my GPS/PC module appears to be decreasing.

The JED PC541 computers should have 240Kb when new. The chip is actually 512Kb Disk-on-Chip and acts as a hard disk, even though it is only Flash-PROM. Much of this 512 Kb is used for CMOS settings and the like, leaving 240Kb of memory. You can read this as much as you like but writing to it can only be done a finite number of times.

There is a special algorithm inside the Disk-on-Chip to jump around and use various different sectors, so that any one particular sector will not be over-used. The Disk-on-Chip will automatically detect bad sectors and no longer use them. This is why you will see the Flash-PROM size decreasing over time. When the Flash-PROM size becomes too small, replace the Disk-on-Chip (costing about $AUD40). This can simply be plugged in and out in the field. Make sure that the TRANSFER.EXE and COMMAND.COM softwares are included on the Disk-on-Chip before replacing.

Thanks for your continued support, good luck!

Appendix B-2

BASE STATION GPS SYSTEM

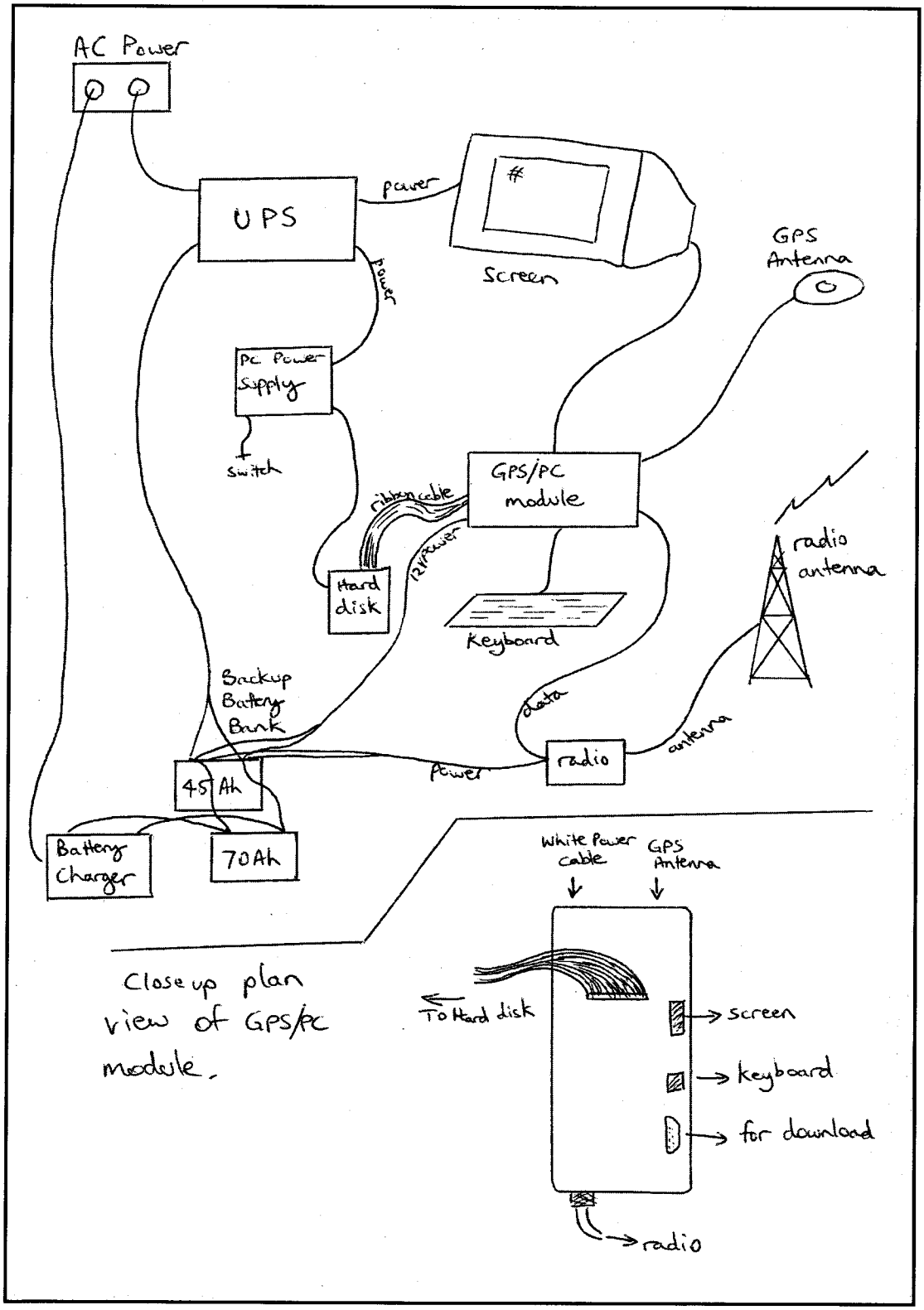

Appendix B-3

SLAVE STATION SCHEMATIC DIAGRAM

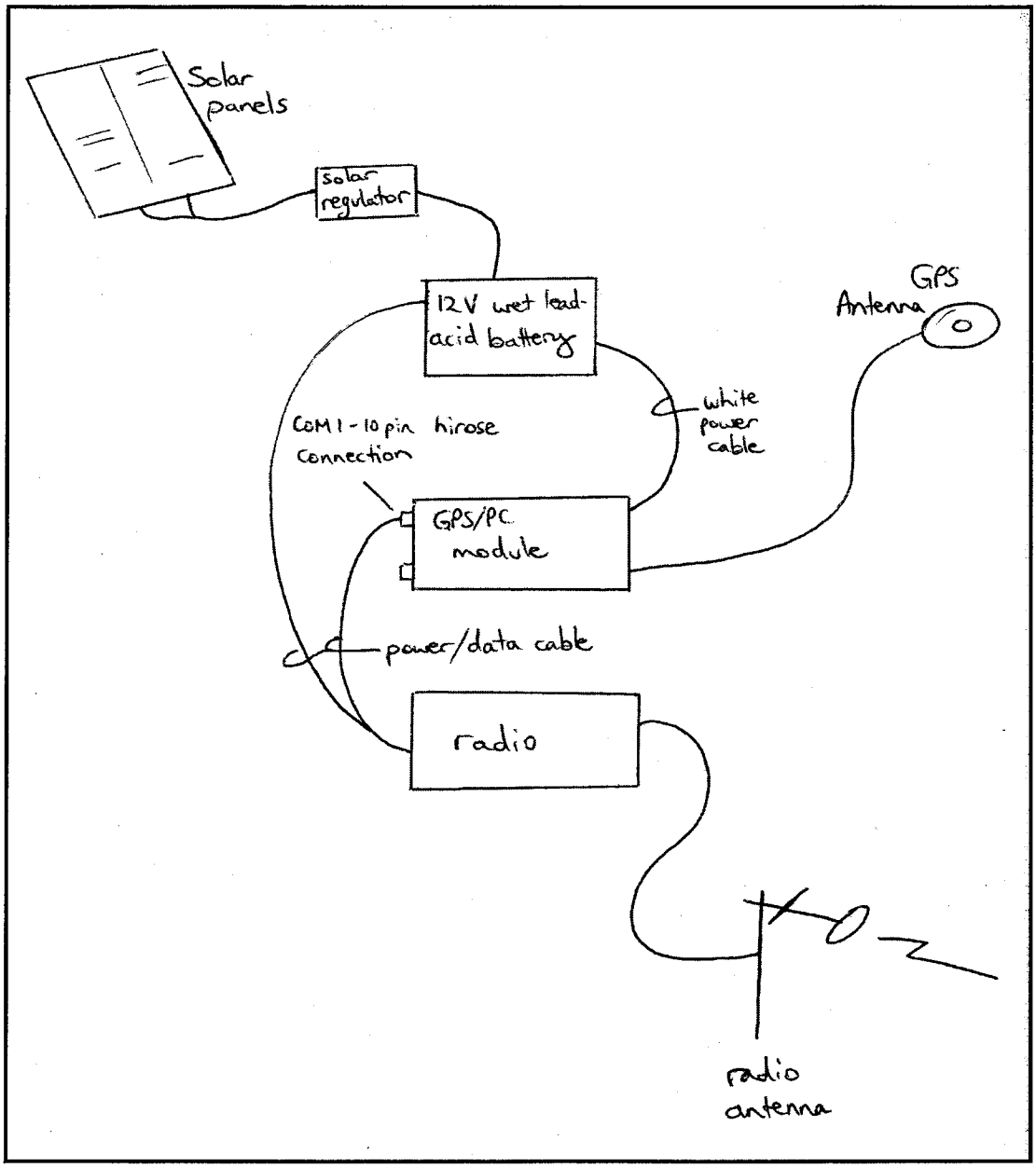

Appendix B-4

SLAVE STATION SETUP IN DETAIL

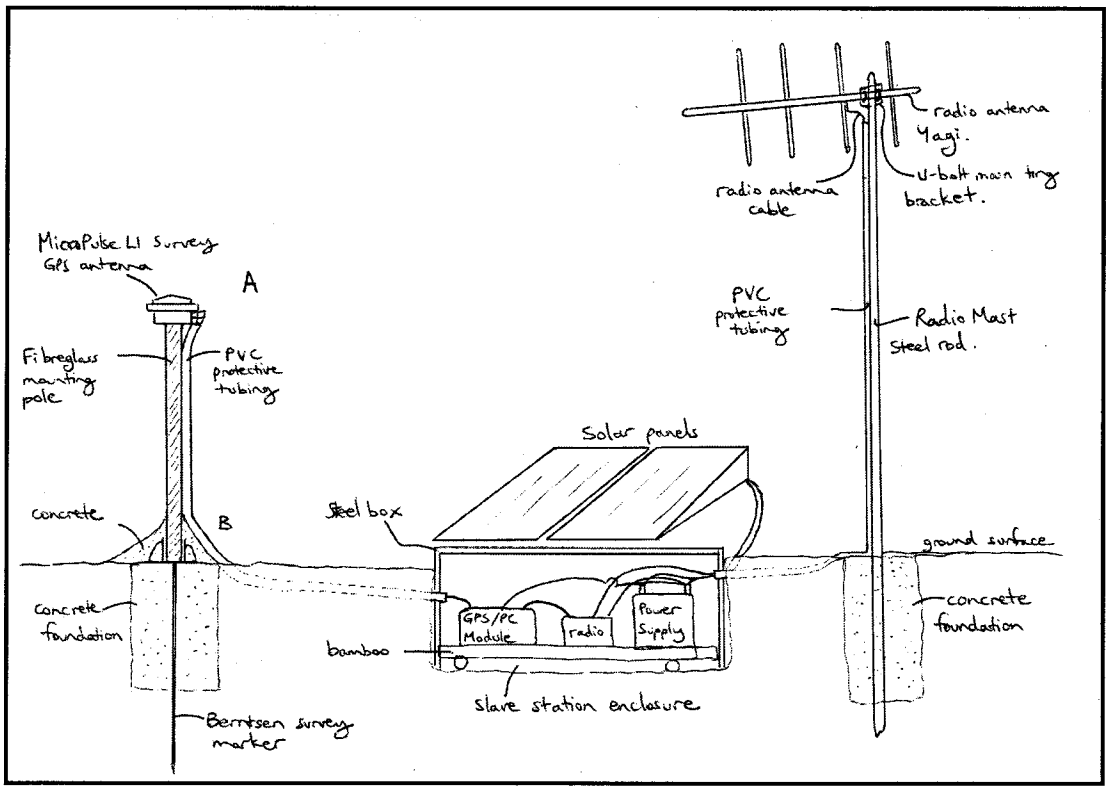

Appendix B-5

CLOSE-UP OF ANTENNA MOUNT

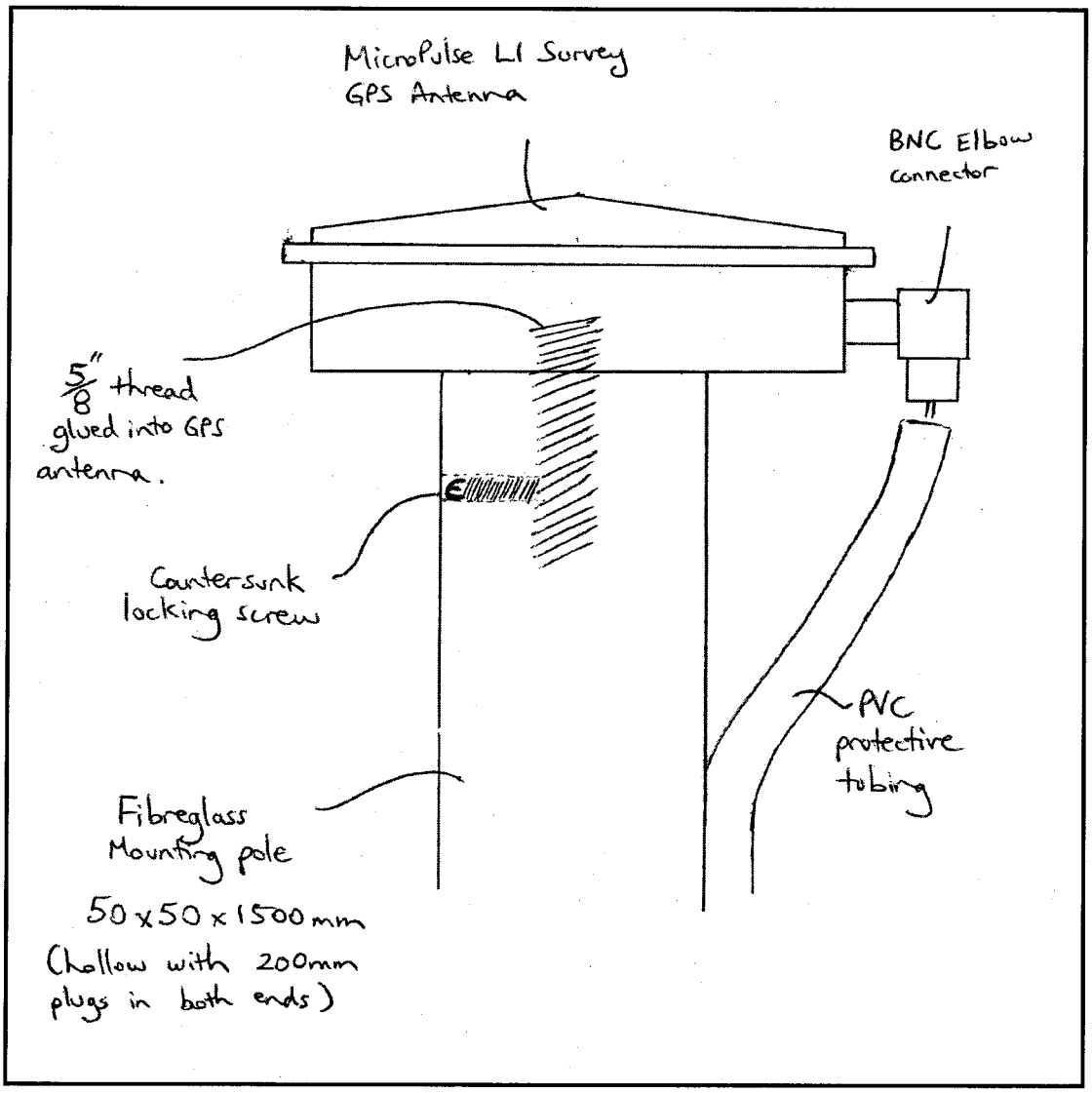

Appendix B-6

CLOSE-UP OF SURVEY MONUMENT DESIGN

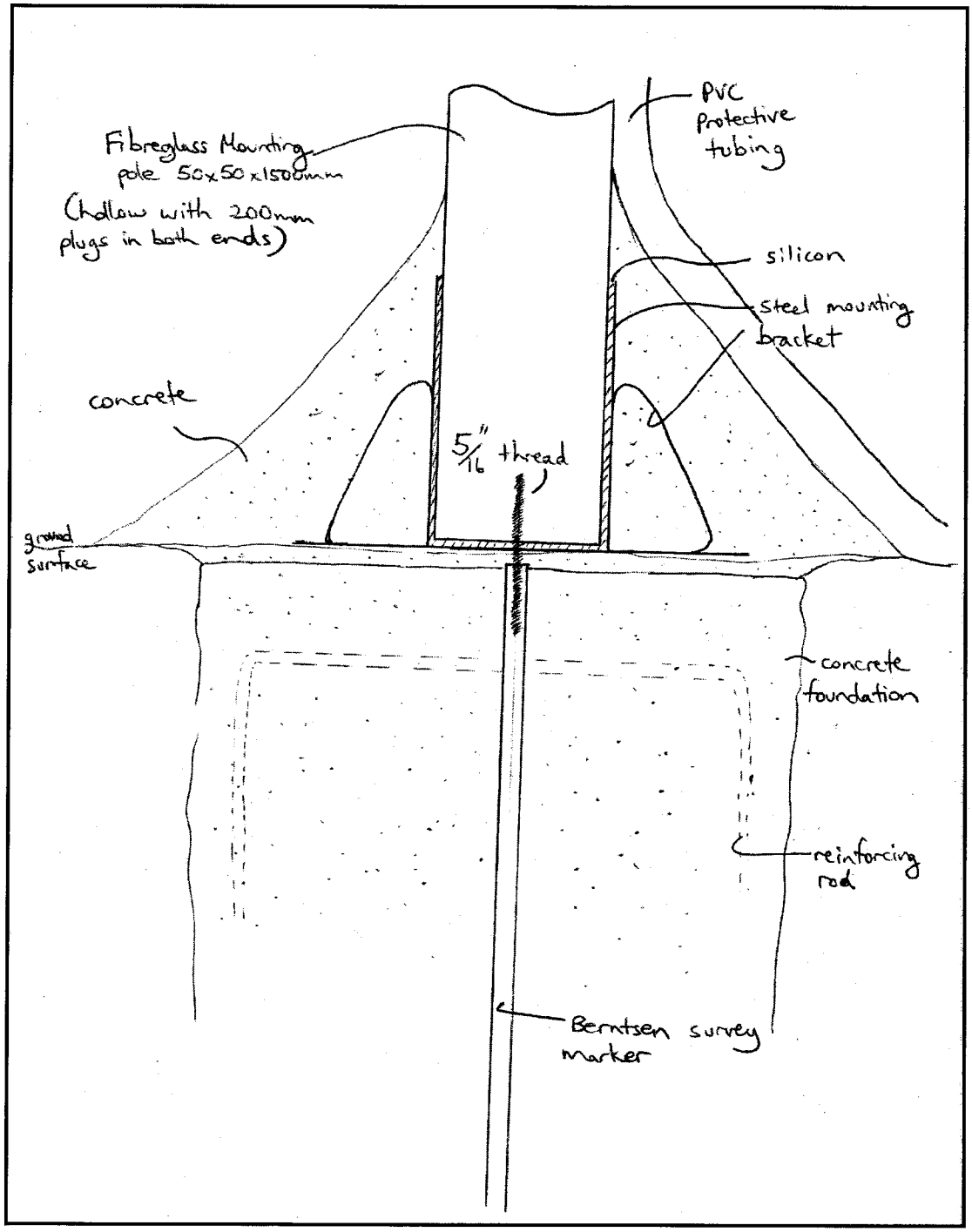

Appendix C

EFFECT OF TEMPERATURE LAPSE RATE ON THE SAASTAMOINEN MODEL

A simple empirical calculation using the Saastamoinen model (equation 5.15) illustrates the negligible difference of using the temperature lapse rate values for the USSA66 model of –6.50°K/km and comparing with Mendes' value of –6.10°K/km in terms of the total tropospheric path delay.

The effect of the temperature lapse rate can be checked using the formulas from the Bernese documentation (chapter 12) (Rothacher & Mervart, 1996) to transfer surface values to a particular height and adopting standard atmosphere values as starting values. The formulas are given below:

$$P = P_s\left(1 - 0.0000226\left(h - h_s\right)\right)^{5.225} \qquad \text{- (C1)}$$

$$T = T_s - 0.0065\left(h - h_s\right) \qquad \text{- (C2)}$$

$$H = H_s.\exp^{-0.0006396\left(h - h_s\right)} \qquad \text{- (C3)}$$

$$e = \frac{H}{100}\exp^{\left(-37.2465 + 0.213166T + 0.000256908T^2\right)} \text{ (Rothacher et al, 1986)} \qquad \text{- (C4)}$$

P_s = 1013.25 mb

T_s = 291.15 °K

H_s = 50 %

Where:

P – pressure

T – temperature

H – humidity

h – height above the ground surface

e – partial pressure of water vapour

exp – natural logarithm

s – indicates on the ground surface

The 0.0065 term in equation C2 refers to the temperature lapse rate for the USSA66 standard model. Assuming a station height of 1000m ie h = 1000m and computing the Saastamoinen zenith tropospheric delay for both the USSA66 (-6.50°K/km) and the Mendes derived value (-6.10°K/km) the results are presented below.

D_{trop}(USSA66) = 2.0840m

D_{trop}(Mendes) = 2.0848m

The difference is at the sub-millimetre level and the discrepancy due to the different temperature lapse rates in the zenith direction can be considered negligible.

Publications from the

SCHOOL OF SURVEYING AND SPATIAL INFORMATION SYSTEMS
(formerly: SCHOOL OF GEOMATIC ENGINEERING)

THE UNIVERSITY OF NEW SOUTH WALES
ABN 57 195 873 179

To order, write to:
Publications Officer, School of Surveying and Spatial Information Systems
The University of New South Wales, UNSW SYDNEY NSW 2052, AUSTRALIA

NOTE: ALL ORDERS MUST BE PREPAID. CREDIT CARDS ARE ACCEPTED.
SEE BACK PAGE FOR OUR CREDIT CARD ORDER FORM.

MONOGRAPHS

Australian prices include postage by surface mail and GST.
Overseas prices include delivery by UNSW's air-lifted mail service (~2-4 weeks to Europe and North America).
Rates for air mail through Australia Post on application.

(Prices effective November 2002)

		Price Australia (incl. GST)	**Price** Overseas
M1.	R. S. Mather, "The Theory and Geodetic Use of some Common Projections", (2nd edition), 125 pp, 1978.	$ 16.50	$ 15.00
M2.	R. S. Mather, "The Analysis of the Earth's Gravity Field", 172 pp, 1971.	$ 8.80	$ 8.00
M3.	G. G. Bennett, "Tables for Prediction of Daylight Stars", 24 pp, 1974.	$ 5.50	$ 5.00
M4.	G. G. Bennett, J. G. Freislich & M. Maughan, "Star Prediction Tables for the Fixing of Position", 200 pp, 1974.	$ 8.80	$ 8.00
M8.	A. H. W. Kearsley, "Geodetic Surveying", 96 pp, 1988.	$ 13.20	$ 12.00
M11.	W. F. Caspary, "Concepts of Network and Deformation Analysis", 183 pp, 2000.	$ 27.50	$ 25.00
M12.	F. K. Brunner, "Atmospheric Effects on Geodetic Space Measurements", 110 pp, 1988.	$ 17.60	$ 16.00
M13.	B. R. Harvey, "Practical Least Squares and Statistics for Surveyors", (2nd edition, reprinted with corrections), 319 pp, 1998.	$ 33.00	$ 30.00
M14.	E. G. Masters and J. R. Pollard (Eds.), "Land Information Management", 269 pp, 1991. (Proceedings LIM Conference, July 1991).	$ 22.00	$ 20.00
M15/1	E. G. Masters and J. R. Pollard (Eds.), "Land Information Management - Geographic Information Systems - Advance Remote Sensing Vol. 1", 295 pp, 1993 (Proceedings of LIM & GIS Conference, July 1993).	$ 33.00	$ 30.00
M15/2	E. G. Masters and J. R. Pollard (Eds.), "Land Information Management - Geographic Information Systems - Advance Remote Sensing Vol. 2", 376 pp, 1993 (Proceedings of Advanced Remote Sensing Conference, July 1993).	$ 33.00	$ 30.00
M16.	A. Stolz, "An Introduction to Geodesy", 2nd extended edition, 148 pp, 2000.	$ 24.20	$ 22.00
M17.	C. Rizos, "Principles and Practice of GPS Surveying", 565 pp, 1997.	$ 46.20	$ 42.00

UNISURV REPORTS - S SERIES

(Prices effective November 2002)

Australian Prices *:	S8 - S20		$11.00
	S29 onwards	Individuals	$27.50
		Institutions	$33.00
Overseas Prices **:	S8 - S20		$10.00
	S29 onwards	Individuals	$25.00
		Institutions	$30.00

* Australian prices include postage by surface mail and GST.
** Overseas prices include delivery by UNSW's air-lifted mail service (~2-4 weeks to Europe and North America). Rates for air mail through Australia Post on application.

S17. C. Rizos, "The Role of the Gravity Field in Sea Surface Topography Studies", Unisurv S17, 299 pp, 1980.

S18. B. C. Forster, "Some Measures of Urban Residential Quality from LANDSAT Multi-Spectral Data", Unisurv S18, 223 pp, 1981.

S19. R. Coleman, "A Geodetic Basis for Recovering Ocean Dynamic Information from Satellite Altimetry", Unisurv S19, 332 pp, 1981.

S29. G. S. Chisholm, "Integration of GPS into Hydrographic Survey Operations", Unisurv S29, 190 pp, 1987.

S31. J. Soetandi, "A Model for a Cadastral Land Information System for Indonesia", Unisurv S31, 168 pp, 1988.

S33. R. D. Holloway, "The Integration of GPS Heights into the Australian Height Datum", Unisurv S33, 151 pp, 1988.

S36. A. R. Marshall, "Network Design and Optimisation in Close Range Photogrammetry", Unisurv S36, 249 pp, 1989.

S37. W. Jaroondhampinij, "A Model of Computerised Parcel-Based Land Information System for the Department of Lands, Thailand", Unisurv S37, 281 pp, 1989.

S39. C. Bosloper, "Multipath and GPS Short Periodic Components of the Time Variation of the Differential Dispersive Delay", Unisurv S39, 214 pp, 1990.

S40. J. M. Nolan, "Development of a Navigational System Utilizing the Global Positioning System in a Real Time, Differential Mode", Unisurv S40, 163 pp, 1990.

S41. R. T. Macleod, "The Resolution of Mean Sea Level Anomalies along the NSW Coastline Using the Global Positioning System", Unisurv S41, 278 pp, 1990.

S42. D. A. Kinlyside, "Densification Surveys in New South Wales - Coping with Distortions", Unisurv S42, 209 pp, 1992.

S43. A. H. W. Kearsley (ed.), Z. Ahmad, B. R. Harvey and A. Kasenda, "Contributions to Geoid Evaluations and GPS Heighting", Unisurv S43, 209 pp, 1993.

S44. P. Tregoning, "GPS Measurements in the Australian and Indonesian Regions (1989-1993)", Unisurv S44, 134 + xiii pp, 1996.

S45. W.-X. Fu, "A Study of GPS and Other Navigation Systems for High Precision Navigation and Attitude Determinations", Unisurv S45, 332 pp, 1996.

S46. P. Morgan et al, "A Zero Order GPS Network for the Australia Region", Unisurv S46, 187 + xii pp, 1996.

S47. Y. Huang, "A Digital Photogrammetry System for Industrial Monitoring", Unisurv S47, 145 + xiv pp, 1997.

S48. K. Mobbs, "Tectonic Interpretation of the Papua New Guinea Region from Repeat Satellite Measurements", Unisurv S48, 256 + xv pp, 1997.

S49. S. Han, "Carrier Phase-Based Long-Range GPS Kinematic Positioning", Unisurv S49, 185 + xi pp, 1997.

S50. M. D. Subari, "Low-cost GPS Systems for Intermediate Surveying and Mapping Accuracy Applications", Unisurv S50, 179 + xiii pp, 1997.

S51. L.-S. Lin, "Real-Time Estimation of Ionospheric Delay Using GPS Measurements", Unisurv S51, 199 + xix pp, 1997.

S53. D. B. Lemon, "The Nature and Management of Positional Relationships within a Local Government Geographic Information System", Unisurv S53, 273 + xvi pp, 1997.

S54. C. Ticehurst, "Development of Models for Monitoring the Urban Environment Using Radar Remote Sensing", Unisurv S54, 282 + xix pp, 1998.

S55. S. S. Boey, "A Model for Establishing the Legal Traceability of GPS Measurements for Cadastral Surveying in Australia", Unisurv S55, 186 + xi pp, 1999.

S56. P. Morgan and M. Pearse, "A First-Order Network for New Zealand", Unisurv S56, 134 + x pp, 1999.

S57. P. N. Tiangco, "A Multi-Parameter Radar Approach to Stand Structure and Forest Biomass Estimation", Unisurv S57, 319 + xxii pp, 2000.

S58. M. A. Syafi'i, "Object–Relational Database Management Systems (ORDBMS) for Managing Marine Spatial Data: ADCP Data Case Study", Unisurv S58, 123 + ix pp, 2000.

S59. X.-Q. Lu, "Strategies for Improving the Determination of Displacements of Sea Surface Temperature Patterns Using Consecutive AVHRR Thermal Images", Unisurv S59, 209 + xiii pp, 2000.

S60. G. Dickson, "GPS-Controlled Photography: The Design, Development and Evaluation of an Operational System Utilising Long-Range Kinematic GPS", Unisurv S60, 417 + x pp, 2000.

S61. J. Wang, "Modelling and Quality Control for Precise GPS and GLONASS Satellite Positioning", Unisurv S61, 171 + x pp, 2001.

S62. Y. Wang, "Knowledge-Based Road Extraction from Aerial Images", Unisurv S62, 178 + xi pp, 2001.

S63. L. Ge, "Development and Testing of Augmentations of Continuously-Operating GPS Networks to Improve their Spatial and Temporal Resolution", Unisurv S63, 230 + xvi pp, 2001.

S64. H.-Y. Chen, "A Study on Real-Time Medium-Range Carrier-Phase-Based GPS Multiple Reference Stations", Unisurv S64, 182 + xxiv pp, 2001.

S65. G. Y. K. Shea, "A Web-Based Approach to the Integration of Diverse Data Sources for GIS", Unisurv S65, 233 + xv pp, 2001.

S66. M. Mirbagheri, "Analysis of Interferometric SAR for Topographic Mapping", Unisurv S66, 135 + xvii pp, 2001.

S67. P. Wang, "Applying Two-Dimensional Kalman Filtering Techniques to Digital Elevation Models for Terrain Surface Modelling", Unisurv S67, 175 + xi pp, 2001.

S68. J. M. Rüeger, "Refractive Indices of Light, Infrared and Radio Waves in the Atmosphere", Unisurv S68, 92 + vi pp, 2002.

S69. C. Satirapod, "Improving the GPS Data Processing Algorithm for Precise Static Relative Positioning", Unisurv S69, 131 + viii pp, 2002.

S70. R. Mason, "Developing Australian Spatial Data Policies – Existing Practices and Future Strategies", Unisurv S70, 258 + xv pp, 2002.

S71. C. Ogaja, "A Framework in Support of Structural Monitoring by Real Time Kinematic GPS and Multisensor Data", Unisurv S71, 191 + xiii pp, 2002.

S72. L. Dai, "Augmentation of GPS with GLONASS and Pseudolite Signals for Carrier Phase Based Kinematic Positioning", Unisurv S72, 188 + viii pp, 2002.

S73. C. Roberts, "A continuous Low-Cost GPS-Based Volcano Deformation Monitoring System in Indonesia", Unisurv S73, 271 + xvi pp, 2002.